E.O. Paton Electric Welding Institute
of the National Academy of Sciences of Ukraine

Laser Technology Research Institute
of the National Technical University of Ukraine
«Kiev Polytechnic Institute»

International Association «Welding»
Local Charity Foundation «Welding Community»

Laser Technologies in Welding and Materials Processing

Proceedings of the Third International Conference

29 May – 1 June, 2007, Katsiveli, Crimea, Ukraine

Edited by
Prof. B.E. Paton and Prof. V.S. Kovalenko

E.O. Paton Electric Welding Institute, NASU
Kiev 2007

(2007) **Laser Technologies in Welding and Materials Processing.** Kiev: E.O. Paton Electric Welding Institute, NASU, 142 pp.

The book contains papers presented at the Third International Conference «Laser Technologies in Welding and Materials Processing», covering the latest achievements in the field of laser welding, cutting, surfacing and other advanced processes of laser machining of materials. Prospects of application of laser technologies are considered. Authors of the papers are the known specialists from many countries all over the world.

Conference Sponsor:
Presidium of the National Academy of Science of Ukraine
E.O. Paton Electric Welding Institute of the NAS of Ukraine

Information Support:
«Avtomaticheskaya Svarka»
«The Paton Welding Journal»

Compiled by *V.S. Kovalenko, I.V. Krivtsun*

Publishing Project *A.T. Zelnichenko*

CRC Preparation *L.N. Gerasimenko, T.Yu. Snegiryova*

Design *I.V. Petushkov*

Editor *N.A. Dmitrieva*

Illustrations in cover page one ---- by courtesy of V.S. Mayorov et al.
(Institute on Laser and Information Technologies of RAS, Shatura, Russia)

State Registration Certificate DK 166 of 06.09.2000

ISBN 966-8872-07-X

Sent to press on 14.12.2007. 60×84 / 8 form. Offset paper. Offset print. Ukr. Pet. Font. 29,0 cond. print. sheets. 20,1 publ. print. sheets.
Camera-ready copy was prepared at E.O. Paton Electric Welding Institute. 11, Bozhenko st., Kiev, 03680.
Published by «Esse». 34 / 1, Vernadsky Ave., Kiev, 03142.

Contents

PREFACE

These Proceedings cover the materials of the 3rd International Conference on Laser Technologies in Welding and Material Processing (LTWMP'07) which took place in Katsively town, Crimea, Ukraine, on May 29 – June 1, 2007.

The International Conference had been organized by the experts in laser technology from the E.O. Paton Electric Welding Institute of the National Academy of Sciences of Ukraine and from the Laser Technology Research Institute of the National Technical University of Ukraine «Kiev Polytechnic Institute» where pioneering research in this field in Ukraine and in the former Soviet Union was conducted since 1963. The Conference had been supported by the International Association «Welding» as well.

At the 1st similar conference held in May 2003 the decision to hold such conferences once per every 2 years was accepted. And thus again in 2005 the experts from 19 countries (Ukraine, Russia, Belarus, USA, Germany, Poland, PRC, Switzerland, Israel, Italy, Belgium, Iran and others) in the field of laser technology have presented the results of their last researches.

In 2007 it was possible to get acquainted with papers of participants from some new countries — Slovenia, Great Britain, Turkey, Cuba and others. Alongside with traditionally established topics the accent was made on rapidly developing new laser applications like those for medicine and medical instrumentation manufacturing, micro and nanoprocessing, etc.

The lasers have dynamically come practically to all spheres of human activity in the last years. More 350 various applications of lasers are known now. Use of lasers for processing materials in various industries is especially effective. And the customer's interest to these technologies has increased especially for last decades because of development of new generations of lasers with increased efficiency: solid-state, powerful $\tilde{N}\hat{I}_2$*, excimer, metal vapor, compact diode, fiber optics etc.*

To this and to other last achievements in the field of laser technology the program report and few plenary papers had been devoted. In total three plenary sessions were carried out.

The further work of Conference was held on following topics: welding, modeling, synthesis of 3D objects, heat treatment, coating, equipment, other advanced processes (8 sessions). The special session was allocated to poster papers (27 in total).

Some reports was devoted to urgent problems of laser sintering of powder materials at realization of processes of 3D products synthesis. The new developments in use of laser radiation for sintering the diamond containing composites at manufacturing the diamond cutting tool was discussed as well.

The significant attention at the Conference was paid to process simulation. The models of different processes were presented which had been visualized in dynamics giving quite adequate mechanism of different effects at laser beam interaction with materials. Such simulation not only helps to understand better these effects but also provides eventually the improvements in laser material processing.

The Conference has shown that laser technology still remains the most dynamically developing area of science and engineering stably raising efficiency of existing processes of laser manufacturing, constantly opening new applications of lasers in industrial sphere and attracting close attention of customers from different fields of industry and national economy.

Friendly, hospitable and creative atmosphere of the Conference promoted development of useful discussions, establishment of business contacts. The participants of the Conference from different countries marking unconditional success of the Conference, expressed wishes to take part in next 4th International Conference LTWMP'09. Thus the tradition keeps going on conducting such conference on laser technology in the post-soviet countries.

Prof. Volodymyr S. Kovalenko
Co-Chairman of the Conference

LASER TECHNOLOGY IN MEDICINE AND MEDICAL INSTRUMENTATION MANUFACTURING

V.S. KOVALENKO
Laser Technology Research Institute of NTUU «KPI», Kiev, Ukraine

The most widespread in medicine are lasers in diagnostics, therapy and surgery. The brief survey on such applications is given in proposed paper. Another very prospective field connected with application of laser in medicine is the use of lasers for medical instrumentation manufacturing. Thanks to possibility to highly localize laser radiation impact in the working zone, different unique industrial laser applications are possible at the level of micro and nano processing of tiny components for the great variety of specific medical devices. Among them are high quality precise sophisticated cutting of stents for cardio surgery operations, microwelding of elements for ears phones, manufacturing of microelectromechanical systems (MEMS), cardio valves, artificial teeth, etc. for implantation into human body. Laser rapid prototyping technology became the very useful technique to manufacture the polymer models of scalps, bones damaged as a result of accident or pathology development. Such models are of great help for surgeons for the fast development of strategy for complicated surgery operation.

For the whole history of civilization the human being was trying first to find and later to develop the best means to achieve the victory over his enemy. All those means were mainly based on the development of different types of weaponry for the physical damage or destruction of the enemy. Eventually the great efforts were taken to try to convert almost every latest scientific and technical achievement into new type of weaponry using tremendous resources of different countries. Except of military aspects those moves had the evident positive impact on different other civil applications developments of the latest results in science and technology as well including the medicine first of all.

Thanks to the latest global political and economic developments the enormous arm race has decreased drastically. So nowadays the civil applications of the newest scientific results have increased to great extent. And this is especially true for laser applications. We witness the wide spreading of lasers in medicine for the last few decades. The dynamic development and manufacturing of the large variety of lasers has greatly influenced that process.

So the scientists are paying the great debt to mankind: after centuries of shortening the human being's life the numerous researchers are taking the great efforts now to safe the life of people and to prolong the human life expectancy…

Among more than 350 different laser applications in almost every field of human activity the applications in medicine and related fields are occupying the second position after industrial laser application.

Medical applications. Considering the laser application in medicine, one has to realize the significant similarity of principal mechanisms of laser radiation interaction with organic tissue and interaction with different types of materials at industrial laser applications: irradiation –– absorption (reflection) — heating –– structural (chemical) changes –– overheating (evaporation, explosion, ablation) — cooling.

Thus, the main difference at interaction with biological matter is the very low reflection of laser beam from human (biological) tissue and very high role of chemical (biochemical) reactions at laser radiation interaction with alive tissue.

There are three main mechanisms of laser beam action at biological tissue [1], namely photo-chemical, photo-thermal, and photo-destruction.

The first one is typical for the reflexotherapy, to activate medicine, sterilize, treat wounds, etc.

The second one could be realized in two different variations: hyper heating up to 37–43 °C (no reverse destruction occurs) and up to 43–60 °C (membrane lost is observed as well as tissue welding).

For the photo-destructive method there are the following possibilities: at temperatures up to 60–100 °C tissue coagulation and necroses are observed, up to 100–300 °C liquid evaporation as well as carbonization takes place and at higher than 300 °C solid tissue evaporation takes place.

Further temperature increase causes destruction through thermal explosion (photo ablation), shock mechanical wave, etc.

Diagnostics. Laser radiation is quite widely used for diagnostic purposes. Laser may be installed into the system for blood testing. The application of laser in spectroscopic systems for material content analysis is well known as well. For studying the processes inside the living sells at high resolution the laser microscopy is used successfully.

Therapy. In therapy laser irradiation at low intensity may reduce the inflammation process both at the skin surface and inside some human organs.

Laser radiation may be used for treatment efficiency increase. Thus many diseases need to be treated by an even level of drugs in the blood. For this the capsule with drugs has a tine laser-drilled hole in its shell which releases a steady, constant dose of medicine.

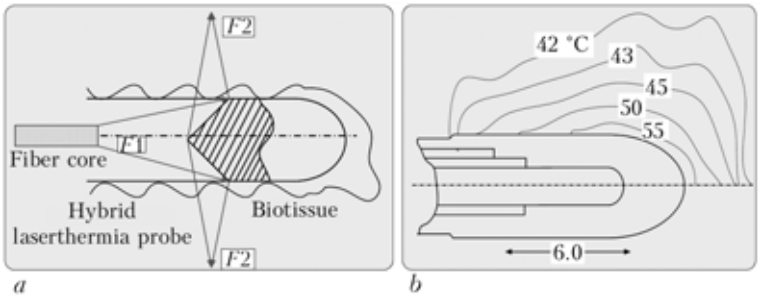

Figure 1. Sketch of hybrid laserthermia probe (*a*), and the measured temperature profile (*b*)

A lot of research is done for treatment different tumors, local inflammations, etc. without surgical intrusion. Our research at the Laser Technology Research Institute has demonstrated that depending on design of laser probe and treatment conditions it is possible to control the depth of internal action, the level of thermal influence reached. This is very important result demonstrating the possibility of non invasive treatment of prostate disease for example.

The positive result has been demonstrated as well at laserthermia for deep seated brain tumors using a hybrid laserthermia probe. In such system the Nd:YAG laser with a hybrid probe was developed to overcome a certain disadvantage of conventional laserthermia system with a frosted tipped contact probe. In Figure 1, *a* and *b* the sketch of hybrid laserthermia probe and the measured temperature profile is shown, respectively.

Vision correction. To restore the normal sight the focused laser radiation is used to correct nearsightedness or farsightedness. Guided by a computer program the excimer laser beam reshapes the cornea thus changing its curvature. To correct nearsightedness the laser beam trims the cornea's center, making it flatter. For farsightedness a doughnut-shaped rings of tissue is removed.

Heart muscle laser perforation at ischemia. Instead of conventional treatment of ischemia (coronary artery disease) by attempting to bypass or widen an occluded artery it is possible to use laser radiation for treatment (Figure 2). Depending on the side of the ischemic area, 30–40 channels 1 mm in diameter are created through the heart muscle. Each channel is created in 20–50 ms by action of a single pulse of CO_2-laser. Blood is then forced into the new channel thus exposing the reperfusable ischemic area to oxygenated blood.

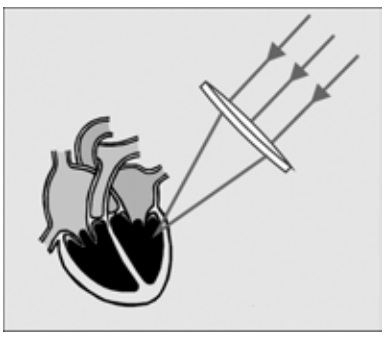

Figure 2. Laser perforation of heart muscle

Surgery. The main advantages of using laser beam in surgery as a scalpel are the high level of sterility, very high energy (heat) localization, the possibility to make «bloodless» resection because of blood capillary welding. The latter allows using laser beam as the sterile instrument for connecting (welding) tissue.

Laser processing in medical instrumentation manufacturing. Unlike in old time when medical instrumentation was limited to few numbers of different tools (mainly surgical) nowadays it is almost impossible to list the variety of medical devices, instruments, components etc. manufactured using laser technologies.

Machining. Among principal applications are the drilling of holes in catheters (to precisely measure blood or precisely control medication, machining of plastic catheter profiles (to facilitate insertion with minimal force), machining of biosensors (to provide accurate metering of patient condition) and fine perforation in membranes (to provide controlled passage of gas or liquids) [2–4].

Benefits are as follows:

- extraordinary edge quality;
- no heat-affected zone;
- accuracy and precision;
- no foreign materials introduced;
- repeatability;
- easy to automate;
- cost effective;
- process control.

Stents production. Cardio-vascular decease is a number one killer in the world. Because of patches formation on the walls of blood vessel the crossection of the vessel is decreasing causing the resistance to the blood flow. This is the main reason for strokes. Despite all the best medical and surgical therapy, stroke survivors are still at a high risk of suffering a relapse. Thus, there is a need to search for better treatment and preventative strategies.

One possible solution is the intracranial stent [5]. It can prevent the development of stroke and thus save life. Stenting can restore the blood flow in cerebral arteries. It represents a minimally invasive technique that is less costly and traumatic. The market for such a medical device is also very promising.

The design of the stent is very important. This stent should be smaller and more flexible than a coronary stent. It has to adapt to the curvatures in the

cerebral arteries. Also, the stent materials must be biocompatible.

A powerful tool that can be used for designing the stent is the advanced FEM (ANSYS). It can perform important simulations like the expansion process when the stent is under various physiological conditions. This is a very useful and important part of the designing process as the degree of restenosis after implantation depends very much on the design of the stent (Figure 3).

First types of stents was manufactured using the machining with quite long pulses (micro-, nano-, picoseconds) with consequent finishing and super finishing (abrasive, electropolishing etc.) operations.

Stents of the higher quality may be manufactured with femtosecond pulses lasers using the material ablation as erosion mechanism. The machining system for such manufacturing uses ultra-short pulses (100 fs) of light. It is a very different process compared to conventional laser machining like excimer or Nd:YAG laser. With ultra-short pulse width, the phenomenon of «multi-photon» process occurs. This means that the peak power is so high that the light energy not only overcomes the bonding forces between the materials (molecules) but also the forces between the atoms. The ultra-high peak power intensity is about 100 TW / cm^2.

Besides, the light-matter interaction time is also much shorter than the time for the heat to propagate into the adjacent materials through conduction. Hence, there will not be any heat-affected zone due to laser ablation. The component tube is usually fixed in a rotational stage with 3-axis of movement. The rotational error is only 1 μm and movement accuracy is 0.3 μm. During fabrication, the laser energy is adjusted to around 400 MW and the rotation speed is about 4 deg / s. The achieved average roughness is about 0.79 μm.

At the Laser Technology Research Institute of NTUU «KPI» there is the international project under development # 3350 «New Medical Stents Design and Their Manufacturing Using Laser Radiation». Project is sponsored by STCU. Partners: the Netherlands, Belgium, and Portugal. The main goal of the project: to develop the design and technology for manufacturing quite cheep stents which might be much more available for the patients with low incomes.

Marking. Laser marking is widespread for identification of different medical components and tools thanks to possibility of noncontact and sterile producing minimal signs without damaging the product quality.

Hardening. There are great variety of different medical instruments, the working surfaces of which needs some additional surface hardening, namely stomatological tools, surgery instrumentation, components for medical devices to increase their wear resistance and reliability. As a rule, after laser treatment the long life of such instrumentation is increasing by a factor 3–5. Quite original application is the possibility to change the biocompatibility of different metal implants in surgery [6]. Thus it was shown that with Nd:YAG laser irradiation of material surface it is possible to affect the cell proliferation and adhesion in stainless steel and Ti–Al–V alloy. Depending on material and working conditions these properties may be enhanced or decreased and in such a way biocompatibility of metal implants may be kept under control.

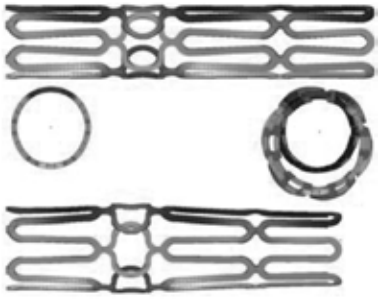

Figure 3. Stent shape as manufactured and after the installation (deformed inside the vessel)

Welding. A method for laser welding of parts used in ear implants has been developed at laser center of Flaming University, Belgium [7]. In order to reduce the size and the efficiency the electronics that produces signals going to the ear nerves is contained in the implant with very small dimensions: diameter of 18.7 mm, height of 3.8 mm and wall thickness of 0.2 mm. The box for electronics is made of Ti6Al4V titanium alloy to be compatible with the human body and has to satisfy the following conditions:

- leak tightness is better than $5 \cdot 10^{-8}$ mbar·l / s (MIL-STD-883D);
- welding depth is 50–75 % of the wall thickness;
- maximum inside temperature during welding is lower than 100 °C;
- no sharp edges;
- no surface contamination;
- no evaporation of titanium during welding;
- no moisture in the box.

The welding was performed with a 400 W pulsed Nd:YAG laser at pulse length of 15 ms, energy of 2 J, frequency of 3 Hz, 120 steps per minute and welding time of 6 min (720 steps). The overlap of 2 pulses is at least 50 %. A lens with a focal length of 80 mm has been used for welding the implants. With those parameters it was possible to fulfil the above requirements. There are many other laser welding operations in manufacturing different components for medical devices.

Rapid prototyping. This technology based on use of laser radiation for stereo lithography or sintering is becoming a good technique for manufacturing implants to replace the damaged bones or bones affected by pathology. With development of new materials with high biocompatibility the complicated surgery operations are getting more versatile and reliable.

Another very prospective application is manufacturing plastic model of scalp of bones damaged because of accident or pathology. Such model is created based on 3D virtual image of the damaged organ obtained by tomography of the patient (Figure 4). With such model the surgeon may develop the strategy of

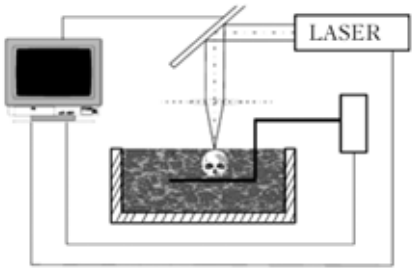

Figure 4. Scheme of manufacturing the model of scalp of acrylic, epoxy, vinyl and other materials by laser stereolithography

the complicated operation quite easily not disturbing the patient.

Laser devices. The ability of laser radiation to cause the bio-stimulating effect has initiated the number of laser applications in different medical devices [8–13].

Hair brush. The hair brush was proposed which has the laser radiation distributed via optical fibers between the brush elements [8]. As a result while hair combing the radiation is transferred to the very hair roots stimulating their growth or decreasing some local inflammation.

Toothbrush. The same principle is used at combination of laser radiation with teeth brush. Such device may reduce the paradentothis just during the everyday teeth cleaning procedure instead of using special laser treatment of this decease.

Laser shower. Combination of shower with laser irradiation may cause the positive effect by bio-stimulation and just due to psychological effect. In this case the laser diodes are installed in the shower head and water streams are used for laser radiation (of one or the variety of colors) transportation.

Liposuction. Experts from Massachusetts General Hospital, USA, had disclosed the new results on possibilities to use laser radiation for liposuction. They use the free-electron laser of specific wavelengths (selective photothermolysis) to heat up fat which was then excreted by the body –– without harming the skin. They suggested as well this technique could be used for treating cellulite, acne and heart disease. The explanation of the mechanism is as follows. The main cause of acne is a lipid-rich gland, the sebaceous gland, which is located a few millimeters below the surface of the skin. One has to be able to selectively target the sebaceous gland. This research showed that if one can build laser at this region of the spectrum he may be able to do this. Thus the problem is to create a fat-seeking laser. Such technique could also be used to eliminate cellulite and body fat. Fat build up in the arteries (plaques), which causes heart attacks, could also be treated. Experts say that they are still a few years away from testing this technique on human beings.

Nanorobots. Speaking about future developments of lasers in medical devices it is worth to mention first of all the micro and nano applications. It is considered quite prospective to combine medical devices with micro or nano information systems.

Thus the microrobot had been developed already which can move along the blood vessel and to diagnose the changes in temperature during the travel. It is possible in such a way to detect the local increase of temperature and thus to determine the source of inflammation or possible disorder in human organ functioning. Now such robot has millimeter size but with time its dimension may few micrometers or even nanometers. Such system designed as few shell construction may be multi functional containing monitoring unit, which is collecting various information, unit with medicine which is injected for local treatment, control unit which transmits the necessary information outside, etc. In this case laser technology is used to manufacture the nanochips, incorporated into the nanorobot –– nanobot.

Future trends. Further radiation localization via short wave and short pulse duration:

- will cause effects inside living cell;
- will bring the possibilities to affect the DNA code;
- will enhance the creation of nano- (NEMS) and microelectromechanical (MEMS) systems to control intercellular processes;
- will give the chance to manufacture compact nanoprocesssors capable to be implanted into human body.

Miniaturization of laser system due to use of new types of lasers: more mobile laser medical devices and thus possibility to manufacture new unique medical devices.

CONCLUSIONS

1. Laser medical applications are becoming more sophisticated and widespread.

2. The spreading of medical devices is enhanced by unique opportunities in manufacturing of laser material treatment.

3. The field is very prospective and achievements are far from saturation.

4. With nanotechnology developments the variety of laser technology use in medicine will increase further.

1. Kovalenko, V., Golovko, L., Konso, Z. et al. (1997) The use of laser radiation for biologic tissue hyper heating inside the body without its resection (I-Modeling). In: *Proc. of ICALEO* (San Diego, USA, Nov. 1997).
2. Meijer, J., Du, K., Giner, A. et al. (2002) Laser machining by short and ultrashort pulses: State of the art. *Annals of CIRP*, 51(**2**).
3. Kovalenko, V.S. (2006) Laser micro- and nanoprocessing. *Int. J. of Nanomanufacturing*, 1(**2**), 173–180.
4. Kleine, K.F., Whitney, B., Watkins, K.G. (2002) Use of fiber lasers for micro cutting application in the medical device industry. In: *Proc. of ICALEO* (Scottsdale, USA, Oct. 2002).
5. Yuan, Q., Ngoi, B.K.A., He, L.M. et al. (2002) Novel intelligent stent development. In: *Proc. of Int. Congress on Biological and Medical Engineering* (Singapore, Dec. 4–7, 2002).
6. Chew, H.R., Lawrence, J., Chong, C.K. et al. (2003) Laser treatment of selected bio-metals for improved biocompatibility. In: *Proc. of ICALEO* (Jacksonville, USA, Oct. 2003).
7. Gedopt, J., Delarbre, E. (2003) Pulsed Nd:YAG laser welding of titanium ear implants. In: *Proc. of LTWMP-2003.* Kiev: PWI.
8. Kovalenko, V.S., Tryvailo, M.S., Dementieva, N.V. et al. *Hair brush*. Pat. 20040604717á Ukraine. Publ. 16.06.2004.
9. Kovalenko, V., Zhuk, R., Tryvailo, M. et al. *Device for vacuum-laser therapy*. Pat. 2003087667 Ukraine. Publ. 13.01.2004.
10. Tryvailo, M., Kovalenko, V. *Laser massager*. Pat. 200503152 Ukraine. Publ. 17.10.2005.
11. Kovalenko, V., Zhuk, R., Tryvailo, M. et al. *Tooth brush*. Pat. 2003087666 Ukraine. Publ. 10.01.2004.
12. Tryvailo, M., Kovalenko, V. *Device for blood irradiation.* Pat. 200503131 Ukraine. Publ. 17.10.2005.
13. Kovalenko, V., Tryvailo, M., Zaininger, L. et al. *Massage ring*. Pat. 200503135 Ukraine. Publ. 17.10.2005.

LASER-BASED WELDING AND BRAZING IN AUTOMOTIVE PRODUCTION — INVESTIGATIONS TO REDUCE FAILURES AND IMPERFECTIONS

F. ALBERT, A. GRIMM, C. KAGELER and **M. SCHMIDT**
Bayerisches Laserzentrum GmbH, Erlangen, Germany

Laser welding and brazing are gaining more importance in today's automotive production. Both methods offer the potential for fast joining processes and a decrease of rework. A robust process management is, however, a precondition to achieve defect-free welding and brazing results. Two research projects are focusing on this problem at the Bavarian Laser Center (Bayerisches Laserzentrum). Solutions for laser welding of zinc-coated steel sheets in an overlap configuration and laser brazing of visible joints are examined.

Welding of zinc-coated thin steel sheets in an overlap joint configuration is mainly used in production of car bodies. Even when latest research results and technological improvements are taken into account, it is difficult to control or predict the behaviour of a laser welding process of such sheets in a zero-gap assembly. In the majority of cases, the coatings on the sheet surface have a lower evaporation temperature than the melting point of steel itself (T^{st}_{melt} > 1800 K; T^{Zn}_{vap} = 1180 K). When welding in a zero-gap assembly, the degassing of the vaporized zinc between the sheets is impossible in most cases. Therefore, it exhausts through the keyhole, disturbing the balance of pressure and the hydrodynamic processes in the weld pool. Results are imperfections or failures in the weld seam (Figure 1).

However, there are several possibilities to have an external influence on the laser welding process and the weld seam quality. One method presented in this paper is based on the modulation of the laser power, which should generate a stable keyhole dynamic and the possibility to permit the permanent degassing of vaporized zinc through the keyhole as well as to avoid failures as a result of keyhole collapses. The interactions of the power modulation with the keyhole and the liquid material are analyzed by means of high-speed images, optical process signals and welding results.

Laser brazing is also an important joining technology for visible joints of car bodies. Even today failures like pores, holes, spilling and one-sided melting of the sheets cannot be completely avoided and post-process quality checks are mandatory. In this case the accuracy of the used robot and fluctuations of laser power or focal position are the determining factors for the formation of failures. The expensive post-process checks could be avoided by means of a pyrometer-based on-line quality control, which is also discussed in this article. The use of this temperature-based on-line monitoring system allows detecting the mentioned failures. Furthermore, it is the basis of a closed-loop process control in order to adjust the position of the robot as well as the laser power and focal position. The realized system-technology and results of brazing experiments and pyrometer signals will be discussed.

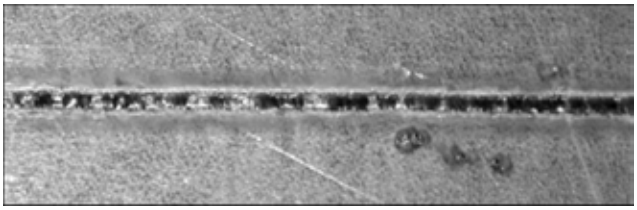

Figure 1. Weld seam of zinc-coated steel sheets in zero-gap overlap joint configuration

Laser welding of zinc-coated steel sheets. *Experimental setup*. The experimental setup is shown in Figure 2. Based on a deep-penetration process, two zinc-coated steel sheets with thicknesses of 0.6 and 0.7 mm are overlap-welded with a technical zero-gap. The zinc coatings have an average thickness of 10 μm. The laser source is a Yb:YAG disk-laser with a maximum continuous output power of 4 kW at 1030 nm. The beam quality product is about 9.2 mm·mrad (M^2 = 27.4), the focus diameter is 600 μm, and the focal length is 450 mm.

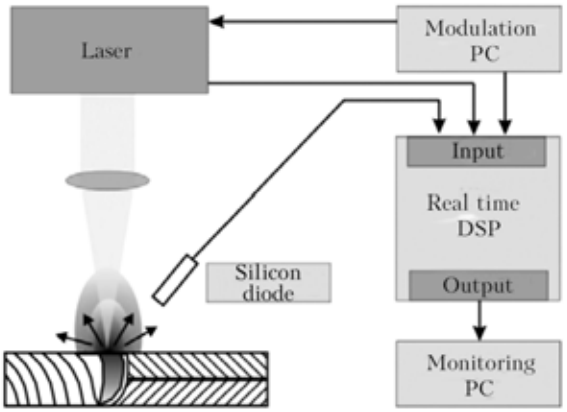

Figure 2. Schematic diagram of the experimental setup

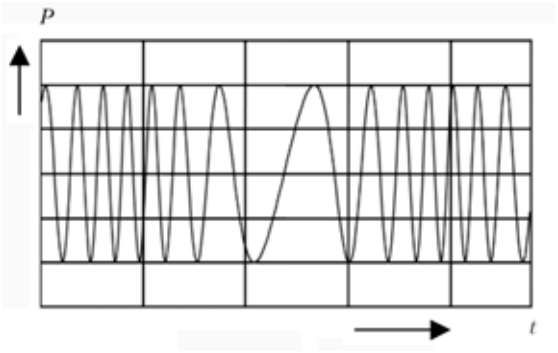

Figure 3. Exemplary waveform of the frequency modulation used to the laser output power control

The optical emissions of the welding process are detected by a silicon-photodiode with a spectral range from approximately 400 up to 1100 nm filtered by a band pass at 530 nm. The laser output power, the modulation signal and the process emissions are detected simultaneously with a sample rate of 50 kHz. The viewing angle from the photodiode is about 80°, oriented to the horizontal reference line.

In order to affect the keyhole oscillations, the laser output power is modulated around an average power P = 3.6 kW. As mode of modulation, a normal sinus curve is mostly chosen. To avoid resonance effects when modulating near the eigenfrequency of the keyhole dynamic over a longer period of time, the carrier frequency is changed by a frequency modulation. The carrier signal directly represents the current laser output power. By changing the frequency shift or the offset, for instance, the range of the laser output power can be defined. An exemplary modulation signal used in the experiments can be seen in Figure 3.

Results and discussion. With regard to avoiding failures during deep-penetration laser welding of zinc-coated steel sheets an important aspect is the existence of small pressure fluctuations of the keyhole in a certain frequency range. Welding results of non-contaminated sheets show that the welding depth, for example, is much more constant, the smaller the frequency range is where the fluctuations arise [1].

To describe this phenomenon some basic considerations are necessary, namely in deep-penetration laser welding complex physical processes superpose each other. A keyhole with an opening towards the laser beam is generated by the vaporizing material. It is surrounded by the pool which consists of liquid steel. The gaseous material flows towards the opening of the capillary causing a decrease of pressure within the keyhole. If a stable welding process is needed, this loss of pressure has to be compensated by continuously vaporizing new material. The equilibration of the vaporization–pressure, generated by the vaporizing steel, and the pool–pressure of the liquid steel keep the keyhole open. This balance of pressures is formed by the external pressure, consisting of the surface pressure p_{surf}, the hydrostatic pressure p_{hst} and the hydrodynamic pressure p_{hdn}, and the internal pressure, consisting of the ablation pressure p_{abl}, as well as the gas flow pressure p_{gas}. The interaction of these internal and external pressures leads to a specific dynamic of the keyhole. A FFT-analysis of the optical emissions during a non-modulated laser welding process of two zinc-coated steel sheets (overlap configuration, 100 μm gap) shows this characteristic eigenfrequency of the keyhole oscillation (Figure 4).

An imbalance of pressures inside and outside of the keyhole can occur by varying process parameters like varying zinc thickness or geometry (gap size), laser power and welding speed. When welding zinc-coated sheets an area of high pressure, vapour exists around the melt pool. If the gap between the sheets is narrow, the vapour cannot extend outwards, pressure fluctuations of the keyhole arise and failures are generated. The explosive degassing process disturbs the welding process and the keyhole collapses due to the disequilibrium of pressures (Figure 5). With expelling, a high amount of the liquid steel from the melt pool is carried away, causing cavities, spillings or pores within the weld seam. As a result the mechanical properties of the weld seam are directly af-

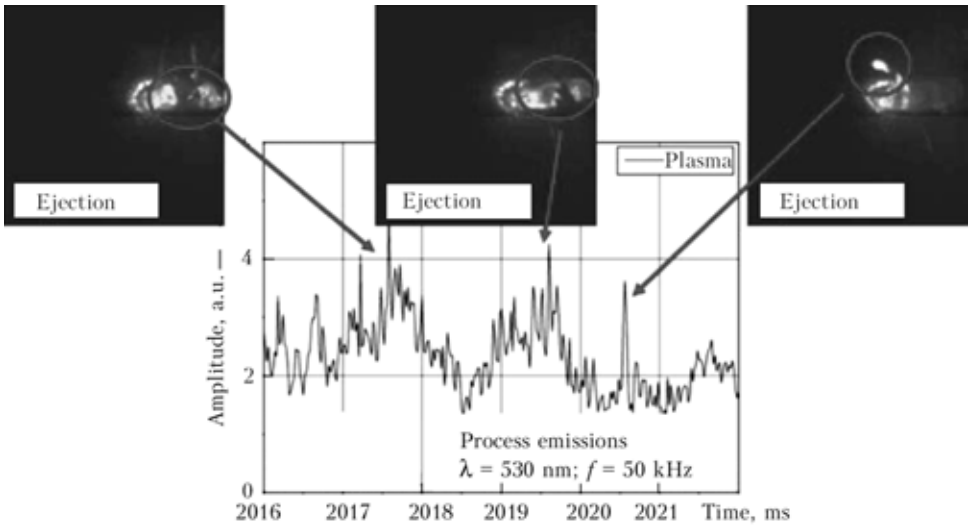

Figure 4. Time signal of optical emissions during CW-laser overlap welding of two zinc-coated steel sheets with thickness of 0.6 / 0.7 mm and zero-gap at P = 3600 W, v = 6 m / min, λ = 1030 nm, d_{spot} = 600 μm

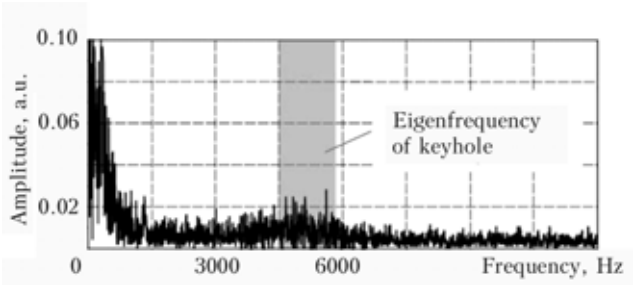

Figure 5. Frequency spectrum of CW-laser overlap welding of two zinc-coated steel sheets with thickness of 0.6 / 0.7 mm and 100 μm gap at P = 3600 W, v = 6 m / min, λ = 1030 nm, d_{spot} = 600 μm

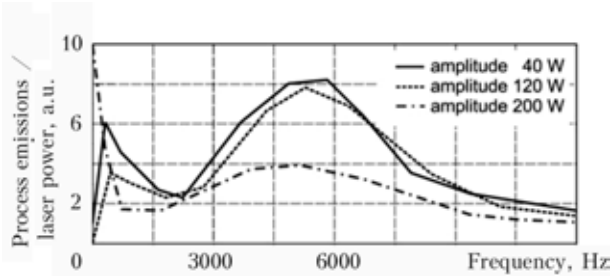

Figure 7. Transfer function for laser welding of zinc-coated steel sheets 0.6 / 0.7 mm thick at P = 3.6 kW, v = 6 m / min, d_{spot} = = 600 μm

fected in a negative way [2–7]. Furthermore the eigenfrequency of the keyhole is not detectable in this case and the whole welding process is instable.

It is the aim to define effective modulation parameters for positively influencing the welding process by an always opened keyhole. This demand is pursued if the frequency range of the power modulation is near the eigenfrequency of the keyhole dynamic. This is equitable if the peaks in frequency range of process emissions are in the same range as the frequency of power modulation. In experiments the attenuation of the process can be determined by calculating a transfer function with frequency information of process emissions and laser power.

During one welding process of at least 300 mm welding length the frequency of power modulation is changed between f = 0 and f = 10 kHz and the optical emissions as well as the modulation parameters are detected. This information allows the generation of the transfer function and the definition of useful modulation frequencies (Figure 6).

Figure 7 exemplary shows such a transfer function for a welding process under conditions described above. A low attenuation can be seen between 4.5 and 6.0 kHz. The necessary carrier frequency for the power modulation has to be in the same range.

Other facts about the modulation like modulation depth (amplitude) as well as the frequency shift and the velocity of frequency shift are not detectable. Last data have to be determined by further experimental investigations.

As can be seen in Figure 8, power modulation with a carrier frequency in the described range leads to an open keyhole during the whole welding process. Without modulation the size of the keyhole will be disturbed and collapses are detectable by high-speed pictures.

First welding results clarify a reduction of failures (cavities) when a power modulation is applied. Figure 9 presents the number of cavities at 300 mm long weld seams. The results prove that a reduction of failures is possible but still to the actual state of research no zero defect rate is reached.

An analysis of further results reveals that failures can also form behind the keyhole. A stable keyhole is thus only one step to minimize failures. Additional efforts have to be made to realize a second degassing possibility and to reach weld seams without defects.

On-line quality control for laser brazing. This part of the article deals with the development of an on-line monitoring system for laser brazing with high-power diode lasers which permits the on-line detection of failures like pores, holes, spilling and one-sided melting. Furthermore, this system is the basis of a closed-loop process control in order to abandon the expensive post-process quality controls.

A promising new approach for on-line process monitoring and control is the locally defined measurement of the temperature field of both joining partners. First tests have confirmed a correlation between temperature and seam quality. The temperature measurement via pyrometers turned out to be most advantageous (Figure 10).

A new on-line process monitoring and control system based on temperature measurement promises an enormous reduction of manufacturing costs for laser brazing. Thus, this process will become even more attractive for the automotive industry. With the assistance of a capable temperature measurement system

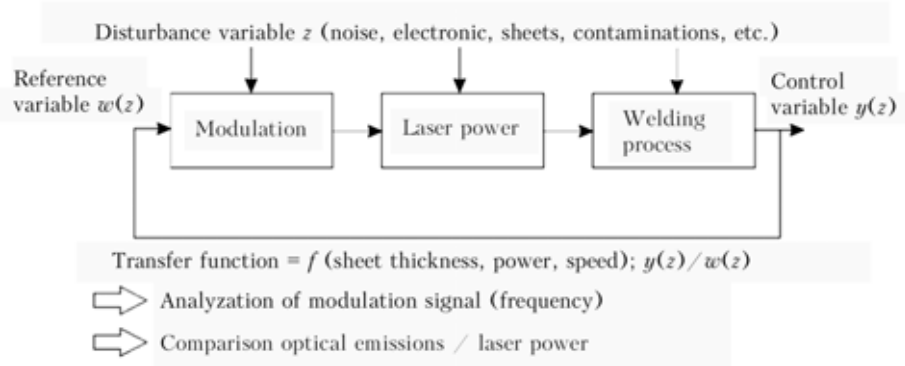

Figure 6. Model for determining transfer function and defining modulation parameters

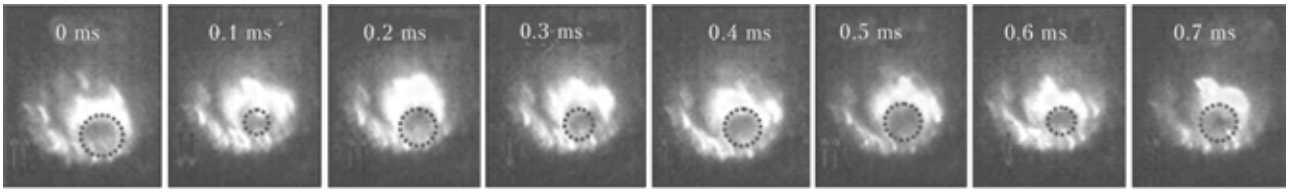

Figure 8. High-speed pictures of the keyhole in welding of sheets 0.6 / 0.7 mm thick with power modulation at P = 3.6 kW, $f_{carrier}$ = = 4.5 kHz, v = 6 m / min, d_{spot} = 600 μm

based on pyrometers, this project wants to detect failures in the seam so that these failures can be avoided in a closed-loop controlled process afterwards. This can be achieved by investigations in the measurement of temperature during the brazing process and integration of thermal detectors as to receive information about the effects of unadjusted temperature control on the brazing result. A further aim is the implementation of the temperature measurement into a brazing head with a wire feeding system for high-power diode lasers with best conditions of detection. Last but not least, the result will be a temperature-based robot- and laser-control.

Experimental setup. The research is realized on a laser brazing system, including a wire feeding device and a fiber-guided high-power diode laser with a maximum output power of 2.7 kW. Due to the optics which are integrated in the brazing head and the light conduction cable, the laser spot diameter at the end of the wire is 3.1 mm. The most important parts of the experimental setup are two integrated pyrometer optics which are connected by optical fibers to pyrometers. A two-color measurement technology is used

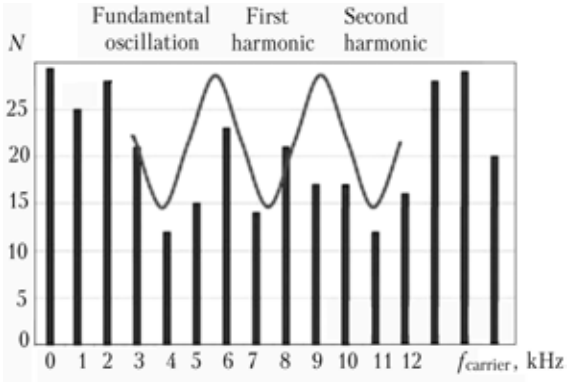

Figure 9. Number of cavities N at 300 mm weld long in relation to the carrier frequency of power modulation at P = 3.6 kW

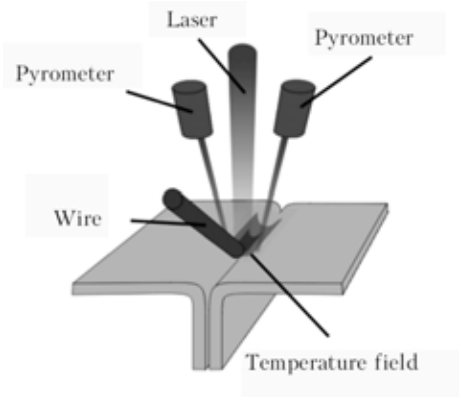

Figure 10. Principle setup of the process monitoring system

to be independent of the emission factor that detects temperatures between 500 and 1300 °C at wavelengths of 1.52 and 1.64 μm with a response time t_{90} of up to 2 ms. The measuring is carried out in mono-mode at ε = 0.8. Due to the process dynamics and the continuous change between molten and solid materials at the processing zone, it has to be considered that a proper identification of the emissivity and thus an absolute specification of the temperature is not possible. The diameters of the measuring spot can be adjusted between 1 and 5 mm.

The investigations are done on linear edge raised joints of DX 54 D + Z100 deep drawing steel sheets with a thickness of 0.8 mm, a typical thin sheet for automotive body parts. Brazing speed of 2.1 m / min and laser power of 2700 W have turned out to be ideal parameters in terms of surface quality of the seam and filling degree.

Results and discussion. Figure 11 shows some top views of intentional defective parts with linear edge raised joints. Starting from an ideal adjustment of the brazing head towards the joint (Figure 11, *a*) the lateral deviation of the path is constantly extended up to 0.3 mm (Figure 11, *b*). Afterwards the brazing head returns back to the ideal position in order to be moved out of this location again. Lateral misalignment in this time is up to 0.5 mm (Figure 11, *c*); at the end there is no intentional misalignment.

The two pictures with the lateral deviation indicate obvious melting of the lower steel sheets, whereas

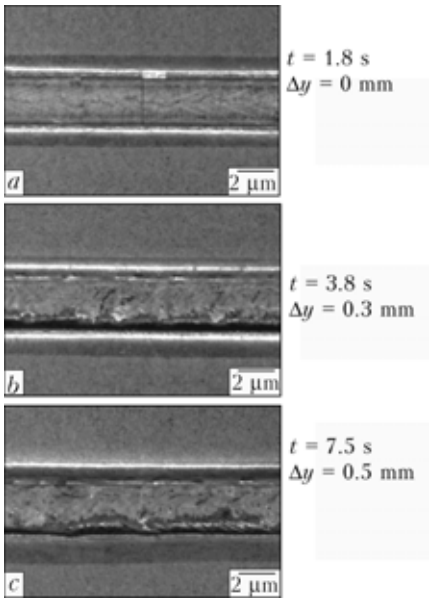

Figure 11. Top views of clear seam (*a*), lateral misalignment of 0.3 (*b*) and 0.5 (*c*) mm

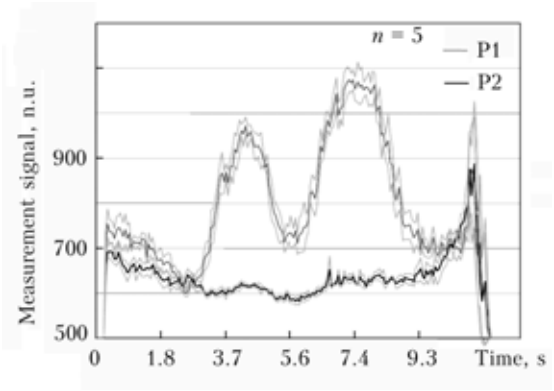

Figure 12. Signal sequence at lateral misalignments of 0.3 mm (3.8 s) and 0.5 mm (7.5 s)

the melting at the misalignment of 0.5 mm naturally exceeds the melting (see Figure 11, *b*).

With the help of the measurement system which is described above, signal sequences of these processes are acquired (Figure 12).

The sequence above clearly reveals the two misalignments. Furthermore, the two failures differ in their signal amplitude which can be traced back to the different deviation and melting respectively.

Intentional variations of the laser power can also be detected in the signal sequences. Both pyrometer signals increase at power variations ΔP = 700 W each at 3.7 and 7.6 s (Figure 13).

Consequently, the sensor signals allow a differentiation between types of failures and different intensity of the failures.

The results prove the possibility of an on-line quality monitoring system for laser brazing. The investigations of best condition for detection as well as first applications of the measurement system at intentional defective parts clearly show the existing potential.

The current steps of the project include the qualification of the measurement system for fillet joints and complex 3D seam geometries. In the future the

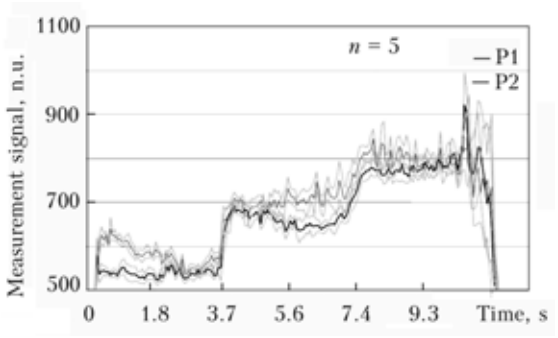

Figure 13. Signal sequence at variations of the laser power of 700 W

knowledge should be the basis for a temperature-based closed-loop process for brazing with high-power diode lasers.

Acknowledgment. This work has been funded by the BMBF — Project FM-LaB and the Stiftung Industrieforschung — Project Temperaturgeregeltes Laserstrahlhartloten mit Hochleistungsdiodenlaser. The authors wish to acknowledge for the support.

1. Otto, A. (1997) *Transiente Prozesse beim Laserstrahlschweissen*: Dissertation. Reihe Fertigungstechnik — Erlangen, Bd. 65, Bamberg, Meisenbach.
2. Geisel, M. (2002) *Prozesskontrolle und -steuerung beim Laserstrahlschweissen mit der nichtlinearen Methodik*: Dissertation. Reihe Fertigungstechnik — Erlangen, Bd. 123, Bamberg: Meisenbach.
3. Hohenstein, R., Otto, A., Geiger, M. (1998) Systemanalyse des dynamischen Verhaltens beim Laserstrahlschweissen. In: *Strahl-Stoff-Wechselwirkung bei der Laserbearbeitung 2*. Bremen: BIAS, 125–130.
4. Kaplan, A. (1994) *Modellrechnung und numerische Simulation von Absorption, Warmeleitung und Stromung des Laser-Tiefschweissens*: Dissertation. TU Wien.
5. Beck, M. (1996) *Modellierung des Lasertiefschweissens*. Stuttgart: Teubner.
6. Kroos, J. (1993) *Stabilitat und Dynamik der Dampfkapillare beim Schweissen von Metallen*: Dissertation. TU Braunschweig.
7. Klein, T. (1997) *Freie und erzwungene Schwingungen der Dampfkapillare beim Laserstrahlschweissen von Metallen*. Aachen: Shaker.

INFLUENCE OF PULSE SHAPE ON MODES OF LASER WELDING OF TITANIUM, STAINLESS STEEL AND ALUMINIUM ALLOYS

A. ALLAS[1], **A. KUDRYAVTSEV**[2], **M. MILENIKY**[2], **L. SAPRYKIN**[2] and **V. NOVOSADOV**[3]
[1]Center TRIZ «Tvorchestvo», Ltd., St.-Petersburg, Russia
[2]RMC «Lasers and Apparatus^{TM}», Zelenograd, Russia
[3]Moscow State University of Food, Russia

The equipment of RMC «Lasers and Apparatus^{TM}» has been employed during the researches on influence of energy, duration and shape of pulses of laser radiation on depth of formation of a weld on the samples executed from aluminium, stainless steel and titanium. To define the weld depth after welding wedge-shaped samples have been chosen. The purpose of research was definition of optimum welding modes with maintenance of the maximal depth of profusion. Two variants of welding were carried out, namely beyond threshold when spitting metal from welding zone occurs, and under threshold without spitting. Under threshold a mode provides the depth profusion of up to 3 mm on aluminium alloys and stainless steel, and up to 2 mm on titanium samples. The maximal profusion at minimal energy contribution in an pulse is observed in the case of use of the pulse shape of an isosceles triangle for all materials. It is the consequence of the achievement of the temperature maximum at the surface of samples in a welding zone at choice of the given shape of pulses.

Since 1970s the pulse laser welding equipment in microelectronics and instrument making for manufacture of medical equipment are widely used. Developed and serially delivered down to 1990 series of laser technological complexes «Kvant-10», «Kvant-12», «Kvant-15», «Kvant-16», «Kvant-17» and «Kvant-18» provided an opportunity of selection of technological welding modes with a variation of peak-time parameters, namely energy, duration and frequency of pulses. The shape of pulses did not vary because of design features of inductance-capacitor converters, and, as a rule, had the half-sine pulse shape.

The RMC «Lasers and Apparatus^{TM}», Moscow, has developed and serially manufacture modern universal welding equipment LTA-4 and ML4, providing an opportunity of programmable control of peak-time parameters of pulses of laser radiation, including the shape of pulses. Researches of influence of energy, duration and shape of pulses of laser radiation on depth of formation of a weld seam have been executed on the following samples: aluminium (alloys À Ì g-2, À Ì g-5, 1102 À Ì), stainless steel (10Kh18N10Ò) and titanium (VÒ1). For experiments the YAG:Nd laser-based complex ML4-2 was used (Figure 1).

Figure 1. Laser complex ML4-2: energy of pulses E = 8–50 J; duration of pulses t = 4–14 ms; frequency of pulses f = 2–15 Hz; welding speed v = 0.8–6.0 mm / s

Rectangular triangle samples (Figure 2) with the legs of 10 × 20 mm from aluminum, stainless steel and titanium 1.2 mm thick have been made. Two samples were preliminary imposed against each other and incorporated by laser spot welding on the corners. Welding was carried out lengthways longer leg. The shape of samples is chosen specially for simplification of the analysis of profusion depth after welding, without necessity make metallographic section.

The shape of pulses was as follows: rectangular, isosceles triangle, right-angled triangle with right-sided peak, and right-angled triangle with left-sided peak (Figure 3).

The purpose of research was definition of optimum welding modes with maintenance of the maximal depth of profusion.

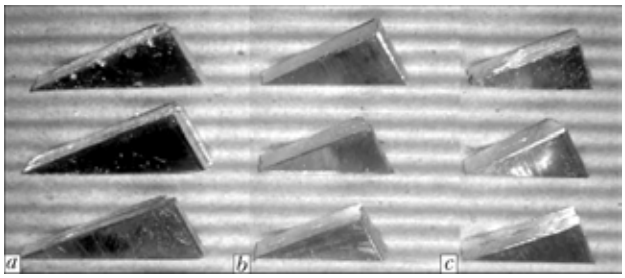

Figure 2. Aluminum (*a*), stainless steel (*b*) and titanium (*c*) samples

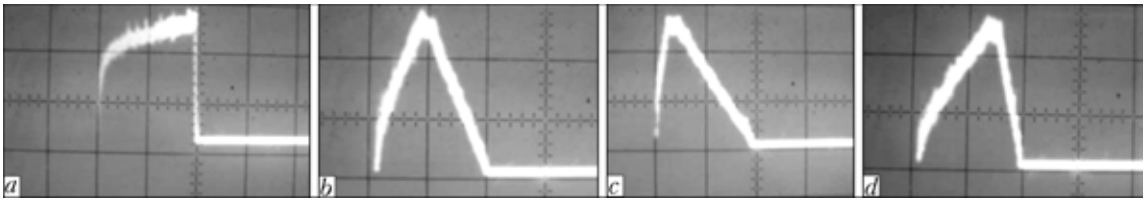

Figure 3. Oscillograms of pulse of rectangular (*a*), isosceles triangle (*b*), right-angled triangle with left-sided peak (*c*) and right-angled triangle with right-sided peak shape (*d*) at duration of 4, 8 and 12 ms

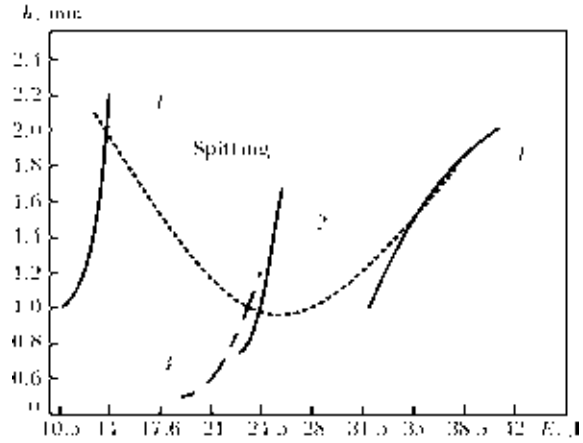

Figure 4. Dependence of profusion depth *h* on energy *E* of pulses with isosceles triangle shape of 4 (*1*), 12 (*2*) and 8 (*3*) ms duration and with rectangular shape of 14 ms duration (*4*) in welding of aluminium

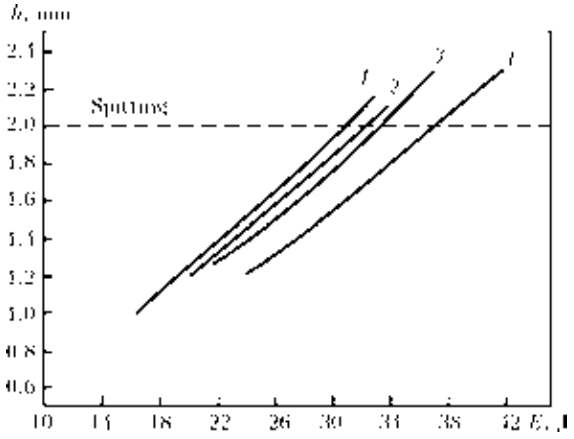

Figure 6. Dependence of profusion depth *h* on energy *E* of pulses with isosceles triangle shape of 12 (*1*) and 14 (*2*) ms duration and with rectangular shape of 12 (*3*) and 14 (*4*) ms duration in welding of titanium

Welding was carried out in two variants: level above threshold when spitting of metal from a weld pool occurs, and level below threshold without spitting of metal from a welding zone.

In above threshold mode, the maximal depth of welding on aluminium samples was up to 5 mm, on samples from stainless steel –– up to 3 mm, thus, on the surface of welded samples cavity with depth of up to 1 mm is formed. On titanium samples in above threshold mode burns through are observed.

Welding in the second variant (below threshold) provides the profusion depth of up to 3 mm on aluminium alloys, up to 2 mm on stainless steel and up to 1.75 mm on titanium samples.

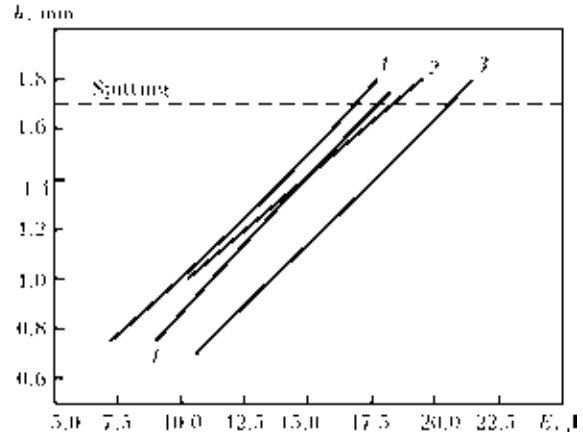

Figure 5. Dependence of profusion depth *h* on energy *E* of pulses with isosceles triangle shape of 12 (*1*) and 14 (*2*) ms duration and with rectangular shape of 14 (*3*) and 12 (*4*) ms duration in welding of stainless steel

It has been certain that the optimum shape of pulses for welding of investigated materials is the isosceles triangle.

Adjustable shape of pulses influences decrease in a threshold. At observation on the screen of the video-control device over processes of welding decrease in the threshold, allowing one to avoid formation of spitting of metal from a weld pool, at simultaneous formation of qualitative weld seams is observed at a choice of pulses in the shape of an isosceles triangle. It speaks smoother achievement of the maximal temperature a surface of samples in a welding zone at reduction of pressure vapor in weld pool [1]. Optimum duration of pulses of the triangular shape lays within the range of 4–6 ms for aluminium, 12–14 ms for stainless steel and 10–12 ms for titanium. Thus it is possible to receive deeper profusion (up to 30 %) at decrease in pulse energy (Figures 4–6), that is impor-

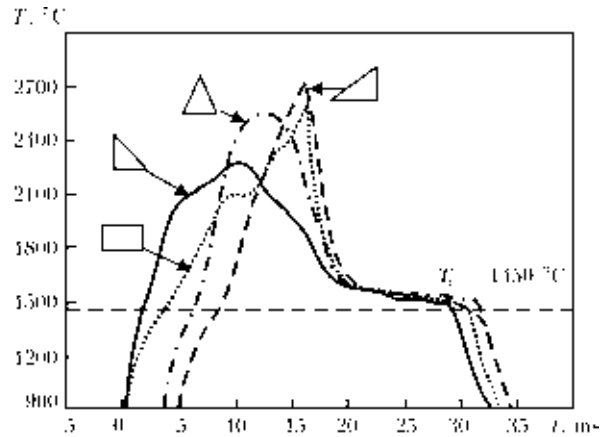

Figure 7. Temperature evolution for the laser pulses with different shape

tant for welding materials of small thickness. That proves to be true the calculations executed in work [2].

At research of dependence of welding zone temperature on the pulse shape, executed by colleagues from French university ENISE with use of a pyrometer, it is shown that the triangle shape with sharp forward front (Figure 7) provides smoother increase of temperature in a welding zone, decrease in the maximal temperature in a welding zone and increase in time from the beginning of melting before crystallization of melt. The shape of isosceles triangle provides rise in temperature in a welding zone at simultaneous reduction of time from the beginning of melting before crystallization of melt. Accordingly to the triangle shape with slowly grow up forward front provide the greatest temperature in the zone of welding and minimal time from the moment of melting before full crystallization of melt. The rectangular shape provides formation of a step on forward front and sharp peak with achievement of the maximal temperature similar to the previous variant. Thus, for a soft variant of heating with the minimal threshold it is possible to recommend pulses of the triangular shape with fast increasing forward front that is very important in welding of dispersion-strengthened alloys.

1. Smurov, I., Bertrand, Ph., Doubenskaia, V. (2006) Advanced pyrometry in industrial laser application. In: *Proc. of 4th Int. Conf. on Beam Technologies and Laser Application* (St.-Petersburg, Russia, Sept. 23–28, 2006), 36–41.
2. Grigoryants, A., Shiganov, I., Misyurov, A. (2006) *Technological processes of laser processing*. Moscow: N.E. Bauman MGTU, 394–395.

STRUCTURE AND MICROHARDNESS OF COATINGS OF HIGH-CHROMIUM CAST IRON POWDER IN HYBRID SPRAYING AND PLASMA SPRAYING WITH SUBSEQUENT LASER GLAZING

O.G. DEVOINO[1], M.A. KARDAPOLOVA[1], I.V. KRIVTSUN[2], Yu.S. BORISOV[2], V.D. SHELYAGIN[2], A.I. BUSHMA[2], V.Yu. KHASKIN[2], A.V. BERNATSKY[2], S.G. VOINAROVICH[2], A.N. KISLITSA[2] and **E.K. KUZMICH-YANCHUK[2]**

[1]Belarusian National Technical University, Minsk, Belarus

[2]E.O. Paton Electric Welding Institute of NASU, Kiev, Ukraine

Technological peculiarities of hybrid laser-plasma and plasma spraying with subsequent laser glazing of coatings of high-chromium cast iron powders, which are a by-product of spark erosion machining of cast billets, were investigated. As found as a result of the experiments conducted, the hybrid process enhances the thermal effect on particles of a spraying material. This leads to formation of the coating zone with a structure that features low porosity and high cohesion strength, which is characteristic of the glazed state. On the other hand, because of a large difference in sizes of the spraying powder particles, they have a wide range of trajectories. This results in overheating of some particles, causes their partial evaporation and, hence, loss of alloying elements. No such phenomenon was detected in laser glazing of preliminarily sprayed coatings. In general, the hybrid spraying process is more promising, although it requires both upgrading of procedures and optimization of hardware.

Basic requirements to wear-resistant coatings include high hardness and hardness to elasticity modulus ratio, minimal porosity and adhesion strength. Different types of cladding and thermal spraying are the most widespread technologies used to deposit protective wear-resistant coatings. All of them ensure a sufficiently good quality of the coatings, providing that the appropriate materials are used. Main drawbacks of cladding are cracking of an insufficiently heated workpiece, or undesirable thermal strains in volumetric heating of the workpiece, as well as the negative effect by fatigue on resistance of the substrate material [1]. Characteristic disadvantages of thermal spraying include porosity of the coatings and not always sufficient strength of adhesion to the substrate. These disadvantages can be eliminated by applying an additional heat treatment, e.g. laser glazing [2].

Scientists of the E.O. Paton Electric Welding Institute of the NAS of Ukraine offered the method for hybrid laser-plasma spraying of coating, which makes it possible to combine the processes of plasma and laser heating of a spraying material [3], as well as the processes of spraying and laser glazing of a coating. An integrated laser-arc indirect-action plasmatron was developed to implement this technology. Plasma is generated in this plasmatron using the special type of gas discharge, i.e. combined laser-arc discharge formed as a result of coaxial combination of the focused CO_2-laser beam and plasma arc burning in the inert gas flow (Figure 1). Preliminary investigations of technological capabilities of the integrated plasmatron show that such devices hold much promise both for spraying of different materials and for deposition of diamond and diamond-like coatings [4].

The purpose of this study was to investigate the possibility of using the hybrid laser-plasma technol-

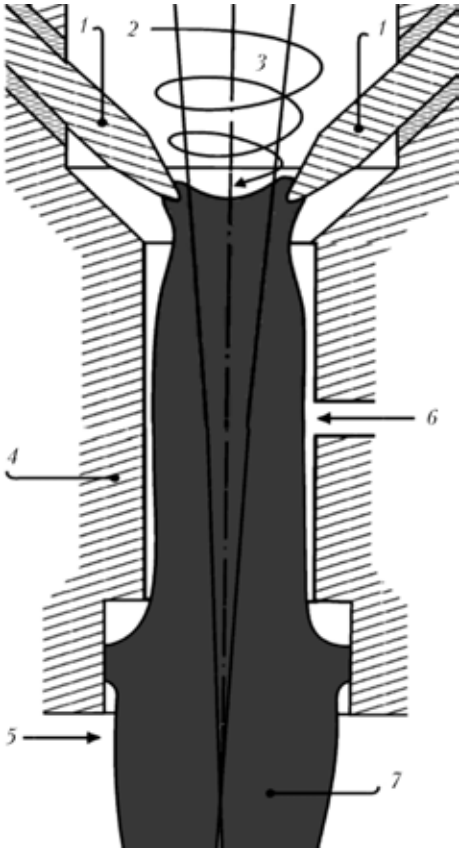

Figure 1. Basic diagram of integrated laser-arc plasmatron having an axisymmetric design: *1* — thermionic cathodes; *2* — inert plasma gas; *3* — focused laser beam; *4* — nozzle-anode; *5* — powder feeding; *6* — active gas; *7* — combined discharge plasma

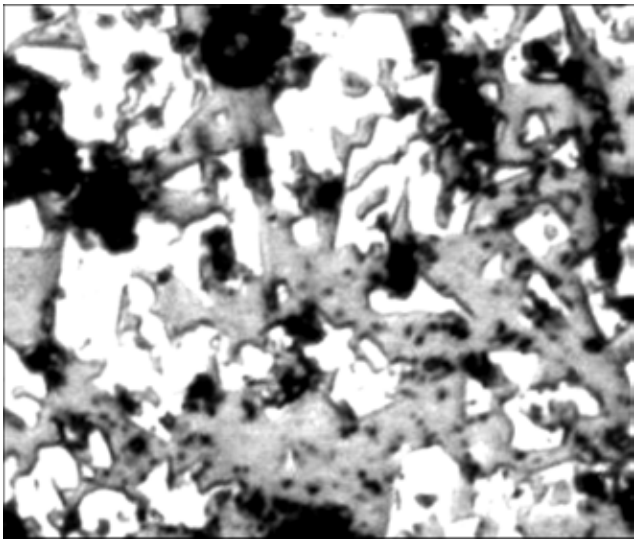

Figure 2. Remelted zone of coating in hybrid spraying

ogy for deposition of coatings from powders of high-chromium cast iron, and evaluate the effect of parameters of laser radiation on structure and properties of such coatings in hybrid spraying and in traditional plasma spraying followed by laser glazing.

Coating materials and parameters, experimental procedure. Powder of high-chromium cast iron of the IChKh28N2 grade, having particles 40–100 and 100–160 μm in size, was used as a spraying material. Chemistry of the powder was as follows, wt.%: 28 Cr; 2.5 C; 2 Ni; 1 Mn, and iron ––– base. The powder was a waste of spark erosion machining of cast billets, which determined the high degree of its oxidation. According to the preliminary investigations, iron oxides of different stoichiometric composition (Fe_2O_3 and Fe_3O_4) were localized mostly in the peripheral layers of powder particles. The oxide layer has low strength of adhesion to a particle, and can be partially removed in friction under an insignificant force effect. High prospects of applying this material are determined by its low cost, provided that a substantial source of raw materials is available, i.e. more than 1 t of wastes of the required particle sizes a year [5].

The UPU-3D unit with the PP-25 plasmatron was employed for spraying. Nitrogen was used as a plasma and transportation gas. The gas flow rate was 3 m^3 / h, arc current was 180–220 A, and voltage was 85–90 V.

The technological laser unit based on the CW laser Kometa-2, working with a mixture of CO_2, He and N_2 gases and generating radiation with a wavelength of 10.6 μm and power of 2 kW, was used to implement the laser glazing processes.

Hybrid spraying was performed using a special bench for laser-plasma spraying, which comprised an integrated laser-arc plasmatron of the axisymmetric design (see Figure 1), CO_2-laser [6] or ROFIN-SINAR diode-pumped Nd:YAG laser DY 044 with a power of up to 4.4 kW. The spraying conditions were as follows: 80 A discharge current; 48 V voltage; 0.7 m^3 / h gas (Ar) flow rate; 2 kW laser (Nd:YAG) radiation power; 500 mm lens focal distance; and 40 mm spraying distance (distance from exit section of the plasmatron to a specimen).

The use of the Nd:YAG laser with a wavelength of 1.06 mm made it possible to avoid the phenomena of absorption of laser radiation in the arc plasma and formation of the combined discharge, which took place in the case of using the CO_2-laser. This allowed implementation of such a flow diagram of the hybrid process where a coating was deposited by using only the arc plasma flow (jet), whereas the laser beam passing through the plasma jet provided additional heating of the spraying powder and then glazing of the coating.

Investigations of the resulting coatings were performed on polished transverse sections of the coated specimens after etching them in 4 % solution of nitric acid in ethyl alcohol. Structural examinations were conducted using the «Neophot-21» microscope at magnifications of ×200 to ×500. Microhardness was investigated using the MPT-3 meter by a standard procedure under a load on the indenter equal to 50 and 100 g.

Results and discussions. *Hybrid laser-plasma spraying*. Analysis of the experimental results shows that an important role in hybrid spraying is played by such a process parameter as the ratio of spraying spot diameter d_s to laser beam diameter d_l on the workpiece surface. For the selected spraying parameters the d_l / d_s ratio was about 0.25. In this case, structure of the coating in a section normal to the treatment direction from axis of the beam to the periphery can be subdivided into the following characteristic zones: first, coating that experienced complete remelting; second, sprayed coating with signs of sintering of the particles; and, third, sprayed coating.

First zone (Figure 2) subjected to the direct impact by the laser beam is formed as a result of the processes similar to those occurring in laser glazing or deposition of coatings. The only difference lies in an additional thermal effect by the beam on the particles, it affected as early as during their movement in the plasma jet. This zone is characterized by high hardness ––– from 10 to 17.5 GPa. The content of the hardening phase, i.e. light regions in the photo (see Figure 2), is 30–40 %, and it is distributed over the surface of the section sufficiently uniformly. Microhardness of these regions is 16–17.5 GPa. This structure is formed in rapid solidification of the material from the liquid state in complete remelting, which is characteristic of the process of laser grazing of coatings with a high content of boron and carbon [7]. The average value of microhardness is 12 GPa. The quantity of pores and their sizes are insignificant. The developed surface of contact of the coating and substrate is indicative of a high adhesion strength.

To provide a uniform quality layer corresponding to first zone, it is necessary to optimize parameters of the coating process. Excessive power of laser radiation at the center of the treatment spot leads to a complete

burnout of the material and formation of a recess along the axis of the laser path. This phenomenon occurs at a rated radiation power of more than 2 kW and diameter of the spot on the specimen surface equal to less than 5 mm. It is very likely that full evaporation of particles, especially of a small size, takes place as early as during their stay in the plasma jet under the simultaneous effect by laser radiation. This is confirmed by the fact that the above regions characterized by high hardness and precipitation of the hardening phase are shifted with respect to the beam axis and located near the boundary of second zone.

Second zone, i.e. the region of which is shown in Figure 3, features a uncharacteristically low porosity of the sprayed coatings and developed surface of contact both between the particles in a coating and between the coating and substrate. This structure is indicative of a high cohesion strength and increased strength of adhesion between the coating and substrate. Besides, whereas structure at the coating–substrate interface looks like the glazed one, closer to the surface it becomes more similar to the sprayed one. Distribution of microhardness through thickness of a coating is chaotic. The maximal values of 7–11 GPa were fixed in individual white (non-etchable) regions corresponding to the initial structure of wear-resistant cast iron with a substantial content of the hardening phases. These regions correspond to the internal volumes of the particles unaffected by the environment during the spraying process.

The major part of second zone is characterized by a microhardness value ranging from 2.5 to 7 GPa (in etched regions with different tints of grey color). The presence of these regions is attributable to an intensive burnout of alloying elements in the subsurface layers of the particles under the effect of laser radiation during the spraying process. This results in decrease in the content of the hardening phases and lowering of the degree of alloying of the metal matrix of a coating. The size of second zone is 0.4–0.6 of diameter of the spraying spot.

All the above coating zones are characterized by the presence of a slightly defined HAZ in the substrate material, which is revealed by microdurometry analysis. Its thickness is 0.7–1.0 of that of the coating, within which a decrease in microhardness was fixed with distance deep into a specimen. Most probably, its formation is caused by low-intensity hardening processes, which do not lead to changes in sizes of grains in metal.

Improvement of structure of second zone, compared with third zone (see Figure 3), is attributable to a number of factors. The main of them seems to be dissipation of the thermal effect of the laser beam over the heat-conducting substrate and coating, which enhances thermal activation of contact surfaces between the coating and substrate. Moreover, an additional melting and intensive diffusion interaction at interfaces take place between the particles in the coating. These phenomena are evidenced by a change in

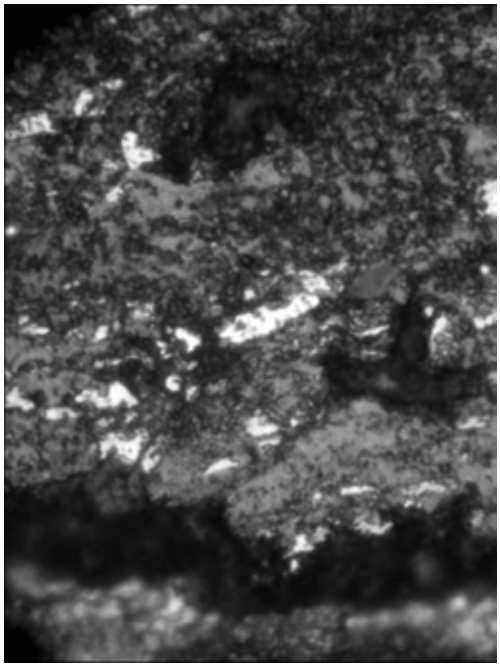

Figure 3. Coating zone with signs of sintering of particles (×250)

structure of the coating from the glazed to sprayed one with increase in distance from the substrate surface. This is explained by the fact that thermal conductivity of the coating is always lower because of a large number of interfaces between the particles, compared with a solid material.

In addition, because of design peculiarities of the plasmatron employed, the particle velocity vector during the spraying process is directed not normal to the surface treated (and, hence, offset to the laser beam), but with a certain deviation. Therefore, some quantity of the powder particles is not directly affected by laser radiation. Most of them fly through the laser beam, thus acquiring an extra thermal energy. However, they have time to leave its ranges before they fall onto the substrate surface. Increase in temperature of such particles, compared with the traditional process of plasma spraying, can also be considered a cause of formation of second zone.

Increase in power of laser radiation in hybrid spraying leads to changes in sizes and some decrease in microhardness, causing no qualitative changes in structure. It is second zone that increases in the main, and a region of the burnt out material expands in the place of first zone. At a power of 3 kW, the average value of microhardness of second zone decreases to 3.5 GPa, compared with 4.5 at a laser power of 2 kW. This phenomenon is attributable to a more intensive burnout of alloying elements in a particle with increase in power of laser radiation. Decrease in hardness of second zone with decrease in consumption of the powder occurs for the similar reasons, but to a lesser degree. The consumption of the powder is proportional to the flow rate of a transportation gas and, hence, velocity of the particles being transferred. As the axis of the laser beam and path of the particles in the plasma flow intersect, decrease in the velocity of the particles leads to increase in the time of the

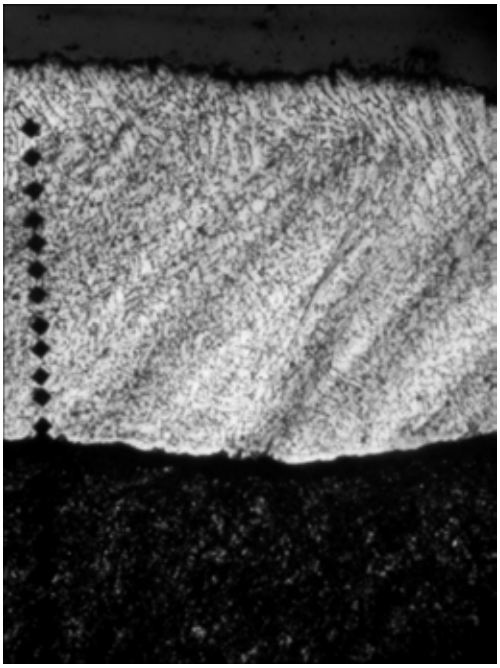

Figure 4. Transverse section of coating produced by plasma spraying and subsequent laser glazing (×125)

effect on them by laser radiation and burnout of alloying elements.

Plasma spraying with subsequent laser glazing. Plasma spraying followed by laser glazing is a process that proved advantageous for many composite materials. However, it was applied for the first time to deposit coatings based on high-chromium cast iron. In this case the goals of laser glazing were to achieve a high coating to substrate adhesion strength and decrease porosity of a coating.

Glazing of the coatings of pure cast iron IChKh28N2 resulted in formation of a classic structure: white (non-etchable) remelted coating layer and slightly defined HAZ in the substrate material (Figure 4). The glazed coating is almost pore-free, the coating to substrate contact surface is well-developed, and flowing of the coating material into the pores on the substrate surface takes place. The latter is indicative of complete penetration of the coating without melting of the substrate. HAZ is characterized by

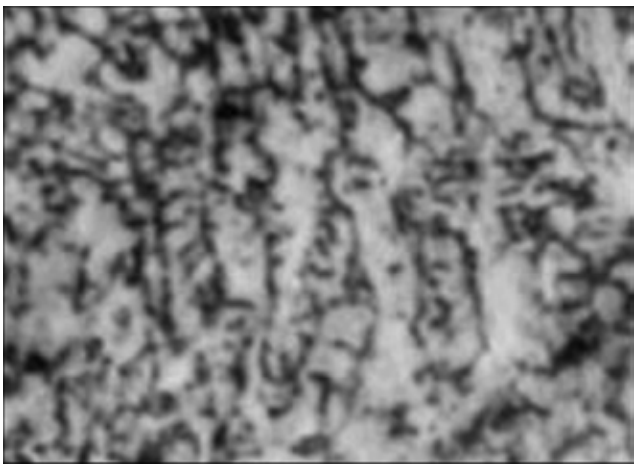

Figure 5. Sub-surface layer of transverse section of coating produced by plasma spraying and subsequent laser glazing (×500)

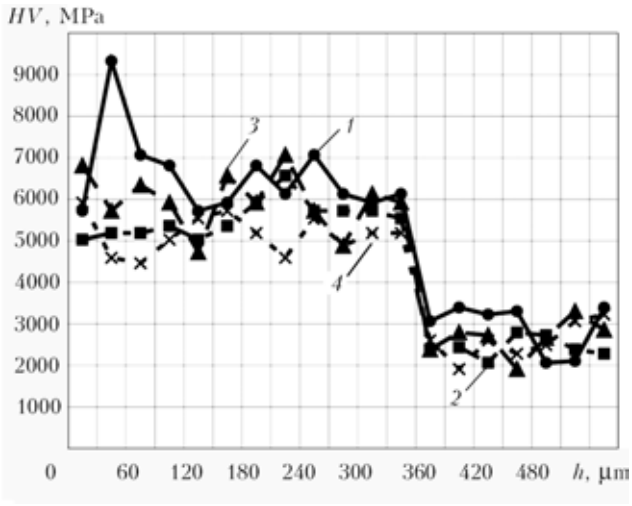

Figure 6. Distribution of microhardness HV through thickness of coatings h at D_{max} = 5 (*1*, *2*) and 3 (*3*, *4*) mm, v_{max} = 250 (*1*, *3*) and v_{min} = 120 (*2*, *4*) mm / min

insignificant decrease in grain size compared with the initial material.

The remelted layer, a characteristic region of which is shown in Figure 5, has a slightly defined dendritic structure mostly with axes of the first order. Dendrites grow in size with distance from the substrate surface, which evidences growth of the temperature gradient with increase in thickness of the coating during solidification. Comparison of the coating structure with results of microdurometry analysis suggests that coatings consist of the meta-stable metal matrix oversaturated with alloying elements, as well as the redundant hard phases precipitated along the dendrite boundaries.

As shown by the comprehensive investigations conducted, variations in glazing parameters have a substantial effect on microhardness of the coatings. Experimental variables were not only the power of radiation, but also the speed of a relative movement of the workpiece and laser beam, as well as the diameter of the latter. Decrease in the movement speed and beam diameter results in a marked deterioration of microgeometry of the coating surface. Increase in the thermal effect causes a clearly defined recess along axis of the beam path, the coating material is partially burnt out and partially forced out from the path center to the periphery. Decrease in the speed of the laser beam from 250 to 120 mm / min, like decrease in its diameter, leads to a 10–15 % decrease in the average value of microhardness, whereas in the case of a simultaneous decrease in the beam speed and diameter, decrease in the average value of microhardness is more than 18 %. Like in the case of hybrid spraying, this can be explained by a more intensive burnout of the hardening carbide phase with increase in power density during treatment.

Figure 6 shows profiles of distribution of microhardness through thickness of the coatings for the above glazing conditions. The coatings produced under conditions with a less intensive thermal effect are characterized by a lower homogeneity and presence

of a large amount of hard inclusions. In this case, hardness of the HAZ hardly differs from that of the initial specimen material, whereas under the glazing conditions with an increased specific thermal energy it markedly decreases.

CONCLUSION

Plasma spraying followed by laser glazing provides quality pore-free coatings with a uniform structure. Their microhardness depends upon the laser treatment parameters, and increases with growth of the speed and diameter of the laser beam on the workpiece surface, amounting on the average to 6.5–7 GPa at a treatment speed of 250 mm / min, laser beam diameter of 5 mm and power of 2 kW. These parameters are optimal for formation of the coatings sprayed from dispersed wastes of electric spark machining of high-chromium cast iron. Hybrid laser-plasma spraying is a promising technology, which is capable of providing high physical-mechanical properties of the coatings due to the intensive energy (heat) effect on the spraying material both during the spraying process and after its deposition on the substrate. To raise efficiency of the hybrid process, especially in deposition of coatings from iron-base materials, it is necessary both to improve design of the integrated plasmatron and to optimize the spraying process parameters, in particular the d_l / d_s ratio and control of distribution of energy across the section of the laser beam. These process parameters should be selected on the basis of thermal-physical properties of spraying materials. The zone of a sprayed coating with signs of sintering of the particles is formed at the periphery of the remelted region due to dissipation of the laser beam thermal effect over the heat-conducting substrate and coating. This phenomenon implies the possibility of improvement of the hybrid technologies for formation of coatings using different concentrated energy sources.

1. (1974) *Technology for electric fusion welding of metals and alloys*. Ed. by B.E. Paton. Moscow: Mashinostroenie.
2. Borisov, Yu.S., Kharlamov, Yu.A., Sidorenko, S.L. et al. (1987) *Thermal spray coatings of powder materials*: Refer. Book. Kiev: Naukova Dumka.
3. Bushma, A.I., Krivtsun, I.V. (2004) Modelling of laser, plasma and combined heating of fine-dispersed ceramic particles. In: *Proc. of 3rd Int. Conf. on Computational Modelling and Simulation of Materials* (Acireale, Sicily, Italy, 2004), Part B, 409–416.
4. Borisov, Yu., Bushma, A., Fomakin, A. et al. (2005) Integrated laser-arc plasmatron for laser-plasma spraying and CVD processes. In: *Proc. of 2nd Int. Conf. on Laser Technologies in Welding and Materials Processing* (Katsiveli, Crimea, Ukraine, 2005), 57–59.
5. Yaroshevich, V.K., Kardapolova, M.A., Avsievich, A.M. et al. (2005) Prospects of application of dispersed high-chromium cast iron wastes for reconditioning and hardening of parts. In: *Rep. Transact. on Engineering*, Issue 21, Vol. 1. Minsk: BNTU, 346–350.
6. Garashchuk, V.P., Shelyagin, V.D., Nazarenko, O.K. et al. (1997) Technological 10 kW CO_2-laser LT 104. *Avtomatich. Svarka*, **1**, 36–39.
7. Grigoriants, A.G., Safonov, A.N. (1987) *Laser equipment and technology*: Manual for High Educational Institutions. Book 3: Methods for surface laser treatment. Moscow: Vysshaya Shkola.

LASER SINTERING OF COMPOSITES USING THE ENERGY OF ULTRASONIC OSCILLATIONS

V.V. DZHEMELINSKY, L.F. GOLOVKO, O. GONCHARUK and **O. KAGLYAK**
National Technical University of Ukraine «KPI», Kiev, Ukraine

Laser sintering of composites is an efficient tool of making parts with complicated spatial configuration or their components with given physical and mechanical properties. This method develops by leaps and bounds all the time broadening the range of its applications in industry. The core element of this process is a liquid-phase sintering that lies in laser melting of one of the components of the selected material composition, further re-crystallization and melt cooling. The crystallized melt, given there exist a reasonable wetting, grabs firmly and binds solid particles of the composition, which undergone partial melting or no melting at all. Taking into account the high rate of thermal processes, it was noted that diffusion could not play dominant role. Nevertheless, deep investigation showed that there are evidences of 2D mass transfer from liquid phase to solid one and vice versa. These processes could be intensified by additional application of ultrasonic oscillations. This leads to a significant increase in composite quality (structure uniformity, absence of microcracks, porosity, etc.) and to the simplification of technological process. The present paper is dedicated to the investigation of the basic laws and peculiarities of laser sintering under the influence of ultrasonic oscillations.

It is known that a lot of composite materials based on metallic matrixes (Fe, Al, Ni, Co) with embedded particles of carbides, borides, nitrides, oxides or super-hard materials (diamonds), which do not dissolve in matrix, have high resistance and are widely used in modern technologies and for tools manufacturing in particular.

The lesser these particles and distances between them, the better they block dislocations, thus improving resistance and rigidity of composites.

It was found that main reasons for softening of composites are damage and cracks of grains that appear at the initial stage of composite formation.

Combined methods, for example CW or pulsed laser radiation coupled with high-frequency oscillations, should guarantee efficient distribution of particles, plasto-elastic deformation of medium, lessening macro- and microinhomogeneity of structures. Efficiency of ultrasonic oscillations at various applications is proved by the majority of research projects and practical experience. Ultrasonic oscillations can intensify different processes that appear on the interface of materials (during welding, gluing etc.). It is used for the dimensional processing of hard brittle materials like ceramics, glass, semiconductors and precious metals, which impossible to process by other means. Ultrasonic oscillations intensify (up to 1000 times) processes in liquid and liquid-disperse phases (crystallization, cleaning, degassing, dissolution) and production of new highly disperse structures.

In given work the new perspectives of the use of ultrasonic oscillations along with laser radiation for the tools manufacturing on basis of cubic boron nitride are shown, technological schemes are investigated and possible methods of manufacturing are considered. The influence of ultrasonic pulses on the composite formation and processing conditions were investigated as well.

Experimental methods and procedures. The goal of the given research is to develop techniques of tools manufacturing from super-hard materials using the energy of ultrasonic oscillations.

There are no references in literature about rational implementation of ultrasonic oscillations for laser sintering. As well as there is no experimental data on the influence of ultrasonic energy on the composite structure formed during high-speed thermal processes.

Cavitations, acoustic currents, ultrasonic capillary effect, that occur in liquids and melts, are used for emulsion production, surface cleaning, alloying, metallization, quality increase etc.

The crucial point of combined processes is the effects that appear during the crystallization of a metal. Ultrasonic fields of high intensity introduced into the melt pool create special conditions for the start of crystallization process. Among them are acoustic currents, radiation pressure, cavitations and forces of viscous tension. Figure 1 shows the scheme of powerful ultrasonic field impact on the metal being crystallized [1].

According to [2–8] the influence of ultrasonic oscillations leads to the following changes in material structure: lessening of grains dimensions, formation of uniform grains, increase of materials homogeneity, prevents the development of liquation processes even redistribution of non-metallic impurities and inclusions in the base material. But the list of these processes is not complete and it does not take into account some peculiarities of the crystallization processes that occur due to ultrasonic oscillations. Sometimes, the columnar structure of crystals thickens, and at some specific values some crystals increase in size. Ultrasonic oscillations modify the dendritic structure of the base metal. Therefore, when we change the microstructure of the metal we change its physical prop-

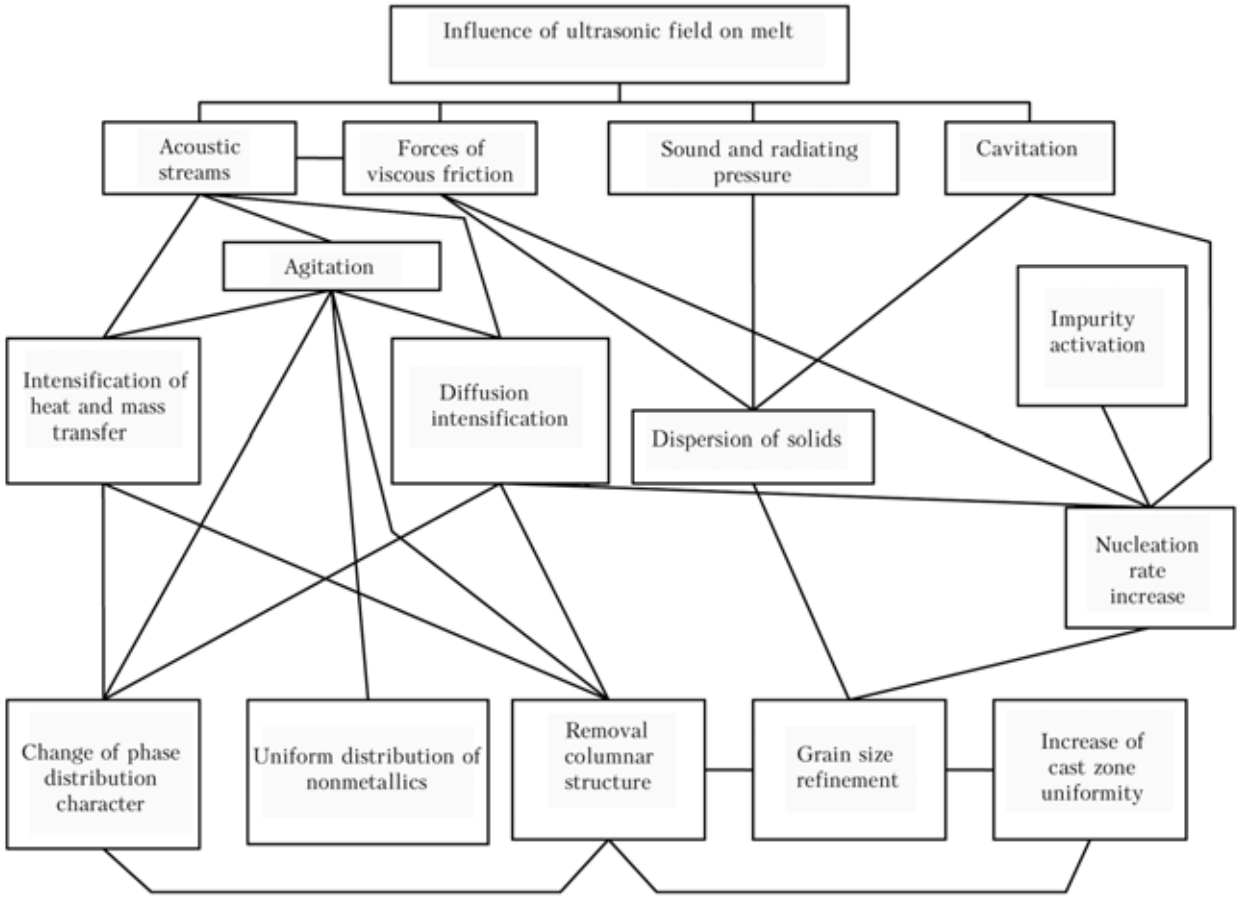

Figure 1. Scheme of influence of powerful ultrasonic field on crystallizing silicon melt

erties. For instance, strength characteristics and plasticity of the material could be increased.

It is known [9] that the pressure of up to 1 Ì Pa in the compression wave caused by ultrasonic oscillations leads to overcooling of up to $(3–5)\cdot10^{-2}$ K of the material during crystallization. Thus, we may conclude that main influential factors during ultrasonic processing of liquid metals are cavitations and acoustic waves leaded to closing of cavitation caverns and occurrence of microwaves which, in turn, granulate crystals and form new «growth» centers for non-metallic inclusions. Powders from cubic boron nitride with particle size of 250 / 200, 200 / 160 μm were used in the experiment as an example of these non-dissolving active particles. Acoustic waves stir and disperse crystals during the crystallization.

The efficiency of laser sintering process combined with high-frequency oscillations, its stability and quality of processing greatly depends on the choice of material for waveguide of magnetostrictor and technological scheme of the processing.

In automatic welding some fluxing agents, ceramics and copper moving inlets introduced ultrasonic oscillations into weld pool through the contact with molten metal, are used. Application of these materials for the manufacturing of these inlets would allow one to control and to manage ultrasonic oscillations, for other thermo-insulating materials are bad conductors of sound.

The main parameters that influence the quality and efficiency of hardening and calibration of a specimen surface pressure and force deforming stylus are the contacts with material, oscillations amplitude and travel speed of the deforming stilus. Ultrasonic hardening at a frequencies of 20 kHz with an amplitude increase from 5 to 30 μm leads to the surface hardness increase from 10 to 125 %.

There are two schemes of laser sintering for the tools manufacturing: application of ultrasonic pulses to the tool body, and application of ultrasonic pulses to the melt pool after the laser beam. It is also possible to apply ultrasonic pulses before laser beam to tighten the composite layer before sintering.

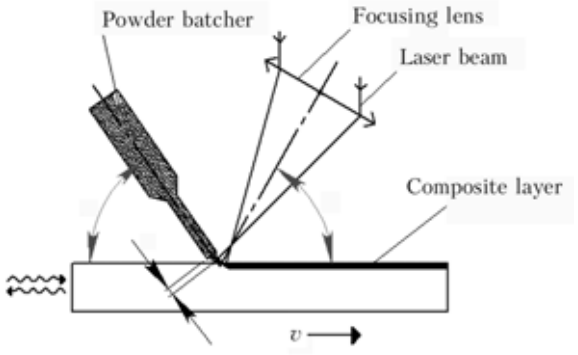

Figure 2. Scheme of imposing UHV at laser sintering beforehand bricketed layer

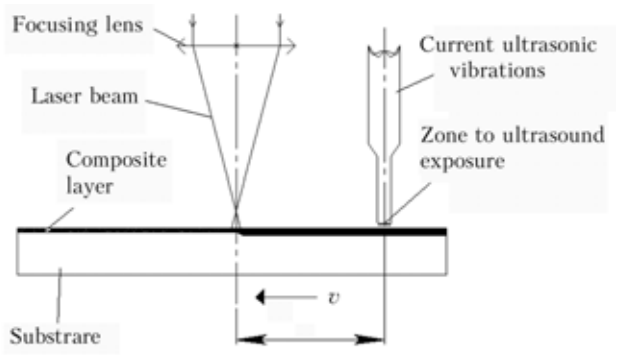

Figure 3. Scheme of imposing UHV in a trace to laser radiation

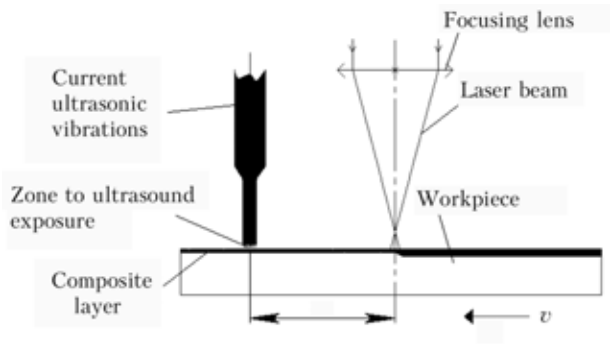

Figure 4. Scheme of imposing UHV together with laser radiation

The following materials were used: bed ---- steel 3, steel 45, steel U8; composite ---- cubic boron nitride KP 250 / 200; binder Br010; powder Cu + Sn.

To increase the productivity and quality of laser sintering of composites the focal plane was deepened at a given depth, the powder was supplied through the dispenser and laser beam was inclined at a given angle. The powder is pre-heated with help of laser beam, enters into the zone of direct laser heating and is alloyed to the metallic bed. Quality of the composite could be increased by modifying the parameters of laser sintering and parameters of ultrasonic oscillations. Schemes of the processes are given in Figures 2–4.

Figure 3 shows the scheme of ultrasonic oscillation imposition on melt pool at a given distance from the irradiated surface. This would result into the refinement of an alloyed material and would create a «cold working» effect on the surface irradiated by laser beam. The liquation effects could be avoided as well. Moreover, one could achieve a uniform distribution of chemical elements in the working zone. Introduction of ultrasonic fluctuations before the laser processing zone would lower the porosity of the generated layer and would redistribute grains in the binder. The major drawback is that this scheme is applicable only for small areas. This scheme could be also used for surface cleaning and preparation.

Although ultrasonic oscillations are widely used in foundry industry to manufacture castings and also for workpiece processing, the combined influence of laser and ultrasonic fluctuations is not investigated. We strongly believe that this combined technology has a bright future, especially its application for tools manufacturing. The benefits of laser processing technology (high speed heating, non-contact processing) and ultrasonic oscillations might open new horizons for its implementation in micro- and nanoprocessing.

CONCLUSION

Possible schemes of laser processing assisted by ultrasonic fluctuations were presented. The main parameters of the process were obtained and investigated. Possible schemes for obtaining qualitative specimens are discussed.

1. Pàrkhimîvich, E.M. (1988) *Welding and deposition in ultrasonic field*. Ì insk: Nauka i Tekhnika, 207.
2. Àbràmîv, Î.V. (1972) *Crystallization of metals in ultrasonic field*. Ì oscow.
3. Såvårdånêî, V.P., Klubîvich, V.V., Stepanenko, À.V. (1973) *Processing of metals by pressure with ultrasound*. Ì insk.
4. Silin, L.L., Balandin, G.F., Êîgàn, Ì.G. (1962) *Ultrasonic welding*. Ì oscow.
5. Kulemin, À.V. (1978) *Ultrasound and diffusion in metals*. Ì oscow.
6. Dànilov, V.I. (1956) *Structure and crystallization of liquid*. Kiåv.
7. Polotsky, I.G. et al. (1957) Action of fluctuations of sound and ultrasonic frequency on process of crystallization of metals. In: *Proc. of All-Union Conf. on Use of Ultrasonic Equipment in Industry*. Ì oscow, 12–14.
8. Russo, V.L. (1958) Research of influence of elastic fluctuations of various frequencies on crystallization of weld pool. In: *Welding*. Leningrad, 3–15.
9. Chàumårs, B. (1968) *Theory of hardening*. Ì oscow: Metallurgiya, 288.

OPPORTUNITIES FOR THIN DISCS RIGIDITY MANAGEMENT BY MEANS OF LASER HEATING OF DISCRETE SURFACE ZONES

L. GOLOVKO[1], S. LUKYANENKO[1], RAHMANI MOHSEN[1], V. SOROSHENKO[2], A. KRASAVIN[1], A. LUTAY[1] and V. BORKOVSKI[1]

[1]National Technical University of Ukraine «KPI», Kiev, Ukraine
[2]Institute for Super Hard Materials of NASU, Kiev, Ukraine

The results of theoretical investigation of sheet metal mode of deformation at different loading schemes are given in this paper. Means of control of deformation mode are analyzed. Results of the influence of laser beam radiation and its parameters on the magnitude and character of residual stresses distribution in various structural materials are submitted. Some aspects of thermal and structure-phase states of the irradiated areas are explained in detail. Finally, possible technological schemes of laser processing of metal sheets and experimental results are considered.

Application of sheet metal for the wide range of manufacturing processes leads to significant economy of material and power resources due to minimization of weight and dimensions of the products, labor input and manufacturing costs. It is the most convenient way to manufacture different housings and frames of machinery components, spacecraft antennas, bearing frames of metal-cutting tools. The expansion of application area is restricted by the rigidity limitations.

It is well known that rigidity is a property of a structure or its elements to withstand external loads in terms of deformation, i.e. changes in dimensions and shape. At a given loads the deformations should not exceed given limiting values and are set according to the requirements to a given structure.

Nowadays, there are numerous ways to increase the rigidity of thin metal parts. First of all, there are constructive methods based on the connection between geometrical parameters of a part with its rigidity. One can increase the rigidity by forming closed cavities, ribbed stiffeners, borders, etc. The main drawback of these methods is an increase of mass characteristics of the part, as well as geometrical parameters. To avoid these limitations the parts are made of composite materials with modular grains and fibers. This measure can partially solve the problem of rigidity. On the other hand, the price of these parts increases significantly.

Laser heating can create in metal materials local zones with structures, hardness and tension that significantly differ from the ones of the base material.

Dimensions, shape and spatial distribution of these zones could be easily controlled by changing the laser beam travel path and heating parameters. If one knows how the properties of the irradiated regions and workload tensions change it is possible to influence the rigidity of the given part. In other words, it is possible to create metallurgical webbings with help of laser irradiation.

The main goal of the given direction of research is to create residual stresses on strictly defined areas of sheet metal, which are equal but opposite in sign to maximum elastic stresses that appear due to the impact of workloads during the exploitation of the given component. This way of influence on a strained state of the material, depending on a priority, would increase the component rigidity or the magnitude of safe loads and would decrease the material capacity of the product. To implement this idea it is suggested to create purposefully required residual stresses by means of local laser heating of the most strained areas that might change the chemical compound of a material as well.

To perform this idea it is necessary to create necessary residual stresses in the most stressed areas of the specimen by local laser heating along with changes of its chemical properties. It is possible to control the value, sign and distribution of residual stresses by altering of the irradiation regimes (pulsed or CW modes, power distribution, irradiation time and pulse frequency), locations of heating zones, materials (with structure changes at heating or not).

Combined methods may lead to even better results (ultrasonic oscillation, heating and deformation, etc).

Part of this work was previously published in [1, 2] and the present study shows some results regarding the opportunities to control modes of deformation of thin discs by creation of temperature fields of necessary configurations.

Mathematical modeling of disc modes of deformations. Modeling of the modes of deformation of a steel disc at various loading conditions were conducted with help of MSC Nastran software.

2D and later 3D models were generated (Figure 1). It was supposed that a thin disc was made of chromium steel (1.3 % Ñ, 1.0 % Cr) 0.5 mm thick and 200 mm in diameter, and rigidly attached to a shaft with the diameter of 30 mm with a rotational moment $\grave{I}$. Modulus of elasticity $\mathring{A}$, shear modulus

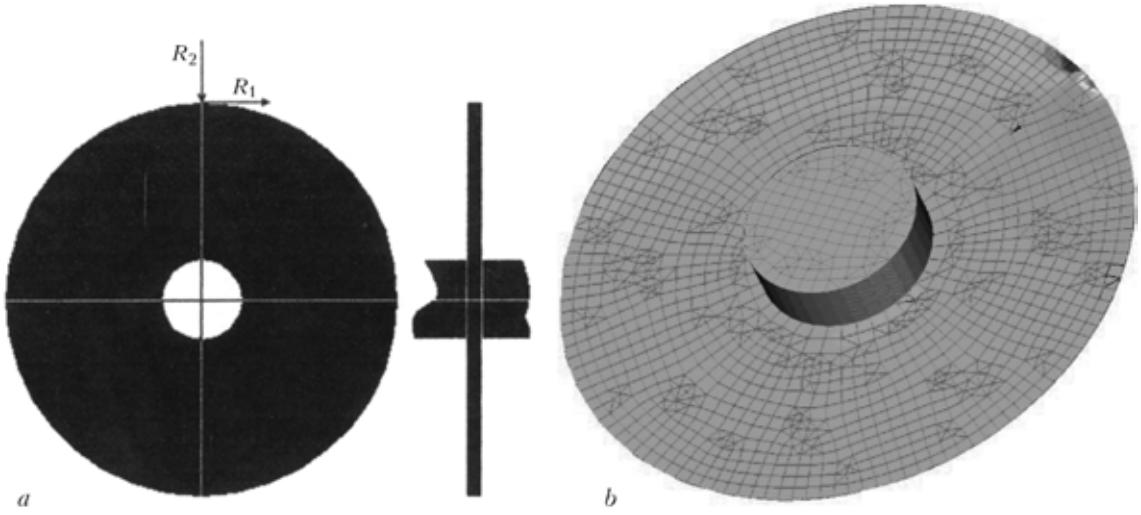

Figure 1. Disc computational scheme (*a*) and computational mesh (*b*)

G, Poisson ratio μ, material density ρ were taken as for mild steel. Stresses that correspond to yield strength at tension, shrinking and shearing were treated as boundary values.

The FEM standard elements were used for the areas which are under consideration, corresponding boundary conditions were set, as well as work load conditions.

While rotating disc interacts with work material it suffers from radial and tangential reactions R_1 and R_2. Their ratio may vary in a wide range. The calculations were conducted at the most common ratios R_1:R_2 (Table). The direction of forces is shown also in Figure 1. The distribution of normal, tangential and maximum stresses was calculated for different planes.

Experimental setup, equipment and research methods. Experimental investigation was conducted with the help of industrial laser system based on Ñ Î $_2$-laser «Comet-2» (wavelength λ = 10.6 μm, beam power Ð = 1.5 kW, beam mode is ÒÅ Ì $_{20}$, beam exit diameter *d* = 42 mm). Focusing lens is made of KCl, and its focal distance is *F* = 300 mm. Beam power was controlled continuously with a specially designed power meter which grabs 1 % of laser irradiation (accuracy of 2 %). Beam analyser LBA from ALL GmbH was also used to measure power distribution in the focal plane and to determine the actual beam diameter.

Carbon steel (1 % Ñ) and alloyed steels 95Kh and V2F were used in the experiments. Specimens 1 mm thick were irradiated at following regimes: focused beam diameter d_0 = 5 mm, beam power *P* = 1 kW, beam velocities *v* = 0.5, 1.0, 1.5, 2.0 and 2.5 m / min.

The irradiated samples were cut in halves with help of electric discharge sawing machine in a direction perpendicular to the direction of laser beam movement (across the grooves) and in the axial direction. A metallographic sample was done according to the standard methods from one of the halves. The microstructure was visualized with a 3 % spirit solution of nitric acid.

The studies of microstructure of hardened surface layers were conducted with help of microscopes ММÐ-2Ð and «Neophot 23». These microscopes were coupled with digital camera connected to a PC unit. The hardness of the microstructures after laser heating were done with help of hardness gage PMT-3 and an indenter load of 100 g.

Influence of load conditions on stress distribution in a disc. Analysis of computational results has shown that various by sign, direction and value stresses are formed when the external load is applied. In the area which is close to the point of load application there exist normal shearing stresses, whereas in the peripheral regions tension stresses occur (Figure 2, *à* and *b*). Configuration of its distribution significantly depends on the ratio between radial and tangential components of the load. If the radial component is too big the shearing stresses are located

Ratio of common loads

No	Tangential load R_1, N	Radial load R_2, N	No	Tangential load R_1, N	Radial load R_2, N
1	20	10	8	260	220
2	80	50	9	270	320
3	100	110	10	280	420
4	110	130	11	100	420
5	170	140	12	80	200
6	170	170	13	100	250
7	180	210	14	300	100

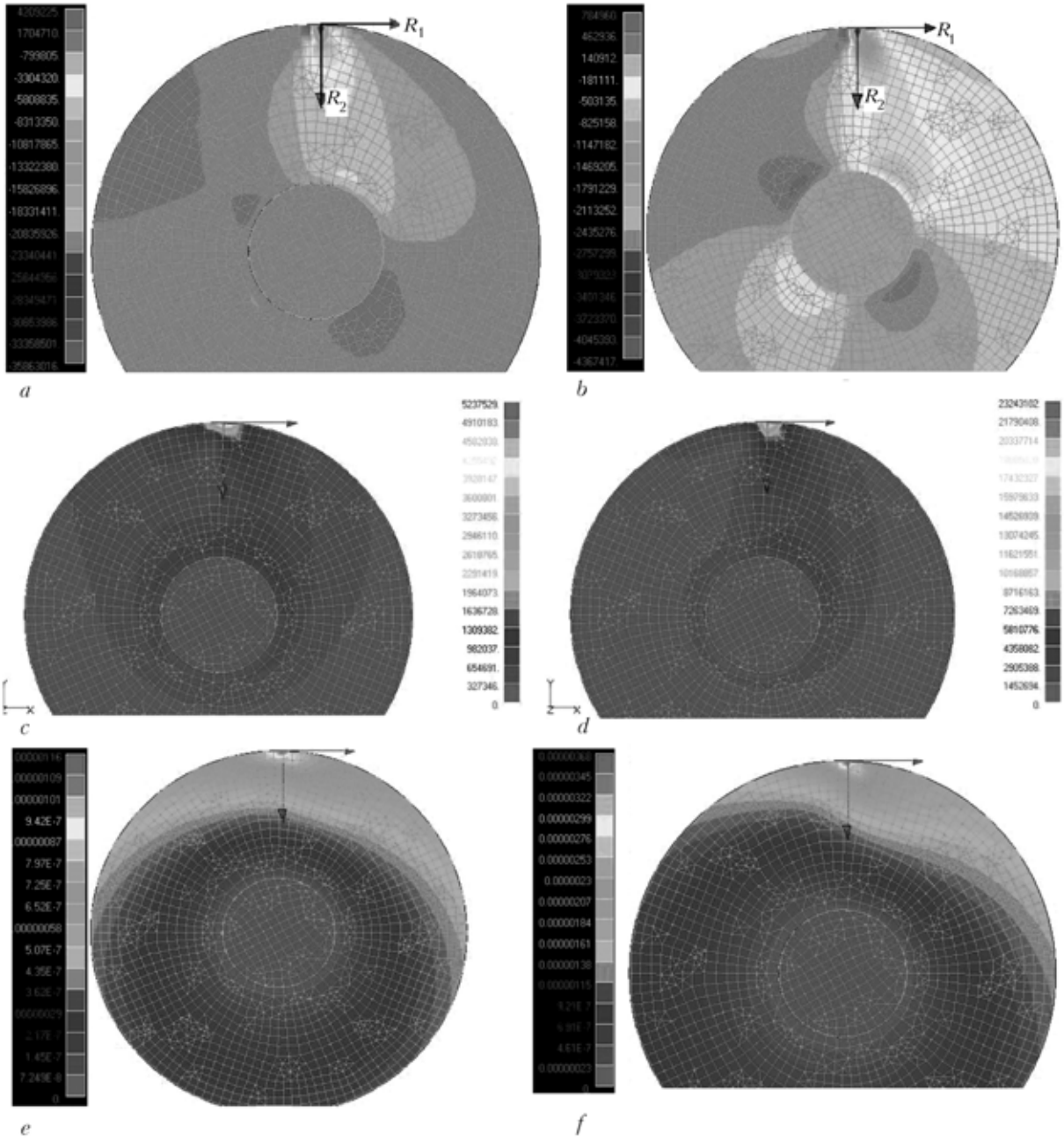

Figure 2. Distribution of normal (*à, b*), tangential (*c, d*) stresses and deformations (*e, f*) in a disc at load ratio R_2:R_1 = 50:10 (*a, c, e*) and 80:20 (*b, d, f*)

close to the radius (see Figure 2, *à*). If the tangential component is too big the trajectory of normal shearing stresses bends in the direction opposite to the direction of disc rotation (see Figure 2, *b*). This tendency is very straightforward. Therefore, the stressed state if the disc and its deformations could be predicted in case the load value is given.

Having the extreme values of deformations it is possible to establish critical load values. These values would determine the disc rigidity. It is possible to increase the values of critical loads by forming the opposite residual stresses in a disc volume. This task could be solved with help of local laser heating.

Depending on the chemical composition of the steel, initial structure state and irradiation regimes, it is possible to form tension and shearing stresses with help of laser heating [1]. Due to the locality of the laser heating process it is possible to get their various distributions along the disc surface.

Peculiarities of structure-phase transformations at laser heating of thin steel discs. The steel V2F in the annealed state consists of granulated pearlite and remnants of carbide grid.

Figure 3, *à* shows the area of laser heating of the VF2 steel thin plate 1 mm thick. Laser prosessing regimes were as follows: $Ð$ =1 kW, d_0 = 4.5 mm, v = = 0.5 m / min. This area could be divided into several layers. In the first layer, where the temperature exceeded critical point A_c, the carbides were fully dissolved. Layer structure contents retained austenite with small part of martensite (Figure 3, *b*). Layer hardness was 7500 Ì Pa. In the second layer, the

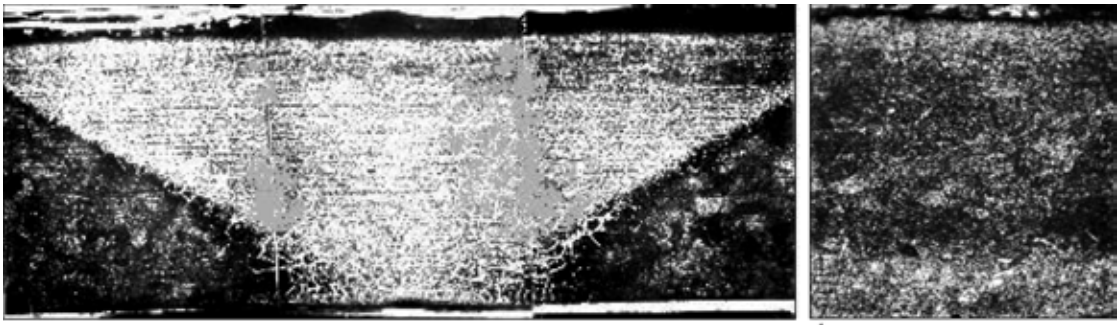

a *b*

Figure 3. Area of laser heating (*a* — ×75) and structure of thin plate 1 mm thick of steel V2F (*b* — ×400) processed at *Ð* = 1 kW, d_0 = 4.5 mm, *v* = 0.5 (*à*) and 1.0 (*b*) m / min

values of heating temperatures were close to optimal tempering temperatures for the given steel and the values of cooling velocities were high enough to enable the formation of martensite. The carbide grid was crumbled and highly-dispersed carbides were formed. Layer hardness was 7500 Ì Pa.

If we move further into the surface it is possible to observe the underhardened zones that include martensite, retained austenite and small carbide particles.

Contrary to the processing of massive part, in our case the intermediate zone has fuzzy borders. Layer structure contents troostite with martensite inclusions.

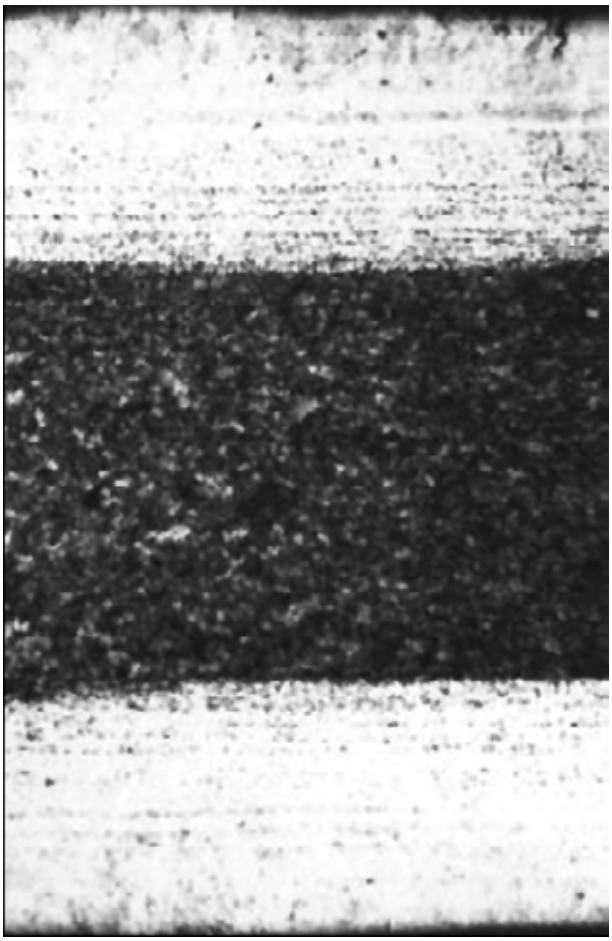

Figure 4. Appearance of thin steel plate (1 % Ñ) hardened from both sides at *P* = 1 kW, d_0 = 5 mm, *v* = 2 m / min

As Figure 1 shows, the areas with changed microstructure are very uneven. It means that stresses would be uneven as well and would lead to disc deformation. The shearing stresses formed by the martensite transformations would be located close to the disc surface. The disc would have to change its shape to dome-shaped in the direction opposite to that of beam propagation. There are two ways to avoid these undesired effects.

The first method lies in laser irradiation of those areas on the opposite sides of disc plate (Figure 4).

To avoid the disc deformations due to the locality of the laser influence it is necessary to process the disc in «locked» state (between two matrices), as shown in Figure 5. The disc is positioned in matrix and is fixed with another matrix which has grooves to enable laser heating of the disc.

After processing, the matrices with disc are turned upside-down and laser processing starts again. The disc is released later from matrix but only upon completion of laser processing procedure. The tensions are counterbalanced along the volume of the disc and, consequently, deformations are eliminated.

There is another way to control tension state of discs. By changing the irradiation parameters it is possible to form the hardened layer with thickness equal to the thickness of the plate and with cross-section equal to the rectangular one. Since the borders of hardened layer coincide with the tempering temperature isotherms it is necessary to determine the irradiation regimes where isotherms would have the necessary shape (Figure 6).

In order to determine this conditions a mathematical modeling of thin disc laser heating processes were conducted.

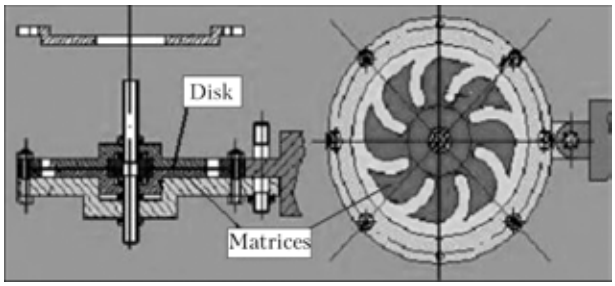

Figure 5. Tool for the double-sided laser processing of disc in «locked» state

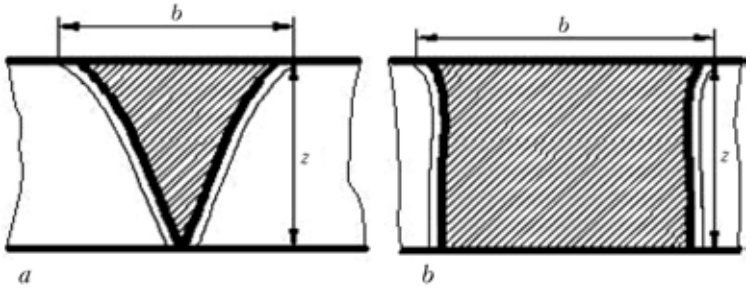

Figure 6. Real (*à*) and desired (*b*) distribution of tempering isotherms in the disc

Mathematical modeling of thermal state of thin discs at laser heating. Laser beam with the intensity q moves along the surface of metal plate with dimensions L_x, L_y, L_z in the direction of the $0Y$ axis with the given velocity V (Figure 7).

The laser beam travel path corresponds to the most common distribution of elastic stresses as shown in Figure 8.

As a model of laser heating process there was used a heat conductivity equation with appropriate initial and boundary conditions:

$$c\rho \frac{\partial U}{\partial t} = \lambda \left(\frac{\partial^2 U}{\partial x^2} + \frac{\partial^2 U}{\partial y^2} + \frac{\partial^2 U}{\partial z^2} \right),$$

$$x \in [0, L_x],\ y \in [0, L_y],\ z \in [0, L_z],\ t \in [0, K_k].$$

Initial conditions:

$$U(x, y, z, 0) = U_{\text{in}}.$$

Boundary conditions:

- on the surface of laser beam influence

$$\lambda \frac{\partial U(x, y, 0, t)}{\partial z} + q(x, y, t) = 0;$$

$$q(x, y, t) = q_{\max}(x', y') e^{-5 \frac{(x - x_c)^2 + (y - y_c)^2}{r^2}};$$

$$x_c = \frac{L_x}{2};\quad y_c = Vt;$$

- out of zone of laser beam influence

$$\lambda \frac{\partial U(x, y, 0, t)}{\partial z} + \alpha[U(x, y, 0, t) - U_c] = 0;$$

- other surfaces of computational domain

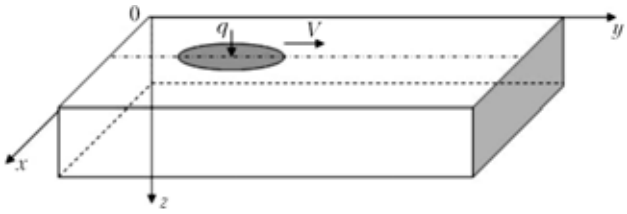

Figure 7. Computational scheme of laser heating of thin plate

$$\lambda \frac{\partial U(x, y, L_z, t)}{\partial z} + \alpha[U(x, y, L_z, t) - U_c] = 0;$$

$$\lambda \frac{\partial U(x, y, z, t)}{\partial x} + \alpha[U_c - U(0, y, z, t)] = 0;$$

$$\lambda \frac{\partial U(L_x, y, z, t)}{\partial x} + \alpha[U(L_x, y, z, t) - U_c] = 0;$$

$$\lambda \frac{\partial U(x, 0, z, t)}{\partial y} + \alpha[U_c - U(x, 0, z, t)] = 0;$$

$$\lambda \frac{\partial U(x, L_y, z, t)}{\partial y} + \alpha[U(x, L_y, z, t) - U_c] = 0.$$

A finite difference method with adaptive mesh was used to solve the system of equations. Moreover, the mesh changed with every time step and thickened in the zones with high gradients.

Laser beam is modeled as a light package consisting of equal and uneven intensity distribution. Figures 9 and 10 represent the above mentioned distributions (tempering isotherms).

As the results show, with the even distribution of laser beam power (see Figure 9), the isotherms of the temperature that leads to structure-phase changes are limited in the area that has an uneven width along the plate thickness (see Figure 3). At an identical

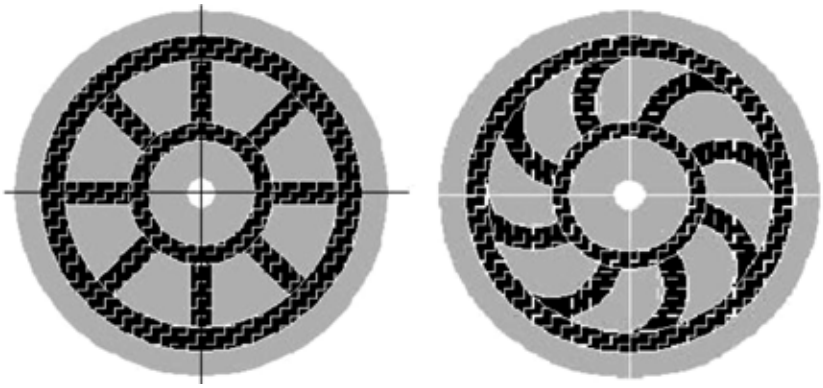

Figure 8. Laser heating paths

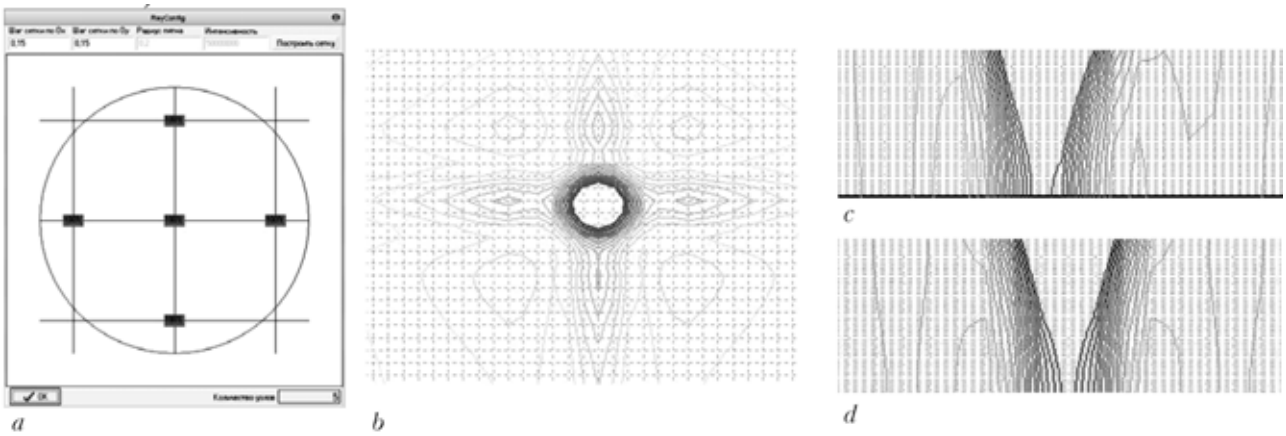

Figure 9. Laser power distribution in the heating zone (*à*) and temperature distribution in the planes $X0Y$ (*b*), $Y0Z$ (*c*) and $X0Z$ (*d*)

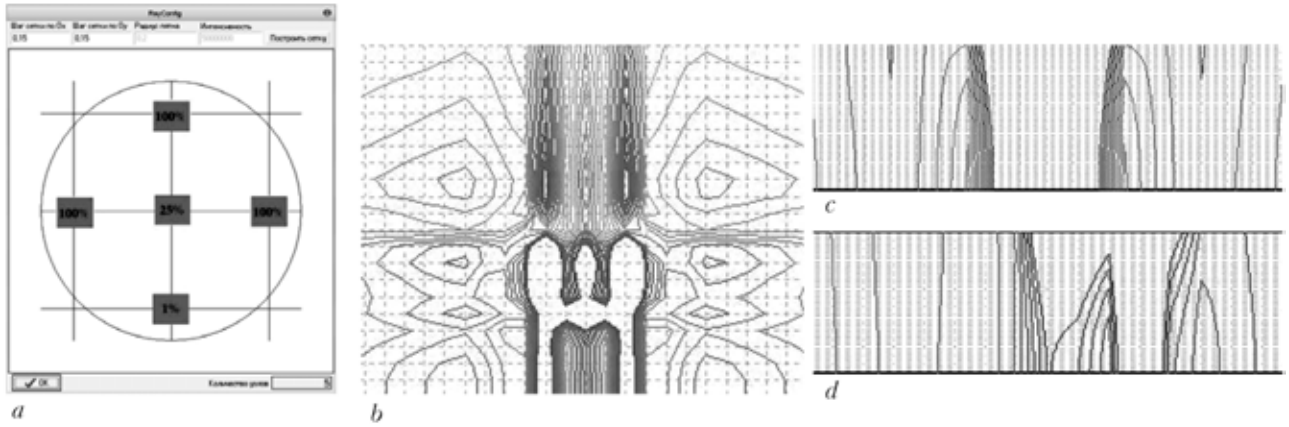

Figure 10. Laser power distribution in the heating zone (*à*) and temperature distribution in the planes $X0Y$ (*b*), $Y0Z$ (*c*) and $X0Z$ (*d*)

irradiation regimes (processing velocity, focal spot diameter, beam power) but at uneven distribution of laser beam power in the focusing spot along the heating zone (100 % I along the focusing spot edges, 25 % I in the spot centre and 1 % I in the tail part) (see Figure 10), the isotherms change its configuration and limit the area of structure-phase changes down to the rectangular area.

It means that with the opportunity to manage the laser power in the focal spot it is possible to form locked-up stresses which are evenly distributed along the plate thickness.

CONCLUSIONS

1. Modeling of modes of deformation is an efficient tool to determine means of rigidity increase and efficiency of material performance.

2. Since laser zone of influence is very small, it allows managing the value, direction and configuration of residual stresses and increasing the rigidity of specimen significantly.

3. Control over the distribution of laser irradiation leads to changes in configuration of isotherms and to control the stress conditions.

4. Use of adaptive meshing methods and increase of the efficiency of computational results significantly reduces computational time. Moreover, the accuracy of the results could be pre-defined and increased by using dense meshing in the zones with high temperature gradients.

1. (2001) *LIA Handbook of Laser Materials Processing*. Orlando: LIA, 249–258.
2. Kovalenko, V.S., Golovko, L.F., Chernenko, V.S. (1991) *Hardening and alloying of machinery by laser beam*. Kiev: Technika.

LAWS OF LASER RADIATION ABSORPTION WITH BIOLOGICAL BODIES

L. GOLOVKO, V. ROMAN, Z. KANSO and **H. SALAVATI**
National Technical University of Ukraine «KPI», Kiev, Ukraine

In the report results of experimental studying of processes of absorption and dispersion of laser radiation with 1.06 mm wavelength by biological fibers are presented. Researches were carried out on specially developed technological complex on basis of the 100 W solid-state Nd:YAG laser with wavelength of 1.06 μm. The complex is equipped with the necessary measuring instrumentation for control of parameters of laser beam (capacity, spatial distribution of intensity), fiber system for radiation transportation on the basis of the 0.9 mm diameter quartz fiber, and special focusing systems allowed receiving various distributions of intensity of radiation. The original technique of measurement of depth of penetration and dispersion of laser radiation in muscular tissue, liver and potatoes fibers is offered, and practically realized values of its optical parameters (factors of absorption and dispersion) are determined. It is established that depth of penetration of laser radiation with the 1.06 mm wavelength changes over a wide range depending on kind and structure of biotissue. For a muscular tissue it achieves 30–45 mm, 20 mm for a liver tissue and less than 20 mm for other tissues. It is shown that its value after achievement of the certain size does not depend on time and intensity of irradiation. Laws of change of a spatial configuration of zone of penetration and dispersion of laser radiation are discussed depending on characteristics of beam falling on biotissue, its kind and structure.

Creation of local superficial and volumetric temperature fields with certain shape, predefined position of temperature maximum inside the biological body, are of interest of medicine, veterinary, biotechnology and plant growing. Due to ability of non-invasive bringing of the certain portion of energy into the local area of the body, laser radiation is applicable for realization of mentioned above task. Its realization requires knowledge of laws of laser radiation interaction with organic bodies.

Many works are dedicated to studying of optical characteristics of biologic bodies. Never the less, their results have significant difference. The reason is imperfection of analysis methods. The only one common conclusion of researchers is that the most deep penetration has laser radiation with the wavelength equal to 1.06 mm.

The areas of this research are development of effective way of determination of optical properties of biological body irradiated with the laser beam, mathematical modeling of temperature processes which taking place during laser heating of biological tissues in the temperature range 37–60 °C and ways of temperature distribution control.

Experimental setup and methodology. Experimental studying of laser radiation absorption within biotissue was carried out with test bench (Figure 1). It consists of Nd:YAG laser LTN-102 (beam diameter 6 mm, power 1–125 W), power measuring device, optical properties analyzers (Figure 2) and thermocouples (Figure 3).

Intensity of laser radiation inside the body was measured in two directions, namely parallel and perpendicular to the laser beam propagation with fiber optical cables (quartz, diameter 0.8 mm) and photodiodes. The body was irradiated with unfocused laser beam 6 mm in diameter. Biological sample was allocated on the test plate.

To determine the absorption coefficients of biotissue, the forward end of optical fiber was inserted into the body from the side opposite to laser irradiation, parallel to the co-ordinate plane xOy (Figure 4).

Figure 1. Experimental setup

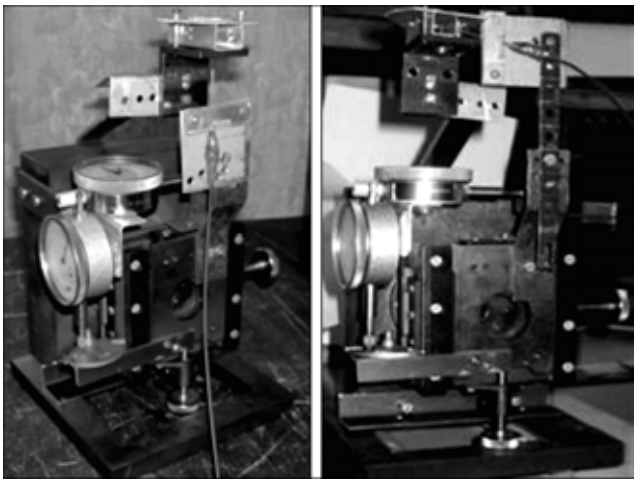

Figure 2. Two-axis device measured depth of radiation penetration

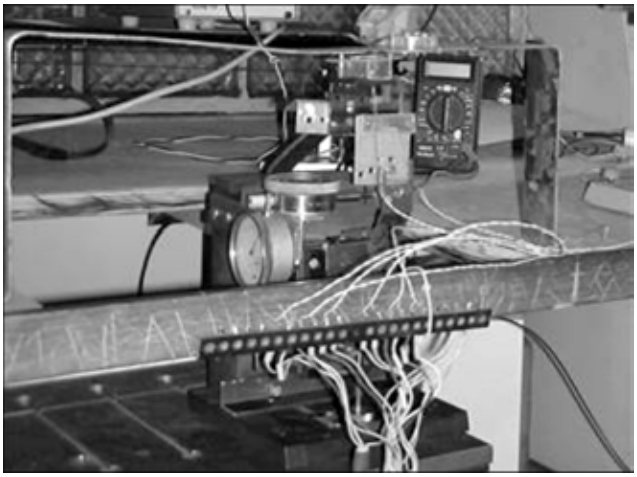

Figure 3. Temperature distribution analyzer

The back end of optical fiber was connected to photodiode. The intensity of laser radiation was measured with oscilloscope. The displacement of the test plate and depth of the forward end of optical fiber was controlled with micro-screws.

In order to determine light scattering coefficient, intensity of laser radiation was measured in the direction perpendicular to the axis of laser beam propagation (optical fiber was inserted into the side surface of the body parallel to the co-ordinate plane xOy) (see Figure 4). With the micro-screw, body was moved in the direction perpendicular to the axis of radiation. So, it was possible do determine the light scattering depending on the position of optical fiber on co-ordinate plane xOy (see Figure 4). The same measurements were done for the various depths Z from the irradiated surface.

Temperature of the irradiated body was measured with Cr–Al thermocouples with electrode diameter of 0.15 mm. Thermal-electromotance was measured with oscilloscope. The position of thermocouples relate to beam and surface was controlled with micro-screws (Figure 5).

Results of experimental studies. Experimental studying of physical properties were carried out with muscular tissue, pig liver and potato. Samples were fixed on the test plate and irradiated with unfocused laser beam. Power of radiation was changed. Intensity of laser radiation inside the body was measured with optical fiber. Results are shown in Figures 6 and 7.

According to the experimental results, all studied bodies have direct propagation of laser radiation in direction parallel to the axis of laser beam and scattering of radiation in radial direction. Moreover, rule of laser radiation scattering is changing depending on depth. Near the surface, changing of scattering has exponential regularity. Increasing the depth, scattering law trends to linear.

All studied biological bodies have the same laws of radiation absorption. The only one difference between them is the attenuation coefficient. Basing on carried out measurements, we obtained the shape of laser radiation distribution inside the irradiated body (Figure 8). It approximation gives possibility significantly increase precision of modeling of laser heating of biological bodies.

Obtained results show that the highest absorption of laser radiation has potato (penetration depth 15 mm), and the lowest absorption has muscular tissue (35 mm). Penetration depth of pig liver is 25 mm.

According to the measurements for the muscular tissue, pork liver and potato, absorption coefficients α are 0.29, 0.4 and 0.66 mm^{-1} and scattering coefficients α^* are 0.417, 0.52 and 0.59 mm^{-1}, respectively.

Absorption a and scattering α^* coefficients were defined as

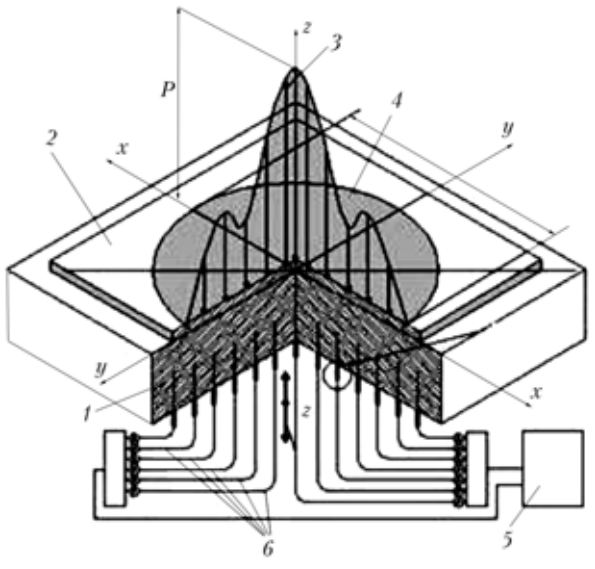

Figure 4. Scheme of measurement of optical characteristics: *1* — biotissue; *2* — optical glass; *3* — laser beam; *4* — beam diameter; *5* — oscillograph; *6* — fiber optic cable

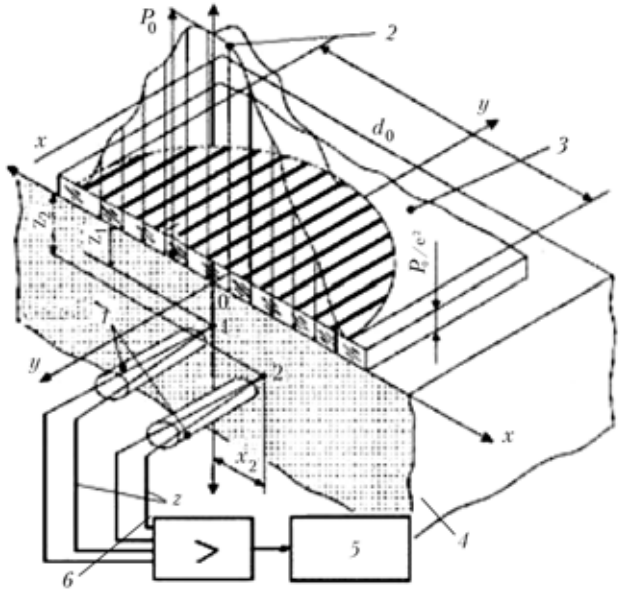

Figure 5. Scheme of temperature distribution measurement: *1* — Al_2O_3 tube; *2* — laser beam (λ = 1.06 mm; $P(x, y) = P_0 \exp(-Z^3 / Z_0^3)$; *3* — optical glass; *4* — biotissue; *5* — 2-beam oscillograph; *6* — thermocouples

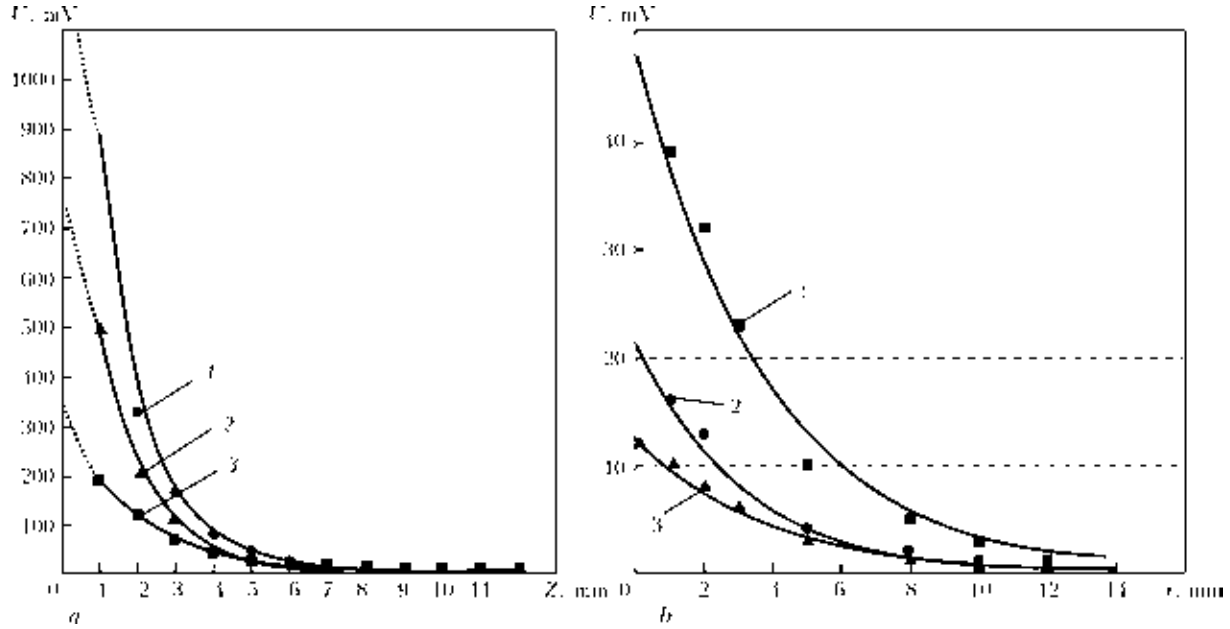

Figure 6. Change of laser radiation depending on depth Z (*a*) for muscular tissue (*1*), pig liver (*2*) and potato (*3*) and on distance from the beam axis r (*b*) at distance from the surface of 2 (*1*), 4 (*2*) and 6 (*3*) mm at the 10 W laser power and 120 s irradiation time

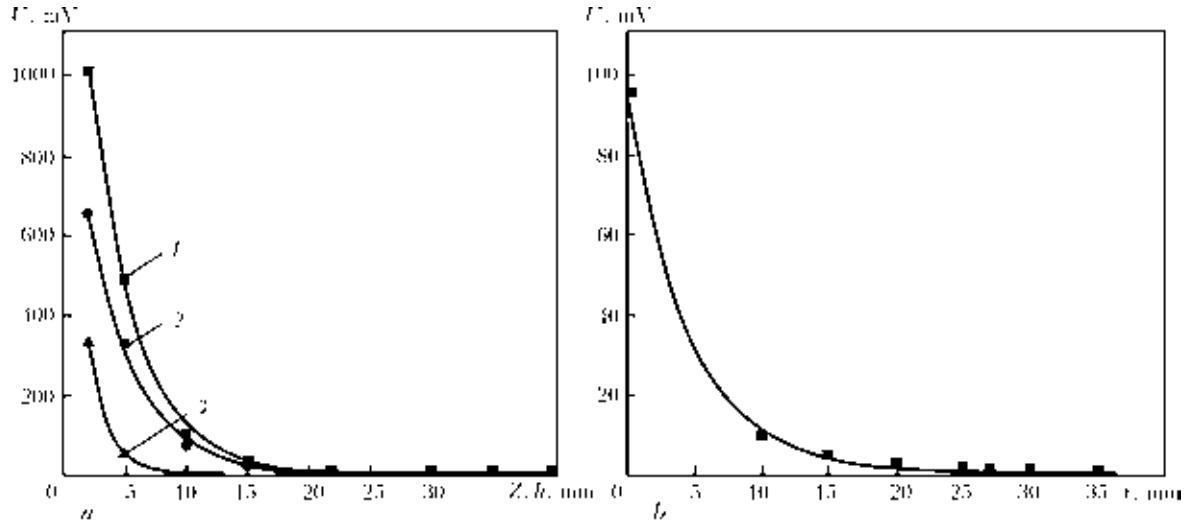

Figure 7. Change of radiation of laser with power of 18 (*1*), 10 (*2*) and 6 (*3*) W depending on depth Z (*a*) and on distance from the beam axis r (*b*) at the 18 W laser power and Z = 2 mm from the surface of muscular tissue

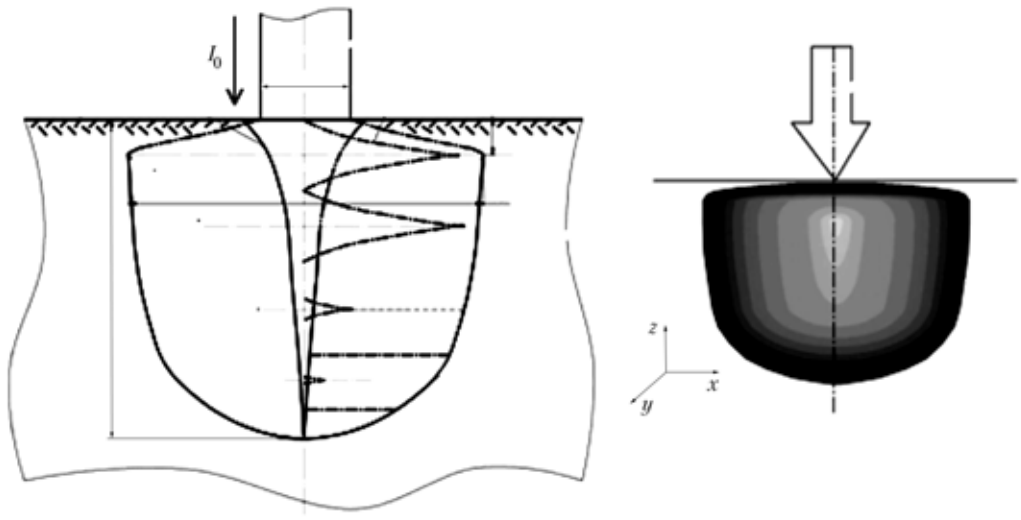

Figure 8. Laser power distribution inside the biological bodies (λ = 1.06 mm)

$$\alpha = \frac{1}{l_z}, \quad \alpha^* = \frac{1}{l_x - r_1} = \frac{1}{l_x - r_b \exp^{-\alpha z}}, \tag{1}$$

where l_z is the distance from the surface in direction parallel to the axis of laser beam, on which laser radiation is fully absorbed; l_x is the distance from the beam axis in radial direction, on which laser radiation is fully absorbed; r_1 is the radius of laser radiation penetration zone in case if scattering is equal to zero; r_b is the radius of laser beam.

Mathematical modeling of biotissue laser heating. One of the possible ways of curing of various diseases is heating of certain volume of biological body up to temperature 37–43 °C. In this case, displacement of temperature maximum from the irradiated surface inside the heated area plays an important role.

Laser radiation (λ = 1.06 mm) can be used as a heat source for such heating. Radiation is delivered to the biological body with optical fiber and special focusing device. Displacement of temperature maximum inside the body can be achieved by cooling of the surface with special liquid at the certain temperature.

If the inner surface of the hollow cylindrical body irradiated with laser beam (Figure 9, *a*), its heat condition can be described with 2D heat equation in cylindrical co-ordinates *rOz* (symmetry at co-ordinate φ):

$$c\rho \frac{\partial U}{\partial t} = \lambda \left(\frac{1}{r} \frac{\partial U}{\partial r} + \frac{\partial^2 U}{\partial r^2} + \frac{\partial^2 U}{\partial z^2} \right) + W, \tag{2}$$

where $U = U(r, z, t)$ is the temperature distribution; t is the time; c, ρ, λ is the heat capacity, density and heat conductivity of biological tissue, respectively; W is the total volumetric heat source.

The total volumetric heat source is equal to

$$W = q_r + q_l, \tag{3}$$

where q_r are the losses of the energy on the surface because of re-irradiation; q_l is the energy absorbed with biological body.

$$q_r = \begin{cases} 0 \text{ at } r \in (0, r_{\max}), \\ \varepsilon\delta(U^4 - U_{cp}^4) \text{ at } r = 0, \end{cases} \tag{4}$$

where ε is the emittance of biological tissue; δ is the Stefan–Boltzmann coefficient; U_{cp} is the temperature of cooling agent.

$$q_l = \left(1 - \left(\frac{1 - n}{1 + n}\right)^2\right) I_0 e^{-(\alpha + \alpha^*)r} e^{-(\alpha + \alpha^*)z}, \tag{5}$$

where n is the refraction coefficient; I_0 is the maximum of radiation intensity.

Power distribution on the plane *rOz* (Figure 9, *b*) is symmetrical relative to the axis of the laser radiation. So it's advisable to locate the beginning of the co-ordinate system at the point of laser beam axis and biological surface interaction. So the task is solving only for the condition $z \geq 0$.

Entry and boundary conditions (taking into consideration one-sided cooling) for the equation (2) are

$$\lambda \frac{\partial U}{\partial r}\Big|_{r=0} = H(U\Big|_{r=0} - U_{cp}), \quad U\Big|_{r_{\max}} = U_{\text{in}}, \\ \frac{\partial U}{\partial z}\Big|_{z=0,\ z=z_{\max}} = 0, \quad U(r, z, 0) = U_{\text{in}}, \tag{6}$$

where U_{in} is the initial temperature of biological body; H is the convection coefficient.

In case of heating in a narrow range, the physical properties of the body can be assumed to be constant.

The task was solved using the finite difference technique and adaptive algorithms. Adaptive algo-

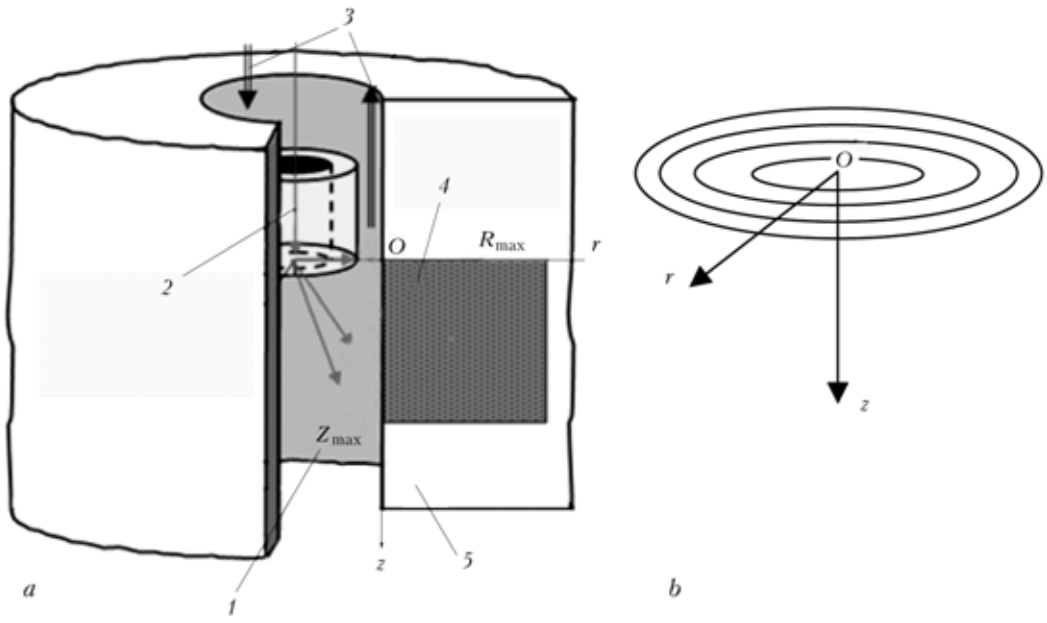

Figure 9. Modeling process (*a*) and laser intensity distribution inside the muscular tissue (*b*): *1* — in-feed channel; *2* — optical fiber with focusing element; *3* — cooling; *4* — calculation area; *5* — biological tissue

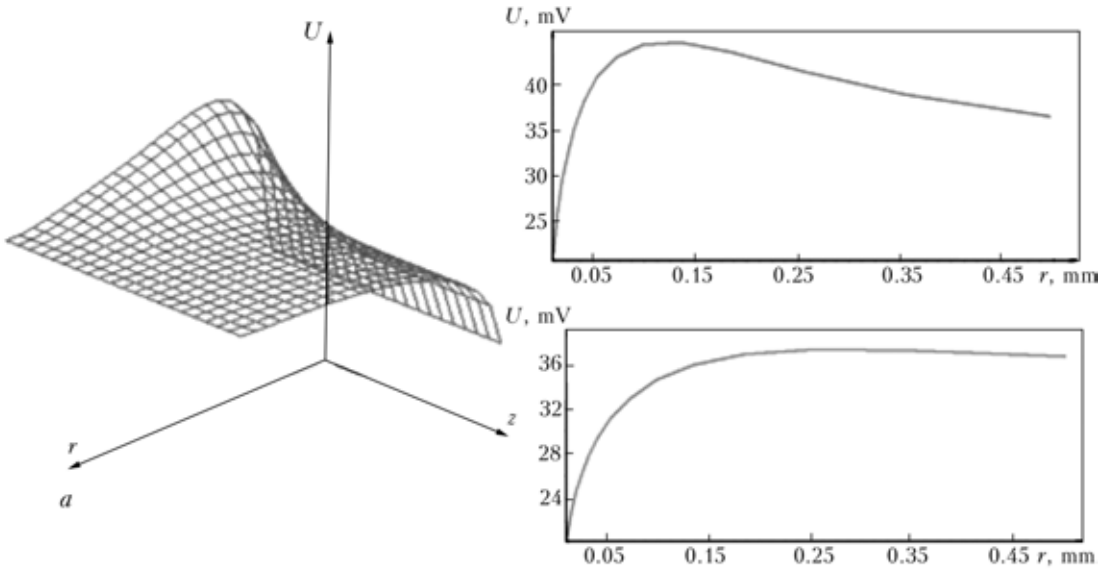

Figure 10. Temperature distribution inside the biological body (*a*), and temperature profiles at depth Z = 0 (*b*) and 0.3 (*c*) mm and t = 6 s

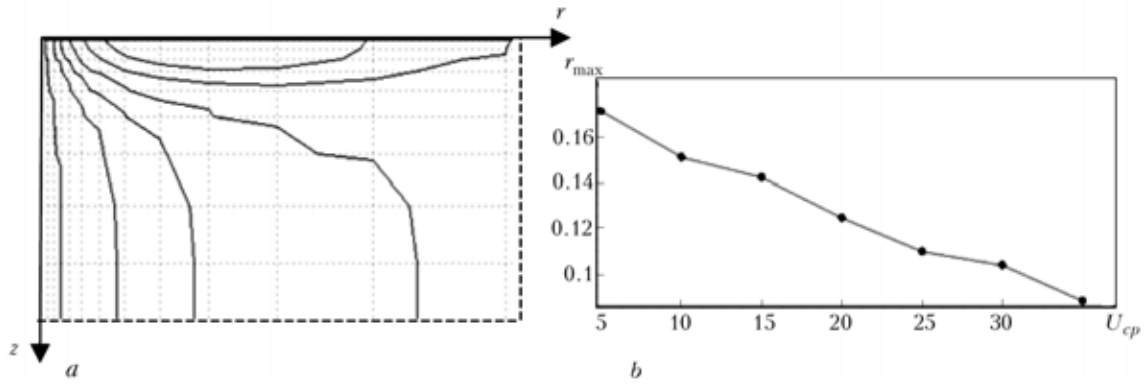

Figure 11. Temperature profiles (*à*), and dependence of temperature maximum position (depth r_{max}) on cooling temperature U_{cp} (*b*)

rithms give us possibility to analyse the temperature on-line, check error and use variable difference grids ---- the more temperature gradients the smaller size of the grid.

Mathematical model was checked and adjusted with experimental measurements. Temperature distribution inside the irradiated body was studied in cases of focused and unfocused laser beam. Basing on the elaborated model we calculated the temperature field inside the body and changing of the temperature profile with the time (Figures 10 and 11). Calculations were carried out for the following parameters: $\varepsilon\delta = 0.539 \cdot 10^{-7}$, U_{cp} = 20, I_0 = 50, $\alpha + \alpha^*$ = 9.99, n = 1.46, H = 20, λ = 0.00628, ρ = 0.0015, c = 1170, irradiation time t = 6 s.

CONCLUSIONS

1. Effective way to determine the optical characteristics of the biological tissues was proposed.

2. Laws of absorption and scattering of laser radiation with wavelength of 1.06 mm within biological tissues were obtained.

3. Effective modelling of biological heating with laser radiation, which is based on finite difference technique with adaptive algorithm, was proposed.

INCREASE OF TRIBOTECHNICAL CHARACTERISTICS OF FRICTION SURFACES BY SELECTIVE LASER CLADDING

L.F GOLOVKO, A.K. SKURATOVSKIJ, A.T. SERDITOV, Y.V. KLYUCHNIKOV (Ukraine),
H. SALAVATI and **M. HAGHERIZADEH** (Iran)
National Technical University of Ukraine «KPI», Kiev, Ukraine

The analysis of conditions of wear processes of friction units details was given in such extreme working conditions, as at the high specific pressure, high temperatures and action of the excited environments containing abrasives. The manufacturing techniques on the friction surfaces by means of laser cladding of accumulators of solid greasing are offered. The results of mathematical simulation mode of deformation of the friction unit details allowed one to define the rational form and topography of such discrete sites depending on sizes of specific loadings, loading circuits and material properties. Results of experimental studying of laws of formation in conditions of laser irradiation of wearproof superficial layers tribotechnical characteristics are shown.

Significant problem of machines and mechanisms working in extreme conditions (high specific pressure and temperatures, higher speeds of relative driving, operation in excited environments and vacuum) is low endurance of their most main details forming pairs of friction. Such terms are characteristic for supports of boring chisels, footstep-bearing of billows of turbines of the system of turbo-supercharging of engines, shoulder-blades of gas turbines and other. The laboured or in general impossibility of delivery and withholding in the area of contact of details of knots of friction of greasing is the distinctive feature of their work. Such details, as a rule, work in conditions of dry friction. The technological measures developed by present tense, powering up rational selection of materials with an optimal correlation of their hardness, creation on conjugated surfaces of oil-retaining regular microrelief, application of composite materials, solid greasings, allowed deciding a lot of the intricate technical problems related to providing of capacity of different mechanisms. However much comparison of terms of work of the heavó-loaded knots of dry friction with the terms of work of machines with the traditional types of greasing shows that they on the resource of work in ten and hundred one time yield to the last.

The aim of this work is development of manufacturing techniques the heavó-loaded knots of dry friction, ensuring, due to architecture of the forced solid greasing, essential increase of reliability and resource of their operation.

For reaching an object in view in the given research solved following problems:

- development of a way of architecture of forced solid greasing of heavó-loaded knots of dry friction;
- mathematical simulation of the intense-deformed condition of surfaces of friction with preliminary produced and special image the located deepenings filled by an antifrictional material;
- definition of the rational shape of deepenings and regularities of their arrangement on surfaces of abrasion;
- development of the antifrictional material executing function of solid greasings;
- study of regularities of process of filling of technological deepenings by an antifrictional material by a laser gas powder cladding method;
- valuation of resources of practical use of the offered technique in the industry.

Development of a method of organization of the solid greasing. For providing of high resistance to the wear besides good bearing strength of surface of friction must possess high antifriction properties. For the examined knots of friction such properties it is possible substantially promote due to application of the solid greasing. For its organization it is suggested on one of surfaces of friction to create the evenly placed deepenings having a different shape in a plan, but the necessarily reserved contour (Figure 1). Solid antifriction material takes place in these deepenings.

In the process of work of such knot under action of loading effort of wall of deepenings resiliently become deformed and cause diminishment of their volume. Antifriction material filling these reserved deepenings is squeezed out in the area of contact, fills microgaps and provides, thus, the forced greasing [1].

Simulation of the intense-deformed condition of a node of friction. For simulation of the intense-deformed condition of a surface of heavó-loaded friction pairs at operation of external loading the physical model (Figure 2) has been created. It represents the round cylinder, on which surface along a generatrix for all length or fractionally slots, in chessboard order, are located. Slots have a closed loop and a rectangular cross-section.

As a material of model steel 14KhN3 Ì À with density ρ, coefficient of elasticity *Å*, module of shift *G*, Poisson's factor *m*, limit of fluctuation *s*, was used. After a choice of area of model for decomposition on finite elements, it was set shapes and their approxi-

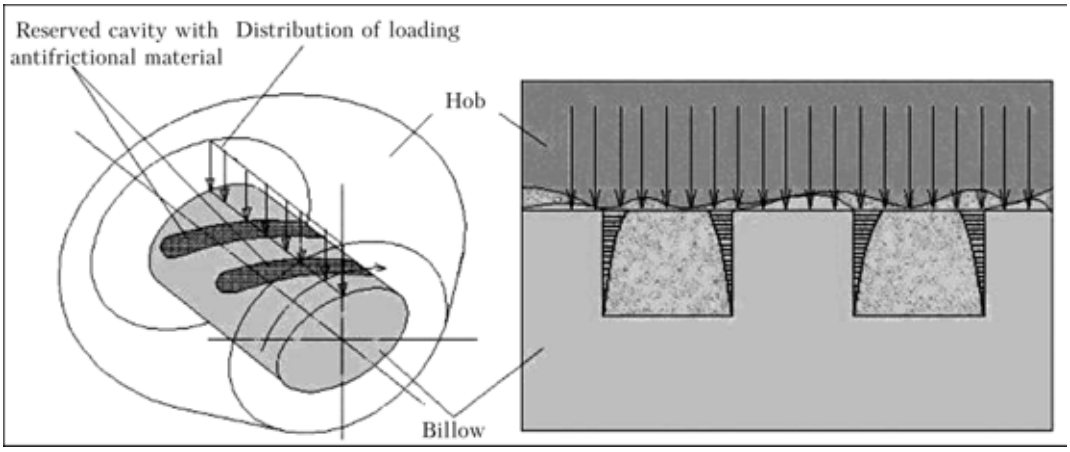

Figure 1. Scheme of organization of the forced solid greasing

mate sizes, their amount was set. Then boundary conditions, zones of the application, a direction of operation and magnitude of external loading (Figure 3) were set. In this Figure distributions of elastic efforts, their sign and magnitudes are presented also. In Figures 4 and 5, distributions of elastic efforts in direct and cross-sections in models with a various arrangement and the sizes of long slots are presented.

The analysis of results of simulation has confirmed working capacity of the offered way of architecture of forced solid greasing of heavó-loaded nodes of friction. Operating the shape and the sizes of slots in view of properties of materials, it is possible to change effectively a level of elastic strains of slots walls (see Figure 5). It allows in each concrete case, in view of magnitude of loading, a construction of details of a node of friction to be rationally designed.

The experimental equipment and holding of research technique. Experimental researches were spent with the purpose of installation of regularities of process of a laser cladding.

Samples with the sizes $40 \times 40 \times 5$ mm from steels 45 and 14ÕhN3 Ì À with various initial structure were treated by radiation of the Ñ Î $_2$-laser on the techno-

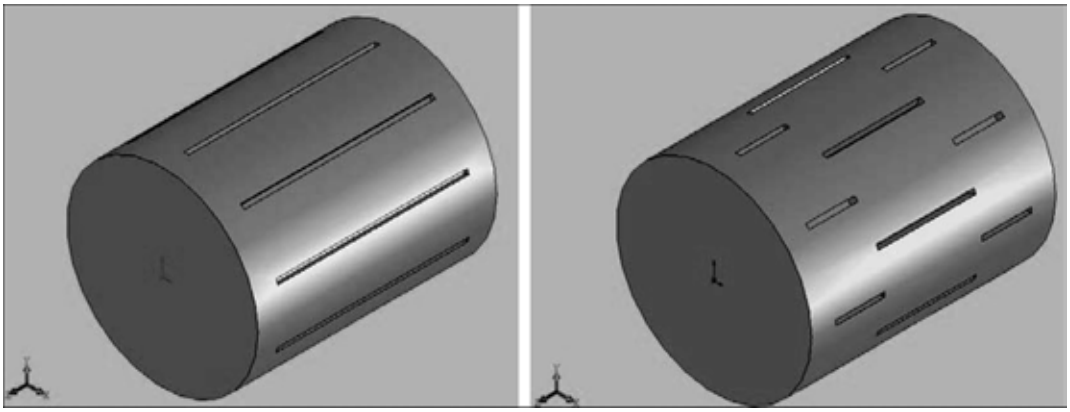

Figure 2. Physical model of friction pairs knot

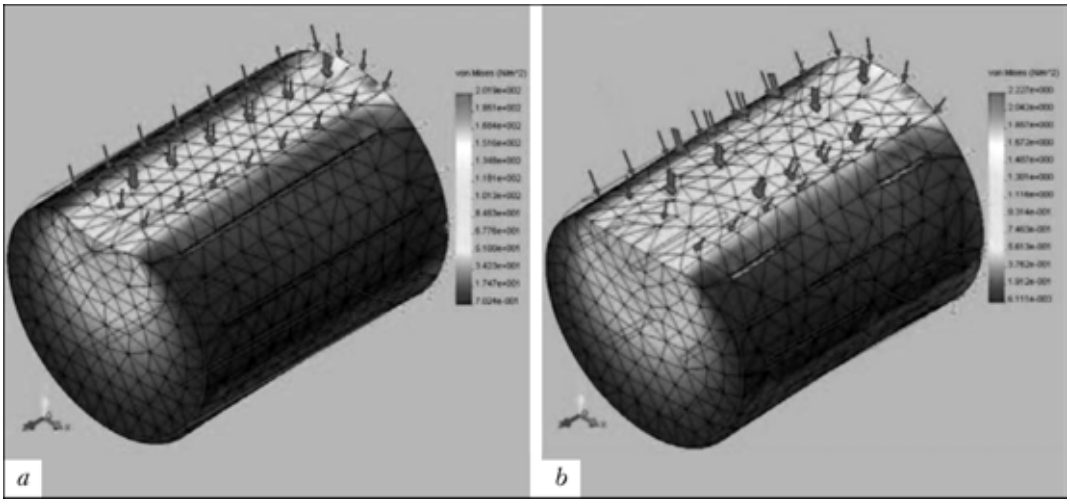

Figure 3. Areas of decomposition of FE-models, zones of application and direction of operation of external loadings and distribution of elastic efforts: *a* — cylinder with long slots; *b* — cylinder with short slots located in chessboard order

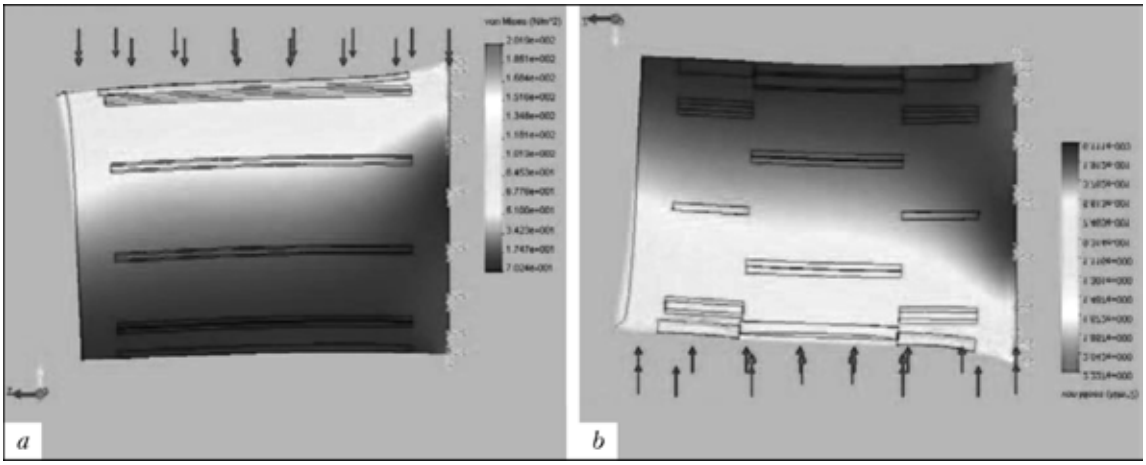

Figure 4. Distribution, sign and magnitude of elastic efforts in direct sections of cylinders with long (*a*) and short (*b*) slots located in chessboard order

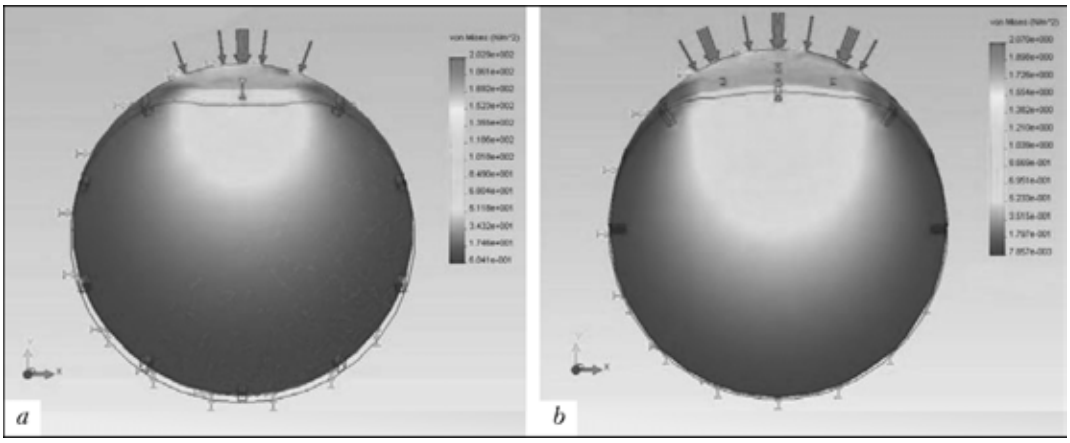

Figure 5. Distribution, sign and magnitude of elastic efforts in cross-sections

logical complex equipped by devices of monitoring of parameters of a bunch, system of batching and feeding a dust, four-coordinate table with CNC (Figure 6). Power of radiation was 1.2 kW, speed of handling varied within the limits of 0.3–2.0 m / min, diameter of a spot of focusing ---- within the limits of 2–5 mm.

At this way in the submelted surface stratum of a deepening of the detail displaced under the certain law, in a trace of a ray, under 45° jet of transporting gas moved powder cladding material. Expenditure of a dust varied within the limits of 0.1–0.5 g / s (Figure 7).

Bronze to be used was supposed for the details of nodes of abrasion working at high speeds of sliding and small loadings, mixture of dusts ---- at a great loading efforts and rather low speeds of sliding.

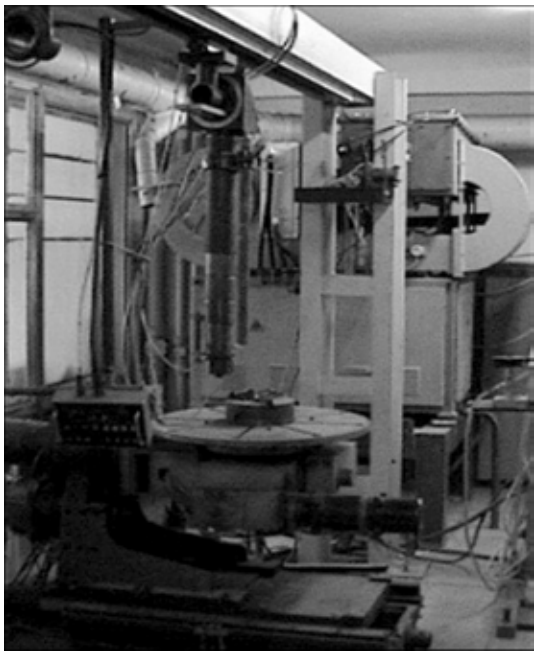

Figure 6. Experimental technological complex on the basis of Ñ Î $_2$-laser for gas powder cladding of antifrictional materials

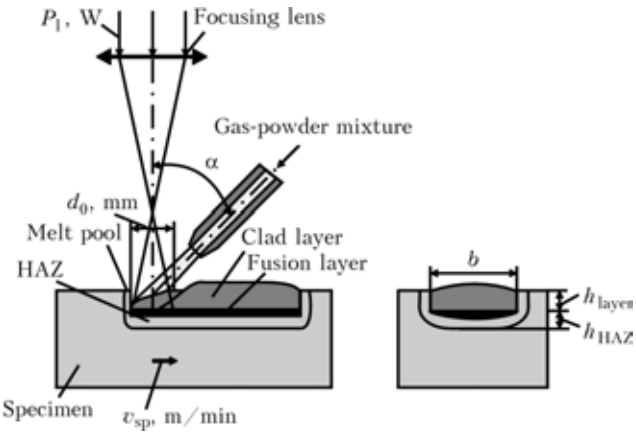

Figure 7. Scheme of filling the slots by antifrictional material in the way of laser gas powder cladding

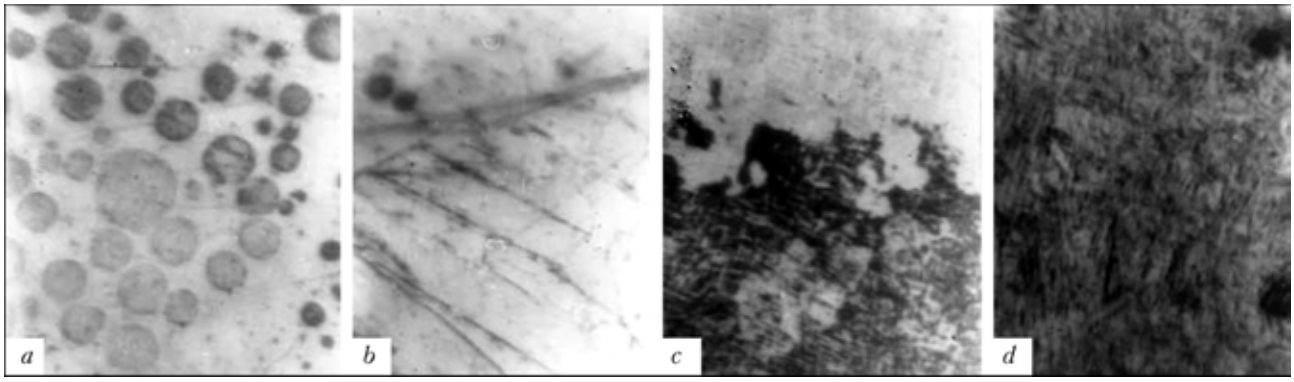

Figure 8. Microstructures of various zones of cladding of bronze on steel: *a* — on the surface; *b* — under the surface; *c* — transitive stratum; *d* — zone of steel quenching

The subsequent grinding of a rough tolerance ensured the necessary sizes and quality of a surface. As cladding antifrictional material bronze Br Î STs10-1 was used, and also mixture of a dust of bronze with a dust from steel 95Kh at a various ratio of components [2].

Virtues of an offered way of drawing of antifrictional materials are sharp selectivity and productivity of process, opportunity of architecture of different compositions due to application of a complex of various powder materials, high adhesive strength clad stratum with a material of a basis in view of presence between them metallurgical link.

After laser handling samples exposed by metallography and durometry, during which structure, microhardness and dimensional performances of clad stratums, transition stratums, where alloying of coverage, basis and HAZ materials occured, were studied.

After the analysis of results, on the selected conditions natural details (pins chisel straight bits and footstep bearings of turbines) which put on trial in real conditions were treated.

Results of experimental researches of the laser gas powder cladding process. During laser gas powder cladding, on a surface of steel the stratum of bronze filling a special deepening with a closed loop is shaped. In microstructure (Figure 8, *à*) non-fused particles of a dust of the bronze, introduced in crystallized liquid melt, which in underlying stratums has homogeneous enough structure (Figure 8, *b*) are visible. The stratum of bronze is strongly connected to a substructure, owing to presence of its stratum of alloying with steel. The structure of a transition stratum is resulted in Figure 8, *c*. Under a zone the liquid basis settle down a HAZ regarding which the temperature of heat was above point $À_{c3}$.

It has caused course of process austenitizing and the subsequent formation as a result of autoquenching superfine martensite structures with high microhardness (Figure 8, *d*).

In Figure 9 distribution of microhardness on clad stratum depth, which precisely reflects its structure, is presented. As follows from this dependence, immediately on a surface the stratum of bronze 0.4 mm width, and below ---- the stratum of alloy of bronze with steel, a basis of which smoothly increasing hardness, are testified. Still below is a small transition stratum and a zone of quenching of steel in a hard condition with microhardness of 8.0–8.5 GPà, initial structure of steel.

As have displayed the received results application of laser radiation for a build-up welding allows solving in parallel one more very important problem, namely strengthening surface stratum walls and slot bottom due to autoquenching a steel basis. As a result, during operation the plastic antifrictional material will be between details which conjugated surfaces have high hardness.

It is expedient to apply to great specific pressure and rather small speeds of sliding cladding mixtures of steel and bronze dusts. As have displayed the researches executed in [2], during trials on wear process in a condition of dry abrasion with loadings of 5.1–15.3 Ì Pà, at speed of abrasion of 20 mm / min have been established, that build-up welding of 60–80 % of bronze have essential heightening resistibility to wear at big loadings (Figure 10).

For structure from 90 % of bronze wear is catastrophically augmented in connection with loss of durability of a material. Essential heightening of endurance and reduction of time of wear-in for build-up welding from 60–80 % of bronze and 40–20 % of steel in structure of an aggregate speaks significant lowering of factor of abrasion between rubbing surfaces.

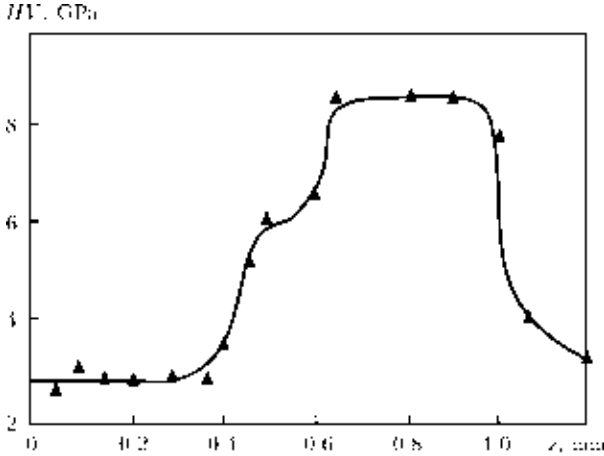

Figure 9. Distribution of microhardness on depth of clad stratum of bronze Î TsS10-1 on steel (0.45 % Ñ)

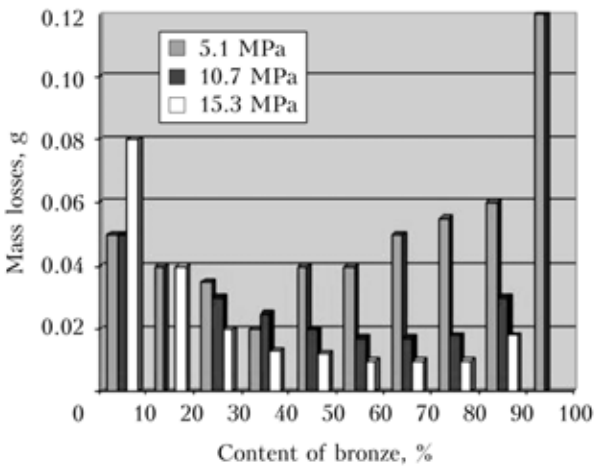

Figure 10. Dependence of wear magnitude on bronze contents in surfacing mixtures at different loadings

Trials on wear were spent without feeding pool greasing to a zone of abrasion. The role of hard greasing was played in this case with bronze.

Opportunities of application of the received results in the industry. At drilling slits in geological prospecting the special straight bits being are widely applied by the instrument destroying rock and shaping its trunk (Figure 11). It represents the case consisting from three welded swing arms. On pins of swing arms, forming a block, three are placed rock-destroying a disk with insertions from a hard alloy. The straight bit is the basic element of the process equipment limiting productivity and the cost price of drilling. It is linked with its low longevity, due to extreme operating conditions of a node of a sliding friction. On pins of swing arms special deepenings, which by laser gas powder build-up welding were filled with mixture steel and bronze dusts, were made. After a build-up welding of a pin of swing arms were ground for giving the demanded sizes and a surface roughness. On pins strengthened and clad swing arms disks with insertions were established. Swing arms with disks gathered on three units, welded forming thus straight bit. Field trials of new straight bits in comparison with standard have detected essential (on 30–60 %) increase shaft deepening on one unit.

The bench trials of footstep bearings produced on new technique with application of a laser build-up welding, have detected double increase in endurance at simultaneous lowering the cost price of a good by

Figure 11. General view of straight bit and swing arm with a pin

means of a laser build-up welding, is effective means of heightening of a resource of operation of hard loaded nodes of abrasion.

CONCLUSIONS

1. The offered way of forced hard greasing which are powering up manufacture on a conjugated surface of special deepenings with a closed loop and their filling with an antifrictional material by laser build-up welding, is effective means of heightening of a resource of operation of hard loaded nodes of abrasion.

2. It is expedient to apply to high specific pressure and rather small speeds of sliding the surfacing mixtures containing 20 % of steel and 80 % of bronze dusts.

3. The laser cladding of the bronze type antifrictional materials on steel details promotes forming under a plastic coverage of a stratum of chilled steel with high microhardness of 8.0–8.5 GPà.

1. Golovko, L.F., Serditov, A.T., Klyuchnikov, Yu.V. (2005) Application of laser surface processing for increase of wear resistance of parts is high-gravity of the loaded clusters of friction. In: *Proc. of Int. Conf. on Laser Technologies in Welding and Materials Processing* (Crimea, Katsiveli, May 21--28, 2005).
2. Pereloma, V.A., Podoltsev, A.D., Likhoshva, V.P. et al. (1998) *Investigation of thermal processes and surface layer structure in laser surfacing of powder materials*. Kiev: IED.

DEEP PENETRATION OF HIGH-POWER CW CO_2-LASER BEAM INTO LIQUIDS

V.S. GOLUBEV, A.N. GREZEV and **N.V. GREZEV**
Institute on Laser and Information Technologies of RAS, Shatura, Russia

Experimental results are presented on research of channeled penetration of high-power (up to 3.5 kW) CW- and long-pulsed CO_2-laser beam into liquid media (water and glycerin). Laser power threshold for channel formation, channel growth phase ($t \sim 10^{-3}$–10^{-1} s) and quasi-stationary phase ($t > 10^{-1}$ s) were investigated. Experiments and qualitative modeling have revealed that in the case of keyhole (KH) in water its depth and diameter depend upon heat exchange and convection conditions inside the KH and the liquid pool, and KH mean diameter roughly ten-fold exceeded the value of the laser beam focal diameter (the same situation was stated for the case of KH in glycerin). The depth and mean diameter of the KH fluctuate at frequencies in the range of 10^2–10^3 s^{-1} with relative amplitudes in the range 10–30 %. A qualitative hydrodynamic model of the KH in water was developed based on the assumption that geometrical and dynamical parameters of the KH (mean depth, mean diameter, velocity of the depth growth) depend upon intensity of turbulent and convective heat transfer from the channel liquid walls into the bulk of the liquid. The KH volume is filled with evaporating microdroplets detached from liquid walls of the KH by the process of capillary-evaporative instability. Energy and momentum balances of the KH are attributed to radial transfer of vapor condensation enthalpy into liquid walls and to the equilibrium of dynamic pressure of vapor radial flow impinging the KH walls with the sum of hydrostatic and Laplacian pressures of the liquid. In the case of glycerin the experimental data and numerical estimations show that KH depth depends upon evaporation losses rate.

Formation and sustaining of laser channels (keyholes –– KH) in liquids is strongly interesting in fundamental science [1–4], as well as for laser practical applications in materials processing [2], medicine [5–8] etc. Experimental investigations of KH in liquids that resulted from penetration of the CO_2-laser focused beam (50 W to 4 kW power) were described in [1–3, 5, 9]. Depth of KH in water increased to the values of about 1–4 cm at the 1–4 kW laser powers. The KH growth and its sustaining in water was accompanied by instabilities of its surface in the form of «goffers» [2, 5, 9], formation and collapse of micro-bubbles [5, 9] of about 10–10^2 μm in size, and emission of acoustic waves into the surrounding water and in ambient atmosphere [3, 5, 8]. The spectrum of acoustic frequencies ranged from 1.5 to 10–15 kHz. In [5] the sound pressure amplitude reached 0.1 atm. The velocity of the KH bottom propagation is ~1–5 m / s at the initial stage of KH formation at the ~10^5 W / cm^2 laser beam intensity. Studies [3, 9] present measurement results on velocity field of closed (vortex) convective water flows in the KH vicinity (at laser beam power of 100–200 W). The values of flow field size and KH depth were of similar order, and convection velocity values approached 10–50 cm / s. Study [10] describes results of experiments and modeling on channel propagation in water and gelatin by a free-running erbium laser at the ~10^{-4} s pulse duration, 30 mJ pulse energy, and radiation intensity in the KH $q = 10^4$–$4 \cdot 10^6$ W / cm^2. It was found that the channel proceeded into water at velocities $v_p \cong 10^2$–10^4 cm / s. The propagation process is described with a hydrodynamic model in terms of energy, mass and momentum equations.

With the aim to create qualitative physical models of the laser KH in liquids we have made [9, 11–13] experimental investigations of quasistationary KH in water, developing KH and laser power thresholds of KH emergency, as well as qualitative physical estimations of the values of power threshold of KH emergency, velocity of KH bottom movement during the phase of KH growth, mean values of the KH depth and diameter and of the velocity of liquid inside turbulent convective whirls around the KH. The results of these investigations, along with recent investigations of the KH in glycerin, are given in the present paper.

Thresholds of emergency and initial phase of the KH growth. Experimental investigation of KH emergency in water and its subsequent growth were made [14] with a 5 ms pulsed CO_2-laser of sub-kW range. Results of $h = f(P)$ measurement are presented in Figure 1. The value dh / dt, as well as the h and $2R$ values, are similar to those which were found in experiments [5]. A model interpreting the results of Figure 1 was proposed in [12]. A hypothesis was proposed that channel emergency at the threshold $Đ = Đ_{th}$ and its growth at $Đ > Đ_{th}$ are driven by vapor pressure of evaporating microdroplets detached from liquid surface of the crater as a consequence of evaporative-capillary instability. Final results for thresholds $R = 0.05$ cm and $Đ_{th} \cong 60$ W are close to experimental data (see Figure 1).

Model [12, 13] of the KH growth phase at $P > P_{th}$ is based upon the concept of downward motion of the channel bottom due to vapor recoil pressure. The vertical position of KH walls is determined by equilibrium between hydrostatic pressure and dynamic pressure of radial vapor flow going from axial zone of KH and impinging its liquid walls. The origin

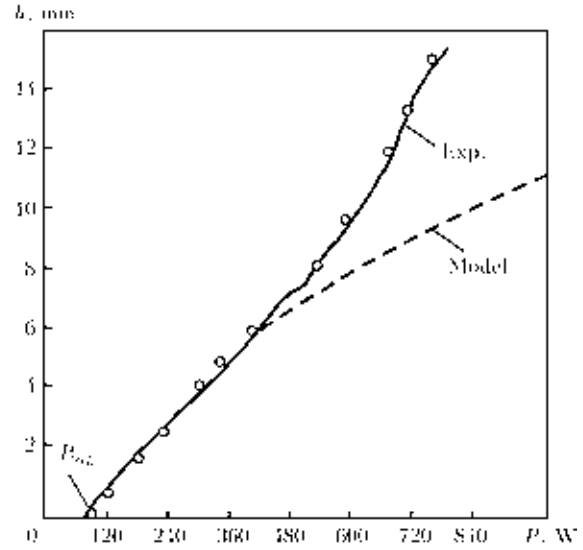

Figure 1. Depth of KH h in the water at 5 ms pulse duration and 0.5 Hz pulse-repetition rate [14]

of vapor flow is the evaporation of microdroplets inside laser beam area, and the origin of microdroplets is the detachment of surface microwaves humps due to capillary-evaporative instability. The cause of instability is the radial heat flux generated by condensation of radial vapor flow upon liquid walls. Finally, mean bottom radius R and KH depth $h(t)$ of the growing KH were found: $R \sim P^{2/3}$; $h(t) \sim Pt / (1 + \text{const} \cdot Pt)$, where P is the laser beam power and t is the current time. If $P \cong 10^3$ W, then $\overline{R} \cong 5 \cdot 10^{-2}$ ñm and $h \approx 0.8$ ñm at $t = 5 \cdot 10^{-3}$ s. These values are close to experimental results (see Figure 1).

Quasistationary KH. An experimental study of KH in water was performed [9] using the 0.5–3.5 kW CW CO_2-laser focused beam with intensity of $1.7 \cdot 10^5 \div 1.2 \cdot 10^6$ W / cm^2. The mean depth h and diameter $2R$ of the KH were measured with 30 % accuracy (Figure 2). Frame pictures of KH and surrounding water bulk showed the presence of small bubbles (0.1–1.0 mm) and water movements around the KH, which represented transient whirls in the KH vicinity. Two

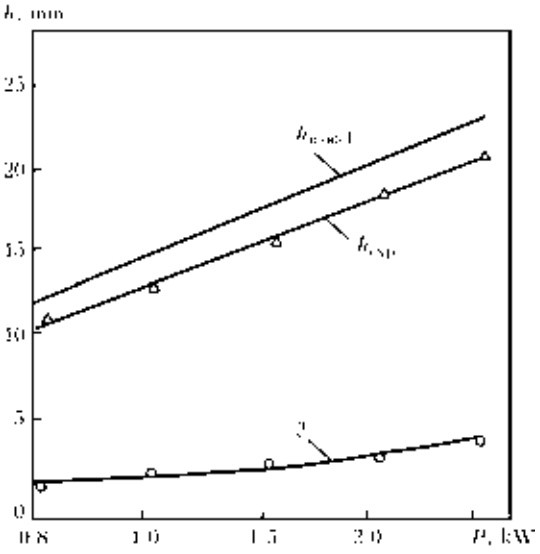

Figure 2. Depth h and outlet diameter $2R$ of the laser KH in water [9]

types of turbulent whirls around KH were observed, namely full-scale quasistationary Archimedean convection whirl and small-scale transient whirls adjacent to the KH surface correlated with the KH collapsive movements (Figure 3). Typical values u of whirls velocities were 10–50 cm / s. The depth and diameter of KH were fluctuating at frequencies in the range of about 10–10^2 s^{-1}. Relative amplitude of these fluctuations reached 50–100 %, i.e. KH presented a periodically collapsing object. At our estimations, the frequencies of gravitational collapse (periodical «flooding» of KH) are 3–10 s^{-1}, and those of capillary collapse (accompanied by development of goffers) [15] are of the order of 10^2 s^{-1}.

Mean geometrical parameters (h, R) of the KH and mean velocity u of the surrounding liquid were estimated [9, 12, 13] using the energy and momentum balance equations [4, 16] for axial and radial vapor flows and formulae [17, 18] for turbulent convection heat and momentum transfer in water bulk, regarding mechanisms of thermocapillary force, buoyancy, vapor recoil pressure and of turbulent viscosity. Resulting equation for the KH depth h is

$$P = P(h) =$$
$$= \left[(3\pi/4)\rho c Pr (\varepsilon\beta g)^{1/2} (\Delta T)^{3/2} + \pi\sqrt{2} (g\rho/\rho_v)^{1/2} E_v (R/h)^2) \right] h^{5/2},$$

where ρ_v is the vapor density; β is the coefficient of liquid volume thermal dilatation; g is the gravitational acceleration; $\Delta T \cong T_b - T_0$; $E_v \cong 1.5$ J / cm^3 is the specific heat of evaporation for 1 cm^3 of vapor at 1 atm.

The first term in square brackets represents heat losses of KH by turbulent convection; the second term represents the evaporation losses through the KH mouth. Evaporative losses in the range of $10^2 << P << 10^4$ W have a share 0.1–0.3 of convection

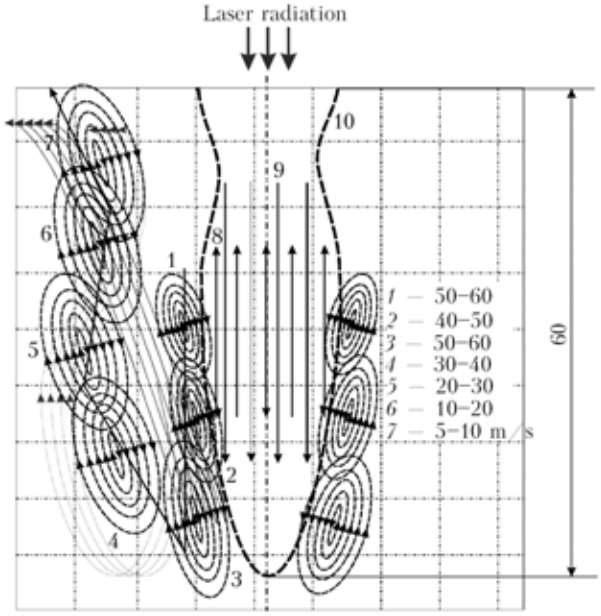

Figure 3. Transient whirls in the water bulk nearby the KH at P = = 3 kW: *1–7* correspond to velocities of rotational movements inside the whirls [9]

losses. Equation $P = P(h)$ (considering $R / h = \text{const}$) gives the law $h \propto P^{2/5}$, that is close to experimental result (see Figure 2). Besides, the law $h \propto P^{2/5}$ correlates with experimentally measured [9] water temperature growth time $t_g \propto P^{1/5}$.

To estimate the mean KH radius value R we implied the hypothesis of microdroplets evaporation in the volume restricted by the focused laser beam and total depth of KH. The droplets are detached from the KH liquid walls due to periodical development of capillary-evaporative instability [19, 20]. Vapor flows radially to KH walls and gives away its condensation energy and its momentum, so determining the value of mean KH radius R. It is assumed that the total flux of the vapor condensation energy equals to the total laser beam power, which is spent to evaporation of the droplets. Dynamic pressure of the vapor flow, impinging the KH wall, equals to mean hydrostatic pressure $\rho g(h / 2)$. Finally, the ratio

$$R/h \cong \frac{3}{8}\frac{\rho c \Delta T}{E_v}\left(\frac{\rho_v}{\rho}\varepsilon\beta\Delta T\right) = \text{const} \cong 0.5\cdot 10^{-1}$$

was found. This value of R / h correlates satisfactorily with the results of our experiments (see Figure 2) and experiments of [2].

Mean velocity $\underline{u}$ of the circular flow in the full scale Archimedean convection whirl (Figure 4) was estimated by a formula

$$u \cong \left[\frac{(\beta g)^2 \Delta T}{\varepsilon^3 \rho c} P\right]^{1/5}.$$

At $P = 3\cdot 10^3$ W and $\varepsilon \approx 10^{-2}$, $u \cong 50$ cm / s. This value correlates with results of experiment of [9].

Thus, the mean macroparameters of KH in water can be estimated by a model based on the concept of turbulent momentum and heat transfer in the liquid and radial vapor flow momentum and heat transfer to the KH walls.

Quasistationary KH in glycerin. CW CO_2-laser generated doughnut-shaped beam with 1.5 mrad full angle divergence and 0.1–1.0 kW power; the duration of laser action upon the glycerin free surface was up to 10 s. The KH depth did not changed substantially during the whole time of laser action. Some fluctuations of the depth of about 10 % relative amplitude range and frequency range of 10^2 s^{-1} have been observed. The KH shape was similar to that reported in [1, 3], i.e. one can see several «waists» and «bubbles» along the channel, and the length of each «bubble» was approximately 1.0–1.5 cm, while the channel depths were in the range of up to 6 cm and the KH mean diameters usually were in the range of 2–4 mm (Figure 5). We attribute «bubbles and waists» to the phenomenon of capillary collapse [15].

We have considered, in a rough approximation, a physical model of the channel in glycerin. Due to elevated value of viscosity, the physical models of KH in water and glycerin are quite different and, according to our estimation, any Archimedean flows

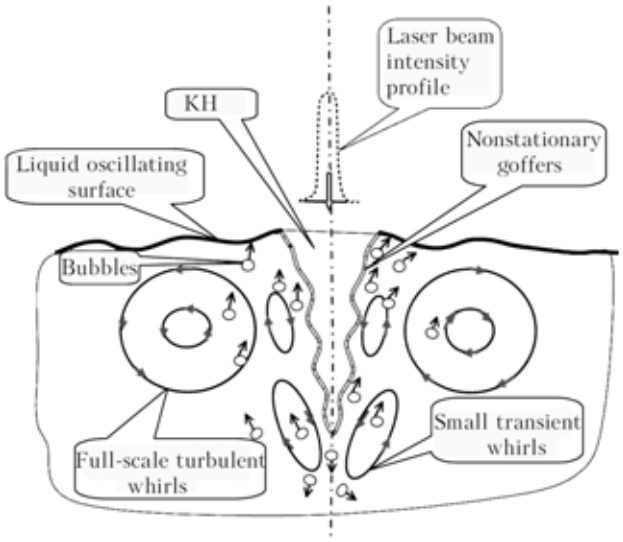

Figure 4. Draft of the quasistationary KH in water

into liquid bulk of glycerin cannot be turbulent. Due to very low value of molecular thermoconductivity of glycerin, the energy balance of the channel governs by evaporation losses. The forces balance is presented mainly by equality of vapor recoil pressure and hydrostatic pressure of the liquid (at least, for channel depths exceeding the range of several millimeters, i.e. for laser powers exceeding some of 10^2 W). The power of these losses, P_{ev}, is presented by expression

$$P_{ev} = [E_{ev} + \rho_v c_p (T_b - T_{amb})]\ (\pi d^2 / 4) u_v,$$

where ρ_v, u_v is the vapor density and outlet velocity, respectively; E_{ev} is the per unit of vapor volume specific energy of liquid–vapor phase transition (for glycerin $E_{ev} \cong 2.1$ J / cm^3 [21]); boiling point $T_b = 563$ K; $T_{amb} \cong 300$ K; $\rho_v c_p (T_b - T_{amb}) = 0.9$ J / cm^3; d is the mean outlet (mouth) diameter of the channel. According to experimental data, a phenomenological fact is $d / h \cong \text{const} \cong 0.8\cdot 10^{-1}$. For the case of glycerin this might be explained, e.g. by a model similar to the model for d for the case of water. The u_v value equals to $u_v = (\rho / \rho_v)^{1/2}(2gh)^{1/2}$, where $\rho = 1.3$ g / cm^3 is the liquid density. Assuming that $P_{las} = P_{ev}$, we have found for h a following modeling expression: h (cm) $\cong$ $\cong 0.3P^{0.4}$ (Figure 6).

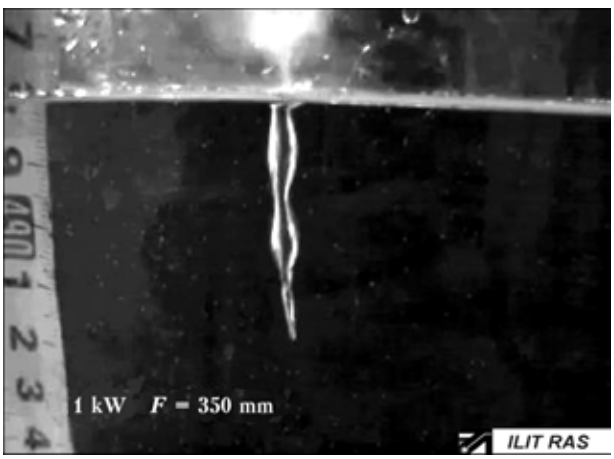

Figure 5. KH in glycerin

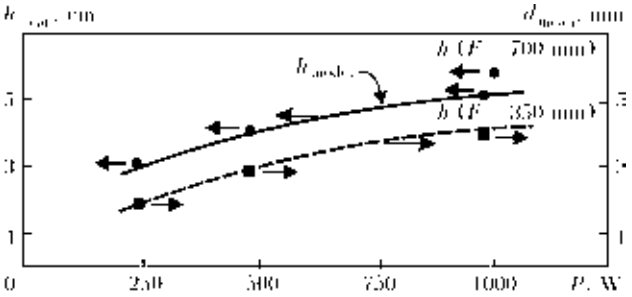

Figure 6. Experimentally measured mean values of KH depth h and diameter d in glycerin: experimental points for h at laser powers P = 250 and 500 W are the same at F = 150 and 350 mm; experimental points for d correspond to the averaged d values for F = 150, 350 and 700 mm; curve h_{model} corresponds to the model formula h (cm) = = $0.32P^{0.4}$

Nonstationary phenomena in KH. *Capillary collapse*. All experimental observations of the developing [5, 14], as well as of the quasistationary [1, 2, 9] KH in water have revealed strong instabilities of the KH walls. The geometrical shape of the walls presents a weakly converging cone with nonstationary goffers. The wavelength of goffers is close to KH diameter. The lower part of KH periodically collapses with repetitive «breakdowns» of KH, succeeded by periodical ejections of vapor jets into surrounding atmosphere, accompanied by acoustic emission. Experimental observations [3, 8] of acoustic spectra in frequency range up to 10^3–$2{\cdot}10^4$ Hz have been reported.

A model [12] of capillary collapse gives repetition frequency of laser «breakdowns» $f \cong 10^3 \div 10^2$ s^{-1}. Vapor pressure bursts generate acoustic waves of frequency f, as well as of resonance frequencies [22] $f_n \sim$ $\sim 10^4$–$3{\cdot}10^4$ s^{-1}.

Oscillations of the quasistationary KH. Free oscillations frequencies ω_0 and f_0 of KH with radius R are $\omega_0 = (g / R + \sigma / \rho h R^2)^{1/2} \cong 10^2$ s^{-1}, and $f_0 = \omega_0 / 2\pi \cong 20$ s^{-1} (if $R \cong 0.1$ ñm, and $h \cong 1$ ñm). A possible cause of the sustaining KH oscillations is the turbulence of the vapor flow ejected from the KH mouth. The frequency spectrum of this turbulence includes frequencies $\omega = \omega_0$, and the KH might be exposed to forced oscillations.

CONCLUSIONS

1. Laser power threshold of the KH origin is determined by the condition of overcoming surface tension force by dynamic pressure of vapor flow from microdroplets evaporated by laser irradiation.

2. The $10^{-2} \div 10^{-1}$ s initial phase of the KH growth is determined by vapor recoil pressure on KH bottom and convective heat exchange of KH wall with surrounding liquid; the convection of the liquid is determined by the motion of the channel bottom.

3. Geometrical and dynamical parameters of KH in water are determined by turbulent convective heat transfer from the KH walls into the bulk of liquid. The KH volume is filled with evaporating microdroplets detached from KH walls due to capillary-evaporative instability. Energy and momentum balances of KH attribute to the radial transfer of vapor condensation enthalpy to KH walls and to the equilibrium between dynamic pressure of vapor radial flow impinging the KH walls and hydrostatic pressure of the liquid. In the case of KH in glycerin, the model of the process is based upon the assumption of prevailing role of direct evaporative energy losses.

4. Geometrical parameters of the quasistationary KH oscillate with frequencies of about 10^2–10^3 s^{-1}, which presumably correspond to capillary collapses and oscillations of the channel wall.

1. Antonov, A.A., Kozlov, G.I. et al. (1987) *Kvantovaya Elektronika*, 14(**6**), 747–753.
2. Spivak, A.V. (1986) *Doklady AN*, 290(**5**), 1107–1111.
3. Cybulski, A., Mucha, Z. *Welding Int.*, 11(**3**), 212–220.
4. Bunkin, F.V., Tribelskiy, M.P. (1980) *Uspekhi Fiz. Nauk*, 130(**2**), 193–239.
5. Jansen, E.D., Frenz, M., Kadipasaoglu, K. et al. (1996) *OE-Reports*, 152(Aug.), 9–12.
6. Vasiltsov, V.V., Golubev, V.S., Dubrov, V.D. et al. (1998) *Proc. SPIE*, **3264**, 145–154.
7. Panchenko, V.Ya., Vasiltsov, V.V., Golubev, V.S. et al. (2000) *Ibid.*, **4241**, 494–498.
8. Kubyshkin, A.P., Panchenko, V.Ya., Vasiltsov, V.V. et al. (2002) *Ibid.*, **4644**, 201–206.
9. Golubev, V.S., Grezev, A.N., Kumar, N. et al. (2004) *Ibid.*, **5449**, 436–442.
10. Forrer, M., Frenz, M., Romano, V. et al. (1993) Channel propagation in water and gelatin by a free-running erbium laser. *J. Appl. Physics*, 74(**1**), 720–727.
11. Golubev, V.S., Dmitriev, A.K., Konovalov, A.N. et al. (2003) *E-print No.1*. Shatura: ILIT RAS, 18.
12. Golubev, V.S. (2004) *E-print No.2*. Shatura: ILIT RAS, 46.
13. Golubev, V.S. (2006) Channeled penetration of high power CO_2-laser beam into water. *Proc. SPIE*, 60530Q.
14. Grezev, N.V., Kumar, N. (2003) *Private communication*.
15. Golubev, V.S. (2002) *Proc. SPIE*, **5121**, 1–15.
16. Vedenov, A.A., Gladush, G.G. (1985) *Physical processes in laser material treatment*. Moscow: Energoatomizdat.
17. Landau, L.D., Lifshits, E.M. (2001) *Hydrodynamics*. Moscow: Fizmatlit.
18. Idelchik, I.E. (1969) *Handbook on hydraulic resistance*. Moscow-Leningrad: Gosenergoizdat.
19. Samokhin, A.A. (1983) *Kvantovaya Elektronika*, 10(**10**), 2022–2026.
20. Akhmanov, S.A., Emelianov, V.P., Koroteev, N.I. et al. (1985) *Uspekhi Fiz. Nauk*, 147(**4**), 675–745.
21. (1991) *Handbook of physical quantities*. Ed. by I.S. Grigoriev, E.Z. Mejlikhov. Moscow: Energoatomizdat, 1232.
22. Rayleigh, J.W. (1944) *Theory of sound*. Moscow: Gostekhizdat, 381.

APPLICATION OF LASER IRRADIATION FOR SINTERING OF CUBIC BORON NITRIDE COMPOSITES

O.O. GONCHARUK[1], L.F. GOLOVKO[1], V.S. KOVALENKO[1], O.D. KAGLYAK[1], N.V. NOVIKOV[2], A.A. SHEPELEV[2] and V.G. SOROCHENKO[2]

[1]National Technical University of Ukraine «KPI», Kiev, Ukraine
[2]V.N. Bakul Institute for Superhard Materials of NASU, Kiev, Ukraine

Cubic boron nitride (CBN) is widely used for abrasive disk manufacturing for steel processing, polycrystalline inlets and milling cutters. In the given work some aspects related to the increase of manufacturing productivity for the abovementioned cutters are portrayed, as well as technological processes of laser sintering for the manufacturing and hardening of working layers of abrasive mills. Results of laser irradiation absorbability by the CBN depending on its state (powder mixture or polycrystalline plate) or on its powder dispersion and surface roughness, heating regimes and initial temperature are presented in details. The direct influence of oblique and exact short-time laser heating on properties of CBN, physical and chemical processes on the boundary of CBN crystals with bonding material is shown. The perspectives for the use of this technology in future are considered. Results of the investigation of laser heating of CBN are sorted according to the type of CBN and depending on the irradiation regimes. The perspectives for the implementation of the new technology into practice are investigated.

Nowadays, the super-hard materials are widely used in industry, and CBN crystals with heat resistance up to 800 °C are one of them. With temperatures above this value some oxidation takes place and consequently leads to the significant loss in durability. These crystals are obtained by the synthesis of hexagonal CBN with the presence of dissolvent in the special containers with hydraulic presses that provide the end-user with the pressure up to 300–980 Ì N / m^2 and the temperature above 2000 °Ñ. Unlike the natural diamond, CBN is chemically neutral to the iron. Reasonable hardness, heat resistance and iron neutrality made the CBN a perspective super-hard material for the processing of the ferrous materials and to make it competitive in terms of the adhesion and diffusion properties with other convenient tools.

Various manufacturing technologies that differ by the method of the creation of the bearing layer and CBN grain fastening exist up to now. Moreover, the variety of bonding materials are synthesized by the galvanic precipitation, sintering of powder materials, super-speed high-pressure sintering etc.

Super-speed heating is the youngest and fast grooving technology that allows optimizing the sintering process and receiving materials with high density and small-grained structure [1]. That is why a lot of non-isothermal sintering methods have emerged. The method we are dealing with lies in direct sintering of metallic materials by means of electric current [2] that is augmented by the laser heating [3–5].

Laser irradiation as a heat source has a lot of advantages, namely accurate non-contact energy introduction into the material, broad range of temperatures for the super-speed local heating, and the possibility to obtain superfine structures. All of them allow us to use laser heating for sintering of thin metallic and composite materials. Experiments with laser heating of ceramic and metallic powders [4] have shown that liquid phase sintering is the best way to obtain the material with the required properties.

The present paper investigates the possibility to use laser heating for the manufacturing of tools based on CBN. Some basic laws of laser beam interaction with CBN-based materials were revealed, as well as the influence of laser beam on the bond performance of these materials.

Equipment and experimental methods. The main purpose of the research is to determine maximum temperature values for super-speed laser heating of different CBN powder mixtures and corresponding irradiation regimes at which there are no changes in tool cutting properties. Moreover, there was made an attempt to investigate the properties of CBN and its applicability for cutting tools manufacturing.

A wide range of beam, metal and powder properties influence laser sintering process. The relationship between these properties and parameters of laser sintering is shown in Figure 1.

Experiment goals were as follows:

- investigate the influence of laser heating on durability of CBN grains;
- choose optimal technological scheme of laser sintering of CBN-based composite materials;
- choose appropriate materials to ensure wear-proof bonding;
- investigate the process of laser sintering of «free» and previously compacted CBN-based powder;
- investigate the influence of laser sintering on physical properties of composite.

In order to determine the absorbability of CBN grains, methods of direct and indirect laser irradiation were used. While implementing the direct irradiation method, the grooves of CBN powder were formed on

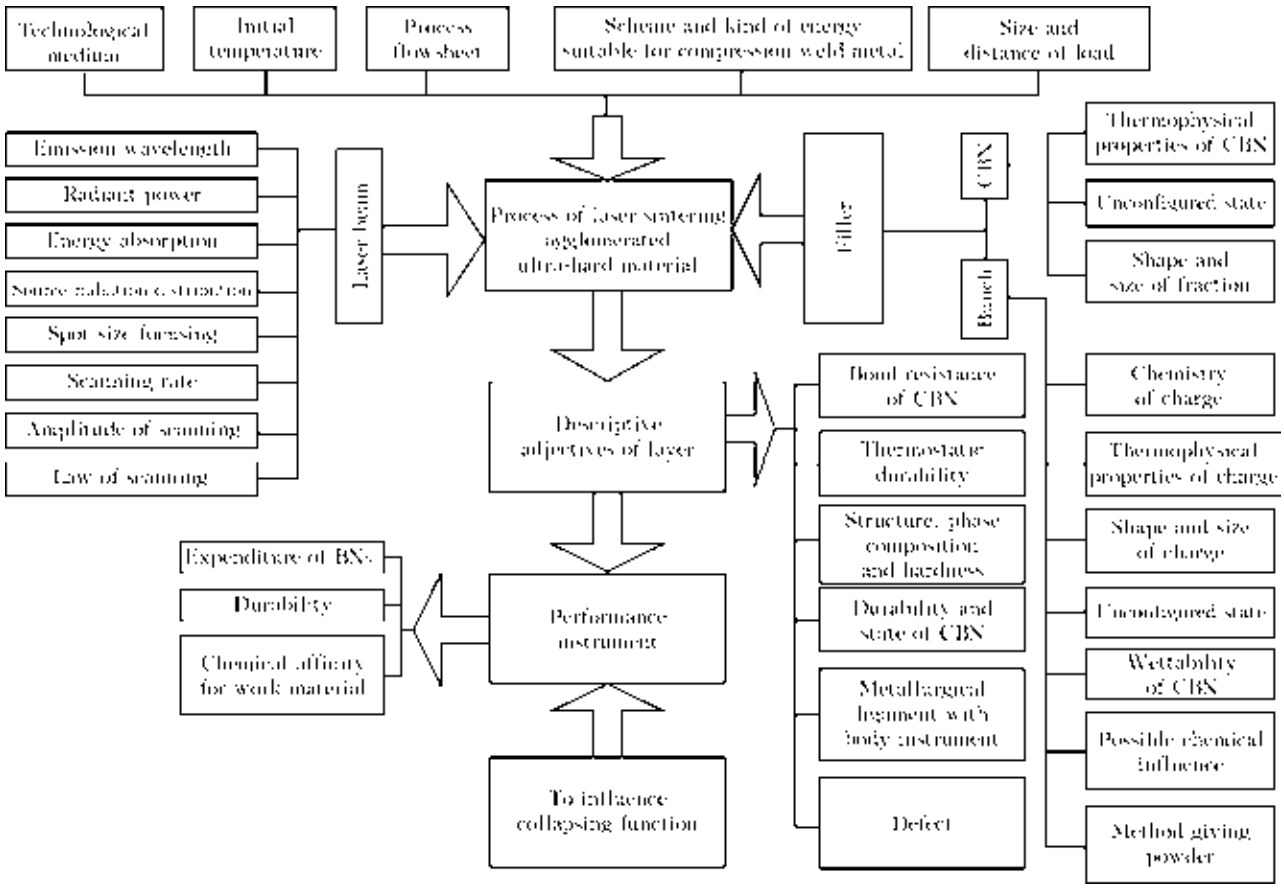

Figure 1. Major factors and parameters of laser sintering process for composites from ultrahard materials and their relationships of cause and effect

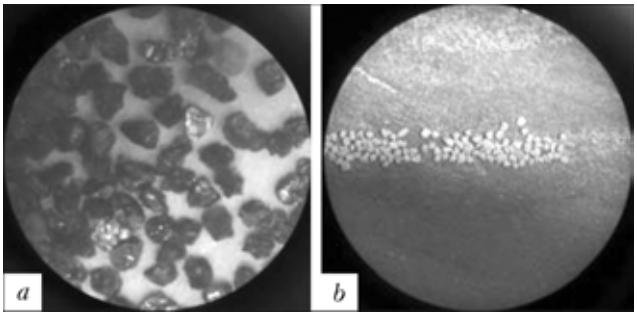

Figure 2. General view of the KÂ 250 / 200 (*a*) and KÐ 200 / 160 (*b*) CBN micropowders

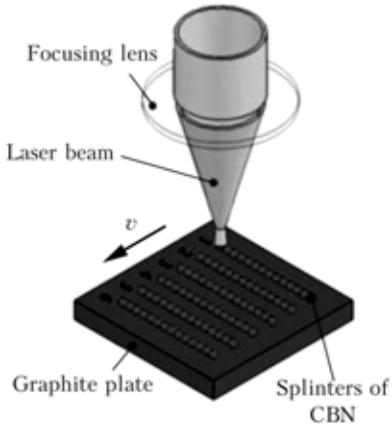

Figure 3. Scheme of set-up for CBN direct irradiation

a graphite surface. In the other case this powder was covered with a layer of metallic powders.

The KB 250 / 200 and KP 200 / 160 CBN powders were used (Figure 2). These powders are used for industrial manufacturing of cutting mills. For each experiment 50 grains of micropowder were selected placed on a graphite plate and were irradiated in CW-mode. The experimental set-up is shown in Figure 3.

CBN grains were positioned on a graphite layer in grooves and were irradiated lately with different regimes (Figure 4).

At beam power of 700 W the following factors were varied: focusing spot (d = 2–7 mm), specimen travel speed (v = 0.2–2.0 m / min).

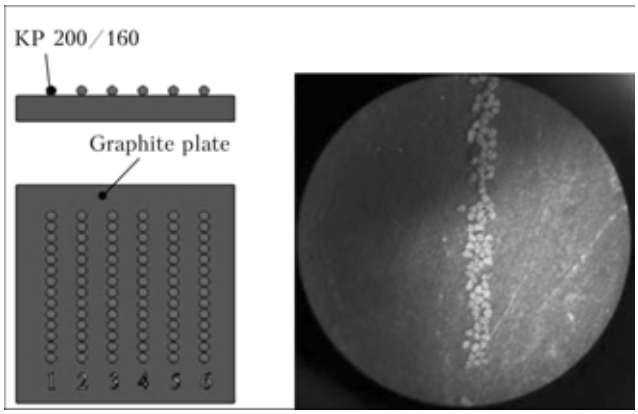

Figure 4. Scheme of CBN grain groove on graphite plate

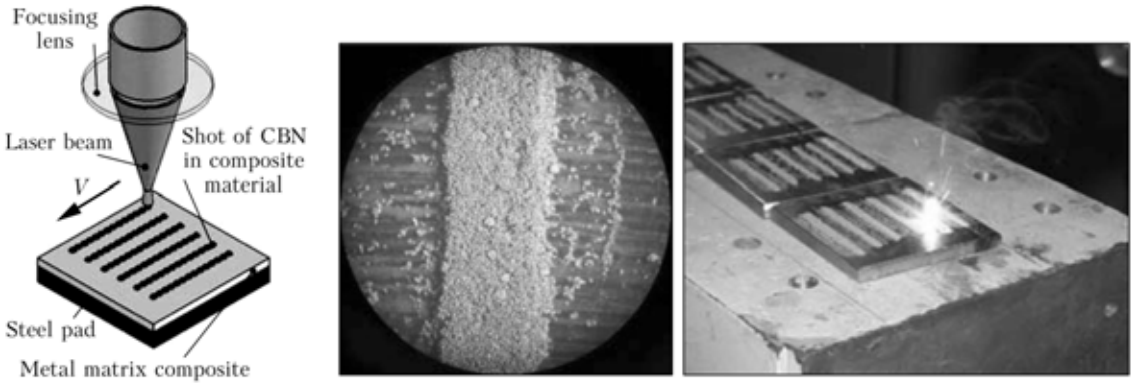

Figure 5. Scheme of indirect irradiation of CBN grain

Composite content, wt.%

Ì aterial	Fe	Ni	C	Cr	Ti	B	Al	Si
PG-12N-01	2.0–5.0	74.4–86.8 (base)	0.3–0.6	8.0–14.0	–	1.7–2.8	--	1.2–3.2

Upon the completion of the experiment, standard tests for static capacity were conducted. The results were later compared with properties of non-irradiated powder.

For the experiments with indirect heating, CBN powder was mixed with metallic powder and was glued to the mild steel plates. The powder layers were compacted down to the thickness of 1–2 mm. The thickness of a compacted layer was measured with help of gauging rod. The specimens were irradiated according to the pre-determined program. The experimental set-up is shown in Figure 5.

Composites with different melting temperatures were used to determine the influence of laser radiation (PG-12N-01, Br010 with 10 wt.% Sn and mechanical mixture of Cu + 20 % Pb), the content of PG-12N-01 is presented in the Table.

Specially designed beds of steels 45 and U8 were used. The composite was made out of mechanical mixture of CBN grains with bonding liquid and was compacted prior the irradiation. The irradiation regimes were as follows: $1.4 \cdot 10^3$–$1.4 \cdot 10^4$ W / cm^2, travel speed of 0.2–2.0 m / min. The experimental results were analyzed with help of electronic microscope, local and integral X-ray element analysis.

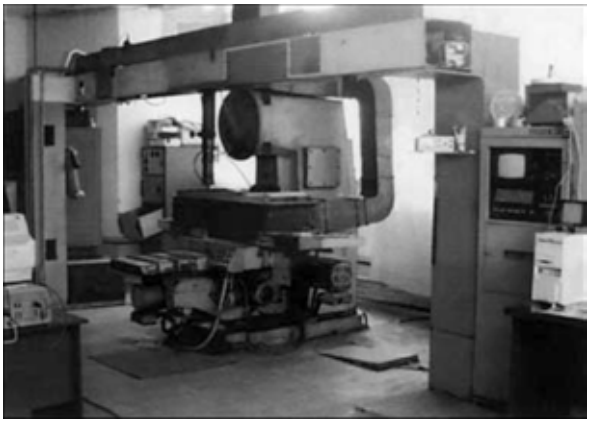

Figure 6. General view of powerful Ñ Î $_2$-laser technological complex KOMETA-2

CO_2-laser KOMETA-2 was used along with transportation unit, loading-unloading system, programmable control unit. Laser wavelength was λ = = 10.6 μm, laser power ---- 700 W, spherical length ---- KCl with focusing distance up to F = 200 mm. Focusing spot was change in the range of d_0 = 1–8 mm, and the travel speed was changing in the range of v = = 0.2–5.0 m / min. The general view of the industrial system is shown in Figure 6.

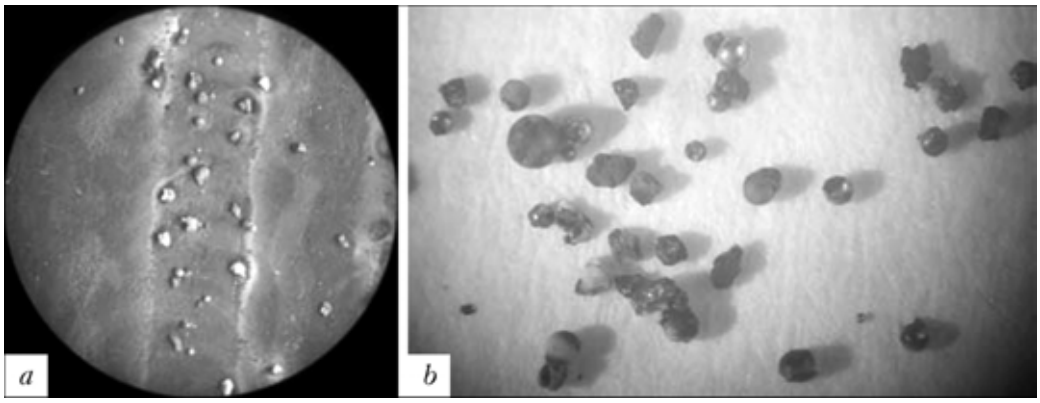

Figure 7. General view of the KP 200 / 160 CBN paths after direct irradiation: *a* — path on graphite substrate; *b* — after removal from substrate

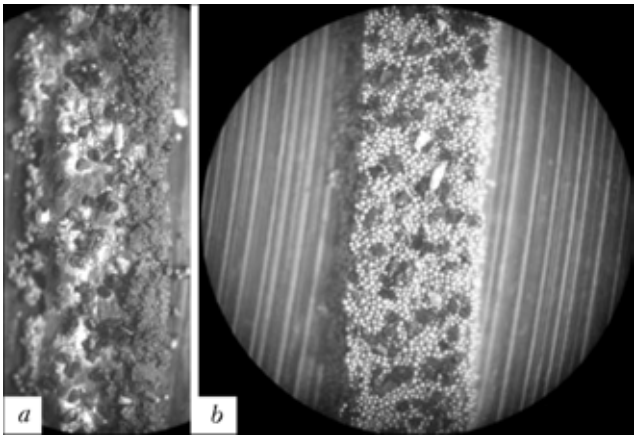

Figure 8. General view of KÂ 250 / 200 grooves in sheaf of Br010 before (*a*) and after (*b*) irradiation at d_0 = 7 mm, v = 0.1 m / min

Results. During laser heating on the surface of graphite bed a visible groove was formed with CBN grains positioned along its borders (Figure 7). The width of the groove corresponds to the effective diameter of laser beam. Since laser beam has a multimode structure and a reasonably even distribution of its intensity, it is possible to conclude that CBN grains were evenly heated as well.

The heating temperature varied in a very wide range, as well as the heating regimes (we could control the beam diameter and heating speed). The maximum value of the heating temperature was close to nickel melting temperature (1453 °Ñ), the average value was equal to the bronze melting point (1020 °Ñ), and the minimum value was equal to 500 °Ñ. The values of heating temperatures were received experimentally by irradiation of CBN grains coupled with nickel powder and bronze bonding Br010 (Figure 8). CBN grains have a good adsorption (80–90 %) for the wavelength λ = 10.6 μm since they are of dielectric nature.

Visual observation of CBN grains with help of microscope showed that they may change color and shape (depending on processing regimes). Grains irradiated at high power density (maximum temperature) partially changed their color ---- from dark to white (Figure 9). Thus, we can conclude that oxidation effects take place at these regimes. Part of the grains remained their color and shape unchanged, but could be easily destructed with a slightest touch of indenter. The remaining grains of this batch, as well as grains processed at different regimes did not change at all.

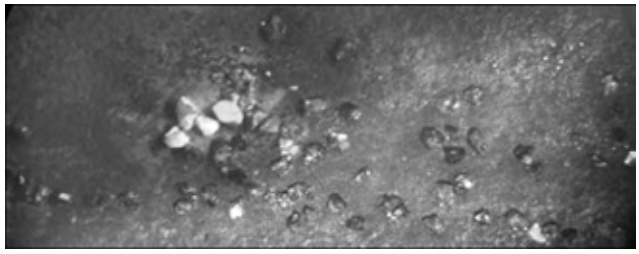

Figure 9. General view of the KÂ 250 / 200 CBN grains after direct irradiation

Studies of the influence of laser heating on physical and mechanical properties of such grains show that the value of static breaking strength for CBN significantly depends upon irradiation regimes and initial strength (brand) of CBN grain. Histograms in Figure 10 show that while heating the specimen up to the temperature 600–1000 °Ñ the average strength of CBN grains reduces by 15–20 % for the KB grain, and for the KÐ grain ---- by 20–23 %. When specimens were overheated to higher temperatures the initial strength reduced drastically. The laser beam power density in a focusing spot plays important role in this phenomena, as well as processing speed (Figure 11). The data listed below were received by averaging of the measurements of breaking strength for a batch of CBN grains (50 grains in each batch) in the initial state and in irradiated ones.

Analysis of the measurements showed that in some repetitive cases the irradiated grains of CBN had high values of strength, namely 1.5–2 times greater than those of the initial one. It would be reasonable to analyze the dynamics of percentage ratio of groups of grains that belong to different fixed intervals of the

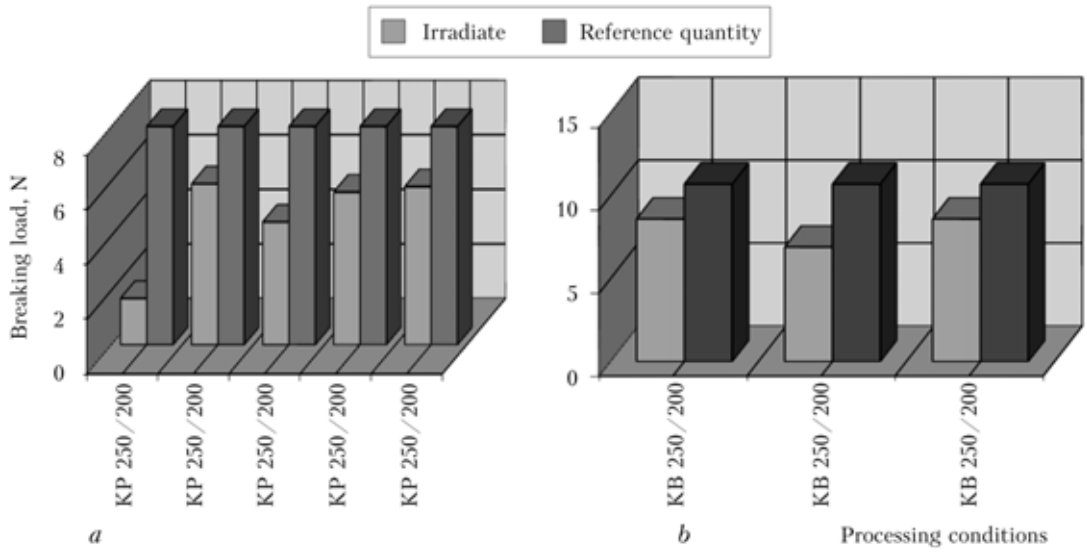

Figure 10. Average durability of KP 250 / 200 (*a*) and KB 250 / 200 (*b*) grains

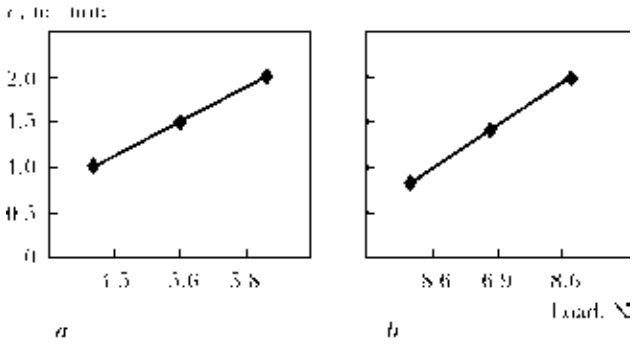

Figure 11. Dependence of durability upon processing speed for KP 250 / 200 (*a*) and KB 250 / 200 (*b*) powder

values of the breaking strength (depending on the irradiation regimes). Figures 12 and 13 show these dependencies and dynamics.

It could be concluded from the plots that CBN grains in the initial state have uneven strength that in most cases could be described by the normal distribution law. The average strength values of CBN grains are a bit higher than those of irradiated ones. Nevertheless, the analysis of above mentioned dependencies shows that for some groups of grains there is a significant or even extreme increase of breaking strength (at a given irradiation regimes). This phenomenon could be explained by the hardening effect of laser irradiation and the existence of some specific regimes that boost the hardening process.

CONCLUSION

CBN grains are good absorbers of laser irradiation with the wavelength of 1.06 mm, and being thermally-insulated could be heated up to the temperatures that cause their destruction. At laser sintering of CBN composites this matter must be taken into account and the control over the thermal state of the heated volume of the material should be provided. Laser irradiation of CBN grains at a specified area of investigated processing regimes (temperature changes in the range of 600–1000 °Ñ) decreases the average values of breaking strength by 15–20 %. It was also shown that laser sintering of CBN decreases the average value of the initial durability but, at the same time, significantly increases strength of number of specimens from the experimental lot. This could be

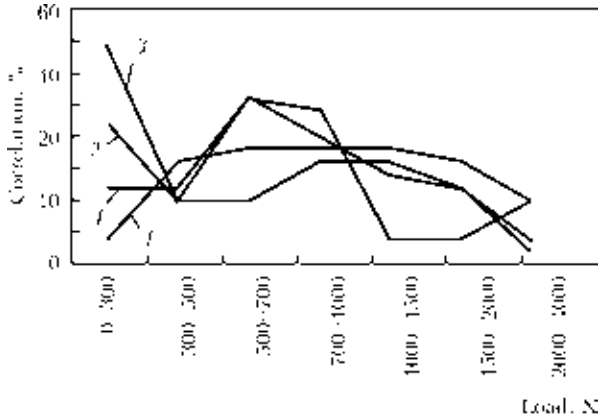

Figure 12. Load dispatch by irradiation of non-treated KB 250 / 200 (*1*) and KB 250 / 200 with *d* = 7 mm treated at *v* = 0.8 (*2*), 1.4 (*3*) and 2.0 (*4*) m / min

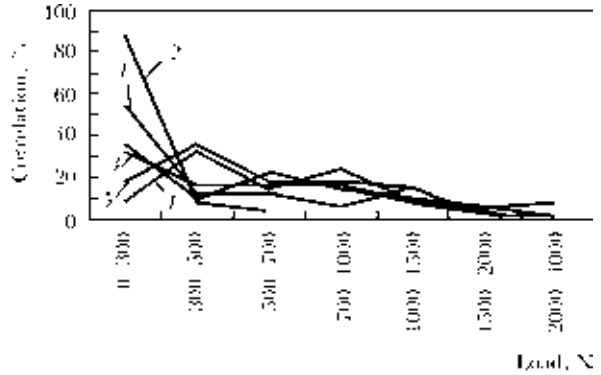

Figure 13. Load dispatch by irradiation of non-treated KP 250 / 200 (*1*) and KP 250 / 200 with *d* = 4 (*2*, *3*) and 7 (*4*, *5*) mm treated at *v* = 0.5 (*2*), 1.5 (*3*, *5*) and 1.0 (*4*) m / min

explained by the hardening effect that laser irradiation causes to a specimen.

1. Skîrîhîd, V.V. et al. (1998) *Sintering of powder materials at electrothermal, plasma and laser heating*. Ì oscow: Metallurgiya, 228–248.
2. Ràichånkî, À.I. (1984) *Bases of process of sintering of powders flashing an electric current*. Ì oscow: Metallurgiya, 128.
3. Blîchànåvich, A. Ì ., Bîchkî, À. Ì . (2004) Laser cutting of materials on basis of diamond and compact modification boron nitride. *Poroshk. Metallurgiya*, **3 / 4**, 47–53.
4. Òîlîchkî, N.K. et al. (1997) Absorption measurement of freely located one-component metal powders and its change during laser processing. *Ibid*., **7 / 8**, 89–94.
5. Ràgulia, À.V. (1998) *Selective laser sintering*. Part 1: Principles. Continual model.

FAST SIMULATION OF THERMAL BENDING USING THERMAL AND MECHANICAL BOUNDARY CONDITIONS

M. GRDEN, Th. PRETORIUS, J. WOITSCHIG and **F. VOLLERTSEN**
BIAS — Bremer Institut fuer angewandte Strahltechnic, Germany

The incremental character of thermal bending makes a finite element simulation often too expensive in terms of time. A three-step approach is presented in this paper which provides a significant acceleration of the thermal-mechanical calculation and results in comparable bending angles. The first step of the provided optimization is done by virtually reducing the sheet to the zone around the irradiation path and defining boundary conditions for the heat flux and mechanical stress along the cutting surfaces. Secondly, a thermal-mechanical simulation using the specified constraints is performed for the shortened section. Finally, the separated parts are reassembled in the third step under equilibrium of forces.

Thermal forming is a flexible way of creating complex sheet metal forms with nearly no spring back effect [1]. This process subsumes the laser bending method which has been investigated by several authors [1–3]. An alternative to the laser utilization is the plasma jet forming. Experimentally results on this subject has been published in [4–6]. Both methods base on the same bending principles which are the local creation of thermal stresses beyond the yield strength and plastic-elastic deformations. The difficulty of the utilization of thermal bending in order to form complex geometries lies in the prediction of correct process parameters like required laser power, velocity or number of irradiations. To avoid high experimental effort attempts has been made to simulate the bending by a FE analysis [7, 8]. This method involves a coupled thermal-mechanical calculation which is expensive in terms of time. For this reason a new approach is presented in this paper where the simulation is applied only to a small section of the sheet and the surrounding material is replaced by boundary conditions.

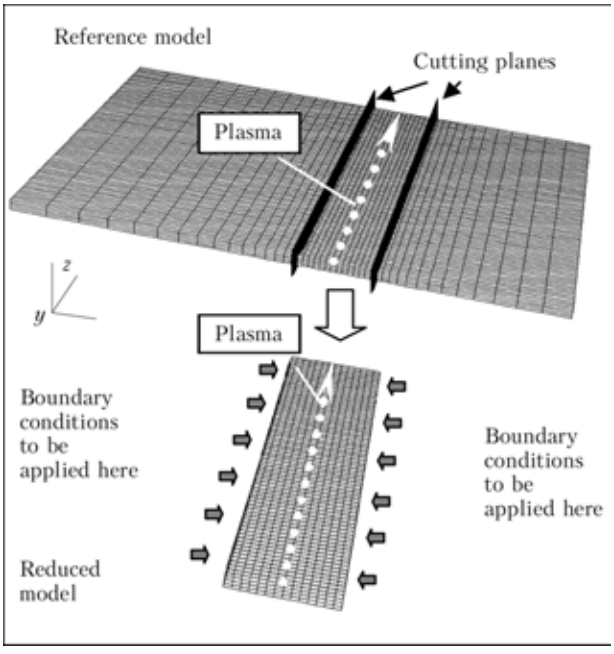

Figure 1. Reduction principle

Simulation parameters. The work discussed in this paper has been done in the context of research on sheet bending achieved by a non transferring plasma jet. Therefore, the heat source considered in the simulation will be one that matches the radius and injected power of the utilized plasma beam. The acceleration method is not limited to this heat source type even more it is suitable for any energy distribution provided by an energy beam. The plasma system has a permanent activated pilot arc with a maximum possible power of 6 kW. Measurements have shown that about 1.2 kW are absorbed by the steel St37 plate of 100 × × 70 × 2 mm within a 6.5 mm radius. The power density is approximated by the Gaussian distribution. One process cycle denotes in this paper an irradiation performed with a velocity of 2.5 m / min with a subsequent 3.32 s pause. The irradiation path is a straight 70 mm long line from edge to edge. Its traversal distance to an outer edge is set to 40 mm. A reference model simulated with ABAQUS that has been verified by experimental data consists of 12,040 elements (hexahedrons). Figure 1 visualizes the reference modeling.

Accelerated simulation. As initially introduced the simulation deals with a reduced sheet model which is limited to the area near to the irradiation path (see Figure 1). The width (14 mm) of the extracted midsection should not be smaller than the diameter of the heat source and the estimated plastic deformation zone. It is necessary to specify boundary conditions which compensate the absent influence of removed parts. Since the simulation involves thermal and mechanical calculations one thermal and one mechanical condition are specified. As thermal boundary condition the heat flux function defined in [9] is used, which has been determined due to temperature field simulations under equal conditions. With the objective of creating a mechanical boundary condition observations on the simulated stress field have been made. A compressive *x*-stress area, which moves ahead

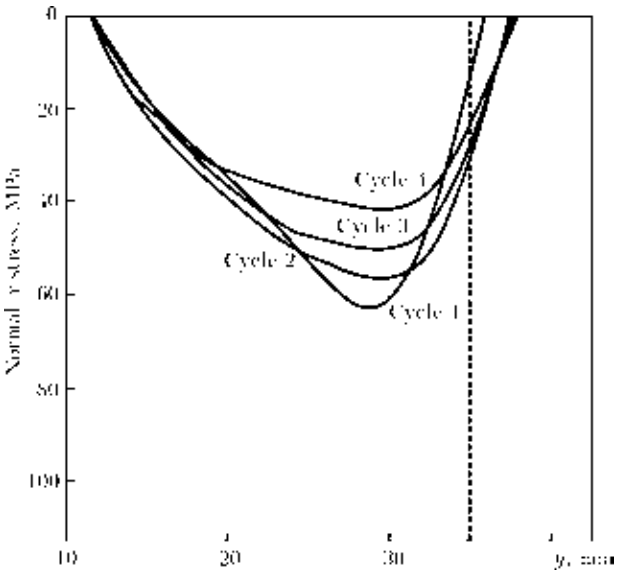

Figure 2. Traversal stress behavior

and sideways of the heat source with a nearly constant magnitude, was present in every process cycle. This compression field also appears within the zones created by the cutting planes (see Figure 1). This fact makes a more accurate consideration of the stress behavior necessary since no traversal compression will be present after the outer parts have been removed once due to model reduction. Figure 2 shows the traversal stress behavior during the first four process cycles. The dotted line within the diagram marks the heat source position along the y-axis. The snapshot is taken at y = 35 mm within the boundary zone at half sheet thickness. It can be seen that the stress magnitude decreases with proceeding cycles. In parallel to this a stepwise increase in temperature can be observed. Therefore the conclusion is made the lower stress magnitudes come from higher temperatures which lead to yield strength reduction.

In order to compensate the absent collateral resistance at boundary zones the missing amount of pressure is artificially added. This is achieved by applying a surface pressure function to the upper half of the boundary side. Suchlike limitation is motivated by the fact that 85 % of all material volume undergoing plastic deformation is placed in the upper half of the sheet. The behavior of the pressure function is put on a level with the compression stress depicted in Figure 2 (cycle 1) and stepwise decreased (by 10 %) over the proceeding cycles. Higher stress magnitudes that appear near the upper surface of the sheet are presently not taken into account. This simplification is accepted in respect to the desired reduction in computation time. In Figure 3 the boundary condition based on previous considerations for the first process cycle is shown. It depends solely on the distance dy to the heat source midpoint along the y-axis. The intention of the given mechanical boundary condition is to improve the accuracy of the calculated bending angle that is traversal to the irradiation path. The condition does not address the effect of a slight longitudinal bending that can be observed due to lower

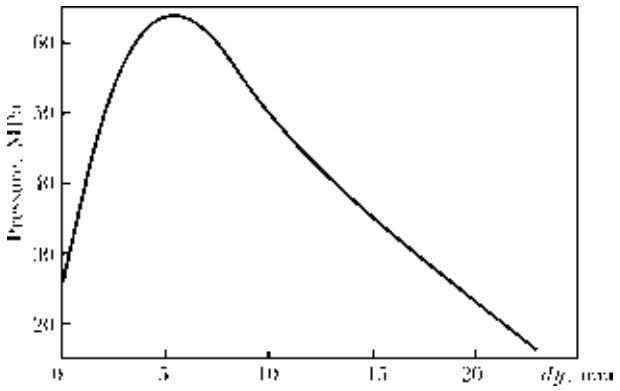

Figure 3. Mechanical boundary condition

stiffness in y-direction. A respective extension of the boundary condition is currently investigated.

With the availability of the reference modeling the reduced midsection is obtained in ABAQUS by the deactivation of undesired elements. The boundary conditions are implemented using the user subroutines DFLUX and DLOAD. After the simulation of the desired number of process cycles is carried out the separated parts are reintegrated in order to create an overall result. For this purpose an intermediate step has been introduced where the previously simulated midsection is cooled down to 20 °C. The time needed for this one-time calculation is very short. The reintegration is then performed by the reactivation of the initially removed elements and the establishing of a balance of forces. The calculation time for this last step can be neglected. As a positive side-effect of the rejoining the previously calculated too large longitudinal curvature is significantly reduced.

Results. The computation time for the simulation of one process cycle using the reduced geometry and boundary conditions is 5 times shorter than the reference simulation time.

The bending angles calculated using the reduced modeling and the introduced boundary conditions have provided a good agreement within a deviation of 4.5–11 % (Figure 4). Another configuration with a modified mechanical condition where the 10 % decrease of pressure per cycle has been removed lead to much too large angles at higher number of cycles. Beside the configuration with the two boundary conditions simulations were also performed with one or

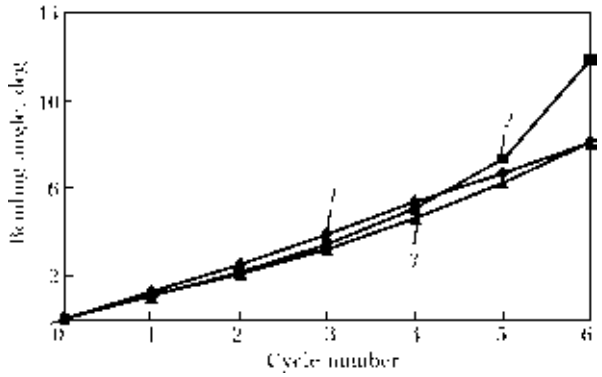

Figure 4. Bending angles behavior over cycles: *1* — reference model; *2* — reduced model, no pressure decrease; *3* — the same, with BCs

Table 1. Results of varied simulation set-ups

Simulation set-up	Bending angle at centerline before rejoining, deg
Reference model	5.35
Reduced model without explicit boundary conditions	3.58
Reduced model with thermal boundary condition	3.17
Reduced model with thermal and mechanical boundary condition	5.48

Table 2. Bending angles before and after rejoining

Simulation set-up	Bending angle, deg	
	Outer edges	Centerline
Reference model	5.30; 5.35	5.35
Reduced model with thermal and mechanical boundary condition before reintegration	3.79; 4.04	5.48
Reduced model with thermal and mechanical boundary condition after reintegration	4.92; 4.94	5.04

both of them being disabled. Table 1 provides the results after four simulated cycles (before the reintegration step). As expected the configuration with no explicit thermal and mechanical conditions lead to a low bending angle. The calculation with just the thermal condition available results in a computed angle lower than the one previously mentioned. Higher yield strength at the sheet upper side due to lower temperature is the reason for this.

The process of rejoining provides a change to the deformation state of the previously simulated midsection. Beside the decrease of the longitudinal bending it has also some influence on the traversal bending behavior. Table 2 displays the results on the traversal angles before and after the reintegration which are measured at different positions. It turns out that the traversal angles at outer edges and the center of the sheet are equalized after rejoining. This condition corresponds better to the situation observed within the reference model simulation.

Conclusion and outlook. The approach discussed above provides a good agreement with respect to the traversal bending angles which lie within a deviation of about 10 % compared to the reference result. The simulation time of one process cycle using the reduced modeling method is about 5 times shorter than the corresponding time for the reference simulation method. For the near future we plan to extend our method in order to handle not only the traversal model reduction but also the longitudinal one. With such a method the simulation could be limited to a small rectangular section that moves along the irradiation path with the velocity of the heat source. The boundary conditions have to be modified for this purpose. Another aim is to allow the irradiation path to be more complex, i.e. to include curves and straight paths.

Acknowledgment. We acknowledge the Deutsche Forschungsgemeinschaft for the financial support of the project VO 530/8-2 in SPP1146.

1. Geiger, M., Kraus, J., Vollertsen, F. (1994) Laserstrahlumformen raumlicher Bauteile. Bestrahlungsreihenfolge wichtig. *Bander Bleche Rohre*, 35(**11**), 26–37.
2. Holzer, S., Vollertsen, F. (1994) Laserstrahlbiegen — Ein beruhrungsloses Blechumformverfahren. *Produktion und Management*, 84(**1/2**), 8–10.
3. Hu, Z., Labudovich, M., Wang, H. et al. (2001) Computer simulation and experimental investigation of sheet metal bending using laser beam scanning. *Int. J. Machine Tools and Manufacture*, 41(**4**), 589–607.
4. Male, A.T., Li, P.J., Chen, Y.W. et al. (1999) Flexible forming of sheet metal using plasma arc. In: *Proc. of 7th Int. Conf. on Sheet Metal*, 555–560.
5. Chen, Y.W., Li, P.J., Male, A.T. et al. (1999) Flexible forming of sheet metal using plasma arc. *ASME/MED*, **10**, 935–940.
6. Li, P.J., Chen, Y.W., Male, A.T. et al. (2000) Flexible forming of sheet metal using a plasma arc. *J. Eng. Manufacture B*, 214(**2**), 117–125.
7. Komlodi, A., Otto, A., Geiger, M. (2004) On the way to real-time simulation of incremental laser beam bending. *LANE*, **4**, 1059–1070.
8. Vollertsen, F., Geiger, M. (1993) FDM and FEM simulation of laser forming: a comparative study. In: *Proc. of 4th Int. Conf. on Advanced Technology of Plasticity*, 1793–1798.
9. Pretorius, T., Woitschig, J., Kurgusow-Link, A. et al. (2005) Fast simulation of the temperature field for plasma jet forming. In: *Proc. of IWOTE on Thermal Forming* (Bremen), 203–210.

MECHANISM OF CAVITY AND WELD POOL FORMATION IN LASER WELDING

A.N. GREZEV
Laser Complexes JSC, Shatura, Russia

Many works dealing with formation of weld cavity and metal transfer to the weld pool in laser welding use two approaches — effect of vapor pressure or capillary forces. This paper reports the results of investigation on formation of a cavity and a weld pool in through penetration welding of metal. The investigations were accompanied with digital video filming and involved caulking of copper cores in steel before welding with further metallographic examination of molten copper motion in the weld pool. It has been ascertained that the metal in the weld cavity moves counterclockwise along the generating line and is released to the weld pool at a certain frequency. Frequency of metal release depends on the welding speed. The metal motion in the weld pool is pulsed in nature with the variable direction vector and resembles the mechanism of whirl emergence in the atmosphere or water. Mechanism of metal motion in the weld pool has also been determined. The work has been performed for the single- and double-beam welding.

In papers [1–4], particular attention has been given to liquid metal transfer in laser welding with incomplete penetration, to formation of the weld pool, as well as to subsequent processes of weld metal crystallization. Two mechanisms for metal transfer have been suggested: due to melt vapors pressure and a thermocapillary method.

This study represents the experimental research of welding cavity formation and of metal transfer from the cavity to the weld pool in laser welding with through penetration.

Digital video filming of the weld cavity with the weld pool performed by a special controlled filter «Chameleon» has permitted ascertain that the overheated liquid metal streams from the cavity to the molten pool tangentially counter-clockwise (Figure 1).

A frame-by-frame measurement of the liquid metal position has allowed defining of the liquid metal velocity. The initial velocity of the metal ejection from the cavity amounts to 30 mm / s and sometimes it exceeds this value. However the liquid metal velocity decelerates up to zero by moving off the cavity. This is derived from liquid metal slowdown by surface tension forces. The process is accompanied by insignificant scaling at the weld front. The liquid metal motion around the cavity precedes its moving at a tangent to the cavity. Evidently, the liquid metal velocity in the cavity exceeds its velocity in the molten metal pool. As soon as the velocity and the mass of the liquid metal in the cavity have reached the critical values, the ejection of the liquid metal into the weld pool occurs.

The measurements of the liquid interlayer surrounding the welding cavity made by the photos (see Figure 1) have permitted a rough determination of its dimensions. The interlayer thickness before the ejection of the liquid metal into the welding cavity is 0.75–0.82 mm and after the ejection it makes up 0.43 to 0.57 mm. Relying on the figures it can be supposed that in the time interval between the liquid aggressive ejections its outflow from the cavity to the molten pool with a lower but uniform and periodical velocity also takes place.

The following technique was used to attain an additional data on the metal melt behavior in laser welding. The specimen of 09G2S steel with the dimensions of 100 × 60 × 10 mm having the special channels with the diameter of 2.1 mm at different height (2, 5 and 8 mm) and with the interval of 10 mm was used for this study. The copper rods were calked into the channels of the specimen for the depth of 12 mm. Then the specimen was welded at the distance of 8 mm from the edge with the 10 kW power beam in helium as the assist gas. The beam was focused by KCl lens of 500 mm focal length with 1 mm focus embedding under the surface being welded. The welding speed was 1 m / min.

A microsection was made for each of the weld zone under study taking into account planes following on the longitudinal axis of the copper rod placed across the weld; the transverse axis of the copper rod along the weld; and the longitudinal axis of the copper rod in the weld plane.

On cavity formation, the metal in the beam-affected zone has mainly two states — liquid and vaporous. The liquid phase amount comes to no less than 97–99 %. The vapor formation process is more active at the cavity top. It decreases approaching the centre of the cavity depth and appears only slightly at the cavity root. This effect owes to lowering of laser radiation intensity as the depth of its penetration

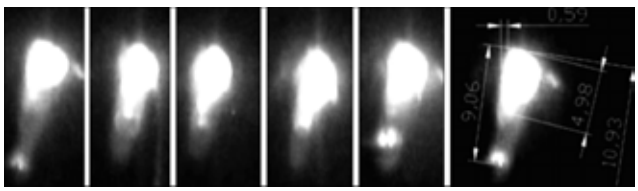

Figure 1. Mechanism of molten metal transfer from the cavity into the weld pool under the laser beam

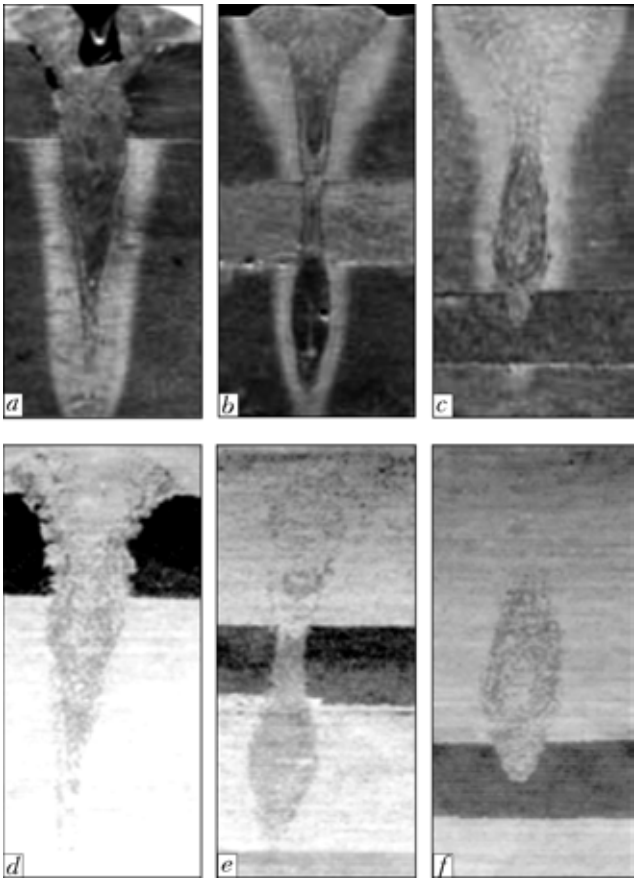

Figure 2. Patterns of copper rod melt moving in the different portions of welded joint cross-section: *a*, *b*, *c* — metallographic images; *d*, *e*, *f* — electron images under copper radiation

into the cavity is increased. This is related to the energy absorption for melting, as well as to vaporizing of metal and nonmetallic inclusions. The molten metal temperature is not uniform along the weld penetration depth at the cavity adjacent zones. The liquid metal temperature at the cavity root (where the laser beam intensity is lower as against that at the top) slightly exceeds the copper boiling point (2360 °C). This is obvious from the metallographic examination (Figure 2, *e*) where the observed process of copper evaporation is less pronounced. The evaporation process is more active (Figure 2, *d*) in the central part of the cavity and the quantity of the fragments with copper traces exceeds by 20–25 % the background amount of parent metal. The beam impact time for the metal is approximately uniform over the cavity depth. So for evaporation of greater metal amount, all other factors being equal, it is necessary to apply a higher temperature to the object. Evidently the metal temperature in the upper and middle zones of welded specimen thickness can approach 3000 °C, but not exceeds the iron boiling temperature (3050 °C) because no evidence of steel fumes was detected.

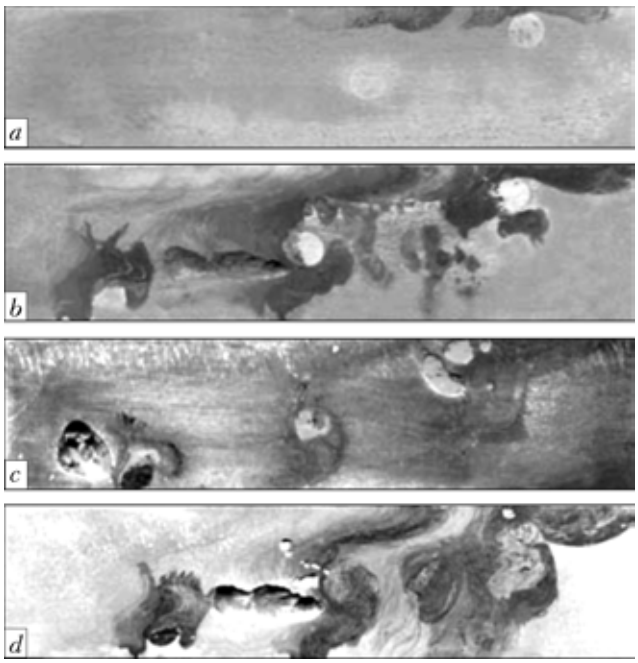

Figure 3. Patterns of copper rod melt moving in the different portions of longitudinal profile of the weld at the distance of 0.9 (*a*), 0.6 (*b*), 0.3 (*c*) mm from the weld axis and along the weld axis (*d*)

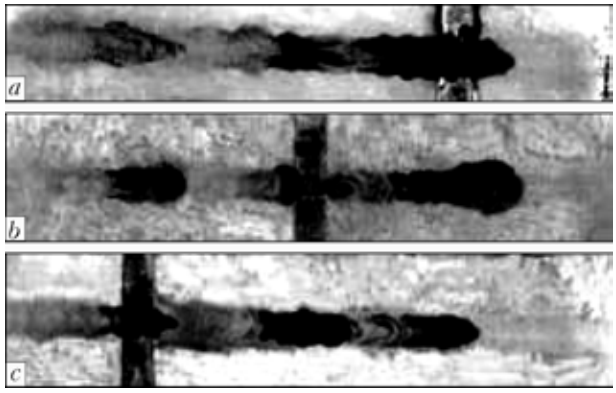

Figure 4. Patterns of copper rod melt moving at the different sheet profiles along the welded joint longitudinal axis: profile of upper (*a*) and central (*b*) weld portions, and of weld root portions (*c*)

It is obvious from Figures 2–4 that copper movement in evaporation is irrespective of the copper rod placement and is directed upwards the cavity depth in the welding direction as well as weld in the formation direction. Copper penetration into the upper melt part is observed in the direction of the shaped joint and in the welding direction at the distance up to 6 mm. At the weld root the copper spread through the same directions is more limited and does not exceed 2–4 mm.

The copper movement in the welding direction occurs also due to the rotation processes of liquid phase around the welding cavity and to the transfer of melt portions with copper additives into the sections adjacent to the weld metal.

It follows from the investigation results that the welding cavity is formed and maintained under laser welding process due to the centrifugal forces of liquid metal. In this case the welding cavity changes its

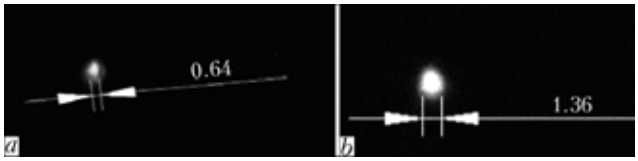

Figure 5. Outward appearance of the upper cavity part before (*a*) and after (*b*) liquid phase ejection from the cavity

diameter (Figure 5) during the welding, i.e. at the instant when the temperature, liquid metal velocity around the cavity and liquid phase mass approach their critical values, the cavity axis dimensions become minimal. At this point an overheated and extra portion of liquid phase is ejected into the weld pool, the cavity diameter is increased and so on. The measurements of the upper cavity part realized by AutoCAD 2000 allowed a rough determination of its dimensions (from 0.64 up to 1.36 mm in diameter). Obviously, the cavity dimensions are changed wavelike over its full depth similarly to the foresaid mechanism of liquid metal transfer, which is due to pulsating change of the vector and velocity directivity of the liquid flux.

The pressure in welding cavity varies simultaneously with liquid phase ejection. The maximal pressure value in the cavity is approached under a minimal cavity diameter. However in this case the pressure does not evidently exceed the atmospheric one or is equal to it. By increasing the cavity diameter in accordance with the foresaid mechanism the pressure in it drops below the atmospheric one, causing the assist gas penetration into the cavity. This is confirmed by different welding conditions in argon or helium as the assist gas, under which the plasma in the cavity influences the weld penetration parameters. The verification of the foregoing suggestion can be found in works [5, 6] which state the fact of helium humidification by water vapors. Under the cavity pressure exceeding the atmospheric one, helium humidified by water vapors could not penetrate into the cavity and the resistance of used steels to cold cracking would not reduce. The saturation with hydrogen through the metal pool surface over its full depth for the time less than 1 / 3 s is unlikely, thus a H_2O molecule dissociation shows of lesser activity in this case.

The welding cavity diameter increases as the laser beam output power is enhanced.

So in laser welding with deep penetration the welding cavity is formed due to the centrifugal forces causing the liquid metal phase rotation. The pressure in the cavity is below than atmospheric one and varies with the transfer of the liquid metal portions. As soon as the critical values of liquid phase rotational velocity and of mass are reached, its portion is ejected into the weld pool at a tangent to the cavity circle. The rotational velocities and mass of the liquid phase are no-uniformly distributed along the cavity depth. At the central part of the cavity the centrifugal rotational velocities of the liquid phase and its mass are lower than the corresponding values in the upper part and at the root. Thus the metal from the central part spires round the cavity and due to higher metal mass and velocities goes upwards to the weld pool in the welding direction. The similar process is observed in the root part of the weld pool.

1. Lopota, V.A. (1989) *Investigation of laser beam welding parameters*. Leningrad, 262.
2. Batanov, V.A., Fedorov, V.B. (1973) Liquid phase washout as a new mechanism of crater creation under plane complex vaporation of metal target by laser beam. *JETP*, 17(**7**), 248–351.
3. Palmer, H.J. The hydrodynamic stability of rapidly evaporating liquids at reduced pressure. *J. Fluid Mech.*, 75(**3**), 487–511.
4. Schuoker, D. (1993) Physical mechanism and modeling of deep-penetration laser welding. In: *Industr. Laser Handbook*. Springer, 67–73.
5. Anisimov, V.N., Baranov, V.Yu. (1983) On development of periodical structures on the surface of metals and semiconductors under pulsed CO_2 laser beam. *Poverkhnost*, **7**, 138–144.
6. Akhmanov, S.A., Emelianov, V.N. (1985) Effect of powerful laser radiation upon the surfaces of semiconductors and metals: nonlinear optical effects and nonlinear optical diagnostics. *Uspekhi Fiz. Nauk*, 147(**4**), 675–745.

HOT CRACKS IN PULSED LASER BEAM WELDS OF Cr–Ni-ALLOYED STEELS: DETECTION METHODS AND PREVENTION BY USING PREDEPOSITED PLASMA SPRAY LAYERS

H. HAFERKAMP[1], O. MEIER[1], B. BOESE[1], F.-W. BACH[2], K. MOHWALD[2] and U. HOLLANDER[2]
[1]Laser Zentrum Hannover, Germany
[2]Institute of Materials Sciences, Leibniz University of Hannover, Germany

Due to their comparably low investment costs, pulsed solid state lasers are used in a wide range of applications. Specific advantages of lasers, such as the low heat input, the high weld quality and the good potential for automation, are used by a wide range of users. With pulsed laser beam welding of high-alloy steels, due to the small molten pool volume, high cooling rates occur and lead to a higher general susceptibility to hot cracking. Industrially relevant stainless steels containing chromium and nickel such as the European grades 1.4404 and 1.4571 are concerned. Therefore it is important to introduce simple crack tests that can be carried out under factory conditions. Simple hot cracking tests for pulsed laser beam welding as found in literature will be evaluated first. Tests in butt and overlap welds with single and continuous spot welding will be shown and their results will be presented. Additionally, the influence of a filler metal layer applied on the substrate by using athmospheric plasma spraying will be shown. With the filler material consisting mainly of chromium and molybdenum, the ferritic content in the weld metal will increase, with a decrease of observed hot cracks.

Due to their comparably low investment cost, pulsed solid-state lasers are used extensively in small and medium enterprises. Therefore, the specific advantages of lasers, such as low heat input, small influence on material properties, minimized distortion and high seam quality, can be exploited by a wide range of users.

However, in pulsed laser beam welding, due to the small molten pool volume, extremely high cooling rates can be observed in the weld. For alloyed materials, this leads to a higher tendency towards hot cracking. Besides fully austenitic chromium-nickel steels and nickel-based alloys, this is also true for standard austenitic steels considered as weldable. Therefore, the prevention of hot cracks is important for a number of applications, for example in the vacuum technology. For the materials named above, there is presently no safe method for avoiding hot cracks during welding with pulsed solid-state lasers.

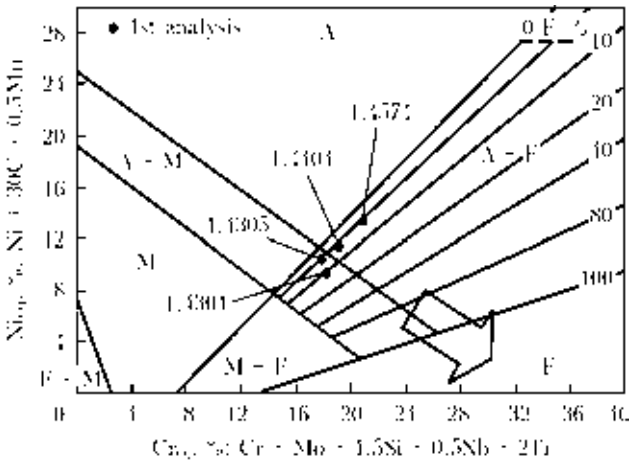

Figure 1. Schaeffler diagram containing featured materials

Hot cracks in austenitic Cr–Ni steels. Austenitic chromium-nickel steels usually have good weldability and a low susceptibility towards hot cracking. This is due to the fact that most steels of this kind solidify primarily ferritic. Only after solidification, the transformation from ferrite to austenite takes place, with a small remaining content of δ-ferrite.

In the material, this ferrite content usually can be metallographically detected by colour etching [1]. The ferrite content in predominantly austenitic structures depends on the chemical composition of the steel,

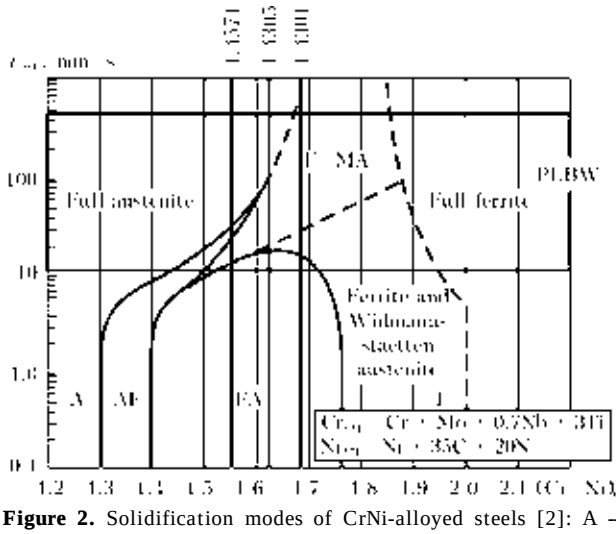

Figure 2. Solidification modes of CrNi-alloyed steels [2]: A — primary austenite; AF — primary austenite with eutectic ferrite; FA — primary ferrite with peritectic / eutectic austenite; F — primary ferrite; F / MA — primary ferrite / massive transformation to austenite

and can be read in the Schaeffler diagram (or in similar, more modern equivalents such as the WRC-92 diagram), as shown in Figure 1. However, an important precondition for the validity of these diagrams is that the cooling process has to be slow.

Unfortunately, in pulsed laser beam welding this precondition does not apply. The cooling time found here is in the millisecond range.

As shown by Lippold [2], the transformation process depends on the cooling rate. Solidification rate is a determining factor for the solidification mode, and therefore to the susceptibility for hot cracking. The connection between these factors can be seen in Figure 2. Using pulsed laser beam for welding CrNi-alloyed steels, the increased susceptibility towards hot cracking can be led back to the primary austenitic solidification. The low δ-ferrite content in the weld metal results in lacks of fusion between the austenite grains, especially when impurities, such as phosphorus or sulphur, are involved. According to the diagram in Figure 2, steels 1.4301 and 1.4305 will solidify primarily ferritic, and steel 1.4571 will change with increasing solidification speed towards primary austenitic solidification.

Process strategy. However, an increase of the Cr / Ni ratio would change the solidification mode towards primary ferritic. This can be done with filler material containing chromium or molybdenum. Due to the small dimensions of the pulsed laser beam welds, the deposition method for filler material has to be adapted. While the use of filler wire is possible, adjusting and maintaining a proper feed process is very complex, and therefore is mostly done by skilled workers with hand guided laser beam welding. Furthermore, the range of welding consumables is also limited, especially for the desired wire diameters of 0.6 mm or less. The use of powder deposition methods is also not feasible, because the powder residue has to be cleaned away before use. Another feasible method is the use of foil filler materials. These have to be set without gap before welding.

An alternative method described here is the deposition of filler material on the base material using the thermal spraying processes. The claddings are locally molten during the welding process and result in an alloying of the weld metal.

Due to its versatility, the atmospheric plasma spraying (APS) process has become important among the thermal spraying processes. It is characterised by high process temperatures, so that a wide range of materials can be processed [3]. The basic principle of the APS process is illustrated in Figure 3. In the plasma torch, an electric arc burns between an anodic copper-made plasma nozzle and a tungsten-thorium alloyed cathode.

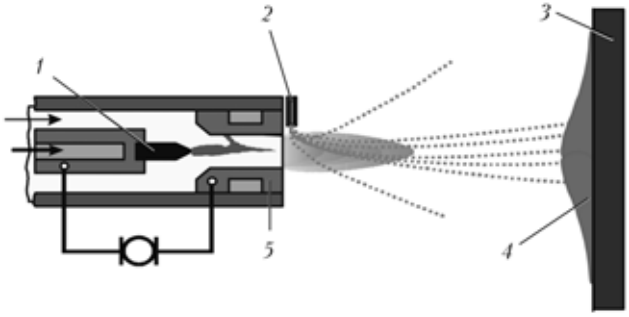

Figure 3. APS process principle: *1* — cathode; *2* — powder injector; *3* — substrate material; *4* — spray clad layer; *5* — anode

The whole system is water-cooled, the arc is started by high tension high frequency ignition. In the electric arc, the process gas, usually argon, nitrogen or argon mixture containing nitrogen, hydrogen or helium, is transferred into the plasma state (ionised). A plasma free jet of 20–50 mm length with temperatures of up to 15000 K is generated. Using a carrier gas (i.e. argon), the powder cladding material is injected into the plasma jet, usually in front of the plasma nozzle. The powder grains are dragged along by the plasma jet and therefore are accelerated towards the part to be clad. In the hot plasma the grains melt partly or completely resulting in small droplets of 5–100 μm in diameter impacting on the surface of the substrate. There, they stick on the surface and solidify spontaneously. Due to the high plasma temperatures and the high energy content of the plasma, materials with high melting temperatures, such as metals, alloys and especially ceramics, can be used for spraying. This is possible because the inert process gas suppresses the atmospheric oxidation of the spraying material.

Presently found in industrial applications are APS burners ranging from less than 10 kW up to water stabilised plasma torches with more than 200 kW nominal power.

Materials used. For the trials, substrate materials as found in Table 1 were used. They were chosen based on industrial relevance. Some rather classic examples of corrosion-resistant steel grades were chosen, namely the Cr–Ni-alloyed steel grade 1.4301 and the similar steel grade 1.4305 with additional sulphur content for improved machinability. As steel grades with additional molybdenum content, grade 1.4404 and the titanium-stabilised grade 1.4571 were chosen.

Table 1. Chemistry of substrate materials, %

Grade No.	C	Cr	Ti	Ni	Mo	P	S
1.4301	0.03	17.92	0.036	8.14		0.036	0.023
1.4305	0.05	17.30		8.10		0.031	0.270
1.4404	0.02	16.65	0.029	10.08	2.04	0.029	0.025
1.4571	0.04	17.36	0.050	11.24	2.20		

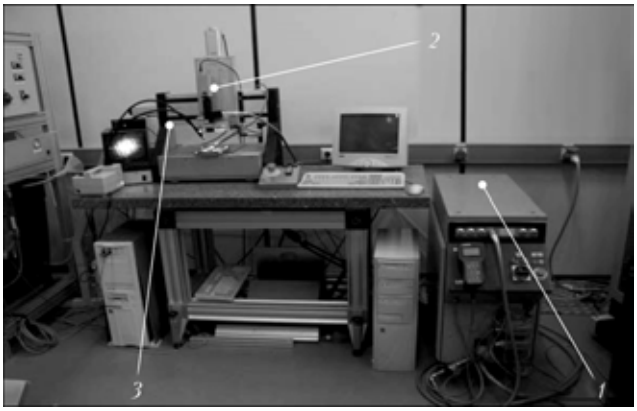

Figure 5. Test setup for welding

Based on the above considerations, the spray coatings used were composed of ferrite-building alloy elements, namely chromium and molybdenum. Based on a simple cylindrical model for the weld metal, the layer thickness needed was calculated with the results shown in Table 2. The weld metal in this model joins a stainless steel foil with 20 % Cr together with a base material with a similar chromium content. In order to achieve a hot cracking-resistant weld metal, an alloy content in the weld metal of 24 % Cr is desired. Based on these considerations, the thickness was calculated for a spray layer containing 100 % Cr / Mo to be used as filler material. As an example shown in Table 2, the calculation for welding common stainless steel metal foil of 100 μm thickness on substrate material with a weld penetration of 400 μm is resulting in a 100 % Cr spray layer of 26 μm thickness

Looking at the results, it can be concluded that layer thicknesses of 50–100 μm are sufficient for use with pulsed laser beam welding. Using the APS process, various layers were produced. For thin layers, the grain size of the powder was smaller than 53 μm, the surface of the base material was glass blasted prior to cladding. As can be seen in Figure 4, the claddings have got a layer structure and tend to be more porous than the base material. The rough blasting surface of the base material is filled by the spray cladding, leaving only a low porosity.

Welding. The specimens were welded using a lamp-pumped pulsed Nd:YAG laser with a mean beam power of 200 W *1* (Figure 5). Using a 400 μm fibre, the laser beam was guided to the process head *2* with an image ratio of 1:1. In setup the NC-controlled positioning system *3* was used.

Table 2. Results for calculation of layer thickness

	Cr / Mo content, %	Material thickness, μm	Cr / Mo content, %	Material thickness, μm
Base material	20	400	20	400
Metal foil	20	100	20	100
Weld metal	24	526	24	577
Desired spray layer	100	26	50	77

Butt welds with milled I-notch preparation and single spot welds on the surface were investigated. In order to minimise sputters, the pulse shape was ramped with a pulse one shown in Figure 6 because of the absorption rate of the material changes during the welding process. Depending on the welding task, the pulse peak power P_L varied between 1 and 2.8 kW, while the pulse length t was varied between 3 and 10 ms.

Results with different crack tests. In order to evaluate the result of the welds, standardised methods have to be used. Ideally, these methods can be applied under limited conditions of industrial use. Therefore, self-restraint tests were favoured. However, the self-restraint tests recommended by standardisation organisations are difficult to apply, as they are usually designed for high-power arc welding processes. Therefore, after a literature study the tests proposed by Weeter [4] in 1986 and Lippold [2] in 1992 were chosen for testing pulsed laser beam welds. Both tests have in common that the restraint level of the welds is defined by the shape of the weld.

Weeter's test for butt welds. Creating a defined weld undercut is the fundamental objective of this test. Comparable to the craters found at the end of electric arc welds, it is believed that undercuts are prone to hot cracking.

In order to make cratered weld spots, holes are drilled into the material prior to welding. These have to be smaller in diameter than the laser spot. Fur-

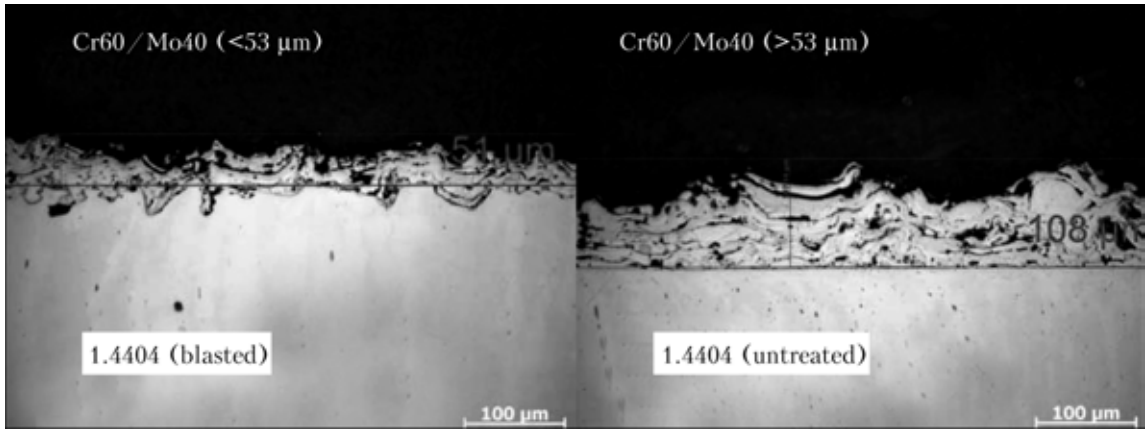

Figure 4. Cross-section of cladding layers

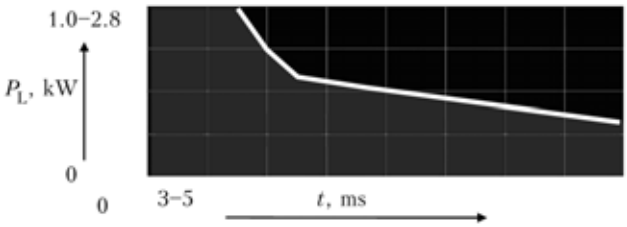

Figure 6. Pulse shape used for laser beam welding

thermore, they have to be rather shallow. The mechanical drilling process is therefore quite difficult to handle, so that experiments with excimer laser ablation were made. As this method was very time-consuming, and as the welding experiments did not show any results, this test was discontinued.

An alternative method described in Weeter's paper was joining parts in butt weld configuration, with increasing gap width of the weld preparation.

For this job, a clamping device was designed, in which the gap can be adjusted precisely using micrometer screws. A specimen welded in this device can be seen in Figure 7. After welding, the crack detection was done by grinding down the material.

Spot welding for the I-joint weld preparation. With the modified Weeter's test, useful results can be obtained for spot welding for I-joint weld preparation. The single spots of the seam in grade 1.4404 steel can be seen in Figure 8. Cracks could be detected starting with a gap width of 90 μm (see Figure 8, *c*). The pulse energy used in this experiment was constantly 12.3 J, with a pulse duration of 9.5 ms. Under these perfectly controllable conditions, the influence of an opening gap can be demonstrated.

The frequently occurring crack problems found in axial welds in shaft-to-collar-connections can be simulated using this test. On the other hand, the gap bridgeability greatly depends on the beam diameter and the material thickness. With specimens spray clad at the joint, the content of base material is low in the welded spots. Due to the layered structure, cracks occur in the spray cladding and wander on into the weld metal. This effect is shown in Figure 9, where the welded spots bridges a gap of 200 μm, with a 80 / 20 Cr / Mo layer having a thickness of 130 μm.

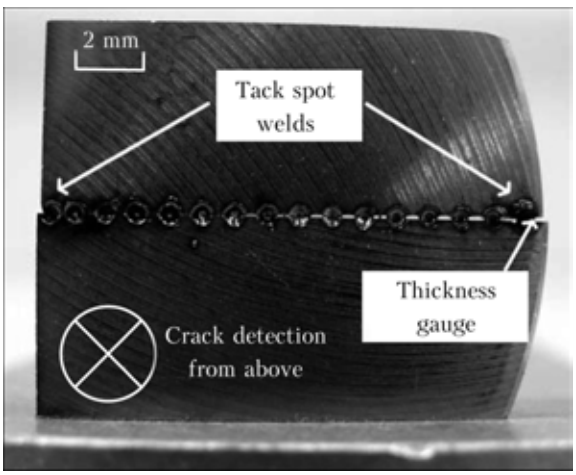

Figure 7. Modified Weeter's test specimen for butt joints

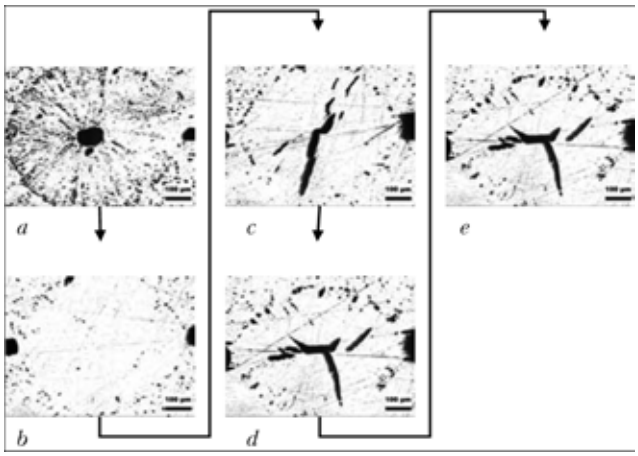

Figure 8. Crack detection in Weeter's test for gap width of 30 (*a*), 60 (*b*), 90 (*c*), 120 (*d*) and 150 (*e*) μm

The cladding of joint surfaces for butt welds is therefore not recommendable for pulsed laser beam welding.

Lippold's test on substrate material. This test [2] bases on the assumption that the welding parameters have a strong influence on hot cracking. Especially the ratio between the weld penetration depth and the weld width has got a high influence on the solidification morphology. The deeper the weld penetration in respect to weld width, the more the solidifying fronts will move towards each other, shoving impurities towards the middle of the weld, leading to hot cracking. Using this test, a matrix of spot welds is created on the substrate material, with variation of pulse peak power and pulse length. The welded samples are then grinded down, so that cracks can be detected metallographically. Ideally, the ferrite content is detected using colour etchants.

Results of Lippold's test on substrate material. Starting the investigations, the focus of the work was put on tests with various substrate materials in order to get a feeling for the performance of different materials in this test.

First reference material was steel grade 1.4301 (X5CrNi18-10), considered as weldable under all conditions. Results are shown in Table 3. A parameter matrix with variation of pulse duration and peak

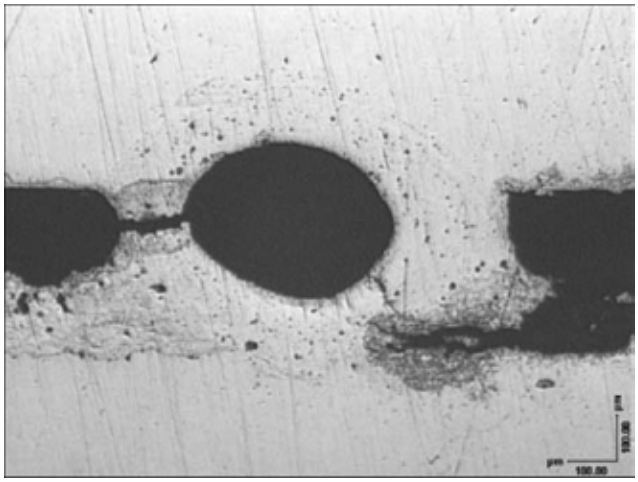

Figure 9. Crack in weld metal having been induced by spray layer

Table 3. Crack detection in steel grade 1.4301

Pulse peak power, kW \ Pulse duration, ms	1.0	1.5	2.0	2.5	3.0	3.5	4.0	4.5	5.0
1.0									
1.1									
1.2									
1.3									
1.4									
1.5									
1.6									
1.7									
1.8									
1.9						■			
2.0									
2.1									
2.2									
2.3									
2.4						xxx			
2.5									

power was welded using the pulse shape shown in Figure 6. Only in one case could be a crack detected, possibly due to a local impurity. The good weldability of this steel grade is proven once more. On the other side of weldability, steel grade 1.4305 (X8CrNiS18-9) can be found. This steel grade is a variant of 1.4301 for improved machineability.

Due to its increased sulphur content and according to the classic hot crack theory, its hot cracking susceptability should be considerably higher. This is confirmed by the results shown in Table 4. Especially with longer pulse duration and with high pulse peak power, weldability is limited. An even more critical behaviour can be observed with steel grade 1.4571 (X6CrNiMoTi17-12-2). Results of crack detection are given in Table 5. With this steel grade, welding is only possible using short weak pulses.

Table 4. Crack detection in steel grade 1.4305

Pulse peak power, kW \ Pulse duration, ms	1.0	1.5	2.0	2.5	3.0	3.5	4.0	4.5	5.0
1.0					■				■
1.1					■	■			■
1.2			■		■	■			
1.3						■	■	■	■
1.4									■
1.5					■				■
1.6						■			■
1.7							■	xxx	■
1.8							■	■	■
1.9				■			■	■	■
2.0							■	■	■
2.1					■	■	■	■	■
2.2							■	■	■
2.3			■		■		xxx	■	xxx
2.4							■		
2.5				■	■	xxx	■	■	■

Table 5. Crack detection in steel grade 1.4571

Pulse peak power, kW \ Pulse duration, ms	1.0	1.5	2.0	2.5	3.0	3.5	4.0	4.5	5.0
1.0					■				■
1.1					■	■			■
1.2			■		■	■			
1.3						■	■	■	■
1.4									■
1.5					■				■
1.6						■			■
1.7							■	xxx	■
1.8							■	■	■
1.9				■			■	■	■
2.0							■	■	■
2.1					■	■	■	■	■
2.2							■	■	■
2.3			■		■		xxx	■	xxx
2.4							■		
2.5				■	■	xxx	■	■	■

Table 6. Crack detection in steel grade 1.4571 with APS layer Cr / Mo: 60 / 40

Pulse peak power, kW \ Pulse duration, ms	1.0	1.5	2.0	2.5	3.0	3.5	4.0	4.5	5.0
1.0									
1.1									
1.2									
1.3									
1.4									
1.5									
1.6									
1.7									
1.8									
1.9									
2.0									
2.1									
2.2									
2.3									
2.4									
2.5									

No cracks!

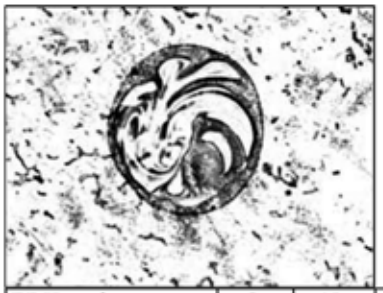

EDX analysis	Cr	Ni	Mo	Mn	Si
Dark zone	19.07	11.07	3.99	1.70	0.72
White zone	26.90	8.29	15.08	0.91	0.54
Base material	17.36	11.24	2.20	2.10	0.77

Figure 10. Spot weld (×200), and phase composition, %

Looking back at Figure 2, it can be seen that the probability of a primary austenitic solidification is much higher with steel grade 1.4571 than with 1.4301. The lack of primary ferrite leads to hot cracking here, although the sulphur content is low.

This problem is solved using filler material in form of a spray layer consisting of 60 % Cr and 40 % Mo and with a nominal thickness of 100 µm. This will increase the chromium equivalent in the material and will force a primary ferritic solidification. As can be seen in Table 6, this method works for pulsed laser beam welding.

With the spray layer, cracks were not observed.

In spot welds prepared with Adler stainless steel etchant, a brightness distribution similar to marmor stone could be observed (Figure 10). The reason for this was imperfect mixing of the elements in the molten pool. In an electron dispersive X-ray analysis (EDX) the reason becomes visible, namely while the dark zone has only slightly increased alloy contents compared to the base materials, the white zone has a high chromium and molybdenum content.

The main goal, i.e. increasing the chromium equivalent, was met. On the other hand, the white zone may contain brittle phases. Presently, an improvement of the mixing is being worked on.

CONCLUSION

With comparatively simple methods, tests for the determination of the hot crack sensitivity of pulsed laser beam welds in various stainless steel grades can be carried out. Two hot crack tests found in the literature were evaluated and modified for the specific welding applications. Especially the hot crack test developed by Lippold can be applied easily, and a wide range of parameters can be varied.

Plasma spray claddings containing chromium and molybdenum have been successfully applied for diminishing the hot crack sensitivity in pulsed laser beam welds in austenitic stainless steel. For butt welds, the new process has some problems due to the porosity of the sprayed layers. On the other hand, the new process has great potential for overlap welding of stainless steel foil on substrate material.

Acknowledgements. The experiments were carried out in the course of the project AiF No. 14.432N, which has been commissioned by the German Association for Welding and Related Processes (DVS) and that has been funded by the German Ministry for Economics and Technology. The authors would like to thank for the sponsorship.

1. Kou, S. (2003) *Welding metallurgy*. 2nd. ed. Hoboken: Wiley.
2. Lippold, J.C. (1994) Solidification behaviour and cracking susceptibility of pulsed-laser welds in austenitic stainless steel. *Welding J.*, 73(**6**).
3. Boulos, M.I., Fauchais, P., Pfender, E. (1993) Advances in thermal spraying-short course. In: *Proc. of Thermal Spraying Conference* (Aachen, March 1–2, 1993).
4. Weeter, L.A., Albright, C.E., Jones, W.H. (1986) Development of a weldability test for pulsed laser beam welds. *Welding J.*, **8**, 65.

LASER TECHNOLOGY IN THE AUTOMOTIVE MANUFACTURING

U. HOESSLBARTH
TRUMPF Laser und Systemtechnik GmbH, Ditzingen, Germany

The CO_2- and solide-state laser are adopted mainly in the automotive engineering. There are many examples of applications including the laser technology advantages. These adoptions take place by means of typical used components, such as for laser cutting of hydroformed tubes and hotstamping parts and also for laser welding of power train parts.

The use of lasers in the automotive industry for material processing has already a long history. With the availability of industrial lasers for material processing, automotive industry was one of the first industries to develop applications for this relatively new tool with the availability of industrial lasers for material processing. In 1973, Ford Motor Company has already purchased an underbody laser welding system for the body shop. The introduction of lasers in the automotive industry has always been in steps and linked to new applications. For example, in the early 1980s, the use of lasers has been expanded by gear parts welding, airbag components and welding of engine components like injection valves. In the 1990s, the laser started its way into the body shop with a very low pace. New applications like the steep increase in the use of tailored welded blanks worldwide and the use of hydroformed parts for pick-up trucks in North America enlarged the number of high power lasers drastically.

Hundreds of lasers show the advantages, cost effectiveness and reliability day after day. Most of these lasers are not installed in the plants of the car manufacturers, instead doing their job at Tier 1 and 2 suppliers worldwide.

Laser applications at Volkswagen. Driven by the VW AG, lasers have now made their way into the body shop. The first implementations in 1993 have led to the present situation of more than 800 installed high-power lasers throughout the global VW plants. The VW Group is the leader of laser applications in the global competition. Joining tasks are overlap welding, brazing of edge joints and the VW typical fillet joint on the trunk-lid and roof. The materials processed are hot dipped and galvanized zinc-coated automotive steels. The VW Golf, VW Touran and VW Jetta hold the «world record» for laser applications with more than 50 m on each body. There are close to 400 solid-state 4 kW TRUMPF lasers applied to perform the joining in the 6 body shops (4 in Europe, and in Africa and North America) producing these models. Laser joints can be found in all areas of the car.

The arguments to apply laser technology over more traditional joining methods are the following:

- increased process speed (joining), with the result of higher productivity and short cycle times. This allows additionally compact manufacturing lines with reduced floor space requirements. The increased process speed in combination with the small focused beam minimizes heat distortion;
- increased strength of the modules compared to most alternative joining methods by continuous welds;
- narrow or no flange can get welded, which allows weight reduction, and additionally it is one key for improved gas consumption;
- high flexibility of the laser technology. The same laser can weld, braze and cut. Additionally, the laser beam can get directed to different work cells by means of fiber optic cables.

What changes have been made between the Volkswagen Touran / Golf / Jetta and the new Volkswagen Passat? The Passat utilizes similar laser applications in the body, but additionally many lasers for cutting the new material ---- ultra high strength steel. Again a new requirement ---- cutting of ultra high strength steel ---- created a new challenge for the manufacturing engineers. The laser was the most economical answer for this requirement. With these new materials in combination with laser technology, the VW engineers designed a car with the highest stiffness values. At the same time, this has been achieved by reduced body weight, which is one of the main parameters to optimize the fuel consumption. Will Volkswagen be the only car manufacturer that uses lasers to this extend? Current applications at the VW Group are still new for most of the other car manufacturers. Most of the car companies are now going in the same direction.

Development of laser technology. The laser technology is rapidly developing. The development of solid-state laser technology has jumped into such a steep turn that nobody has seen before. With the improved beam quality of TRUMPF TruDisk lasers, the laser beam can be used more efficiently. The gain in maximum welding speed for a 4 kW laser beam is shown in Figure 1.

Possible applications for TruDisk lasers with beam quality of 8 mm mrad and power level of 4–8 kW are the use of scanners on robot arms. This high-power

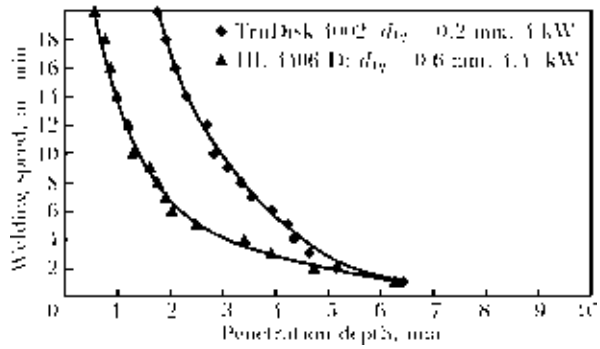

Figure 1. Maximum welding speed of mid steel for a 4000 W laser beam with different beam quality and using focusing optics D70

system was developed mainly by TRUMPF and German Car Manufacturer, and is now available on the market by TRUMPF. The new high beam quality TruDisk lasers allows the use of large focal length (of about 500 mm) with the result of large work envelopes. Figure 2 shows a typical arrangement of a TruDisk laser with a TRUMPF-PFO scanner welding a door assembly.

Why are now the robotically mounted laser scanners from such a huge interest?

Up to know the utilization factor of solid-state lasers in body in white lines have been rather low, in the range of 30–50 %. The reasons are the short standoff (useable focal length of 200 mm) and the time to travel from one weld location to another. Most of the time the laser welding head has to move around tooling and dive into the tooling due to standoff of less than 150 mm. Travel time from one weld location to another is now cut down from several seconds to a few milliseconds, by the fast moving mirrors of the scanner head. By mounting the scanner welding head on a robot arm, the work envelop is turned into a full 3D work envelop. There are practical no 2D parts in a car and this shows that this new feature is needed.

One of the first systems utilizing a 4 kW TruDisk laser in combination with a robotically mounted TRUMPF-PFO was applied at Volkswagen to produce the rear shelf of the new Passat.

The magnitude of using laser scanners goes much further than just replacing resistance spot welds through straight laser step welds. The laser scanner systems offer the full flexibility in location and geometry of the laser welds without a penalty in welding speed. The designers can now place joints with the best fit geometry to the location of choice to accommodate the results of the calculation / simulation programs. This will optimize the number of welds needed, the stiffness / crash behaviour and has the potential to optimize manufacturing cost.

In order to keep the laser technology as a competitive technology, there are many steps to reduce the cost for the laser technology. Due to new developements in laser technology the cost for laser beam sources has been reduced and this development will continue. The electrical efficiency has been increased from 2 up to 25 % during the last 3 years. The target for further cost reduction is now in the

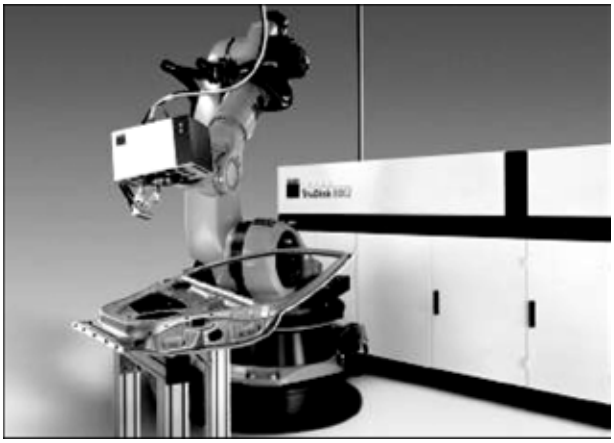

Figure 2. Work envelopes robotic scanner

auxiliary equipment and even in the enclosure. With the introduction of safe robots and safety improvements in the laser controls, the use of less costly enclosures are possible, as shown in Figure 3.

Future applications. The intensive use of laser applications in body in white has been demonstrated by Volkswagen and is now followed with the newest generation laser technology by other companies. The majority of automotive manufacturers, including Audi, BMW, DaimlerChrysler, Toyota, Nissan, Volvo and Hyundai, have based some of their joining tasks for years on laser technology. Ford and General Motors are exploring the benefits of lasers joining in BIW, as well and there are already some signs of implementation within both companies.

We have to keep in mind: laser technology is just one of many joining methods. The decision to implement the one over the other is determined by economical factors. Nevertheless, welding of zinc-coated steels by laser still needs special attention. There are only a few robust production ready solutions to weld zinc-coated steels in an overlap design available. The use of TRUMPF TruPulse laser is one of them.

The future of lasers in the body shop depends on the upcoming design of cars. The use of closed profiles in car design will bring many advantages to the car companies. Just to mention the material utilization of over 90 % and the production rate of more than

Figure 3. State of the art safety enclosure in combination with safe robots

Figure 4. Flexible manufacturing cell of automotive components based on standard machine tools

20 m / min. All this can be reached with integrated profiles that might already include fasteners. The production systems utilizing laser technology are ready and working for other industry sectors.

Another main area is the use of «standard machine tools» in a flexible manufacturing cell to produce parts without any parts specific tooling, as shown in Figure 4. In case the parts are designed for the cell, the cell can produce any mix of the parts in any single parts volume as long as it stays in the maximum cell production volume. Reuse of equipment will be a given as long as the parts follow the design guidelines. Using «standard machine tools» offer a step reduction in equipment costs and huge gains in quality of the manufacturing cell.

The body shop is the heart of automotive manufacturing and most visible part, and lasers are used mainly for welding and cutting. Moreover, the laser is also getting used for measuring, marking, structuring, cladding.

Summary. The transportation industry is in the middle of a revolution driven by some «mega trends». The customer's trends change faster and this requires more modells by reduced production volume per model. Additionally, there is a tendency to change the design of the cars, from the present unibody design to space frame design with plastic panels. This would require one-sided joining applications, plastic trimming / joining. The laser is one of the tools that could fullfil this task. The customers and the government demand further improved passenger safety. The use of high performance materials is needed, and these materials are difficult to joining or trim. And last but not least, our all task is to turn cars in environment-friendly transportation tools. Weight reduction with the use of new high performance materials, the use of a larger material mix per car and alternative propelling systems (like fuelcells and hybrid-engines) are some of these developments. With the «design for lasers», the laser technology is a very cost efficient tool to meet most of the new requirements.

LASER DRILLING AND PERFORATING OIL AND GAS WELLS BECOMING THE REALITY

S. HOSHOVSKIY and **P. SIROTENKO**
Ukrainian State Geological Prospecting Institute, Kiev, Ukraine

Perspective of growing energy potential of Ukraine consists in permanent increasing of deep production of hydrocarbons. Today in Dnipro-Donetsk hollow, which is the main oil and gas basin of Ukraine, are wells drilled with deep till 6000 m, that is why technical problems and expenditure considerably increase. So it will be impossible to drill rocks without new revolutionary methods. One of them is a laser drilling. Besides another important factor in production fluids is effective perforation of complete wells. However existent traditional methods of perforations with application of bullets and cumulative charges do not allow penetrating in formation more than 20--30 cm. That is not enough for good flowing of fluids. Consequently, laser drilling of oil and gas wells and their perforation completely is more perspective for oil and gas industry. Today laser drilling of vertical oil and gas wells and their perforating complete are perspective reality. The nearest technology to inculcation in oil and gas industry is laser perforating of oil and gas wells, which realizes unattainable possibilities for traditional methods of perforating. This method allows increasing flow fluids to well due to deeper penetrating of perforation into formation and high permeability perforating by laser method rocks. The nearest investigation tasks will be methods of delivering lasers radiation and rock removal from wells drilled by laser radiation, economics, portability, reliability, durability, safety, and environmental considerations.

Today wide-spread traditional method of rotary drilling gas and oil wells in which is used a drill bit on the end of a long length of the drill pipe also called a drill string, the last is rotated mechanical by apparatus from a surfaces. The drill bits which actually cuts up the rock are made of different shapes and of many materials, such as tungsten carbide, steel, diamond, which are specialized for different tasks of drilling and formation of rock. The drill bits are often abraded or shattered while drilling a deep well. Each replacement of bit demands drilling string removal from the deep well. The protection of the drilled well from destruction demands steel casing, which is installed and attached by concrete cement to a well bore. All this considerably increase time and expenditures on a drilling of borehole. The major reduction of expenditures of the boring can be reached with executing boring faster and reduction operation removal of a drill string, substitution of a bit and intervals of the installation casing. For the last time for solving mention problems researchers paid much attention to improvement of component structure of drill bits and applying of microwave technology during their fabrication [1, 2]. However, the greatest result can bring the usage of revolutionary laser technology of drilling and construction deep oil and gas of wells.

The urgency of the problem of the creation new instruments and technologies for well drilling proves to be true by necessity of jointing of an energy potential of Ukraine, which is possible under drilling oil and gas wells on a greater depths. Today gas pool in the Dnipro-Donetsk basin, the most perspective oil and gas basin of Ukraine, happens to drill at a depth up to 6 km. In Russia and the USA also increase the depths of the mining of oil and gas, and the need of the drilling hydrocarbon already on depth 4--6 km is appeared. Therefore oil and gas companies need instruments and technologies, which easy can execute the destruction of super hard rocks and structural materials in heavy condition of surrounding medium, in particular under high temperature 150--225 °Ñ and pressures 60--100 MPa.

In oil and gas industry for getting follow of hydrocarbons in development well is used the perforation with punching a wall casing and behind its cement for ensuring the tunnels through which fluids of a formations can be entered into well. Bullets or special explosive charges are used for preparing perforation. The high speed stream of the cumulative charge creates the high striking pressure 104 MPa on tunnel entry and 103 MPa at the end to perforation, which crushes rock, grain of sand of fractures, buries the broken down grains of grouting, loosen the clay particles and creates to tunnels, which has dimensions as a rule from 0.6 up to 2.5 cm in diameter and from 15 up to 30 cm of depth [3].

This traditional technology of perforation of oil and gas wells has the following deficiencies:

- insufficient control of the size of perforation holes and their shape;
- low flow features, aroused by depressing of practicability of broken down rocks for hydrocarbons;
- practicability of the changed zone is greatly lower than native forming of the shaping at the average on 80 % [4];
- optimization of charges and constructions of perforators does not greatly perfect the situation, as saved small depth of perforation hole in a formation of rocks and low their permeability after intensive mechanical affecting on rocks of explosive charges are saved.

Hereupon oil and gas industry needs for new technology of the perforations, which not only create effectively holes, but also minimize the breaches working quality of layer [3, 5]. In present condition, when

necessary to drill as possible deeper for extraction hydrocarbon, and provide the good influxes in working bore holes greater prospect has a laser drilling deep oil and gas wells and their perforated completion.

History of development of the studies on laser drilling and perforating oil and gas wells. The first early steps in study of the possibility of realization of the laser drilling and perforated completion oil and gas of the wells were made by «laser team», which has executed the project «Laser Drilling» (DOE Agreement DE-FC 26-NT 40917). The team included Gas Technology Institute (prime contractor and co-funder), Brian C. Gahan, Samih Batarseh; U.S. Department of Energy (DOE), NETL (sponsor and co-funder), Bill Gwilliam; Colorado School of Mines (subcontractor), Ramona Graves; Argonne National Laboratory (subcontractor), Zhiye Xu; Parker Geoscience Consulting {subcontractor), Richard A. Parker; PDVSA--Intevep, S.A. (participant), Humberto Figuerca, Alejandro Lagreca; Halliburton Energy Services (participant), Neel Skinner [6, 7].

The first study sponsored by Gas Technology Institute preceded this project, according to which super-power military lasers to prove that lasers were checked can cut all types of the rocks and that the super-power lasers are not required for flaking-off, melting and evaporation of rocks. During the second study, financed by NETL, were used two lasers of Argonne National Laboratory to determinate a minimum energy amount for cutting and melting rocks and to define the laser parameters for efficient cutting different types of rocks [7].

The following project «Application of High Powered Lasers to Drilling Deep Wells» (FWP-49066) has put the purpose more detailed to study processes under laser drilling of rocks through water and to construct wells head for laser beam drilling of rocks [1, 3]. The studies of the physical processes in rocks at laser beam drilling also initiated in 2004 at the Lebedev Physical Institute of RAS [8, 9].

Today doubts concerning an opportunity of possibility of the using high powered laser for drilling and perforation of oil and gas wells, which were on start of the laser project in the USA have been take off. Now studies are conducted for the reason determinations of the concepts of the building prototype laser drilling and perforations for ensuring the possibility of undertaking the field test for laser technology of the boring and perforating oil and gas wells [10]. Naturally, many problems still stand before researcher and the main of them are the heavy conditions of usage of the high powered laser equipment in well, but about this will be described below.

Study of different mode interactions between laser radiation and rocks and fluids. Carried out on studies at the Lebedev Physical Institute of RAS have allowed determining three following mechanisms of laser breaking down of rocks [8, 9]:

- ablation of dry materials;
- effervescence of water in surface layer of porous materials impregnated with water, and the consequent explosive expansion of water vapor conducting to effective breaking down of rocks;
- breaking down of hard materials by shock waves, forming a sample while screening of the plasma by a thin stratum of fluid transparent for IR radiations, put on a surface of a sample.

For qualification of these regularities the Laboratory of Gas Laser (Lebedev Physical Institute of RAS) in collaboration with Moscow State University of Mines, Colorado School of Mines and Solution Engineering (USA) has conducted the experiments on study of interaction of pulsed CO- and CO_2-laser with rocks, typical for oil and gas fields. Under the density power of the laser radiation on surfaces sample of up to 107 W / cm^2 to depending on conditions of the surfaces sample and conditions of its radiations, type and amount of sample liquid, are determined:

- energy of the laser pulse required for taking out a unit of the volume of material;
- specific mechanical impulse, passed to sample during its interaction with laser radiation;
- ablation pressure in zone of the interaction, and speed of scattering of expanding plasma torch in different gas-dynamical modes.

The most fundamental studies of the mechanism of the laser radiation interaction are conducted in USA with rocks for different types technological laser [7, 11--16]. So, the professor Ramona Graves (Colorado School of Mines, USA) confirms that depending on using and control laser energy it is possible to break off, melt or vaporize rock. This does not depend on the type of the rock the experiment is produced whit, all depends on used values of laser energy. It is forecasted, as for laser breaking down of rock the hardness of rock does not matter, the lasers will drill faster than in conditions of traditional mechanical drilling. Accordingly it is established to Ramona Graves, the presence of the liquids in rock can practically to help than prevent the process of the drilling. The rock saturated by oil or water under the action of generated by laser heats generates the additional pressure, and helps the process of the destruction. In Colorado School of Mines professor Ramona Graves and her team has studied the different sandstones, limestone, shale and granites in row laboratory experiments, and have shown that in each type of tested rock porosity and gas permeability was increased, but elastic modules were changed toward weakening of the rocks thanks to creation micro-fissures and dehydration of the clays.

However, it is necessary to mark that drill fluid present in wells influences mostly to transmission of laser energy to rocks. The opacity of laser radiation results in significant losses of the laser energy by its transmission from laser head to rocks [7]. It requires implementation of transmission of laser energy to destroyed rocks, having eliminated its interplay with down-hole drill fluids, constructional methods, some

of which is shown in [17]. It is necessary to stress that salt is the one of the most difficult rocks for laser destruction, it requires the significant specific energy of the laser radiation [6]. The carried out analysis of interaction of the laser radiation with rocks shows that rocks with oil and gas collectors are possible to destroy with the help of energy of technological lasers.

Potential advantages of the laser drilling and perforation of oil and gas wells. Laser drilling can raise efficiency of the drilling oil and gas wells thanks to more quick penetration into rocks; to removal of necessity to place a well casing in many situations; necessities to bring to the ground surface a string for substitution of a drilling bit; the more quick getting of well data; the reduction of pure drilling-time and influences on surrounding ambient.

The laser perforation of oil and gas wells can allow one to enlarge permeability of the rocks and as a consequent to augment inflow of fluids from a formation into the well [18]; to augment the depth perforated holes into formations rocks; to do them in any direction concerning a well bore; to set the sizes and shape perforating hole; to study different physical and chemical properties of formations rocks in real time during implementation of a laser perforation and to provide alternative to explosive technology of perforations, and to raise up ecological safety also.

Laser technology can be used for horizontal drilling, if the small sizes of down-hole equipments of the laser system of the drilling are provided.

Choice of type of laser for drilling and perforation of oil and gas wells and concept of constructing the laser drilling and perforation system at this base. Having analysis the sources of information on laser drilling and perforations of oil and gas wells it is possible to select two following approaches in constructing of the system of the laser drilling and perforation. First variant ---- when laser generator is situated on transport facility on day surface near the well, and second variant ---- when the laser generator is arranged inside the well in place conducting of operations of drilling or perforation [1, 3, 5, 6, 17]. Each of the mentioned variant has an advantage and defects. In the case of surface location of the laser generator restrictions on its sizes and mass are took off, conditions of the generator cooling is facilitated, however, the difficult problem of transmission light energy on greater distances in well is remain. At down-hole arranging of the laser generator there are problems of location of the one in protected housing of a small diameter and with providing the cooling since high powered laser generators, as a rule, require liquid cooling.

From the large variety of industrial laser for applying in system of the laser drilling and perforations with a location on a surface of the laser generator it is necessary to prefer fiber lasers with high power because of their high efficiency (up to 25 %), small sizes and masses, and also good coordination with fiber-optic line transmission of a light energy to well. However, even such modern laser can not provide transmission of light energy through the optical fiber on the large distances, today it is about of 200 m. Such result is insufficient for laser drilling and perforations of oil and gas wells, but certainly it is better than when working under gas laser generator, which, to it regret, agreed badly with optical fiber line that brings to its destruction during exploitation.

The most suitable laser generator for placing in the well during drilling and perforation are a powerful diode lasers. Yes, they have very small size and big efficiency. However, they have inherent to them defects when using in bore hole: it is necessary of the supplying for their usages with comfortable temperature conditions, which are as a rule provided by liquid cooling. Therefore diode laser generator for working in borehole needs a cooling system. The most likely this will to be a coil tubing system of cooling, in which is realized winding of flexibility tube on a spool, located on surface, and on though this tube is given coolant accordingly with greater velocity than during the usages laser generator in overland condition.

Take into account that the laser perforator does not need long operation in well, unlike for laser generator for a rig, therefore in this respect it will to be closest for engineering realization. The restraining factor here is need of the ensuring the small sizes of well equipments. Other bounding factor of the using high-power diode laser generator for bore hole will be a high price, today it forms $150--200 per 1 W of radiated power. The adduced problems of the using high power laser in bore hole must not to be a blind alley, from which there is not going out, this is only the cause for above mentioned developers to worked actively on the laser technology and constructors of geotechnical equipment, which have an experience in development of the different equipment for complex well conditions.

An important for a given moment is a creation of hyper thermal electronic basis [19], in composition of which today there is no only chips of low integration, but also microprocessors, which are very required for of well laser system. This will relieve creation of a control system over laser drilling and perforation of bore holes. The modern control system over laser boring and perforation must possess the broad function of the technical vision of the processes in bore hole, as well as conduct physical and chemical analysis of rocks in real time [17]. It is necessary to mark that all other traditional methods of the boring and perforations have no such possibility therefore in this case will be natural a rise in price of laser system of drilling and perforations because of extension of functional and technical possibilities.

The positive moment in construction of the laser system of drilling and perforations is that already today there are from row of the companies the offers to concepts of the constructing both such systems [6, 7], and radiating laser heads [1, 3]. This witnesses

that laser technology of the drilling and perforations approaches field experiments, certainly that they will open some problems else, but the motion to delivered purpose is impossible to stop already. In the near future researchers will go from concept of the construction of the laser system of the boring and perforations to principle of its construction and technical realization in prototype. According to the last information received from USA, professor Ramona Graves and her team plan to carry out development of prototype of system of the laser drilling during the following two years and to start its field testing in real conditions of the bore holes.

CONCLUSION

Today significant way for proof of realization of laser drilling and perforations of oil and gas bore holes is passed, researchers came closely to creation prototype systems of the laser drilling and perforations oil and gas bore holes. Proposed laser drilling has a most prospects of the using while constructing deep bore holes when an arise problem of drill the super hard rocks. In practice the ordinary mechanical boring is reasonable to execute in soft rocks, located at a small depth.

The most important task at a present time for realization of laser technology for drilling and perforations is a creation transmitting lines, capable to send the light energy on greater (5–6 km) distances with small losses.

To accelerate the development of prototype systems of the laser drilling and perforating oil and gas bore holes is possible by creation of thermo-baric cameras which is capable to completely reproduce the depth conditions of the bore holes on temperature, pressure and liquid on ground surface, and allowing one to conduct the laser destruction of a rock samples.

For efficient control of the process of laser drilling and perforations of oil and gas bore holes it is necessary to create a system of the technical vision which is capable to work in complex down-hole conditions. This will allow executing the processes of the drilling and perforations «not in blind», but with image them on ground surface for operator and other personnel of drilling company.

To receipt most advantage of the laser drilling and perforation technology in contrast with traditional technology of the drilling and perforations of oil and well bore holes it is necessary to provide the system of a laser drilling and perforations not only functions of control, but as well as checking-measuring functions for navigations and physical and chemical characteristic of the rocks, in which are executed operations of the drilling or perforations that will allow «intellectual» systems of the laser drilling and perforations to be provided.

Today synonymously is possible to speak that the most suitable laser generator for constructing of the laser drilling and perforation systems are the fiber and diode ones, which have high efficiency and small sizes. The high power fiber lasers are fit for realization of the system of the laser boring with surface location of the laser, but high power diode lasers will be utilized directly in bore hole under the appropriate their cooling, as well as thermal and hydraulic insulation during constructing of the system to laser perforation, since unlike system of the laser drilling it is not required a long cycle of stay in bore hole.

1. Reed, C.B., Xu, Z., Parker, R.A. et al. *Methods of using a laser to spall and drill holes in rocks.* Pat. 2006237233 USA. Priority 19.04.2005. Publ. 26.11.2006.
2. Xu, Z., Reed, C.B., Konercki, G. et al. (2003) Specific energy for pulsed laser rock drilling. *J. Laser Appl.*, 15(**1**), 25–30.
3. Parker, R.A. *Downhole lens assembly for use high power lasers for earth boring*. Pat. 6755262 USA. Priority 11.01.2001. Publ. 17.01.2003.
4. Xu, Z., Reed, C.B., Leong, K.H. et al. (2003) Application of high powered lasers to perforated completions. In: *Proc. of Int. Congress on Applications of Laser and Electro-Optics* (Jacksonville, USA, Oct. 13–16, 2003).
5. Salisbury, W.W., Stiles, W.J. *Method and apparatus for perforating oil and gas wells.* Pat. 4199034 USA. Priority 10.04.1978. Publ. 22.04.1980.
6. Gahan, B.C. (2004) *An overview of high power laser applications research for well construction and completion.* Gas Technology Institute.
7. Gahan, B.C. (2002) Laser drilling: understanding laser / rock interaction fundamentals. *GasTIPS*, Spring, 4–8.
8. Î'Brayen, D., Grews, R., Zvorykin, V.D. et al. (2004) In: *Fizika i Khimiya Obrab. Materialov*, **2**, 16–26.
9. Î'Brayen, D., Grews, R., Zvorykin, V.D. et al. (2005) *Ibid.*, **1**, 47.
10. Gahan, B.C. (2005) Fiber lasers show promise in processing rock and earth materials. *Industrial Laser Solutions*, Sept.
11. Gahan, B.C., Batarseh, S., Watson, R. et al. (2005) Effect of downhole pressure conditions on high-power laser perforation. In: *Proc. of SPE Annual Techn. Conf. and Exhibition* (Dallas, USA, Oct. 9–12, 2005).
12. Gahan, B.C. (2005) Putting the pressure on fiber laser perforations. *GasTIPS*, Fall, 18–21.
13. Gahan, B.C. (2005) Fiber laser offers fast track to clean perforations. *Ibid.*, Spring.
14. Gahan, B.C. (2005) Application of fiber lasers to rock and earth materials. *Ibid*.
15. Gahan, B.C., Shiner, B. (2004) New high-power fiber laser enables cutting-edge research. *Ibid.*, Winter, 29–31.
16. Gahan, B.C., Bataseh, S., Parker, R.A. (2003) Laser may offer alternative to conventional well bore perforation. *Ibid.*, Fall, 25–29.
17. Skinner, N.G., Smith, H.D. Jr., Jones, C.M. et al. *Drilling, perforating and formation analysis.* Pat. 2006102343 USA. Priority 12.11.2004. Publ. 18.05.2006.
18. Xu, Z., Reed, C.B., Graves, R.M. et al. (2004) Rock perforations by pulsed Nd:YAG laser. In: *Proc. of 23rd Int. Congress on Applications of Laser and Electro-Optics* (San Francisco, USA, Oct. 4–7, 2004).
19. Rogers, J.D., Ohme, B., Normann, R. (2005) New paradigm in electronics needed to take the heat of deep gas drilling. *American Oil and Gas Reporter*, Nov.

RESEARCH ON LASER REMANUFACTURING OF STEAM TURBINE BLADES

JIANHUA YAO[1], **CHUNYAN YU**[1], **QUNLI ZHANG**[1], **XIAODONG HU**[1], **CHENGHUA LOU**[1] and **V.S. KOVALENKO**[2]
[1]Zhejiang University of Technology, China
[2]Laser Technology Research Institute of NTUU «KPI», Kiev, Ukraine

Electric power industry is the basic industry of national economy. About 75 % of power all over the world comes from boiler-steam turbine-electric generator of heat-engine plant and reactor-steam turbine-electric generator of nuclear power station. Turbine blade is the key component of steam turbine, which operational life span directly influences the overhaul life of turbine generating units. Using CO_2-laser as the heat source, this research introduced laser cladding technique for recovering the failure dimension and laser alloying technique to strengthening the repaired layer, and thus to perform the laser remanufacturing of turbine blade. This paper described the method of laser remanufacturing for the 2Cr13 stainless steel blade and analyzed the microstructure, wear and cavitation resistance. The results showed that through laser remanufacturing technique the microstructure of treated blade was significantly changed, and the hardness of laser-treated layer was changed tremendously from surface to core material, which is in the range of *HV*0.2 737–250, while the hardness of matrix is *HV*0.2 200–250. The wear and cavitation resistance of the treated blade were increased to at least twice compare to that of the untreated ones after performance testing. Therefore, the laser remanufacturing technique may be applied more extensively in the failure turbine blades with its high flexibility, strongly controllable performance and free of pollution.

Along with the rapid economic development, questions about power shortage become highlighted. Steam turbine equipment plays more and more important roll in some important fields, such as petroleum, chemical industry, light and heavy industries. Turbine blade is the heart of steam turbine, which operational life span directly influences the overhaul life of turbine generating units [1–4]. It works in high temperature with high speed. Due to high-speed impact of the steam and water droplets, the leading edge of steam turbine blades is often prone to cavitations [5–6]. This makes blade loss its value and has to be abandoned. Generally, there are two solutions to the failure leaves: one is replacement, and the other is repairing. The traditional repair methods, such as surfacing, spraying and mosaic ceramic lining, are difficult to meet its working conditions. So it is urgent to find a new remanufacturing method to meet its requirements.

Since the development of applications of high-power laser in the 1970s, laser cladding technology has been developing rapidly. Using high-energy and high-speed laser beam as the heat resource, it can form a metal coating of dense, homogenous, high performance with high heating and cooling rates and adjustable metal powder material composition [7–9]. With the growing maturity of laser cladding technique, it was considered a particularly effective means of remanufacturing technology [10]. The paper introduced laser cladding technique for recovering the failure dimension and laser alloying technique to strengthening the repaired layer, and thus to perform the laser remanufacturing of turbine blade. Based on steam turbine blades of 2Cr13 martensitic stainless steel, this paper mainly analyzed the microstructure, microhardness, wear and cavitation resistance.

Experiments. In this paper, both laser cladding and laser alloying were used on turbine blade to realize the remanufacturing. First of all, laser cladding was carried out for 3D restoration through multi-cladding with special alloy powder. In this process, the interaction time between the laser beam and the powder material plays a crucial role for the desired successful cladding. Cladding was accomplished by delivering the selected powder through a powder feeder (FS-1 model) with a feeding rate of 3.04 g / min. The main cladding parameters were scanning speed v = = 0.30 m / min and power density q = 222 W / mm^2. Secondly, laser alloying method was used to enhance the properties of the cladding layer surface, and thus to perform the entire laser remanufacturing. The main laser alloying parameters were scanning speed v = = 0.35 m / min and power density q = 44 W / mm^2. Two processes were carried out in a laser system consisting of a 7 kW CW CO_2-laser and a CNC controlled working table. Temperature detection system (Sonser Therm MI16 model) was used to measure the temperature of both laser cladding and laser alloying on line. The basic principle of laser cladding and laser alloying is schematically illustrated in Figure 1, *a* and *b*, respectively. The argon was used as shielding gas during laser irradiation.

Before remanufacturing, the substrate and selected powder should be pretreated, so as to meet the demands of laser cladding and alloying. At first, specific mechanical polishing was performed to remove the surface oxides and improve the wetting property. Secondly, alcohol or acetone was used to clean the surface oils. The chemical compositions of 2Cr13 steel substrate, selected powders for laser cladding and alloying are shown in Tables 1–3, respectively. Two pow-

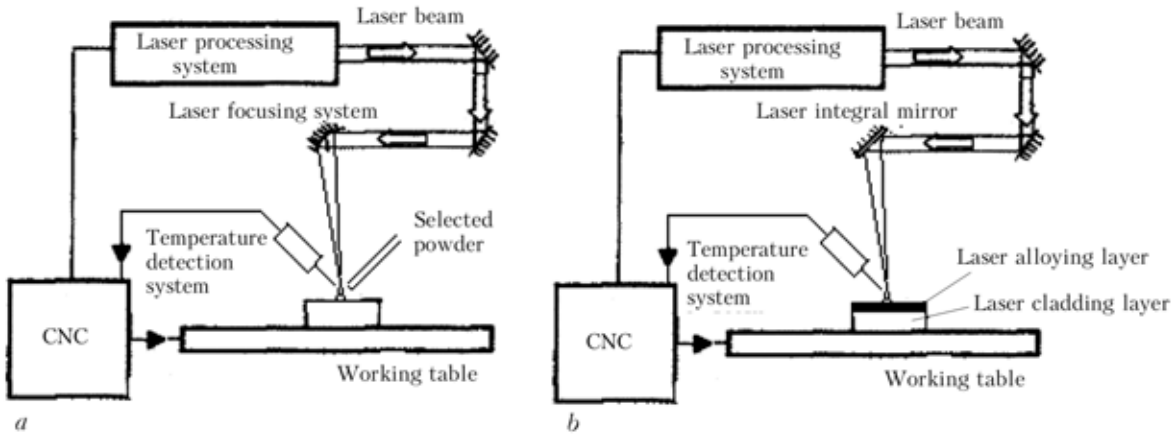

Figure 1. Schematic diagram of laser cladding (*a*) and laser alloying (*b*)

Table 1. Chemical composition of materials used, wt.%

Material	C	Cr	Mn	Si	Ni	Co	W	Fe
2Cr13SS	0.16–0.21	12.0–14.0	≤ 0.8	≤ 0.6				Balance
Powder for cladding	20.1	13.0		1.16	0.77			Balance
Powder for alloying		5.72			6.58	76.47	6.67	Balance

ders should be preheated to 110 ° C for 2 h and cooled in the oven to about 50 °C.

Results and discussion. *Microhardness and microstructure of layer by laser remanufacturing*. The surface microhardness was tested by HXD-1000 digital hardness tester. The load was 200 g and the action time was 15 s. The cross-section microhardness distribution after laser remanufacturing is shown in Figure 2. The test result showed that the surface hardness of remanufacturing section was increased obviously; the microhardness was between *HV*0.2 800 and 650 and the average hardness was *HV*0.2 737. Compared to the substrate *HV*0.2 200–250 microhardness, the layer after laser remanufacturing was 2 times harder. In the experiment, the thickness of laser remanufacturing layer was controlled in 0.7 mm through controlling the thickness of laser cladding. And the microhardness from laser remanufacturing layer to the substrate declined uniformly from *HV*0.2 800–250.

The sample after laser remanufacturing was cut along the scanning direction vertically, inlayed, marked, polished, burnished and displayed according to the standard of metallographical sample. The $FeCl_3$ was chosen as the corrosive. After eroding, the metallographical structure was observed using HXD-1000 digital microhardness apparatus. The cross-section is divided into four regions, namely remanufacturing layer, integration layer, heat-affected zone, and substrate (Figure 3). There are no pores or cracks. Compared with substrate (Figure 4), the remanufacturing layer surface microstructure was much finer, and there is a metallurgical bond between the remanufacturing layer and the substrate. The remanufacturing layer was composed of laser cladding and alloying layers.

In order to further research the microstructure of laser remanufacturing layer, the samples were observed under the FEI SIRION-100 scanning electron microscope. Figures 5 and 6 showed that the selected power for cladding fed to the molten pool of the substrate occurred some physical and chemical reactions. Some of the primary crystal of high-temperature melting point first separated out in fir-tree crystal from the molten pool. With the temperature reduced, the others solidified between the fir-tree crystals and then formed multi-eutectic microstructures with non-equilibrium crystal characteristics.

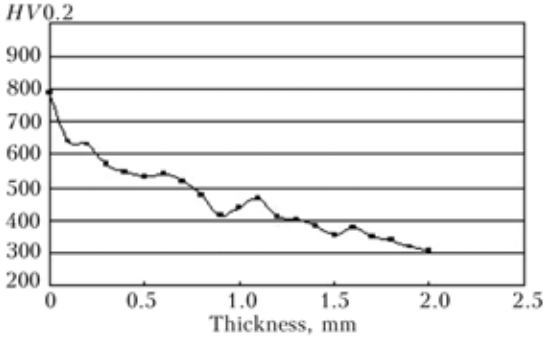

Figure 2. Cross-section microhardness after laser remanufacturing

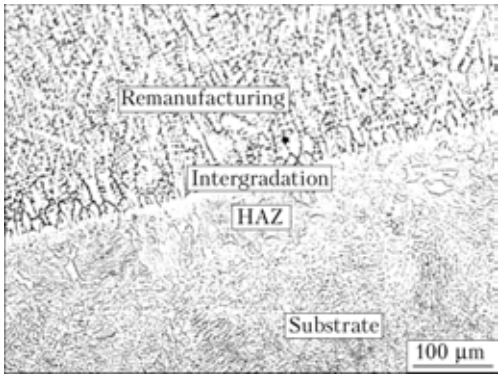

Figure 3. Cross-section structure of laser remanufacturing

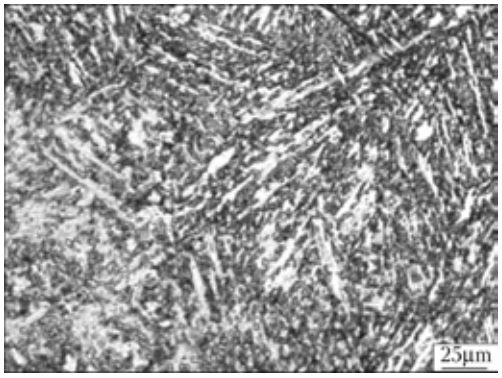

Figure 4. Metallographical structure of substrate

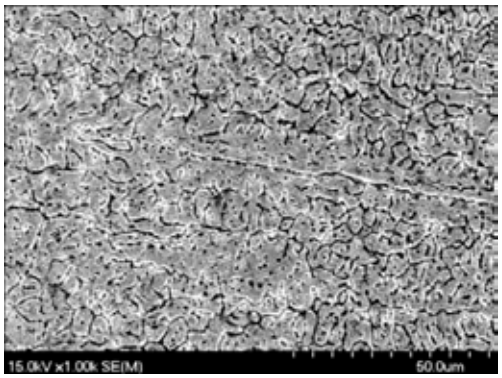

Figure 5. SEM-image of laser cladding layer

Figures 7 and 8 showed that the physical and chemical reactions of laser alloying were more complex than those of laser cladding. The main changes in alloying process included. Firstly, the surface was melted because of the laser irradiating, formed a molten pool, infiltrated the alloying elements (W, Cr, Ni etc.) instantly and carried some chemical reactions. The W and C formed WC ceramic particles distributing in the surface of the substrate dispersedly, increasing the hardness of the alloyed layer effectively; Cr and C formed Cr_7C_3 particles contributing to the hardness; Ni enlarged the austenite section and prevented from forming the second-phase particles, increasing the performance of corrosion resistance. Secondly, a few of the austenite could not transform duly due to the heating quickly and cooling quickly of laser irradiation. This layer possessed of high hardness and plasticity because the residual austenite existed in the surface. Both laser alloying and cladding layer formed the laser remanufacturing layer and the alloying layer outside made the laser remanufacturing possess of excellent wear and corrosion resistance because of its fine microstructure and high microhardness.

Wear resistance performance analysis. For some steam turbines of bad sealing, the blades of turbine could be worn inevitably because of some impurity

Table 2. Result of wear experiment of laser remanufacturing layer

Sample	Mass loss, mg	Coefficient, μ
Substrate	0.68	0.260
Laser remanufacturing layer	0.31	0.209

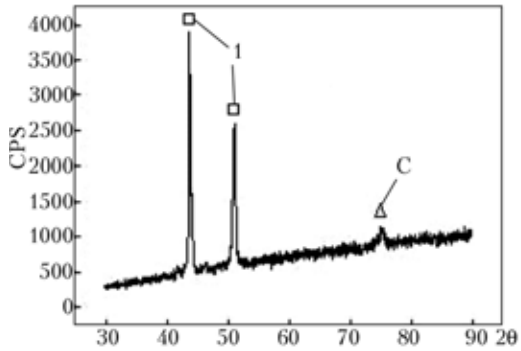

Figure 6. XRD analysis of laser cladding layer: *1* — Fe–Cr–C; *2* — C

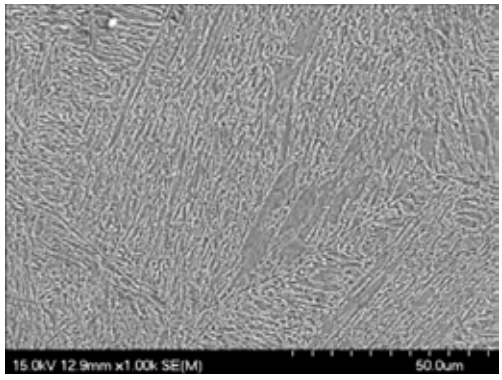

Figure 7. SEM-image of laser alloying layer

in cylinder. In order to analyze the wear resistance, frictional wear equipment (WM-2002 model) was used. The samples were cut into 8 mm disks, load was 150 g, and the standard compared sample was Si3N4 ceramic ball. After 2 h testing, the samples were weighted by BS-224S electronic balance (Germany). The testing result are shown in Table 2.

Observed the whole process of wear test, the wear process between laser remanufacturing layer and the standard compared sample was greatly stable. The Table also shows that the coefficient of friction was reduced about 20 %, and the relatively wear performance was $\varepsilon = 0.456$, which indicated that the wear resistance of laser remanufacturing layer was one time higher than that of substrate, then prolonged the operational life span of steam turbine.

After 2 h dry friction, the substrate and remanufacturing layer were observed under SEM for researching the wear pattern, which is shown in Fi-

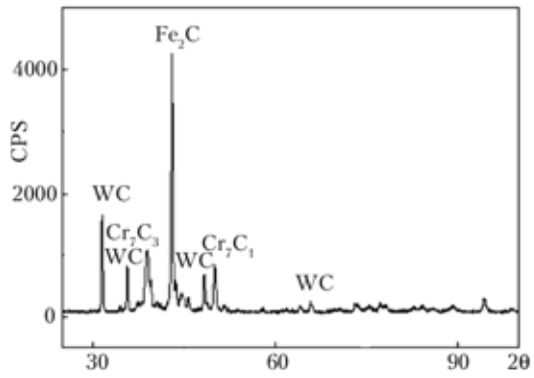

Figure 8. XRD analysis of laser alloying layer

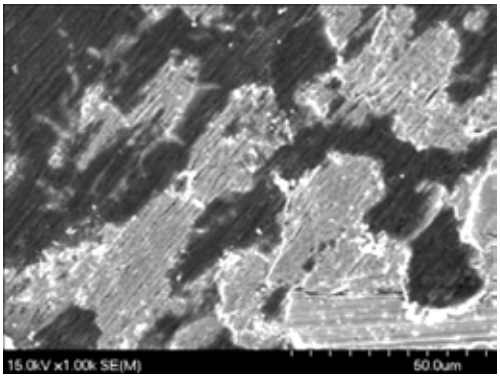

Figure 9. Wear morphology of substrate

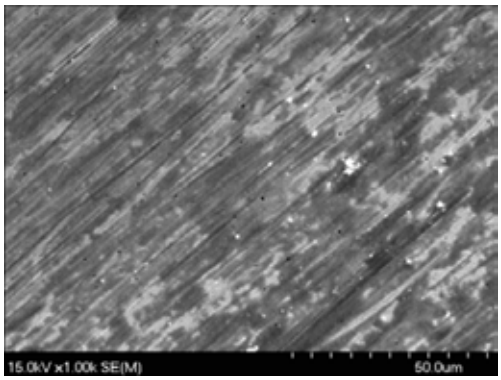

Figure 10. Wear morphology of laser remanufacturing layer

gures 9 and 10. The wear of laser remanufacturing layer and substrate were mainly abrasive particle wear, but the wear pattern was different. Figure 9 shows that after wear test, the scratch of the substrate surface was the same direction and the width of furrows was not uniform. Some adhesive objects were found on the surface with different size and different shape. Following the trace of flake-off, the area of the adhesive objects was also different. Figure 10 shows that the distribution of furrows of laser remanufacturing layer was uniform relatively and found no adhesive objects. The furrows were a bit shallow and narrow, which reduced the contact area of Si3N4 ceramic ball, so the wear coefficient and mass loss were lower than those of substrate. Some white disperse distribution spots were found on the wear surface. EDS analysis showed that the spots were WC and Cr_7C_3 hard phase, which improved the surface hardness and wear resistant effectively. The surface of laser remanufacturing layer owned uniform microstructure, fine grains and high microhardness of

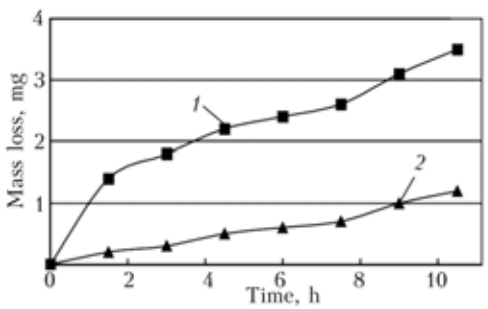

Figure 11. Mass loss–time curve for substrate (*1*) and laser remanufacturing layer (*2*)

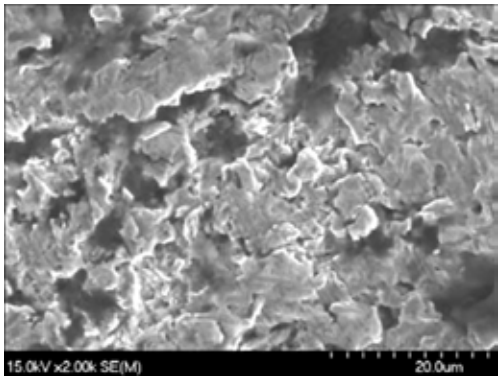

Figure 12. Cavitation morphology of substrate

*HV*0.2 737. This makes a great help to improve the wear resistance.

Cavitation resistance performance analysis. The JY96-ultrasonic wave cell breaking machine was rebuilt a US wave shock cavitation instrument, which included US wave generator, energy conversion device and taper amplitude pole on energy conversion device. The sample surface was abraded by metallographical abrasive polished and polished by buffing machine, then cleaned the sample for 10 min and weight by BS-224S electronic balance. The experimental solution was 3 % NaCl, test time ---- 10.5 h, weighted and cleaned the sample every 90 min and changed the NaCl solution. The mass loss–time curve is shown in Figure 11. After cavitation experiment, surface shape of the substrate and laser-alloyed layer were observed by SIRION-100 SEM.

The mechanism of cavitation has not been identified by a uniform knowledge until now. The main viewpoint is that the cavitation is HF blast wave coursed by collapsing cavity, which is equivalent to hundreds or one thousand atmospheric pressure acting on the material surface. Under continuous alternating stress, the surface of material was mechanical damaged, which resulted in the fatigue flake. After SEM researching the cavitation surface, cavitation pits were found (Figure 12), which were deep, uniform and massive, formed by flaking metal of surface. Figure 13 shows that in the same cavitation condition, the cavitation pits of laser-alloyed layer were a bit shallow and uniform relatively. No any crack was found on cavitation surface and none-cavitation surface because of the effect of quick heating and quick

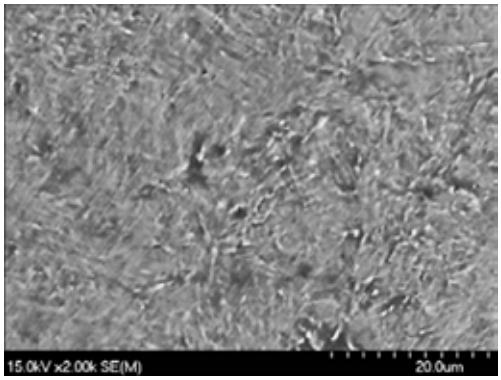

Figure 13. Cavitation morphology of laser remanufacturing layer

cooling of laser beam. The surface hardness was increased and the microstructure was fined. A mass of diffused carbide harden phase restricted the expansion of cracks, the flaking of surface metal and then reduced the erosion rate, which resulted in increasing the cavitation resistance one time than that of substrate.

CONCLUSION

Turbine blade was successfully remanufactured by laser cladding and laser alloying. Laser cladding technique was to recover the failure dimension, and laser alloying to strengthening the repaired layer. The surface structure of remanufacturing layer was much finer. There is a firm metallurgical bond between the remanufacturing layer and the substrate. After laser remanufacturing on 2Cr13 matrix, it was analyzed that the remanufacturing layer was different from the substrate obviously through adding new alloying elements and high power laser beam, obtained finer grains, formed diffused carbide harden phase and chemical compound, increased surface hardness 2 times than that of substrate. The microhardness and microstructure of laser remanufacturing layer were changed obviously, which resulted in better wear resistance and cavitation resistance than those of substrate. Laser remanufacturing is an easy processing with high efficiency and low cost, which has expansive application on increasing the wear and cavitation resistance, and enlarging the life span of steam turbine blades.

Acknowledgements. The authors would like to appreciate financial support from the Key International Science & Technology Cooperation Project of Zhejiang Province, China (2005C14009), Scientific Research Fund of Zhejiang Provincial Education Department, China (20051394).

1. Zhu, X.Y., Wang, Y.H. (2000) The development and actuality of fatigue life and failure diagnose. *Inform. on Electric Power*, **2**, 12–15.
2. Qiu, J.L. (1998) The fracture accident of heavy steam turbine. *Electric Power*, **4**, 8–11.
3. Sun, J.X., Zhang, Z.W., Sheng, M. (2001) Steam turbine fixing technology. *Shanghai Electric Power*, **5**, 42–43.
4. Lewis, B.L. (1982) Unfield approach to turbine blade life predication. *SAE Techn. Paper Series*, 821439.
5. Li, Y.G. (1994) A study on the cavitation erosion resistance of bead welding layer or nickel-based alloy. *J. Xi'an Highway University*, **14**, 77–80.
6. Zhao, M.H. (1999) Study on cavitation resistance of a new type precipitation hardening stainless steel. *Materials Sci. and Eng.*, 7(**4**), 60–63.
7. Wu, W., Wang, M.C. (2001) Advanced laser cladding and welding process for GT. *Gas Turbine Technology*, **4**, 25–30.
8. Ju, Y., Guo, Y., Li, Z.Q. (2002) Status and development of laser alloying and laser cladding in China. *Materials Sci. and Eng.*, 20(**1**), 143–145.
9. Kathuria, Y.P. (2000) Some aspects of laser surface cladding in the turbine industry. *Surface & Coatings Technology*, **132**, 262–269.
10. Yang, X.C., Li, H.S., Wang, Y.S. (2003) Laser refabricating technology for repairing expensive and important equipments. *Laser & Optronics Progress*, 40(**10**), 53–57.

CONTROLLED DEFORMATION OF SHEET METAL WITH DUAL-BEAM LASER HEATING

O.D. KAGLYAK, L.F. GOLOVKO, O.O. GONCHARUK and **V.S. KOVALENKO**
Laser Technology Research Institute of NTUU «KPI», Kiev, Ukraine

Application of laser beam for creation of 3D objects out of a sheet metal (rings, arcs, whirls etc.) is of high demand nowadays. For this purpose, the behaviour of the variety of materials (stainless and mild steels, aluminium, sheet plastics) [1–3] with different thickness was investigated, as well as various geometric shapes (stripes, disks, sectors). The researchers offer versatile irradiation and specimen placement schemes to obtain a range of parameters for process control. The present paper describes new method of sheet metal deformation with laser heating. There were obtained main factors and influential parameters of the process. Methods of mathematical modeling were used to figure out the core parameters of process. The temperature distribution in specimen during one and two-sided heating was obtained.

Key parameters of the process. We think that two groups of factors are of a great importance (Figure 1): firstly, group of energy factors determined thermal input, and, secondly, group of factors included properties of material and its ability to receive the thermal energy. To the first group we should attribute the irradiation parameters, power of energy input, distribution of energy on the irradiated zone, area of irradiated surface, shape of irradiated zone, velocity of movement of thermal source, trajectory of its movement and topography of irradiated zones. To the second group we attribute chemical structure of material, thickness of sample, geometry of sample cross-section, and initial stressed-strained state.

It is known that materials, which are not disposed to polymorphous transformation during heating and cooling, have the mechanism of thermal gradient as main mechanism of deformation [3]. In materials, which have polymorphous transformation, deformations determined by tension occurred as result of transformations, are added to the thermal deformations.

Dual-beam laser heating. Mode of deformation of irradiated material is described as a correlation of thermal tensions and tensions which occur during structure-phase transformations. So, in order to get maximum value of bending angle, we should provide optimal conditions for tensions to come into effect with appropriate sign and direction. During the one-sided irradiation, the rigidity of lower (not-heated) area of plate deteriorates the deformation process. Therefore, we recommend to use dual-beam irradiation.

The first beam irradiates upper side of plate to form defined tension. The second beam irradiates lower side of the plate to increase the material plasticity and its rigidity. The second beam is applied at some displacement S with respect to the position of the first beam in order to heat the lower area while cooling the upper area. Displacement S can be applied before or after the main laser beam, or on both sides (Figure 2). In other words, if we use Cartesian coordinates with the position of the main beam as a starting

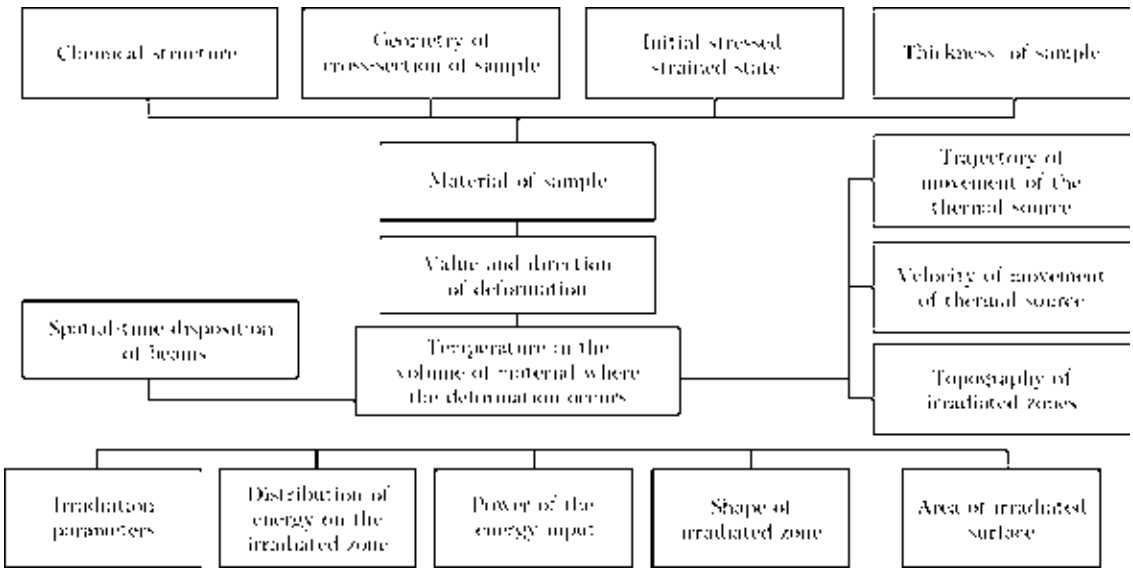

Figure 1. Most affecting parameters

point then point of application of the secondary beam has coordinates (–*S*; 0) in first case, (0; –*S*) in second case and (–*S*; –*S*) in third case. The value of displacement *S* may be the factor to regulate the value of deformation given that other factors remain unchanged.

Computational method of complicated cross-sections. In order to determine and to control the full plate deformation it is necessary to be familiar with the width of plastic deformation affected zone. For this purpose (with certain approximation) we can use the method of complicate cross-sections developed in NTUU «KPI» [4].

This method enables us to determine width zone of plastic deformation of contraction in the perpendicular direction to the axis of single run, and to determine distribution of maximal plastic deformation of contraction across the width of plastic deformation zone. This method is worked out for the butt-welded metal plate. The thermal task in butt welding of thin plate material is identical to the task of linear irradiation of single plate.

Assumptions for the method of complicated cross-sections:

- full longitudinal deformation in cross-section of the plate during heating can be represented by linear function of coordinates with different coefficient depending on the distance between laser beam and cross-section;
- stressed state in plate during heating and after the full cooling is linear;
- material of sample corresponds to the model of plastic-elastic body;
- elastic deformation on the ε_s level is stable at temperatures up to 500 °C (for steel). Then it decreases to 0 at the temperature of 600 °C according to the linear rule:
- thermo-physical properties of material do not depend on the temperature;
- deformations which take place during structure-phase transformations are not taken into account.

Core of the method of complicated cross-sections. This method has an assumption that the distribution of plastic deformation of contraction in the plate doesn't depend on its thickness. In such case the main characteristic of material shrinkage we can consider the diagram of zone of plastic deformation of contraction (ZPDC) in cross-section to the direction of the laser beam run.

The analysis of isochrone for the thermal field of similar scheme of heating in longitudinal section of the run shows that the temperature increases in the point at some distance from the axis of the run and causes temperature loads, and consequently results in the initiation of elastic longitudinal deformation of contraction [5]. These deformations gradually increase and for the points within the width of ZPDC and sometimes reach the value $-\varepsilon_s$ ($\varepsilon_s = \varepsilon_t = \sigma_t / E$). Then, at mentioned points, the plastic deformation of contraction gradually increases to the maximum

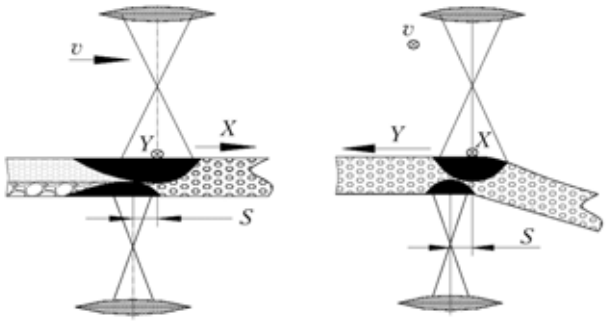

Figure 2. Schemes of second beam displacement

value while reaching the maximum temperature in this poins. That happens when the curve $\tilde{A}_m$ crosses this point. This curve is a projection on the area of the run of a movable space quasi-stationary curve of maximum temperatures $\dot{O}_m$.

Such mechanism of elastic-plastic deformations within ZPDC is investigated by kinetic researches of elastic-plastic deformation in similar thermal processes like butt welding of sheet material. So, within the area of the run we should consider two curves: $\tilde{A}_m$ mentioned above, and $\tilde{A}_b$ (Figure 3). The curve $\tilde{A}_b$ within the width ZPDC is a locus where the elastic deformations of contraction reach the value $-\varepsilon_s$ simultaneously for all points and the longitudinal plastic deformation starts to appear. In all points of curve $\tilde{A}_m$ excluding the zone of melted metal within the width of ZPDC during the heating we have maximum deformation of contraction which has different values for each point of the curve. The curves $\tilde{A}_m$ and $\tilde{A}_b$ intersect each other at some distance from the axis of the run on both sides of it. The points of intersection are the boundaries of ZPDC.

So, we have obtained two parts of ZPDC. They are represented by the segment *bnL* (from the point of crossing mentioned above curves to the axis of the run) and the right segment *bnR* (from the right point of crossing to the axis of the run). Correspondingly, the width of ZPDC may be estimated as a sum of *bnL* and *bnR*.

To analyze the maximum plastic deformation of contraction $\varepsilon ph(y)$ we introduce notation: $\varepsilon fh(y)$ is the full deformation; $\varepsilon\theta(y)$ is the thermal strain; $\varepsilon eh(y)$ is the elastic deformation, and

$$\varepsilon ph(y) = \varepsilon fh(y) - \alpha^* T_m(y) - (-\varepsilon_s). \qquad (1)$$

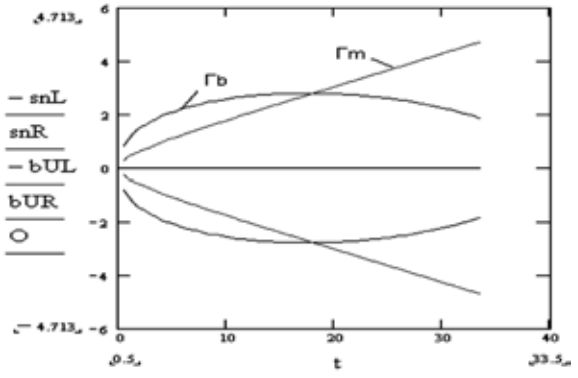

Figure 3. Curves $\tilde{A}_m$ and $\tilde{A}_b$

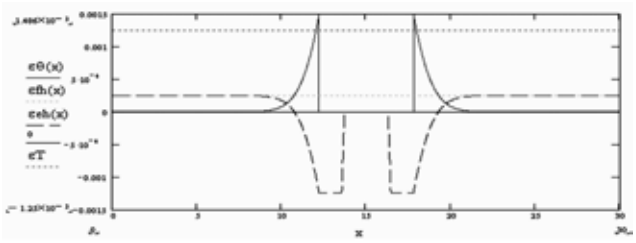

Figure 4. Values of thermal $\varepsilon\theta(x)$, elastic $\varepsilon eh(x)$ and full $\varepsilon fh(x)$ deformation during heating of sample

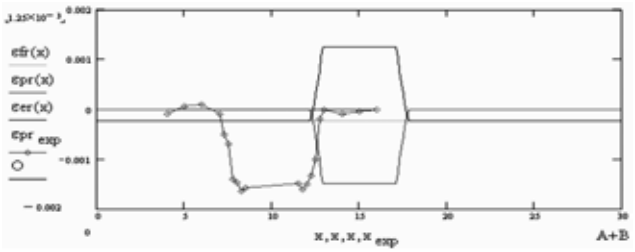

Figure 5. Values of residual deformations appeared after cooling of the sample

That is the equation for maximum plastic deformation of contraction in points across the width of ZPDC in terms of the full and thermal strain at these points when they are intersected by the movable quasi-stationary curve $\tilde{A}_m$ with the elastic deformation ε_e to the level $-\varepsilon_s$. We then can determine dependencies in the movable frame of reference XOY with the start in the point where the source of heating is applied, and with axes X and Y directed along and across the run correspondingly:

$$\frac{2q_n}{\delta_0}\sqrt{\frac{b}{\pi f(y)}}\exp\left[\frac{-f(y)}{4a}-\frac{by^2}{f(y)}\right]=T_m(y)\times \\ \times\frac{-\nu}{\omega}\left(\sqrt{a^2-\omega y^2}-a\right)=\Gamma_m(y). \qquad (2)$$

Example of calculation. The calculation and construction of graph was made using MathCAD. For instance, we propose to consider the calculation for the St3sp steel sample. Its thickness is δ = 0.5 mm, length of 70 cm, and the linear energy is q_n = = 1200 J / s. We enter the value of coefficient of thermal conductivity, volume thermal capacity, coefficient of heat transfer for the chosen material into the calculation scheme, along with the time value t which past from the moment when the heat source crossed across-section with the point on the distance Y from axis of the run. Then we calculate the value bnL and bnR using the formula:

$$tL-\frac{1}{\omega}\left(\sqrt{a^2+\omega bnL^2}-a\right)=0 \qquad (3)$$

and get bnL = bnR = 2.784 cm.

Then we obtain the values of thermal $\varepsilon\theta(x)$, elastic $\varepsilon eh(x)$ and full deformation $\varepsilon fh(x)$ during the heating of sample (Figure 4) and the values of residual deformations which appear after the cooling of the sample (Figure 5).

CONCLUSION

New method of controlled deformation of sheet metal with dual-beam laser heating is proposed. Calculation method of complicated cross-section is adapted to calculate residual deformations which take place during laser heating. By this method we can determine the width of zone of plastic deformation of contraction and the value of residual deformations.

1. Yoshioka, S., Miyazaki, T. et al. (2003) Laser forming of thin foil by a newly developed sample holding method. *J. Laser Appl.*, 15(**2**).
2. Okamoto, Y., Uno, Y., Namba, Y. (2003) Laser forming of plastics by YAG laser. In: *Proc. of LTWMP'03*.
3. Ramos, J., Magee, J., Watkins, K. (2001) Microstructure and microhardness study of bent Al-2024-T3. *J. Laser Appl.*, 13(**1**).
4. Prokhorenko, O.V. (2006) *Development and application of method of complicated cross-sections for calculation of residual deformations appeared during welding of unidimensional structure by longitudinal welds*: PhD Diss. NTUU «KPI».
5. Gatovsty, K.M., Krakhin, V.A. (1980) *Theory of welding deformations and stresses*. St.-Petersburg.

FACILITY FOR RESEARCH ON HYBRID WELDING PROCESSES AT COMBINATION OF PULSED MICROPLASMA AND LASER BEAM WITH CONTROLLABLE PULSE SHAPE

V. KIRICHENKO[1], **N. GRYAZNOV**[1] and **I. KRIVTSUN**[2]
[1]Central Scientific Research Institute of Robotics and Technical Cybernetics, St.-Petersburg, Russia
[2]E.O. Paton Electric Welding Institute of NASU, Kiev, Ukraine

Functional structure of a technological complex for hybrid (laser-microplasma) welding with application of a solid-state Nd:YAG laser, operating in a repetitively pulsed mode with wide range of energy and pulse shape, and integrated direct-action coaxial plasmatron is designed. Suggested algorithms of synchronizing operation of pulsed heat sources for study of joint action from positions of required welding properties achievement give the opportunity to obtain experimental results of laser-microplasma welding process with mild steel for automobile industry, aluminium alloy processing, and nanomaterials sintering.

Potentialities of the modern industry significantly depend on progress in technologies of material processing and joining. It is hard to overestimate the importance of creation and development of welding, cutting or surface modification techniques, based on application of arc discharge plasma as the most cheapest and available energy source. At present, the development of plasma technologies requires [1] concentration of energy in the plasma arc and stabilization of discharge at simultaneous increase of welding process productivity.

The alternative way, widely developed and used in the industry, is based on application of laser radiation as the only thermal source, so jointly with other traditional heating techniques [2, 3], including arc discharge, HF wave, or light irradiation. Due to high concentration of energy in the beam and opportunity of local action, a laser provides high productivity, deep penetration and high accuracy in adjustment of shaping parameters and weld metal properties.

Despite obvious advantages, opportunities of the laser as a thermal source are significantly limited for some applications. First of all, it is due to low efficiency of metal heating by laser radiation because of its high reflectivity at radiation wavelength, typical for the most of technological lasers. Another factor, decreasing efficiency of power laser application, is induced by laser radiation plasma over the metal surface, which reduces the energy part, contributed by a laser beam into a processed object.

A new approach to solution of the mentioned above problems is based on use of combined laser-arc and laser-plasma processes, essence of which is in joint action on processed object of laser radiation and arc plasma [4, 5]. At practical realization of the combined processes both thermal sources act on metal surface inside the common heating zone. Heating of metal by the electric arc leads to a rise of its temperature and, as a result, to increase of absorption of laser radiation. In turn, a small spot of laser beam creates on the metal surface a definitely localized zone with increased concentration of free electrons that raises the efficiency of the discharge. As a result, application of two different sources can lead to occurrence of positive synergetic effect, which reveals itself in action efficiency rise both for laser radiation and arc discharge [6].

To study the process of hybrid repetitively pulsed laser-arc processing of materials, an experimental facility, containing a pulsed microplasma source and a laser with a controllable pulse shape and beam coaxial to the arc, was created. It has been designed to consider the following tasks: estimate of potential synergetic effects in studies on penetration with variation of delays between the pulses of different sources; preliminary investigations on action of spatial and temporal parameters of the laser radiation and arc interpositioning on processing efficiency; revision of technical requirements to hybrid heating source; design of functional schematics and structure of equipment for repetitively pulsed laser-arc material processing; applied technological studies of hybrid welding for refinement of the functional structure and parameters of the complex; formation of the technical requirements to subsystems of the complex; study of technological potentialities of the equipment for hybrid material processing; experimental application of the technological process and equipment.

Actuality of the development is defined by the following key issues:

- creation of a low-power technological facility for laser-arc processing of materials ensures a wide variation range of processing capabilities for formation of the required properties of the weld metal;

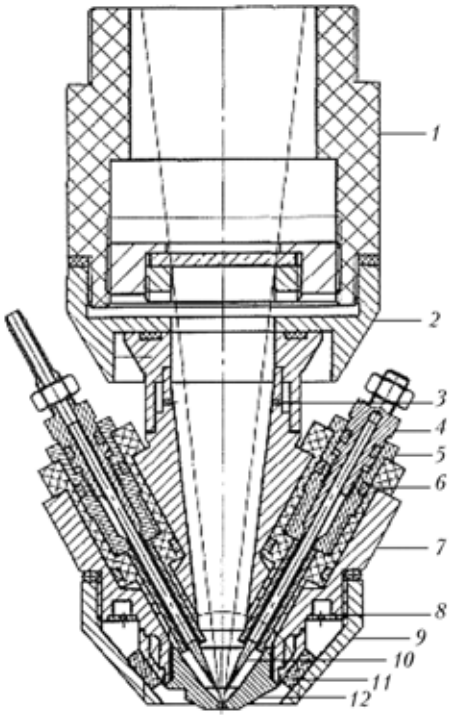

Figure 1. Construction of the integrated plasmatron with focusing system *1*, alignment mounting unit *2*, channel for input of plasma gas *3*, collet *4*, cathode unit body *5*, isolator *6*, plasmatron body *7*, gas splitter *8*, input nozzle for protection gas *9*, thermocathode *10*, porous filling *11* and plasma-shaping nozzle *12*

• joint action on metals can lead to increase in efficiency of energy transfer for as laser, so arc heating sources;

• maximum depth of penetration into metals, defining the thickness of welded parts, is more than one and a half higher in comparison with the only arc source that results in practical productivity doubling [7].

Technical parameters and structure of the laser-arc facility. As the laser base of the technological equipment for hybrid material processing, we have chosen a laser technological complex, intended for cutting of thick metal sheets and deep engraving. Main parameters of the prototype laser technological equipment are as follows:

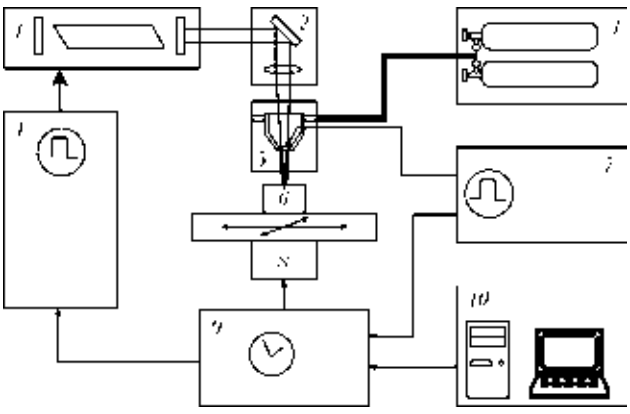

Figure 2. Functional schematics of the laser-arc facility (for designations see the text)

Laser type	Nd:YAG
Operation mode	repetitively pulsed
Pulse shape	digitally controlled, variable in a wide duration range
Operating frequency (limited by 120 W average power level), Hz	up to 100
Average power, W	up to 120
Pulse energy (limited by 120 W average power level), J	up to 3

As a source of electric arc, we have chosen the direct-acting plasmatron developed in the E.O. Paton Electric Welding Institute [8]. It has changeable plasma-shaping copper nozzle with output hole diameter of 1 or 1.5 mm, intended for limitation of lateral dimensions and spatial stabilization of the arc discharge. Construction of the integrated plasmatron allows us to bring focused radiation of the pulsed laser in the welding zone coaxially with the plasma beam.

Figure 1 shows the schematics and design of the plasmatron. It is designed to provide several modes of arc discharge, including CW and repetitive with straight and reversed polarity of the pulses at total power of up to 600 W. Figure 2 presents the functional schematics of the laser-arc facility. The laser complex consists of laser oscillator *1*, beam-delivering system *2*, and laser supply unit *4*. The plasmatron complex consists of pulsed plasmatron *5*, plasmatron supply unit *7*, and gas-delivering system *3*. The integrated plasmatron *5* is mounted to the laser focusing system *2*, and this fixation provides alignment of the beams. The control system *10* and clock system *9* ensure synchronization of the laser pulses with arc discharge pulses and two-axis table *8* motion for realization of hybrid mode processing of workpiece *6*. Appearance of the facility is given in Figure 3, and operation of the complex is shown in Figure 4.

Results and discussion. Figure 5 shows penetration of welded samples obtained with stainless steel and the laser-arc facility. The technical parameters of the arc source, corresponding to the presented welds, are given in Table 1. Motion of the table has been

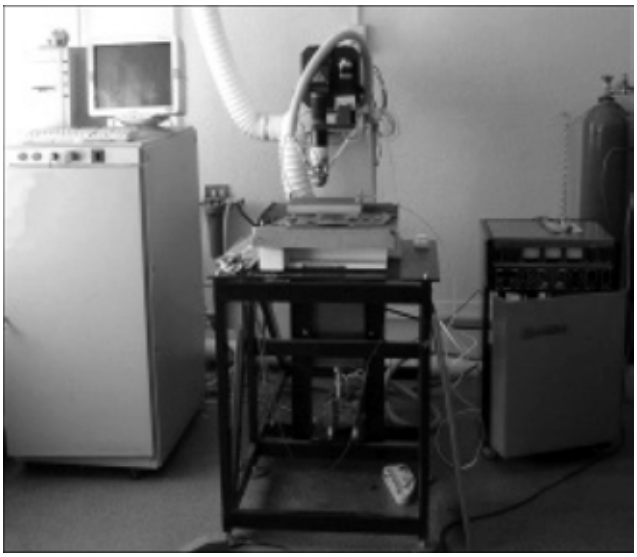

Figure 3. Appearance of the facility for research on hybrid welding processes

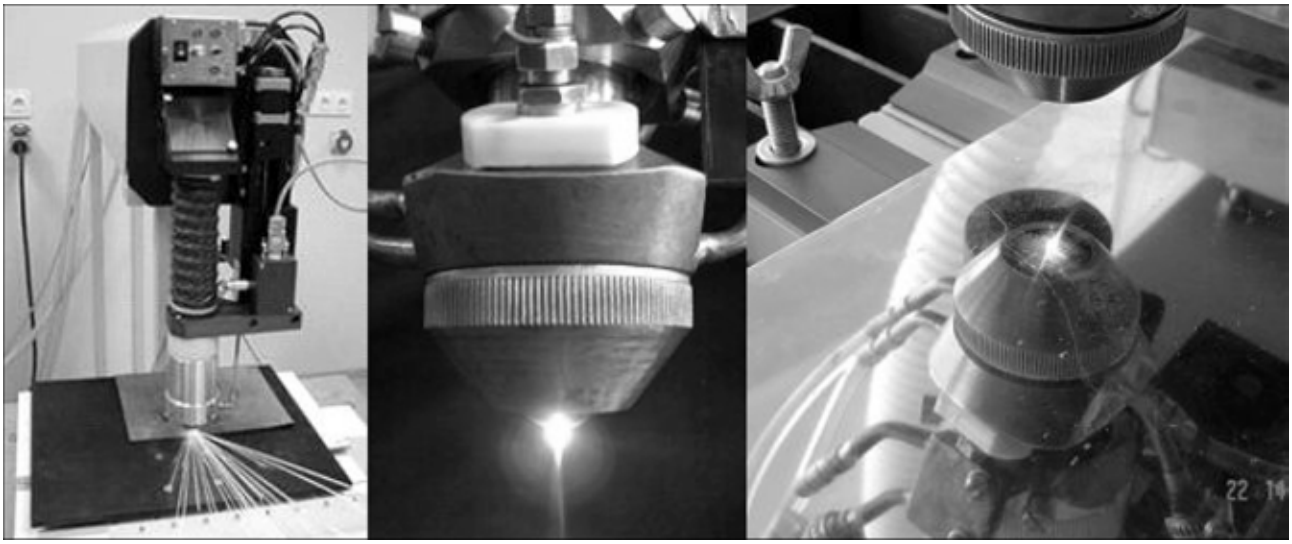

Figure 4. Different modes of laser-arc facility operation

leftward, and it is seen from the picture that addition of laser radiation to arc plasma action results in noticeable weld structure.

The preliminary results of experimental studies have shown noticeable refinement of the weld (shape stabilization) in comparison with the arc welding, even when a part of the laser radiation power is only 10–15 % of total input power.

To analyze the mechanism of this phenomenon, a series of experiments have been performed. First of all, electric measurements show reduction of the electric arc discharge voltage at laser plasma emerging (Figure 6). It can be considered as indirect qualitative proof of discharge efficiency increase at simultaneous usage of both tools. This effect theoretically described in [9].

Measurement of the arc discharge gap resistance in presence of laser radiation has been produced with low supply voltage of 5 V and limiting ballast resistor of 1000 Ohm to prevent arc discharge initiation (Figure 7). It is important to note that resistance of the gap during the laser pulse is even lower than that of ballast resistor (with the voltage on the gap below 2 V). It means that electron concentration in the laser torch is even higher than in the arc discharge.

Interaction effects for combination of laser radiation and arc plasma in welding of aluminum are even more noticeable due to surface alumina film, preventing stabilization of the anode spot for the arc discharge of the straight polarity. The laser energy in this case can be used for removal of the film in the limited zone

Table 1. Technological arc parameters for the welds obtained (see Figure 5)

Mode	Arc current, À	Pulse duration, ms	Pause duration, ms	Frequency, Hz	Welding speed, m / min
Pulsed	18	10	7	60	0.18
Pulsed					0.12
CW	16	–	–	--	0.30

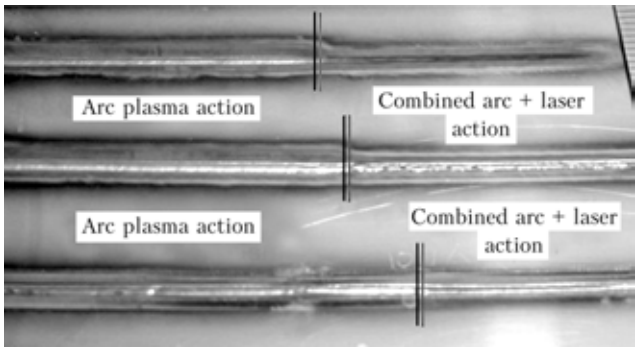

Figure 5. Weld structure at addition of laser radiation to the arc discharge in penetration welding stainless steel 1 mm thick at average power of synchronized laser pulses of 35–40 W (for the rest parameters see Table 1)

of laser focal spot. Figure 8 presents the results of the experiments on weld penetration for aluminum samples with arc pulsed discharge action and joint arc and laser action. Parameters of laser pulse in the experiments are presented in Table 2.

Variation of the laser power allows us to define experimentally the threshold intensity of laser radiation required to remove the oxide film. At excess of this value, arc discharge jitter disappears, and reliable binding of the anode spot to the laser focal spot takes place, as it is seen in Figure 8, *d*. The previous image (see Figure 8, *c*) corresponds to the threshold value of laser intensity and gives, according to Table 2, the required intensity for removal of the alumina film, equal to $6.5 \cdot 10^6$ W / cm^2.

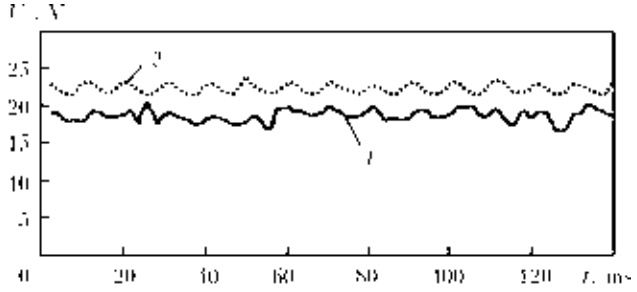

Figure 6. Arc voltage in conditions of arc and laser discharges with (*1*) and without (*2*) laser radiation

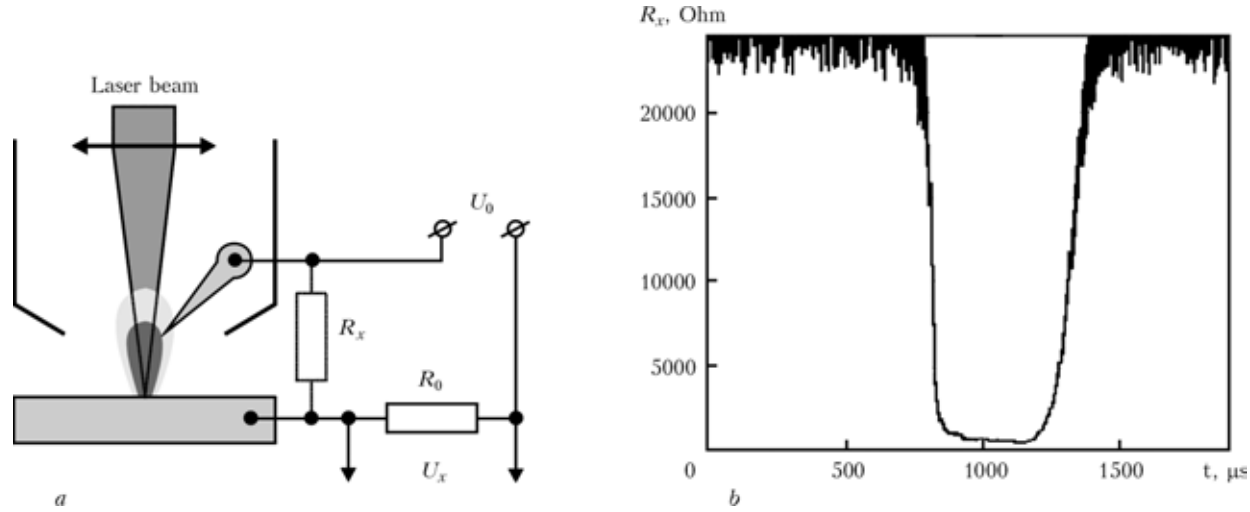

Figure 7. Schematic (*a*) and measurement (*b*) on resistance R_x of the arc discharge gap in laser torch at supply voltage U_0 = 5 V and ballast resistor R_0 = 1000 Ohm

Analysis of the film destroy mechanism has shown that two variants are possible: first of them is connected with absorption in the film itself with further evaporation, and the second one is due to absorption in the aluminum substrate (Figure 9). To estimate the temperature of the aluminum heating, it is necessary to solve the problem of thermal conductivity. In our case, lateral conductivity can be neglected, so the temperature rise for the rectangular laser pulse is defined by the following expression [10]:

$$T = \eta I \frac{\sqrt{\chi t / \pi}}{\lambda}, \qquad (1)$$

where η is the absorption coefficient of the aluminum surface; I is the power density of laser radiation; χ is the temperature conductivity; t is the time of action (pulse duration); and λ is the thermal conductivity.

In supposition that all energy goes on heating till the evaporation temperature, it is possible to obtain the expression for the required laser intensity. In this case, one obtains estimate from below, since it does not take into account losses of energy on melting, partial evaporation, needed to break the film, and weak lateral conductivity. The value of laser intensity, calculated by formula (1), is $4.5 \cdot 10^6$ W / cm^2, that well agrees with the experimentally received results.

Estimate of the second possible mechanism due to absorption in the film itself according with the expression, taking into account double pass of radiation through the film because of reflection from the aluminum surface

$$I = \frac{c\rho T}{\alpha t(2 - \eta)}, \qquad (2)$$

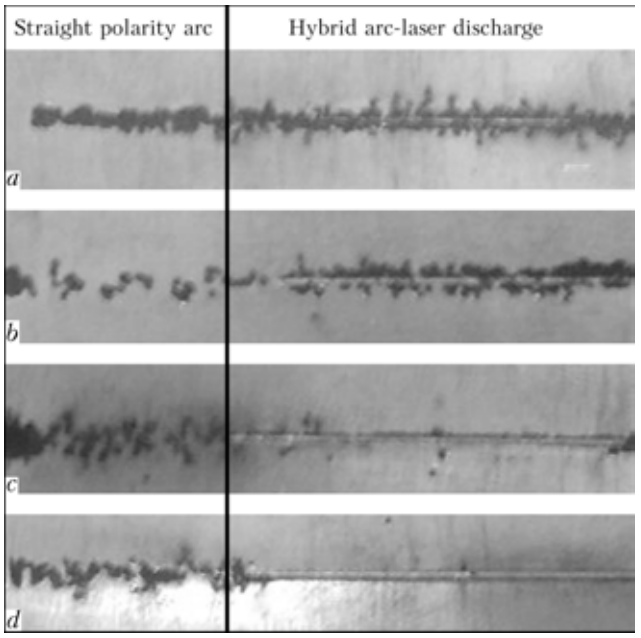

Figure 8. Weld penetration on aluminum surface in conditions of straight polarity arc and hybrid arc-laser discharge

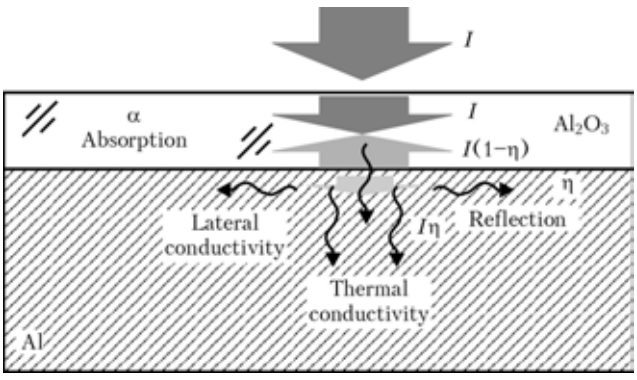

Figure 9. Processes of radiation absorption, reflection and heat transfer at removal of the oxide film on the aluminum surface

Table 2. Technological laser parameters for welding of aluminum samples with penetration at frequency of 70 Hz and pulse duration of 1 ms

Acc. to Figure 8	Current, À	Average power, W	Pulse power, W	Intensity, W / cm^2
a	100	61	870	$5 \cdot 10^6$
b	150	72	1000	$5.8 \cdot 10^6$
c	200	80	1150	$6.5 \cdot 10^6$
d	250	87	1250	$7 \cdot 10^6$

where c is the heat capacity; ρ is the density; and α is the absorption coefficient, gives the significantly lower value of $2.5 \cdot 10^6$ W / cm^2. This fact can be explained by effective heat transfer from the film to the aluminum substrate due to low thickness of the film that ensures sufficient conductivity in the millisecond range.

Pulsed mode allows us to plan experiments on quantitative study of the potential synergetic effect. To exclude mutual influence of laser radiation and arc plasma, we can use temporal delays between their pulses so that the studied object starts to act on metal surface just after completion of the auxiliary action. In this case, estimate of the delivered power and effect value must be based on a precise technique, and its development is one of the main scientific problems of the project.

CONCLUSIONS

The developed hybrid laser-arc facility has the following peculiarities:

- laser source provides radiation pulses with peak power up to 4 kW and intensity up to 10^7 W / cm^2 in the processing zone;
- arc source supplies four different modes, including pulses of reversed polarity, with repetition rate up to 70 Hz and pulse current up to 30 A;
- clock system ensures variation of a delay between arc current pulse and digitally shape-controlled laser radiation pulse;
- coaxial scheme of laser radiation delivery and arc current channel results in maximum efficiency of torch–arc interaction;
- construction of the plasmatron makes it possible to regulate the contents of the gas mixture and separate delivery of plasma and protection gases;
- two-axis table gives the opportunity of automatic adjustment of workpiece motion parameters in the linear speed range of 0.006–0.6 m / min with independent vertical displacement of the plasmatron over the surface being processed.

The initial experiments performed with its application shows high potentialities of the equipment for study of hybrid welding mechanisms and development of the technological modes. The obtained results prove the opportunity of the essential influence of laser and arc pulse interaction on the molten zone shape. Classification of the factors and their quantitative estimation require further studies with application of metallographic analysis for investigation on the pulsed hybrid welding processes.

1. Steen, W.M., Eboo, M. (1979) Arc augmented laser welding. *Metal Construction*, 11(**7**), 332–335.
2. Diebold, T.P., Albright, C.E. (1984) Laser-GTA welding of aluminium alloy 5052. *Welding J.*, 63(**6**), 18–24.
3. Paton, B.E., Gvozdetsky, V.S., Krivtsun, I.V. et al. (2002) Hybrid laser-microplasma welding of thin sections of metals. *The Paton Welding J.*, **3**, 2–6.
4. Gorny, S.G., Lopota, V.A., Redozubov, V.D. et al. (1989) Peculiarities of metal heating in laser-arc welding. *Avtomatich. Svarka*, **1**, 73–74.
5. Dykhno, I.S., Krivtsun, I.V., Ignatchenko, G.N. *Combined laser and plasma arc welding torch*. Pat. 5700989 USA. Publ. 23.12.97.
6. Seyffarth, P., Krivtsun, I.V. (2002) Laser-arc processes and their applications in welding and material treatment. In: *Welding and Allied Processes*. Vol. 1. London: Taylor and Francis Books.
7. Dilthey, U., Lueder, F., Wieschemann, A. (1998) Process-technical investigations on hybrid technology of laser beam-arc welding. In: *Proc. of 6th Int. Conf. on Welding and Melting by Electron and Laser Beams* (Toulon, France).
8. Krivtsun, I.V. et al. (2005) *Experiments on microplasma welding of different metals with small thickness and choice of the corresponding modes of arc discharge for hybrid welding*: Sci. Research Report. Kiev.
9. Abdurahmanov, A., Lopota, V., Sysoev, V. et al. (2006) Simulation of laser induced quartz ablation for nano powder production. In: *Proc. of 5th Int. Conf. on Beam Technologies and Laser Application* (St.-Petersburg).
10. Turichin, G., Grigoriev, A., Zemlyakov, E. et al. (2006) Special features of formation of plasma torch under conditions of hybrid laser-arc welding. *High Temperature*, 44(**5**), 647–655.

QUALITY ASSESSMENT OF LASER-WELDED JOINTS OF DIE-CAST MAGNESIUM ALLOYS

P. KOLODZIEJCZAK[1] and **W. KALITA**[2]
[1]Warsaw University of Technology, Poland
[2]Institute of Fundamental Technological Research of PAS, Warsaw, Poland

The paper presents the methods applied for the quality assessment of the magnesium alloy joints obtained by the CO_2-laser welding. Die-cast magnesium alloys AZ91 and AM50 have been butt-welded using helium as a shielding gas. The primary assessment of properties of joints of similar and dissimilar alloys was performed by the microstructure analysis and measurements of hardness and elemental distribution in the weld cross-sections. The microstructures and the hardness profiles have been evaluated on the cross-sections perpendicular to the direction of beam scanning, as well as on the cross-sections done parallelly to the facing surface along the weld. In order to find any changes due to the action of laser beam (e.g. evaporation of material and convection), the analysis of distribution of basic elements has been performed with X-ray microprobe. The mechanical properties of the joints have been examined by the tests on the Instron stand for static tensile strength and transverse bending. After the fracture of workpieces with welds, the SEM images of fractures were obtained to compare with the parent metal fractures. The corrosion resistance tests performed by the electrochemical method on samples of as-cast materials and welds, have not displayed the differences in the corrosion resistance. However, the microscopic and SEM observations of surfaces of welded samples presented the effect of the joints on corrosion development.

The magnesium alloys gained lately increasing interest of automotive industry mainly because of their much lower density with respect to traditional materials like steel and aluminum alloys. In the recent years the development of new magnesium alloys with mechanical properties comparable with traditional materials [1] led to their applications as the die-casting parts [2]. In effect it was possible to fulfill the sharpening requirements for enviromental protection [3] and transportation safety [4] through the vehicle mass reduction and consequently the fuel savings. However, the production and processing of sheet elements and modular lightweight structures are still in progress. In this matter the special concern is given to welding, particularly to laser beam welding of magnesium alloys [5–17]. The unique features of laser welding may be summarized as follows:

- very high power density of focused beam enables to join the elements with keyhole effect of welding (deep and narrow seam);
- specific energy (defined as the ratio of laser power to welding speed) necessary to obtain the firm joint is much smaller than in conventional methods so the heat-affected zone is thin;
- no filler material is required.

The main parameters of laser welding, i.e. laser power and velocity of scanning, are the ones of simple choice: usually for given thickness of elements to be joined the maximum disposable power is applied and appropriate velocity is accomodated for stable and full penetration welding. The process parameters are the focal point position, the kind of shielding gas and the means of it supplying. Although the helium shielding is much more expensive than argon or nitrogen, the welding with helium provides better shape of the seam, surface quality, less pores and faster welding. The optimum position of beam focal point (with respect to facing surface) depends on the material properties, its thickness and focus length. For magnesium alloys with low melting point (~ 660 °C) and boiling point (~ 1100 °C) the plates of up to 5 mm thickness may be butt-welded with focal position at the facing surface [5].

Several methods should be utilized for the quality assessment of the laser-welded joints. Due to the action of the laser beam and fusion zone creation the microstructure of processed material changes considerably. Microscopic structure inspection provides informations about the shape of the fusion zone, changes in grain size, appearance of precipitates, porosity and occurrence of cracks. In consequence the hardness profiles on the cross sections perpendicular to the direction of beam scanning are different from those of parent material. The irradiation by the focused laser beam may cause evaporation of material and thermocapillary convection, and recrystallization can alter the chemical compound after welding so the analysis with X-ray microprobe to determine the elemental distribution is desirable. The mechanical properties of the joints are revealed by the tests on the Instron stand for static tensile strength and the resistance of the joints to transverse loads. After the fracture of workpieces the SEM images of fractures may be compared with fractures of the parent material.

Corrosion properties of magnesium alloys strongly depend on the method of their production. The development of new technologies permitted to obtain high purity alloys and the corrosion resistance greatly improved [18, 19]. The changes in the processed material introduced by laser welding (modification of composition, compound separation, occurrence of intermetallic phases, increased precipitations) may alter the corrosion resistance of the weld in comparison to

parent material. For the samples of as-cast materials and samples with the joints the comparative corrosion resistance tests can be performed by simple immersion test as well as by electrochemical method followed by microscopic examinations. For more detailed examination of welded structural components also the fatigue tests and the tests for strain rate sensitivity (as for crashworthy components [20]) may be included.

This paper presents some results of application of these methods for the quality assessment of the joints of magnesium alloys obtained by the CO_2 laser beam keyhole welding.

Experimental details. The butt welding of plates of similar and dissimilar alloys has been performed with CO_2 fast axial flow laser at maximum power of 2.5 kW. The beam with the mode close to TEM_{10} was focused to the diameter of 0.25 mm by the ZnSe lens of 5". No filler metal has been used. Two cast magnesium alloys AM50 and AZ91 with the chemical composition given in the Table were machined from the as-cast bars to the plates with thicknesses from 2.0 to 4.5 mm, width of 50 mm and the length of welding edges of 100 mm. In this paper we present results obtained for the plates 4.5 mm thick.

After some attempts the conditions of welding were chosen as follows: laser power has been set at 2 kW, welding speed — at 4 m / min, and after evaluation of the influence of the focal point position (with respect to material surface) on the profile of fusion zone, the beam focal position has been set on the upper surface of plates. The helium shielding of the facing surfaces was provided from the nozzle of 4 mm in diameter with the flow rate of 15 l / min, and the bottom surfaces were shielded by the blow of argon.

The microstructures and the hardness profiles have been evaluated on the cross-sections perpendicular to the direction of beam scanning as well as on the cross-sections done parallelly to the facing surface along the seam. In order to find any changes due to the action of laser beam (e.g. evaporation of material and convection) the analysis of elemental distribution of basic elements has been performed with X-ray microprobe. The mechanical properties of the joints have been revealed by the tests on the Instron stand for static tensile strength and on the 3-point bending stand. After the fracture of workpieces the SEM images of fractures were obtained to compare with fractures of the parent material. The comparative corrosion resistance tests have been performed by electrochemical method (cyclic voltametry) followed by microscopic examinations.

Chemical composition of welded alloys

Alloy	Content of elements, wt.%		
	Al	Mn	Zn
AM50	5.0	0.30	< 0.2
AZ91	9.0	0.17	0.7

Results and discussion. The macrostructures of the butt-welded joints of similar and dissimilar alloys are presented in Figure 1. The boundaries of the fusion zones are nearly parallel and the aspect ratios of welds (thickness of a plate to mean width of the fusion zone) are of high value indicating that the keyhole effect of beam penetration was responsible for the joining. The parent materials contained no pores and after welding the fusion zones are practically free of them. Also, no cracks are observed.

Due to the short (less than 4 ms) time of beam irradiation and fast solidification, the fusion zones are characterized by significant grain refinement. The sharp transitions from the base metal to the fusion zone may indicate that there is no heat-affected zone. On the microscopic blow-up it may be observed that

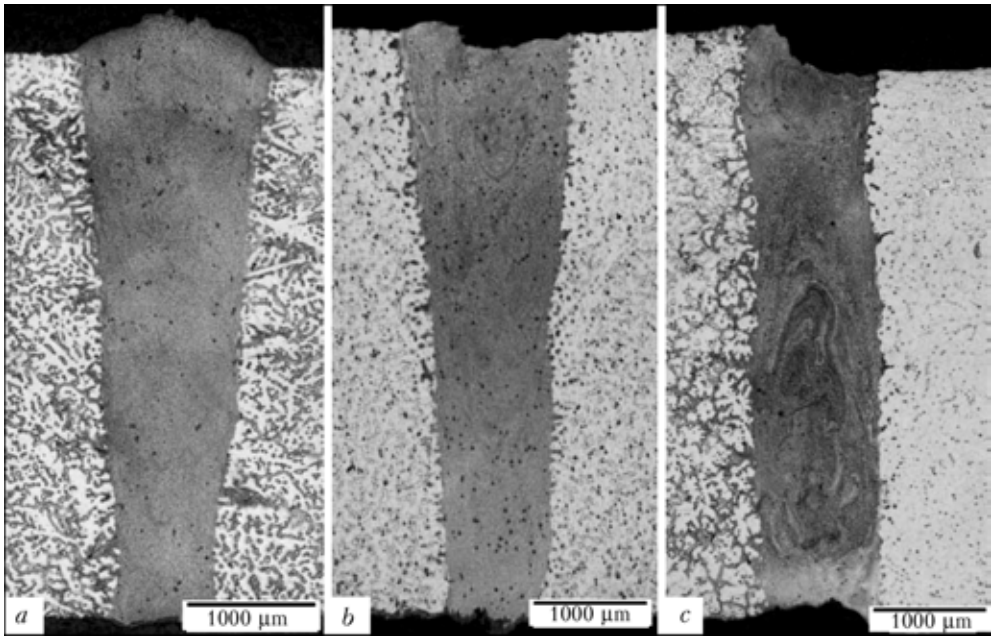

Figure 1. Macrosections of butt-welded joints of similar and dissimilar alloys: *a* — AZ91–AZ91; *b* — AM50--AM50; *c* — AZ91--AM50

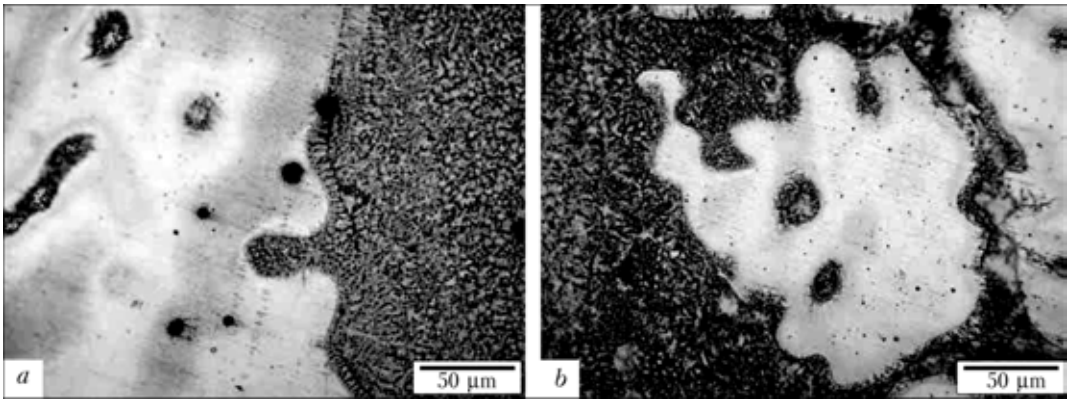

Figure 2. Microstructure in transition zones from the base alloy AM50 to fusion zone (*a*) and from the fusion zone to base alloy AZ91 (*b*) in AM50–AZ91 joint

the distinguished direction of crystallization concerns only one-grain layer on the AM50 side of the joint (Figure 2).

The measurements of hardness distributions in the cross sections of welds (perpendicular to the direction of welding) for joints of similar alloys have shown significant increase of hardness in the fusion zones in comparison to the base material. These results may be associated not only with the high grain refinement in the weld but also with the increase of precipitations at the grain boundaries and appearance of intermetallic compounds. For the joints of dissimilar alloys no such effects are observed (Figure 3).

For the determination of the changes in the chemical composition of material caused by the influence of beam action the measurements of elemental distributions have been performed by means of the Philips X-ray microprobe XL-30. It was found that due to the very low boiling point of magnesium (~1100 °C) in comparison with that of aluminum (~2300 °C), the percentage share of magnesium in the joints has been slightly decreased by evaporation of this element (especially in the AZ91–AZ91 joint). Due to the high grain refinement in the fusion zones the amplitudes of the elemental concentration changes have been much smaller than outside welds. Particularly, interesting are the elemental distributions in the joints of dissimilar alloys AM50–AZ91. Measurements performed at different depths of the joints may indicate the influence of thermocapillary convection and consequent mixing. In effect the greatest changes in the composition across the joint can be observed near the facing and bottom surfaces while the profiles of elemental distributions at the half of the thickness are relatively smooth (Figure 4).

The static tensile tests of samples of parent alloys and the welds were performed on the Instron stand. The stress versus strain curves for joints of similar alloys and the base metals are presented in Figure 5. It has been observed that the fracture of welded samples for all alloys appeared far from the fusion zone boundaries, namely in the region of base metal. As it could be expected, the samples with joints have smaller elongation at fracture than the parent materials, however there are differences for tensile stress: for AM50–AM50 joint the stress at fracture is lower and for AZ91–AZ91 higher than those for base metal samples. For the AZ91–AM50 joints the workpieces broke at the AZ91 side, also far from the fusion zone. The comparison of stress–strain curves for all joints is given in Figure 6. According to anticipations the elongation at fracture for dissimilar joints has the value between those of the joints of brittle alloy AZ91 and the ductile alloy AM50. Since the fracture of the welded samples occurred far from the fusion zones, the SEM images of fracture surfaces of the workpieces of parent materials and samples with the joints displayed no differences.

The static bend tests were performed on the 3-point bend stand (support rollers spacing of 70 mm, the rollers diameter of 30 mm). The differences between the samples with weld and unwelded material have

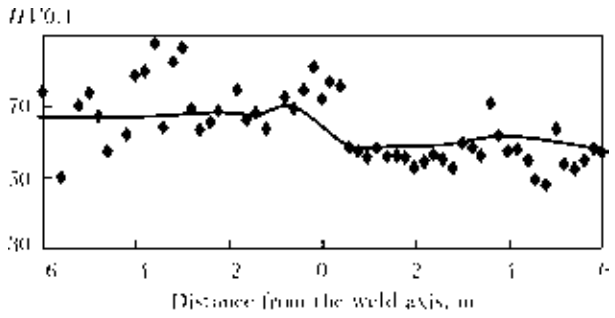

Figure 3. Microhardness profile for joint of dissimilar alloys AZ91–AM50 measured at 1.5 mm from the facing surface

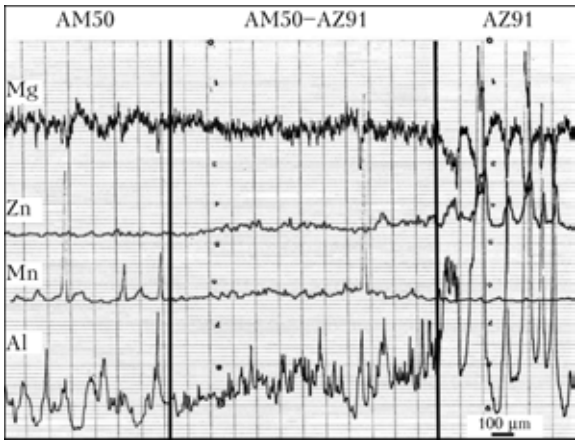

Figure 4. Elemental distributions across the joint of AM50 and AZ91 alloys measured at the half of the cross section thickness

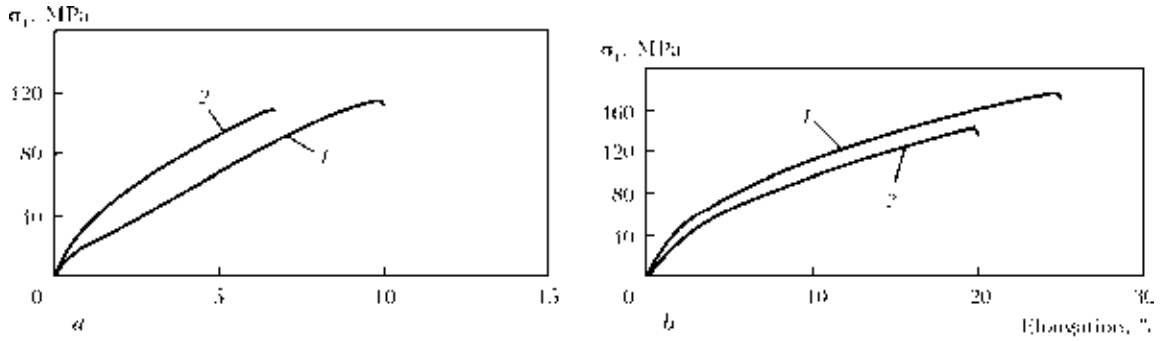

Figure 5. Tensile stress–strain curves for samples of parent materials (*1*) and the joints (*2*) of AZ91–AZ91(*a*) and AM50–AM50 (*b*)

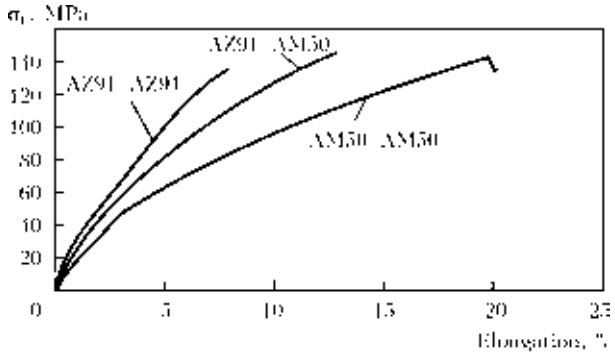

Figure 6. Tensile stress–strain curves for the joints of similar and dissimilar alloys

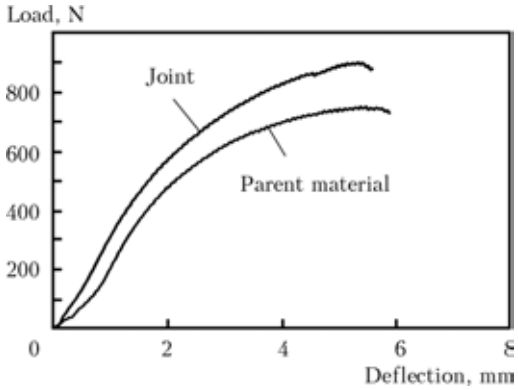

Figure 7. Load versus deflection for AZ91 alloy

been observed only for the joint of brittle AZ91 alloy, where the peak load for base metal is lower than for the joint (Figure 7).

Corrosion behavior of welded and unwelded samples of approximately equal (1 cm^2) surface area was examined by means of electrochemical method. Measurement were carried out in the aerated 0.9 % NaCl solution; three electrode cell consisted of working electrode (magnesium alloy), counter (platinum) and reference electrode (saturated calomel electrode). The measurements were realized with a potential sweep 1 mV / s from –100 to +300 mV. The polarisation curves for welded and unwelded surfaces for AZ91 and AM50 alloys are shown in Figure 8.

From the comparison of polarisation curves for welded and unwelded samples it may be concluded that practically there are no difference in corrosion resistance.

CONCLUSIONS

1. Welding of similar and dissimilar alloys in the same conditions (for plate 4.5 mm thick, 2 kW laser power, 4 m / min speed, in helium shielding and focal position at facing surface) resulted in high aspect ratios of the fusion zones with nearly parallel boundaries, practically pores free and without cracks. No heat-affected zone may be observed.

2. The high grain refinement and increased precipitations in the fusion zones heightened the hardness in these regions in comparison with parent material.

3. In the static tensile tests the fractures for all joints occurred far from the weld, namely in joints

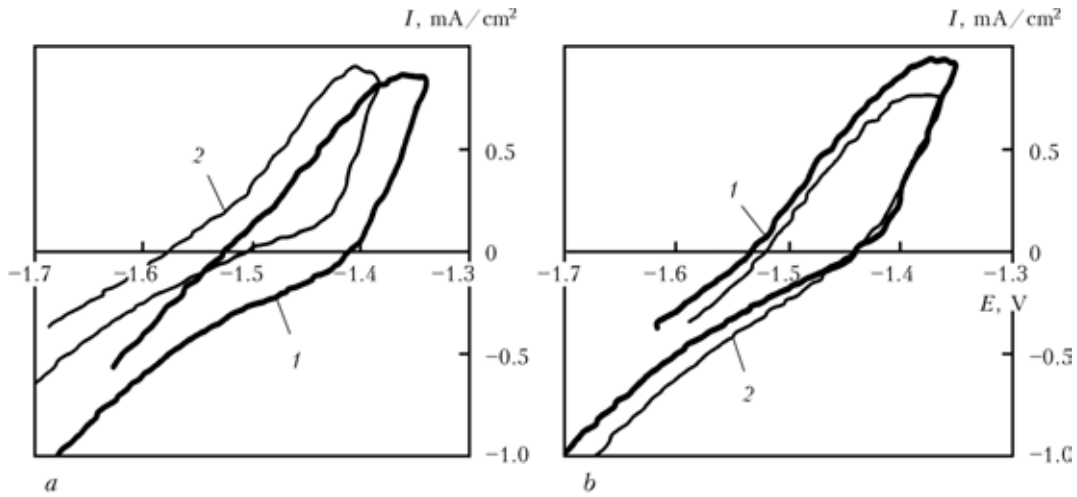

Figure 8. Current–potential curves for welded (*1*) and unwelded (*2*) AZ91 (*a*) and AM50 (*b*) alloys

of dissimilar alloys on the side of brittle alloy AZ91. The plastic properties of samples with welds are lower than for the parent materials. In the bending tests the differences between the welded and unwelded samples can be observed only for the joints of brittle AZ91 alloy.

4. The results of corrosion immersion tests performed in 0.9 % NaCl solution showed that welding of dissimilar magnesium alloys, in this case AZ91–AM50, increases a susceptibility to galvanic corrosion even if the difference between electrode potential values are not apart each other. However an influence of a weld is rather negligible. The corrosion resistance tests performed by electrochemical method for joints of similar alloys have shown practically no differences in comparison with parent material.

1. Friedrich, H., Schumann, S. (2001) Research for a «new age of magnesium» in the automotive industry. *J. Materials Processing Technology*, **117**, 276–281.
2. Longworth, S.J.P. (2001) *The bolting of magnesium components in car engines*: Diss. for Master of Philosophy Degree to University of Cambridge.
3. Aghion, E., Bronfin, B., Elieze, D. (2001) The role of magnesium industry in protecting the environment. *J. Materials Processing Technology*, **117**, 381–385.
4. Mordike, B.L., Ebert, T. (2001) Magnesium. Properties–applications–potential. *Material Sci. and Eng. A*, **302**, 37–45.
5. Weisheit, A., Galun, R., Mordike, B.L. (1998) CO_2 laser beam welding of magnesium-based alloys. *Welding Res. Suppl.*, 77(**4**), 149–154.
6. Dhari, M., Masse, J.E., Mathieu, J.F. et al. (2001) CO_2 laser weldability of WE43 magnesium alloy for aeronautic industry. In: *Proc. of LANE* (Erlangen, Germany, Aug. 28–31, 2001), 297–310.
7. Zhao, H., Debroy, T. (2001) Pore formation during laser beam welding of die-cast magnesium alloy AM60B — mechanism and remedy. *Welding Res. Suppl.*, 204–210.
8. Sun, Z., Wei, J., Pan, D. et al. (2001) A comparative evaluation on microstructures in TIG and laser welded AZ31 magnesium alloy. In: *SIMTech Technical Report PT/01/008/JT*, 1–8.
9. Hakekamp, H., Goede, M., Bormann, A. et al. (2001) Laser beam welding of magnesium alloys — new possibilities using filler wire and arc welding. In: *Proc. of LANE* (Erlangen, Germany, Aug. 28–31, 2001), 333–338.
10. Watkins, K.G. (2003) Laser welding of magnesium alloys. In: *Proc. of Magnesium Technology Conf.* (San Diego, USA, March 2–6, 2003), 153–156.
11. Stern, A., Munitz, A., Koln, G. (2003) Application of welding technologies for joining of Mg alloys. Microstructure and mechanical properties. *Ibid.*, 163–170.
12. Lathabai, S., Barton, K.J., Harris, D. et al. (2003) Welding and weldability of AZ31B by gas tungsten arc and laser beam. *Ibid.*, 157–162.
13. Kalita, W., Kolodziejczak, P., Pokhmurska, H. (2003) Welding of Mg-based alloy AM20 by CO_2 laser beam. In: *Proc. of Int. Conf. on Laser Technologies in Welding and Materials Processing* (Katsiveli, Ukraine, May 19–23, 2003), 214–216.
14. Dasgupta, A.K., Mazumder, J. (2004) Laser welding of AM60 magnesium alloy. In: *Proc. of Magnesium Technology Conf.* (Charlotte, USA, March 14–18, 2004), 43–48.
15. Kolodziejczak, P., Kalita, W., Hoffman, J. et al. (2004) Laser welding of magnesium-based alloys of MgAlZn group. *Advances in Manufacturing Sci. and Techn.*, 28(**4**), 45–53.
16. Kalita, W., Kolodziejczak, P., Kwiatkowski, L. et al. (2004) Properties of the butt-welded joints of CO_2 laser welded Mg alloys. In *Proc. of LANE* (Erlangen, Germany, Sept. 21–24, 2004), Vol. 1, 317–328.
17. Kalita, W., Kolodziejczak, P., Kwiatkowski, L. (2005) Properties of the CO_2-laser welded joints of dissimilar magnesium alloys. In: *Proc. of 2nd Int. Conf. on Laser Technologies in Welding and Materials Processing* (Katsiveli, Ukraine, May 23–27, 2005), 79–84.
18. Li, P.Y., Yu, H.J., Chen, S.C. et al. (2003) Factors affecting the corrosion resistance of cast magnesium alloys. In: *Proc. of Magnesium Technology Conf.* (San Diego, USA, March 2–6, 2003), 51–58.
19. Kwiatkowski, L., Grobelny, M., Kalita, W. et al. (2005) Corrosion properties of the butt-welded joints of laser welded Mg alloys. *Inzynieria Powierzchni A*, II(**2**), 191–197.
20. Abbott, T., Easton, M., Schmidt, R. (2003) Magnesium for crashworthy componenents. In: *Proc. of Magnesium Technology Conf.* (San Diego, USA, March 2–6, 2003), 227–230.

MODEL OF ENERGY TRANSFER OF PULSED LASER BEAM

O. KOZYREV, V. ROMANENKO and **V. KOVALENKO**
Laser Technology Research Institute of NTUU «KPI», Kiev, Ukraine

For construction of model of interaction of laser radiation with material of a target it is necessary to know distribution of energy in a beam in any point of space at any moment. The distribution of laser radiation that comes out of real resonator is presented in this paper. Also the basis of the provisions and shapes of equal phase surface of a clear correlation between the intensity of a single beam anywhere in the cross plane and the intensity at any point in the other planes used are described to fit the laser pulse approximation.

For construction of model of interaction of laser radiation with material of a target it is necessary to know distribution of energy in a beam in any point of space at any moment. Also the basis of the provisions and shapes of equal phase surface of a clear correlation between the intensity of a single beam anywhere in the cross plane and the intensity at any point in the other planes used are described to fit the laser pulse approximation. For this purpose it is necessary to solve the following tasks: to construct a beam pack, having determined geometrical parameters of an each beam, and to determine a share of energy transferred by one ray at any moment of a laser impulse.

Beams pack construction. The direction of a light wave energy carrying is defined by a Poynting vector direction. In the isotropic environment Poynting vector coincides with a direction of an equal phase surface movement.

We shall consider distribution of a spherical wave from the any resonator. In this case the direction of Poynting vector will coincide with a direction of a normal to equal phase surface in any point of this surface.

For more exact description of radiation distribution formed by the real optical resonator, it is possible to offer the following expression [1]:

$$\omega(x) = \omega_0 \sqrt{1 + \left(\frac{x}{x_R}\right)^2}, \qquad (1)$$

where x_R is the Rayleigh length.

Both of x_R and beam waist radius x_R depend from mode structure:

$$x_R = \frac{\pi\omega_0^2}{M^2\lambda}, \quad \omega_0 = M^2 \frac{\lambda}{\pi\theta},$$

where θ is the full divergence angle; M^2 is the modal multiplier.

Let us enter factor $K = \dfrac{M^2\lambda}{\pi}$.

Then it is possible to write $\omega_0 = \dfrac{K}{\theta}$, $x_R = \dfrac{\omega_0^2}{K}$.

Having substituted these expressions in (1), we shall receive

$$K = \theta \sqrt{\omega_e^2 - \theta^2 x_e^2}. \qquad (2)$$

Expression for modal multiplier is $M^2 = \dfrac{\pi K}{\lambda}$.

Direction of Poynting vector will coincide with a direction of a tangent to $\omega(x)$:

$$\frac{d\omega(x)}{dx} = \frac{\theta^2 x}{\sqrt{\omega_0^2 + \theta^2 x^2}}. \qquad (3)$$

For the full description of energy distribution it is necessary to find the equation of energy distribution from a point with coordinates $(0, r_1)$, when $0 \le r_1 \le \omega_0$ (Figure 1). We shall search for such equation in the form of

$$r(x) = \sqrt{r_1^2 + T^2 x^2}, \qquad (4)$$

where T is the unknown parameter.

Consider on an axis $\vec{x}$ point with coordinates $(x_e, 0)$. It is obvious that radius of a beam in a plane perpendicular axis $\vec{x}$ and passing through $(x_e, 0)$ will be $\omega(x_e) = \sqrt{\omega_0^2 + \theta^2 x_e^2} = \omega_e$. Having determined a corner of tangent inclination in a point $(x_e, 0)$ to a curve $\omega(x)$, it is possible to find the centre of the wave front curvature which is passing through a point with coordinates (x_e, ω_e) from $\dfrac{\omega(x_e)}{x_e - x_c} = \dfrac{d\omega(x_e)}{dx}$, hence

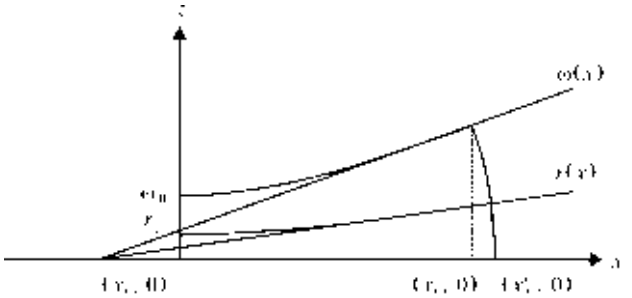

Figure 1 (for designations see the text)

$$x_c = -\frac{\omega_0^2}{\theta^2 x_e}. \quad (5)$$

The curvature radius of this wave front can be defined as a distance between points $(x_c, 0)$ and $(x_e, \omega(x_e))$:

$$R = \sqrt{(x_e - x_c)^2 + \omega(x_e)^2} = \frac{\omega(x_e)}{\theta^2 x_e}\sqrt{\omega(x_e)^2 + \theta^4 x_e^2}. \quad (6)$$

A curve $r(x)$ crosses the equal phase surface in a point $(x_e', r(x_e'))$. As the shape of wave front is considered spherical, two conditions should be satisfied:

1. The tangent to a curve $r(x)$ passing through a point $(x_e', r(x_e'))$ should pass also through the centre of wave front curvature $(x_c, 0)$ the same as also a tangent to $\omega(x)$ in a point $(x_e, \omega(x_e))$.

2. As the radius of wave front curvature R is constant in all points of this front, distance between points $(x_c, 0)$ and $(x_e, \omega(x_e))$ is equal to distance between $(x_c, 0)$ and $(x_e', r(x_e'))$.

At performance of a condition 1 it is received to curve $\omega(x)$:

$$\frac{d\omega(x)}{dx} = \frac{\theta^2 x_e}{\sqrt{\omega_0^2 + \theta^2 x_e^2}} = \frac{\sqrt{\omega_0^2 + \theta^2 x_e^2}}{x_e - x_c} \quad (7)$$

and same to curve $r(x)$:

$$\frac{dr(x)}{dx} = \frac{T^2 x_e'}{\sqrt{r_1^2 + T^2 x_e'^2}} = \frac{\sqrt{r_1^2 + T^2 x_e'^2}}{x_e' - x_c}. \quad (8)$$

After modification (7) and (8) $T = \frac{r_1}{\omega_0}\theta\sqrt{\frac{x_e}{x_e'}}$.

Considering that $\frac{x_e}{x_e'} = \frac{x_c + R\cos\theta}{x_c + R} \approx 1$ finally we have

$$T = \frac{r_1}{\omega_0}\theta. \quad (9)$$

Hence, expression (4) can be rewrited as

$$r(x) = \sqrt{r_1^2 + \frac{r_1^2\theta^2}{\omega_0^2}x^2} = \frac{r_1}{\omega_0}\sqrt{\omega_0^2 + \theta^2 x^2} = \frac{r_1}{\omega_0}\omega(x). \quad (10)$$

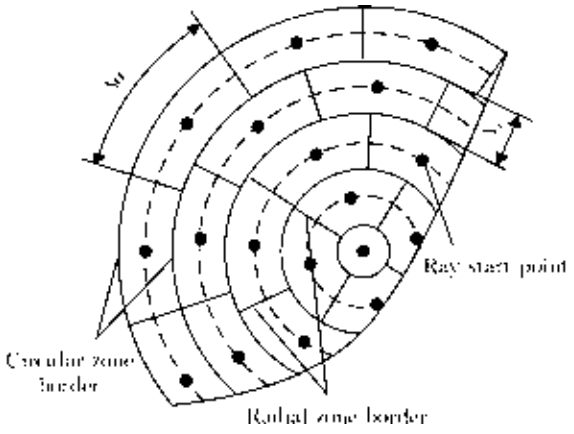

Figure 2 (for explanations see the text)

By means of this expression it is possible to receive a direction of Poynting vector in any point of beam section for any x-coordinate. Besides by means of (10) it is possible to find the unequivocal conformity between intensity of an individual beam in any point of a beam waist plane and intensity in any point in other planes of beam section. For this purpose it is necessary to know power distribution in a beam.

Initial power distribution is necessary to find experimentally, with the subsequent approximation on a minimal squares method. As approximating function it is possible to use

$$I = I_0 \exp\left(\frac{-(y - y_c)^2}{\omega_y^2} - \frac{(z - z_c)^2}{\omega_z^2}\right). \quad (11)$$

Than we need to define power, transferable by an individual beam, depending on starting coordinates of this beam. For this purpose we shall present section of a beam in the shape of the circle divided into ring sites which, in turn, are divided into sectors, each of which will be a source of one beam (Figure 2).

It is obvious that amount of radial zones will be equal

$$N_r = \frac{r}{\Delta_r},$$

where Δ_r is the radial step and, simultaneously, radius of the central (circular) zone. Let us accept the central zone for a reference mark. Its area will be $S_1 = \pi(\Delta_r)^2$.

For reception of start points coordinates, we shall take advantage of the methods applied at aberrations approximation. A final distribution of a field to targets is consequence of spherical aberrations on optical system elements [2]. According to it, for a finding of start points we shall demand the maximal conditionality of a constructional matrix. Then, if the index of a radial zone i accepts values $[1, \ldots, N_r]$, the number of sectors in a ring will be $N_i = 2i - \mathrm{int}(1/i)$.

If each circular zone is divided into radial zones of the identical area (elementary squares) the area of each elementary square in i-ring zone will be $S_{ie} = S_i / N_i$, or for circular zone (from second) ----

$$S_{ie} = \pi\Delta_r^2 \frac{2i - 1}{2i}. \quad (12)$$

Total number of rays in a beam pack will be

$$N_\Sigma = 1 + \sum_{i=2}^{N_r} 2i = N_r^2 + N_r - 1. \quad (13)$$

Coordinates of each ray can be certain in cylindrical coordinates by radius-vector ρ and turn angle φ:

$$\begin{cases} \rho_i = \Delta_r\left(i - \frac{1}{2} - \frac{1}{2}\mathrm{int}\left(\frac{1}{i}\right)\right) \\ \varphi_{ij} = \frac{360^\circ}{N_i}(j - 1) + \alpha. \end{cases} \quad (14)$$

Here N_i is the number of radial zones in i circular zone (i = 1, ..., N_r); j is the index of radial zone (j = = 1, ..., N_i); α is the starting turn angle.

Amount of power gained from each elementary square during laser impulse is

$$P_{ij} = \int\int_{S_{ij}} I dS,$$

where S_{ij} is the elementary square.

For calculation of this integral we shall take advantage of the theorem of average value of double integral:

$$P_{ij} = S_{ij} I(y_{ij}, z_{ij}),$$

where $I(y_{ij}, z_{ij})$ is the intensity in a ray start point. Then the full power of laser pulse will be

$$P_{\Sigma} = \sum_{i=1}^{N_r} \sum_{j=1}^{N_j} P_{ij}.$$

Next we have to determine power gained from elementary square for a certain time interval Δt inside laser impulse with duration τ. It is obvious that the form of distribution of intensity (11) is defined by a scale multiplier I_0 and this multiplier varies in time, i.e. expression (11) can be written as

$$I = I_0(t) \exp\left(- \frac{(y - y_c)^2}{\omega_y^2} - \frac{(z - y_c)^2}{\omega_z^2} \right). \qquad (15)$$

Let us determine intensity falling off in unit R_{ij} concerning a maximum:

$$\mu_{ij} = \frac{I(y_c, z_c)}{I_{\max}} = \exp\left(- \frac{(y - y_c)^2}{\omega_y^2} - \frac{(z - y_c)^2}{\omega_z^2} \right). \qquad (16)$$

For definition of current (instant) value of power it is necessary to determine all over again the form of an impulse which then to approximate, for example, by spline.

The current power value will be sum of powers carried by each ray. Thus, power transferable by one beam R_{ij} possible to define as

$$P_{ij} = \frac{P(t_0)}{\Sigma_{\mu}} \mu_{ij}, \qquad (17)$$

where $\Sigma_{\mu} = \sum_{i=1}^{N_r} \sum_{j=1}^{N_j} \mu_{ij}$; $P(t_0)$ is the current power value in a time moment t_0. Also we can define amount of energy. Also it is possible to define the amount of the energy which has allocated for a time interval Δt and carried by single beam:

$$E_{ij} = \frac{P(t_0)}{\Sigma_{\mu}} \mu_{ij} \Delta t. \qquad (18)$$

Presented model describes geometrical and energetical characneristics of laser pulse and can be used in different models of interaction between laser beam and target material. With a small correction presented model also can be used to describe a continuous laser irradiation.

1. Schwarzenbach, A.P., Ladrach, P. (1995) Recent progress in laser processing. In: *Proc. of Int. Symp. for Electromachining* (Lausanne, Switzerland, 1995).
2. Zinoviev, V.E. (1989) *Thermophysical properties of metals in high temperatures.* Moscow: Metallurgiya.

INVESTIGATION OF HYBRID LASER-PLASMA PROCESSES OF WELDING OF ALUMINIUM ALLOYS AND STAINLESS STEELS

I.V. KRIVTSUN, V.D. SHELYAGIN, V.Yu. KHASKIN, V.F. SHULYM, A.G. LUKASHENKO, E.G. TERNOVYI, O.V. SIORA and **T.G. CHIZHSKAYA**
E.O. Paton Electric Welding Institute of NASU, Kiev, Ukraine

Features of hybrid laser-plasma welding of aluminium alloys and stainless steels using CO_2- and diode lasers were investigated. To this effect, a prototype hybrid plasma torch and power source which provides welding on straight polarity and by heteropolar current pulses were manufactured. Optimal conditions for hybrid welding were established depending on specimen material, necessity of filler wire use, mechanical properties of joints and laser radiation wavelength. To ensure quality cleaning of oxide films at high-speed laser-plasma welding of aluminium alloys, current values to straight and reversed polarity pulse duration ratios were established. Main defects of joints of these alloys were defined, mechanisms of their formation were investigated and methods of their elimination were developed. Macro- and microstructures, microhardness and mechanical properties of welded joints obtained by laser, plasma and hybrid methods were investigated. The investigation results evidenced the advantage of laser-plasma welding. Manufacture of profile tubes from AMts (δ = 0.3 mm) for multiple glass panes was proposed as an example of industrial application of hybrid laser-plasma welding of aluminium alloys.

Preliminary heating and melting of metal by GMA (MIG / MAG) process allows one to substantially expand the range of laser welding application [1]. To that very goal, combination of laser radiation and plasma transferred arc may be applied [2]. One of the most topical applications of laser-plasma welding is manufacturing of airspace equipment details from stainless steels and aluminium alloys [3]. Therefore the object of our work was investigation of hybrid laser-plasma processes of welding of these materials. Here we first set the problem to define the influence of different wavelengths and conditions of focusing of laser radiation upon welding processes. Solution of this problem underlies development of basic techniques of welding of these materials.

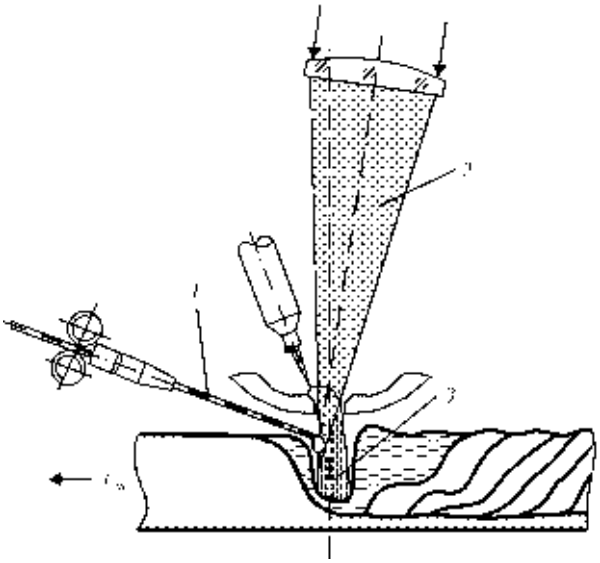

Figure 1. Scheme of experimental arrangement for hybrid laser-plasma welding by integrated plasma torch: *1* — filler wire; *2* — laser beam; *3* — plasma arc

The investigation was carried out using CO_2-laser LÒ-104 with power up to 10 kW [4], and diode laser DF020HQ with power up to 2 kW (Rofin-Sinar, Germany). The experiments were made using the scheme in Figure 1. According to this scheme, focused laser radiation was transmitted through the plasma transferred arc to form a common weld pool. Besides, a possibility of filler wire feed at v_f = 40–200 m / h was provided for. In compliance with this scheme, a hybrid plasma torch was manufactured to combine it both with diode- and CO_2-laser radiation and to move it relative to a specimen being welded at v_w = 10–300 m / h.

At the initial stage of the experiments, principal necessity of filler wire use was being checked. It was established that for welding stainless steels such a welding speed can be selected, at which for given powers of laser beam and plasma arc a minimal reinforcing root bead steadily forms. Due to certain extension of remelted metal, no undercuts are formed in this case, and there is no necessity in using filler wire. For aluminium alloys, selection of a similar mode is more complicated.

Aluminium alloys were welded using heteropolar pulses, while stainless steels were welded in a continuous current mode. In all cases arc voltage was U_a = 18 V. During welding, reversed polarity pulses guaranteed cathodic cleaning of the specimen surface of oxide film. The experiments carried out allowed determining the relationships given in Figures 2–4, in which the distance between curves *3* and *4* is a numerical expression of the so called hybrid effect [5]. It is seen from the diagrams that in welding of stainless steel by the hybrid method using diode laser radiation the hybrid effect does not practically show (see Figure 2). Similarly, when welding aluminium alloys, the hybrid effect occurs (see Figure 3). In

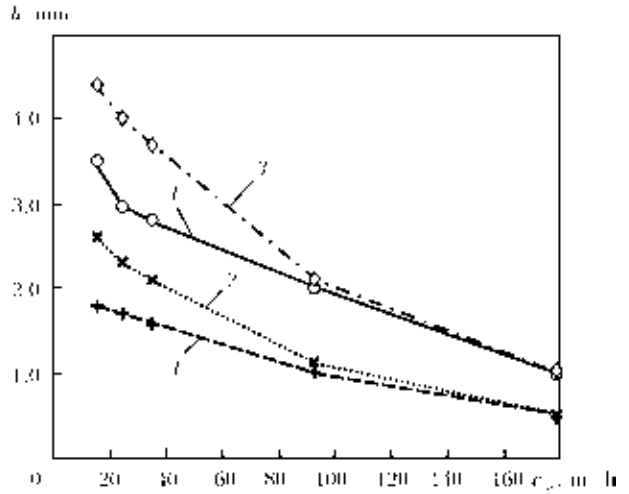

Figure 2. Dependence of penetration depth h on welding speed v_w in laser-plasma welding of stainless steel 1.0–3.5 mm thick with diode laser radiation at P = 2 kW, I = 100 À and U_a = 18 V: *1* — laser welding; *2* — plasma welding; *3* — summation curve for laser and plasma welding; *4* — hybrid welding

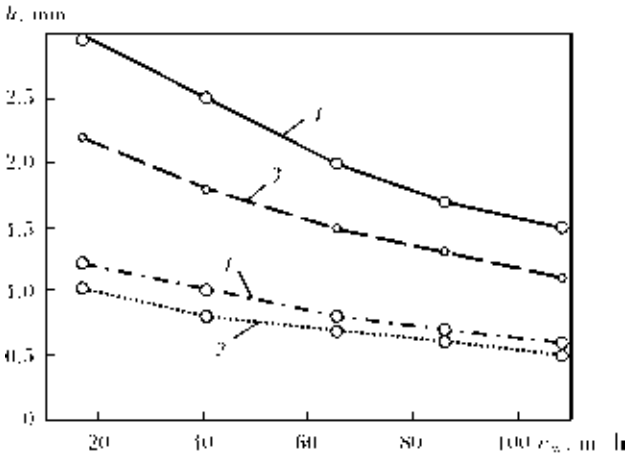

Figure 3. Dependence of change of penetration depth h on welding speed v_w in laser-plasma welding of À Ì ts, À Ì g3, À Ì g5m, À Ì g6, 1915 alloys using diode laser radiation at P = 1.2 kW, I_{str} / I_{rev} = = 50 / 50 and U_a = 18 V: *1* — laser welding; *2* — plasma welding; *3* — summation curve for laser and plasma welding; *4* — hybrid welding

hybrid welding of aluminium alloys using ÑÎ$_2$-laser radiation, the hybrid effect is much more intensely pronounced (see Figure 4).

To define the influence of radiation wavelength on hybrid welding process in more detail, a comparison of relation of energy input rate to thickness of stainless steel sheets to be welded was made. It was established that from the point of view of laser power losses decrease, steels up to 1.2–1.5 mm thick are expedient to be welded by a hybrid method using diode laser radiation, while thicker steels are to be welded using a ÑÎ$_2$-laser. It is connected with the heat conduction character of melting of thin metal and with better absorption of short wavelengths. As the thickness of steel sheets increases in case of hybrid welding using a ÑÎ$_2$-laser, deep penetration mode shows more clearly, which allows significant rising of process output as compared to welding with a diode laser, at which deep penetration is absent.

Next stage of the investigation was to define the difference between welding of aluminium alloys using filler wire À Ì g6 1.2 mm diameter and without it. X-ray nondestructive testing indicated presence of pores in the welds obtained by hybrid welding of aluminium alloys À Ì g3 and À Ì g6 (δ = 0.8–3.0 mm) without filler wire and their absence in case of its use. An analysis of distribution of magnesium and manganese alloying elements in the direction «parent material–weld» made it clear that in the absence of filler wire their burnout occurs (especially in the transition zone), while in its presence not only such burnout is eliminated, but additional alloying of weld metal becomes possible, too. Besides, a study of residual distribution of hydrogen in the welds was carried out. In the absence of filler wire the welds are saturated with hydrogen, which results in residual porosity. Presence of filler material eliminates hydrogen porosity.

The mechanical test carried out showed that hybrid welding of aluminium alloys permits achieving

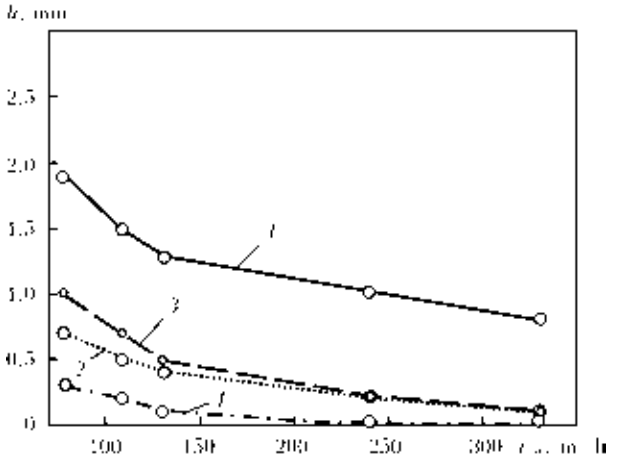

Figure 4. Dependence of change of penetration depth h on welding speed v_w in laser-plasma welding of À Ì ts, À Ì g3, À Ì g5m, À Ì g6, 1915 alloys using ÑÎ$_2$-laser radiation at P = 1.2 kW, I_{str} / I_{rev} = = 50 / 50, U_a = 18 V: *1* — laser welding; *2* — plasma welding; *3* — summation curve for laser and plasma welding; *4* — hybrid welding

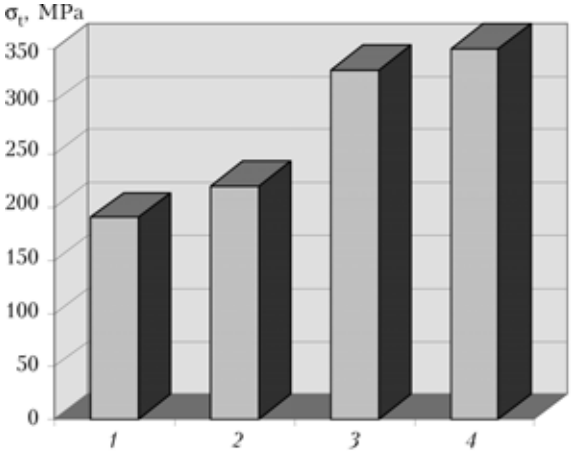

Figure 5. Results of tensile strength test of weld (*1, 3*) and base (*2, 4*) metal of À Ì g3 (*1, 2*) and À Ì g6 (*3, 4*) aluminium alloys welded by hybrid method

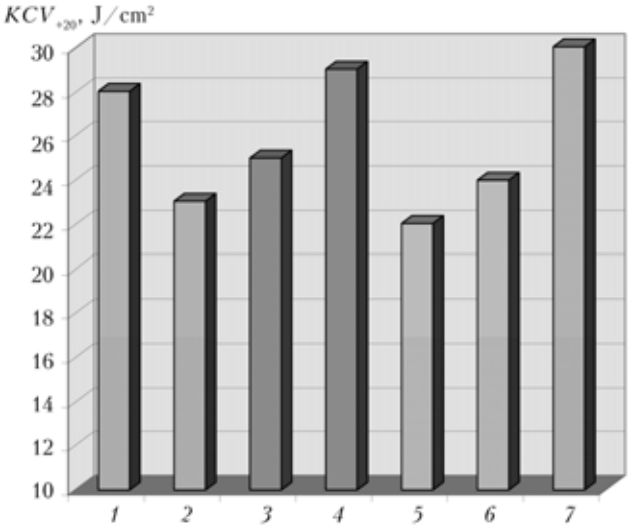

Figure 6. Impact toughness *KCV* at 20 °Ñ of weld (*1, 3, 5*), HAZ (*2, 4, 6*) and base (*7*) metal of 08Kh17Ò steel 3.5 mm thick welded by laser (*1, 2*), hybrid (*3, 4*) and plasma (*5, 6*) methods

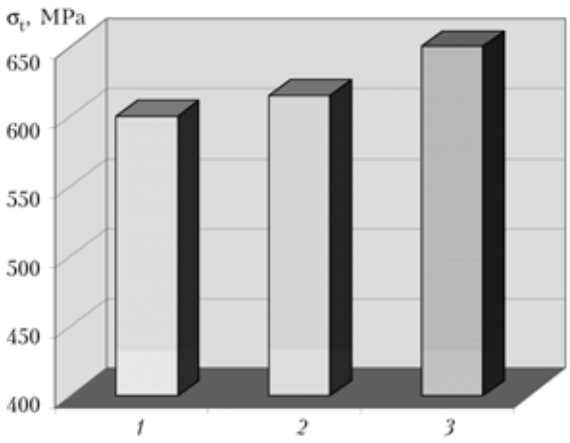

Figure 7. Results of tensile strength test of the 08Kh17Ò steel base (*3*) and joint (*1, 2*) metal 3.5 mm thick welded by laser (*1*) and hybrid (*2*) methods

strength about 90 % of parent metal (Figure 5). For reference, plasma welding ensures strength up to 80 %. The results of impact toughness test of welded samples of ferrite-pearlite stainless steel allow one to assert (Figure 6) that, although laser welding guarantees maximal impact toughness of weld metal (due to obtaining fine-grain equiaxial structures), the best results for the transition zone are guaranteed by hybrid welding. In case of stainless steel, the welds obtained by the hybrid method had the maximal strength (Figure 7).

Since presence and intensity of the hybrid effect are influenced by both power density in the focal plane, and radiation wavelength (though into a much lesser degree), future trends of research development are connected with use of fiber-optic or Nd:YAG lasers due to small wavelength and focal spot sizes.

CONCLUSIONS

1. It was established that in the investigated parameters range optimal welding conditions correspond to such a speed which provides stable formation of the smallest possible root reinforcing bead at maximum power. Taking into account the geometry of welds, such conditions in most cases allow one to avoid using of filler materials due to bulking of remelted metal.

2. For hybrid welding by diode laser radiation, the laser to plasma power ratio should be close to 1:1 or change towards laser power increase, which is concerned with improvement of conditions of hybrid welding process stabilization proportional to metal evaporation increase under exposure to laser radiation.

3. In laser-plasma welding of aluminium alloys by heteropolar pulses, reversed polarity pulses ensure specimen surface cathodic cleaning of oxide film. In high-speed welding, to achieve quality cathodic cleaning, the straight to reversed polarity pulse duration ratio should be close to 1:1. Here, reversed polarity pulse current should make 70...100 % of straight polarity pulse current.

4. The results of X-ray nondestructive testing of AMg3 and AMg6 alloy specimens (δ = 0.8–3.0 mm) are evidence of presence of internal pores in the welds obtained without a filler material and of absence of defects in case of Sv-À Ì g6 1.2 mm filler wire use in hybrid laser-plasma welding of À Ì g3 è À Ì g6 alloys.

5. The investigation of chemical inhomogeneity showed that such elements as magnesium and manganese burn out in hybrid welding without a filler material. This results in formation of pores in cast / remelted part of the welds. Analysis of hydrogen content in welded joint metal verified the dependence of their quality, in particular growth of pore number, on increase of hydrogen content. The use of filler wire permitted to control the process of alloying welds and eliminate the effect of pore formation.

6. Application of laser-plasma welding of aluminium alloys enables to enlarge weld penetration depth by 2–4 times as compared to laser welding and to raise welding speed approximately the same way as compared to plasma welding.

7. Comparison of Ñ Î $_2$- and diode laser showed that presence of hybrid effect, rooting of plasma arc within laser radiation heating zone and stability of high-speed hybrid welding process are rather stipulated by radiation focusing rate than by its wavelength.

8. Tensile strength and impact toughness mechanical test of joints of À Ì ts3, À Ì g5, À Ì g6, 1915 aluminium alloys, as well as of 08Kh17Ò and Kh18N9Ò stainless steels, proved the advantage of hybrid method over laser and plasma ones.

1. Petring, D., Fuhrmann, C., Wolf, N. et al. (2003) Investigations and applications of laser-arc hybrid welding with the «integrated nozzle». In: *Proc. of 2nd Int. WLT Conf. on Lasers in Manufacturing* (Munich, June 2003), 1–6.
2. Paton, B.Å., Gvozdetsky, V.S., Krivtsun, I.V. et al. (2002) Hybrid laser-microplasma welding of thin sections of metals. *The Paton Welding J.*, **3**, 2–6.
3. Grigoriants, A.G., Shiganov, I.N., Chirkov, A.M. (2004) *Hybrid technologies of laser welding*: Tutorial. Moscow: N.E. Bauman MGTU.
4. Garaschuk, V.P., Shelyagin, V.D., Nazarenko, O.K. et al. (1997) 10 kW technological Ñ Î $_2$-laser LT 104. *Avtomatich. Svarka*, **1**, 36–39.
5. Shelyagin, V.D., Khaskin, V.Yu. (2002) Tendencies in development of laser-arc welding (Review). *The Paton Welding J.*, **6**, 25–28.

APPLICATION OF MATHEMATICAL MODELING TO OPTIMIZE THE PROCESS OF LASER BRAZING-WELDING OF DISSIMILAR TITANIUM-ALUMINIUM ELEMENTS OF PASSENGER AIRLINER STRUCTURES

V.I. MAKHNENKO and **A.S. MILENIN**
E.O. Paton Electric Welding Institute of NASU, Kiev, Ukraine

The advanced requirements to quality of aircraft constructions and growing lately competition at the market of aircraft building force producers to apply the newest science intensive technologies in industry. One of priority directions in this field is application of beam welding technologies to produce the permanent connections of metallic details. For achievement of necessary set of properties of units dissimilar welded structures can be used. In particular, to decrease the weight, to increase the corrosion resistance and working life of seat tracks of passenger airliners A380 of the production of Airbus for their making aluminum and titanium elements are used. To their joint the laser brazing-welding technology was developed. To estimate the influence of some technological parameters of this process on performance properties of dissimilar structures a mathematical model that gives an opportunity to find the rational modes of the given welding cycle, was created.

Well known advantages of beam welding, such as high energy concentration, flexibility, controllability, cause actual progress in developing and manufacturing application of beam welding technologies and particularly of laser beam welding. They give an opportunity to carry out production cycles of high complexity and science intensity [1, 2].

Welding of dissimilar materials with sufficient difference in thermal, physicochemical or mechanical properties has always been a challenge for specialists because such welded structures have unique properties but it is very difficult to achieve their satisfactory quality. There are several common reasons of decrease of exploitation properties of dissimilar welded joints: formation of brittle intermetallic compounds as a result of limited mutual solubility of metals under processing; shift of the welded parts relatively to each other caused with different coefficient of thermal expansion; overheating of the heat-affected zone because of deference in thermal conductivity; tendency to galvanic corrosion if two dissimilar metals form galvanic couple in corrosive medium [3–5].

One of the most relevant pair of metals for dissimilar welded joints is aluminium and titanium. High strength and corrosion stability of titanium combined with light weight of aluminium lead to set of rather useful properties of dissimilar structures for aerospace, automotive, chemical industries. But the welding these metals faces some difficulties. One of them is that welding techniques those intend the mixing of liquid phases of metals are excluded because of very low solubility of titanium in aluminium [6, 7].

In view of sufficient difference of titanium and aluminium melting temperatures, joining of these metals could be effectively carried out using brazing-welding technique without melting of titanium but in presence of aluminium molten pool [8]. Such process is very sensitive to technological parameters and their fluctuation, so the use of beam technologies to obtain the titanium-aluminium joints seams to be preferred.

Particularly, for welding of dissimilar seat tracks of passenger airliner A380 in Bremer Institut fuer angewandte Strahltechnik the technology of laser beam brazing-welding has been developed [9]. For more effective optimization of this process from the point of view of possible brittle intermetallic phase formation, hot cracking of aluminium part of joint and residual stress-strain state of dissimilar structure, corresponding mathematical model has been developed.

Description of brazing-welding of the titanium-aluminium seat-tracks. Seat track is used in construction of passenger airliner A380 is a flange beam of complex profile, one part of which is made from titanium alloy Ti6Al4V, another one –– from aluminium alloy AA6056 (Figure 1). Chemical compositions of AA6056 and Ti6Al4V alloys are as follows, wt.%: 0.7–1.3 Si, 0.5 Fe, 0.5–1.1 Cu, 0.4–1.0 Mn,

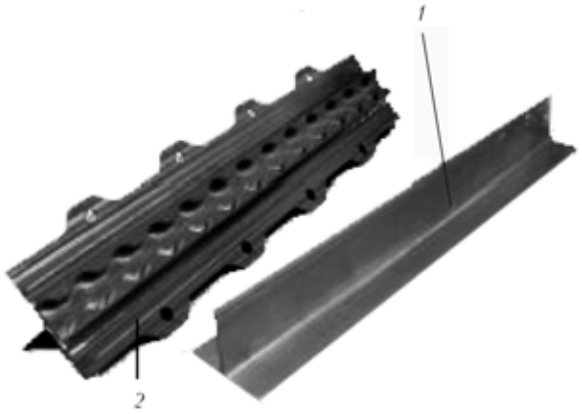

Figure 1. Aluminum (*1*) and titanium (*2*) parts of dissimilar seat track

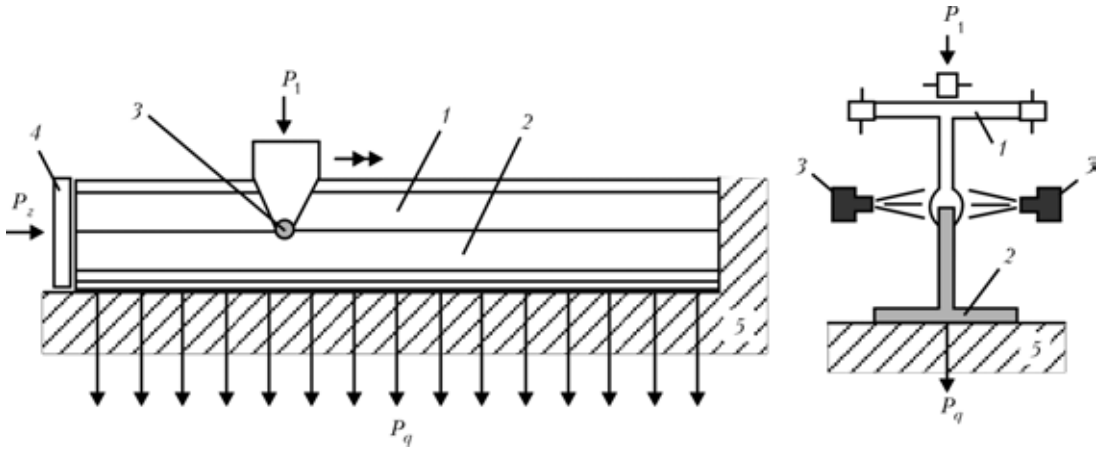

Figure 2. Scheme of the laser brazing-welding of titanium-aluminum joints: *1* — aluminum part; *2* — titanium part; *3* — laser welding heat source; *4* — plunger providing axis force; *5* — supporting table

0.6–1.2 Mg, 0.25 Cr, 0.1–0.7 Zn, and 5.3–6.8 Al, 3.5–5.3 V, 0.05 N, 0.1 C, 0.0125 H, 0.3 Fe, 0.2 O.

The main concept of brazing-welding under consideration lies in melting of the aluminium edge with the concentrated welding heat source but without melting of titanium one; liquid aluminium spreads over the surface of solid titanium under the action of gravitation and forms the brazing-welding dissimilar contact.

Welding process, the scheme of which is shown in Figure 2, is carried out with two symmetrical laser welding heat sources from both sides of the workpiece simultaneously by their moving along the welded joint. The workpiece is positioned in force attachments, where three types of forces are applied: distributed force P_q that presses titanium part of seat-track to supporting table; axial force P_z applied with the help of plunger of the form of seat-track cross section; and concentrated pressing force P_1 in the region of laser welding heat source action, that is made with sliding unit. The values of the forces and some other technological parameters of brazing-welding of dissimilar seat track are given below:

Welding heat source motion rate, mm / s	4.33
Power of each of welding heat sources, kW	1.75
Welding spot diameter, mm	5.0
Height of the beam wall aluminum part, mm	38.4
Height of the beam wall titanium part, mm	42.6
Distributed force P_q, N / mm	4.41
Axis force P_z, N	376
Pressing force of sliding unit P_1, N	756

In fact the value of the laser heat sources power and their motion rate could be varied over some range but not only possess the chosen ones given above. These ranges were determined by the analysis of a number of experiments and the main criterion of choice was the good formation of the seam. It was found that normal wetting of solid titanium with liquid aluminium and satisfied stability of the seam along the welded contact take place with power of each heat source within the range 1.5÷2.0 kW and their motion rate within the range 2.33÷5.33 mm / s. Because of different heat input at the variation of technological parameters the seam geometry different, e.g. within the limits of proposed values of welding heat source motion rate and power the length of wetting of titanium with aluminium varies within the range from 2 to 6 mm.

Mathematical modeling of brazing-welding process and its optimization. As it was already mentioned there are several processes, those should be taking into account at optimization of dissimilar joint welding. In case of brazing-welding of titanium to aluminium main problem is to avoid the formation of such defects as brittle intermetallic compounds in the region of dissimilar contact and hot cracks in aluminium part of welded joint.

In addition to risk of defects formation there is a possibility of high residual bending state of welded beam caused with kinetics of strain-stress state of the welded workpiece. This effect should be also diminished or excluded by means of choosing of rational parameters of welding process.

There are several conventional approaches for optimization of production cycles, but if many interrelated factors determine quality of the final product the most efficient way of optimization is to combine theoretical prediction with experimental observation and validation. This approach seems to be the most appropriate in case of brazing-welding of titanium to aluminium under consideration because in this case the processes of thermal expansion, melting and flow of liquid aluminium, wetting and forming of seam, reactive diffusion, fields of strain and stress formation and progress are interdependent and should be taken into account.

Within the framework of developed mathematical model the processes of liquid flow and seam formation (i.e. dependencies of the geometrical parameters of the seam on the technological parameters of the process) are taken into account on the basis of experimental data. Moreover, because the time of the seam formation is relatively small and the influence of this process on the temperature, strain and stress kinetics is insufficient, it is accepted that the shape of the seam is given preliminary.

The scheme of dissimilar welded joint is shown in Figure 3. As an example of the dependencies of geometry of welded joint on welding parameters, the

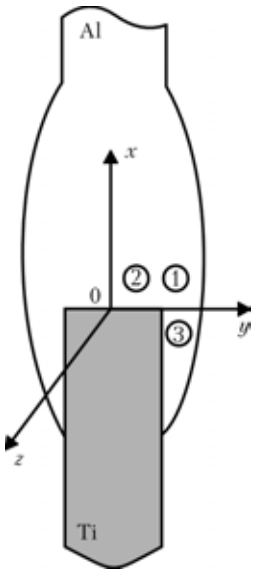

Figure 3. Scheme of dissimilar joint. Regions 1–3 are chosen for investigation of the hot crack formation risk

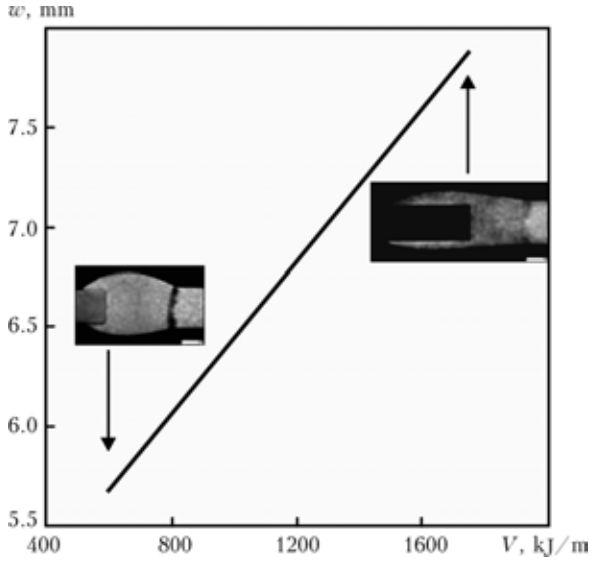

Figure 4. Dependence of seam width w on rate of energy supplied to laser beam welding source V

length of the seam as a function of the heat input is shown in Figure 4.

First step of the modeling of the brazing-welding of titanium-aluminium seat-track is numerical determination of temperature field kinetics during welding. With this aim the thermal conductivity equation was numerically solved:

$$c\rho(x, y, z, T)\frac{\partial T(x, y, z, t)}{\partial t} = \frac{\partial}{\partial x}\times \left(\lambda(x, y, z, T)\frac{\partial T(x, y, z, t)}{\partial x}\right) + \frac{\partial}{\partial y}\times \left(\lambda(x, y, z, T)\frac{\partial T(x, y, z, t)}{\partial y}\right) + \frac{\partial}{\partial z}\times \left(\lambda(x, y, z, T)\frac{\partial T(x, y, z, t)}{\partial x}\right), \quad (1)$$

where $T(x, y, z, t)$ is the temperature at the point (x, y, z) of rectangular axes at the moment of time t; $\lambda(x, y, z, T)$ is the thermal conductivity of the metal at the point (x, y, z), temperature in which equals to T; $c\rho(x, y, z, T)$ is the volumetric heat capacity of the material.

Surface distribution of energy across laser beam welding spot $q(x, y, z)$ is accepted according to Gaussian distribution law [10]:

$$q(x, z, t) = \eta(x)Q\frac{k}{\pi}\exp(-k(x - x_0)^2 - k(z - vt)^2), \quad (2)$$

where $\eta(x)$ is the efficiency of heat input that depends on x-coordinate because aluminium and titanium have different reflectivity of laser radiation; Q is the power supplied to each laser welding heat source; v is the motion rate of welding heat source along the joint being welded; $k \cong 14/d^2$; d is the diameter of laser beam spot; x_0 is the position of welding spot centre. In welding process under consideration welding spot is positioned at the level of titanium edge, i.e. $x_0 = 0$.

To obtain valid results it is necessary to have accurate values of efficiency of laser welding heat source above aluminium and titanium surfaces. In general case these values depend on great number of parameters, such as state of the surface, incidence angle of the laser beam, local atmosphere in the region of the welding spot and so on. So, it is reasonable to estimate efficiency for every concrete welding process.

For the laser beam welding process under consideration the method of determination of the laser heat source efficiency above the aluminium and titanium was as follows: sets of thermocouples were set up at the different cross-sections of the seat-track being welded; then variation of the efficiency coefficients within the limits of the mathematical model up to the best correlation of experimental and calculated thermal cycles allowed obtaining the efficiency of laser beam for this case.

The properties of used metals are given in the Table.

Numerical solution of the thermal conductivity equation (1) gave an opportunity to estimate the values of heat input efficiency depending on the type of material ---- aluminium η_{Al} and titanium η_{Ti}. The best

Physical and mechanical properties of aluminum alloy AA6056 and titanium alloy Ti6Al4V [16, 17]

Alloy	σ_t, Ì Pa, at T, °C		$E\cdot10^{-5}$, Ì Pa, at T, °C		λ, W / (mm·°C) at T, °C		$c\rho\cdot10^2$, J / (mm^3·°C), at T, °C	
	20	500	20	500	20	500	20	500
AA6056	220	100	0.98	0.60	0.11	0.20	0.250	0.295
Ti6Al4V	1060	460	1.19	0.91	0.0059	0.0128	0.248	0.301

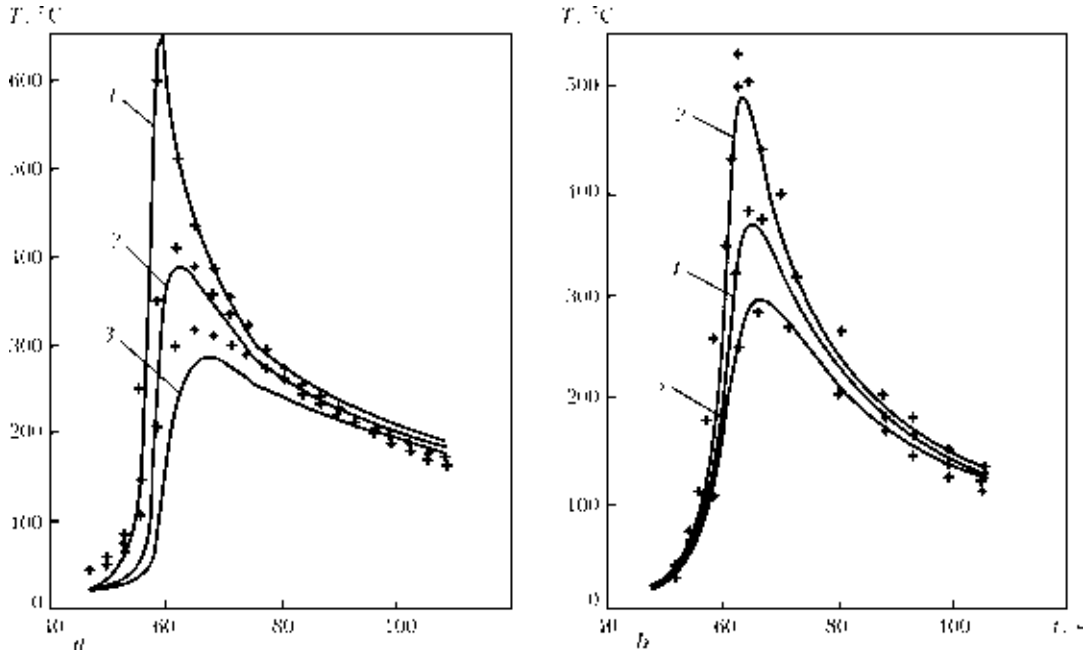

Figure 5. Calculated (solid line) and experimental (dots) values of temperature cycles at distance of 3 (*1*), 6 (*2*), 9 (*3*), 12 (*4*) and 18 (*5*) mm from the titanium edge towards the titanium (*a*) and aluminum (*b*) part of workpiece

adequacy of experimental and calculation data were observed with η_{Al} = 0.17 and η_{Ti} = 0.30. Obtained calculated temperature cycles in several regions and their comparison with the experimental data are shown in Figure 5.

Even though the liquid phases of titanium and aluminium are not mixed during brazing-welding process there is a risk of formation of intermetallic compound layers in the region of the dissimilar contact [11].

Experimental and theoretical researches in this field showed that in case of surface contact of liquid aluminium and solid titanium during relatively small period of time (exactly how it takes place in brazing-welding process) $TiAl_3$ layer can form [12]. This intermetallic compound has very low exploitation properties so presence of $TiAl_3$ layers of high thickness in the titanium-aluminium dissimilar seam can sufficiently reduce the quality of the welded joint.

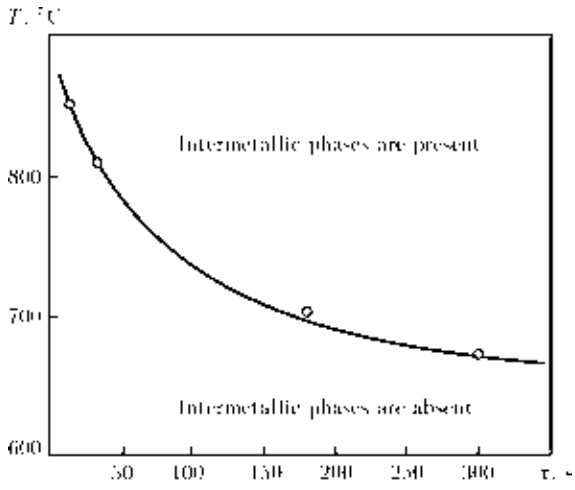

Figure 6. Temperature-dependent latent period of $TiAl_3$ formation in region of the solid titanium and liquid aluminum surface contact [11]

Because of specificity of reaction diffusion processes there is temperature-dependent latent period of the $TiAl_3$ layers formation [8]. So in case of corresponding optimization of brazing-welding process it is possible to obtain dissimilar titanium-aluminium joints without such defects.

The temperature dependence of the latent period of intermetallic formation for the stationary case is shown in Figure 6. For the nonsteady case the conception of coefficient of intermetallic phase formation χ can be used. Its mathematical expression is as follows [11]:

$$\chi = \int_0^{t_0} \frac{dt'}{\tau(T)}, \qquad (3)$$

where t_0 is the observable time of staying of the given point of the contact of solid titanium with liquid aluminum; $T = T(t')$ is the time-temperature dependence at the given point on the moment of time t'; $0 \le \le t' \le t_0$; $\tau(T)$ is the duration of temperature-dependent latent period.

In this case the fulfilling a condition $\chi < 1$ along the contact surface guaranties the absence of the intermetallic layers of sufficient thickness.

As an example in Figure 7 the distribution of values of χ in case of welding under technological parameters given above is shown. It can be seen that under such condition maximum value of χ (that takes place near the *x*-position of the welding heat source) does not exceed 0.015. It means that chosen geometry of the welded joint practically excludes formation of brittle intermetallic layers.

But as it was mentioned, there are ranges of variation of main welding parameters ---- motion rate and power of laser beam welding source. The changing of these parameters influences on the maximum value of

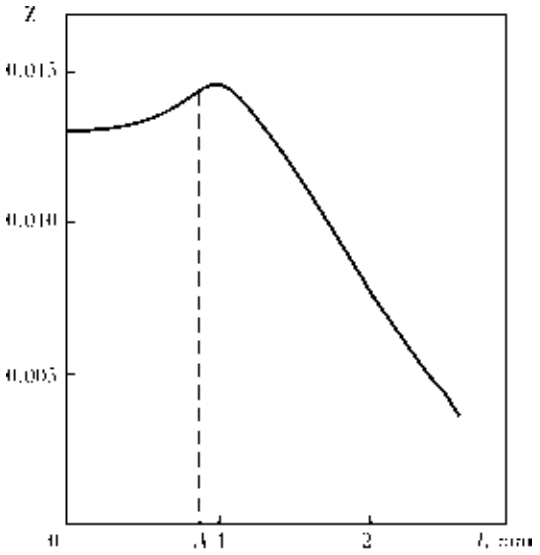

Figure 7. Distribution of χ values along the dissimilar contact: *l* — length of the contact line between the given point and 0

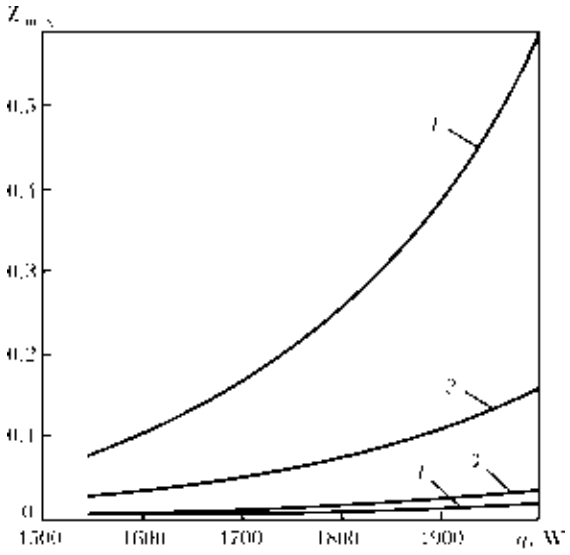

Figure 8. Dependence of maximum χ values on technological parameters at the laser source motion rate of 2.33 (*1*), 3.0 (*2*), 4.33 (*3*) and 5.0 (*4*) mm / s

coefficient of intermetallic phase formation. Results of numerical research of this influence are shown in Figure 8. It can be seen that value of χ increases with increasing of the welding source power and decreasing of its motion rate. This can be explained by higher maximum temperature achieved in the region of dissimilar contact and also by longer staying of titanium-aluminium surface contact under high temperature. Maximum value of coefficient of intermetallic phase formation is lower than 1, but relatively small fluctuation of the position of welding heat source, its power or the geometry of the seam could result in high probability of intermetallic layers appearing in case of power near to maximum possible and minimal possible motion rate.

But one of advantages of laser beam welding consists in high stability of welding parameters. It allows one to state that in all range of possible changing of motion rate and power of welding heat source the risk of formation of brittle intermetallic layers is small enough.

One more well known problem is possible hot cracking of aluminium during welding. Moreover alloy AA6056 used for aluminium part of seat-track is inclined to hot cracking [13].

Formation of hot cracks takes place in temperature interval of brittleness and is caused with thermodeformational processes in the region of seam or heat-affected zone. Hence for estimation of the risk of hot cracking the kinetics of strain state of workpiece being welded should be studied.

For this aim on the basis of calculated kinetics of temperature field the mathematical model of thermodeformational processes was developed.

The technique of the numerical determination of stresses and strains during the welding process is based on the numerical solution of the corresponding problems of the nonstationary thermoplasticity by means of the successive tracing of the development of elastic-plastic deformations starting with primary state before the welding and finishing with the final state after the cooling and unloading of the welded seat-track.

The principle of the presenting of increment of deformation tensor components ε_{ij} as sum of increments of elastic ε^e_{ij} and plastic ε^p_{ij} deformations is put into the basis of elastic-plastic deformational state tracing:

$$d\varepsilon_{ij} = d\varepsilon^e_{ij} + d\varepsilon^p_{ij}. \qquad (4)$$

From (4) on the basis of Hook's law and plastic yielding law, the correlation between strains and stresses could be expressed as follows [14]:

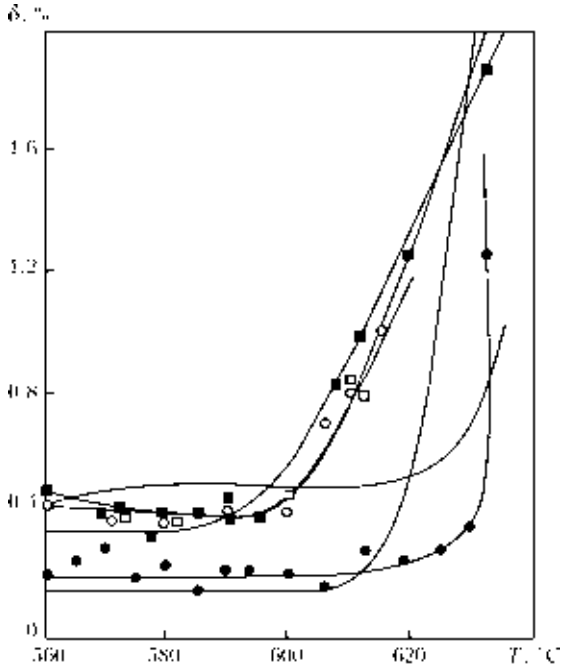

Figure 9. Critical δ values of deformation in temperature interval of brittleness for typical aluminum alloy [15]

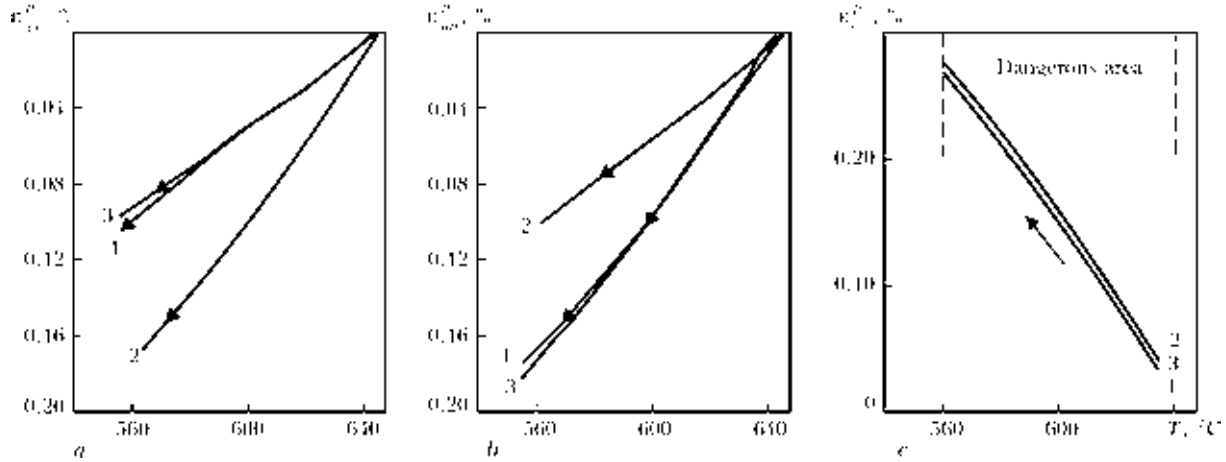

Figure 10. Kinetics of accumulation of plastic deformations ε_{xx}^{p} (*a*), ε_{yy}^{p} (*b*) and ε_{xx}^{p} (*c*) in temperature interval of brittleness at cooling for chosen areas 1–3 (see Figure 3)

$$\begin{cases} d\varepsilon_{xx} = d\left(\dfrac{\sigma_{xx} - \sigma}{2G} + K\sigma + \varphi\right) + (\sigma_{xx} - \sigma)d\Lambda \\ d\varepsilon_{xx} = d\left(\dfrac{\sigma_{yy} - \sigma}{2G} + K\sigma + \varphi\right) + (\sigma_{yy} - \sigma)d\Lambda \\ d\varepsilon_{xy} = d\left(\dfrac{\sigma_{xy}}{2G}\right) + \sigma_{xy}d\Lambda, \end{cases} \qquad (5)$$

where σ_{xx}, σ_{yy} and σ_{xy} are the components of stress tensor; $\sigma = 1/3(\sigma_{xx} + \sigma_{yy} + \sigma_{zz})$; G is the shear modulus; K is the modulus of volume compression; φ is the function of relative elongation; Λ is the scalar function, the value of which depends on strain-stress state in every region of workpiece being welded.

Component $d\varepsilon_{zz}$ is determined from the position of beam theory as linear function of x and y with taking into account of axis curvature of the beam being welded and momentum of applied external forces.

Solution of the boundary problem is carried out by finite-element method.

Conventional criterion of the hot cracking consists in simultaneous fulfilling of two conditions in the region of the size sufficient for generation of hot crack (specific linear dimension more than 1 mm): first, plastic deformations those have been accumulated during cooling at the temperature interval of brittleness should be greater that some critical value, and, second, correspondent normal components of stress tensor should be positive. So with the object to check the fulfilling of these conditions growth of the plastic deformations in characteristic regions of the aluminum part of dissimilar welded joint should be studied.

Critical values of plastic deformations of aluminum alloy, similar to used one, are shown in Figure 9. For more conservative estimation it was accepted that critical value of plastic deformation in temperature interval of brittleness 560–640 °C is equal to 0.2 %.

Figure 10 shows an example of kinetics of accumulation of different components of the vector of plastic deformations in the regions marked in Figure 3. The technological parameters of welding process correspond to those listed above.

It can be seen that values of ε_{xx}^{p} and ε_{yy}^{p} are negative and can't cause hot cracks formation. As for ε_{zz}^{p} two conditions of hot cracking are obviously fulfilled, so formation of transversal hot cracks is possible. If linear dimension of the region of fulfilling of theses conditions is larger than 1 mm, the risk of formation of macrodefects is inadmissibly high. But as numerical research within the framework of developed mathematical model for this welding mode showed the di-

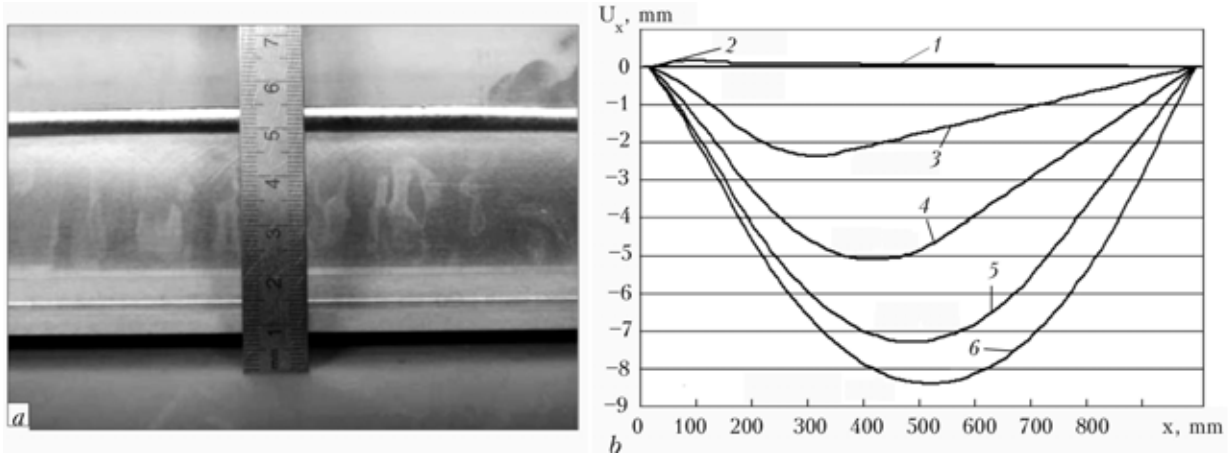

Figure 11. Experimentally measured maximum residual displacement U_x of the seat track axis (*a*), and calculated kinetics of the axis shape (*b*) at 5 (*1*), 50 (*2*), 100 (*3*), 150 (*4*), 200 (*5*) s after the end of welding and unloading and in residual state (*6*)

mension of this region doesn't exceed 0.6 mm in all characteristic regions of the welded joint.

Calculated kinetics of the deformational state of the welded seat-track gives an opportunity to estimate its final shape after the end of welding and unloading of the welded structure.

Experimental research showed that chosen geometry isn't successful, because the residual bending is very high (about 8 mm, Figure 11, *a*). That result corresponds to the data obtained with help of mathematical modeling (Figure 11, *b*). It means that in case of these technological parameters postweld treatment (straightening) of the welded seat-track is necessary. But additional stage in product cycle undesirable because it increases manufacturing cost of seat-tracks.

The rational way to diminish residual bending of the beam and to avoid postweld treatment is to optimize technological cycle. Increasing of the loading of the welded dissimilar beam in force attachment is the most straightforward method, but not effective one. Numerical research showed that even rigid clamping of the welded beam to the supporting table can not reduce residual strain state sufficiently. The most efficient way is to move dissimilar welded joint towards the titanium shell. In this way the higher stiffness of titanium wall will be compensate with the greater mass of aluminum one. It allows decreasing the residual deformation of the welded beam and also the weight of seat-tracks, because for aerospace structures minimal weight is one the most important problem to be solved.

Optimum position of the seam in case of same other geometrical parameters is at distance 2.2 mm from titanium shell. Such changing of welded seam position allows reducing the maximum residual bending more than by the factor of 4, namely maximum value of residual bending is less than 2 mm. The influence of the change of laser welding heat sources motion rate and their power is not sufficient.

It should be noted that all other calculations (estimation of risk of defects formation) in case of changed seam position remain valid because they concern of local processes under high temperatures.

CONCLUSIONS

1. Mathematical model of thermodeformaional processes during brazing-welding of dissimilar titanium-aluminium seat-tracks of passenger airliners A380 has been developed; with the help of developed model the optimization of this technological cycle from the point of view of defect formation (brittle intermetallic layers and hot cracks) and residual strain state of welded product has been carried out.

2. It was shown that the geometry of welded joints and characteristic properties of laser beam welding process allows the risk of the formation of brittle $TiAl_3$ layers to be minimized for all accepted range of variation of main welding parameters (motion rate of laser welding heat sources and their power).

3. It was found that there is possibility of transversal hot cracks formation in the aluminum part of dissimilar region, but the linear size of the area of high plastic deformation is too small for formation of macrodefects and is slightly dependent on variation of main technological parameters within the determined range.

4. With the help of prediction of residual bending state of dissimilar seat-track within the framework of developed mathematical model it was shown that the most efficient way of diminishing of residual distortion is to move the welded seam towards the reducing of titanium part of beam wall and enlarging of aluminum one. It gives an opportunity to obtain low residual axis curvature of the beam and to reduce the structure weight.

Acknowledgments. The authors of this research appreciate the contribution of Dr. Th. Pretorius and his colleagues from BIAS (Bremen, Germany) that has been made to validation of developed mathematical models.

1. Williams, J.C., Edgar, A., Starke, Jr. (2003) Progress in structural materials for aerospace systems. *Acta Mater.*, **51**, 5775–5799.
2. Turner, M.W., Schmidt, M.J.J., Li, L. (2005) Preliminary study into the effects of YAG laser processing of titanium 6Al–4V alloy for potential aerospace component cleaning application. *Appl. Surface Sci.*, **247**, 623–630.
3. Rabkin, D.M., Ryabov, V.R., Gurevitch, S.M. (1975) *Welding of dissimilar joints*. Kiev: Tekhnika.
4. Kamachi Mudali, U., Ananda Rao, B.M., Shanmugam, K. et al. (2003) Corrosion and microstructural aspects of dissimilar joints of titanium and type 304L stainless steel. *J. Nuclear Materials*, **321**, 40–48.
5. Mai, T.A., Spowage, A.C. (2004) Characterisation of dissimilar joints in laser welding of steel-kovar, copper-steel and copper-aluminium. *Materials Sci. and Eng. A*, **374**, 224–233.
6. Wagner, F., Zerner, I., Kreimeyer, M. et al. (2001) Characterization and properties of dissimilar metal combinations of Fe / Al and Ti / Al sheet materials. In: *ICALEO Proc., LIA Congress Proc.* (Orlando, USA), 365–374.
7. Ryabov, V.R. (1983) *Welding of aluminium and its alloys with other metals*. Kiev: Naukova Dumka, 24.
8. Sabokar, V.K., Zamkov, V.N., Kireev, L.S. (1998) Features of argon-arc and diffusion welding of titanium and aluminium. *Avtomatich. Svarka*, **1**, 14.
9. Kreimeyer, M., Vollertsen, F. (2005) Processing titanium-aluminum hybrid joints for aircraft applications. In: *Proc. of 3rd Int. WLT Conf. on Lasers in Manufacturing* (Munich, June, 2005).
10. (1988) *Theory of welding processes*. Ed. by V.V. Frolov. Moscow: Vysshaya Shkola, 154–155.
11. (1986) *Metallurgy and technology of welding of titanium and its alloys*. Ed. by V.N. Zamkov. Kiev: Naukova Dumka.
12. Dybkov, V.I. (2002) *Reaction diffusion and solid state chemical kinetics*. Kyiv: IPMS, 144.
13. Cicala, E., Duffet, G., Andrzejewski, H. et al. (2005) Hot cracking in Al–Mg–Si alloy laser welding — operating parameters and their effects. *Materials Sci. and Eng. A*, **395**, 1–9.
14. Makhnenko, V.I., Velikoivanenko, E.A., Pochinok, V.E. (1999) Numerical methods of the predictions of welding stresses and distortions. In: *Welding and Surfacing Rev.*, Vol. 13, Part 1. Harwood AP.
15. Prokhorov, N.N. (1976) *Physical processes in metals and alloys during welding*. Vol. 2. Moscow: Metallurgiya, 332.
16. (1967) *Physical properties of steels and alloys used in power engineering*. Moscow: Metallurgiya.
17. (1994) Titanium alloys. In: *Handbook on Material Properties*. ASM Int.

ROLE OF CAPILLARY THERMO-CONCENTRATION INSTABILITY IN LASER-INDUCED PROCESSES OF HEAT AND MASS TRANSFER

V.S. MAYOROV
Institute on Laser and Information Technologies of RAS, Shatura, Russia

The paper shows a new approach to thermo- and concentration-capillary convection in connection with simultaneously flowing processes of components redistribution, their interaction, competitiveness and transition from one to another. This consideration is connected with the capillary thermo-concentration instability (CTCI). The CTCI phenomenon has a considerable, and often a decisive influence on the course of physical processes under laser radiation interaction with a substance having at least one liquid phase. Thermodynamic analysis shows that for solutions of any substances, both surface-active and surface-inactive, surface tension grows with temperature in the broad range of variation of the thermodynamic system parameters. Only for pure (more likely, highly pure) substances the traditionally used regularity $d\sigma / dT < 0$ (where σ is the surface tension, and T is the temperature) is valid. As well as all natural substances are more or less «dirty», i.e. they necessarily contain impurities or microimpurities, the case $d\sigma / dT > 0$ occurs in experiments more often than the case $d\sigma / dT < 0$. Only at considerable overheating of the liquid (far from the solidus temperature) the case $d\sigma / dT < 0$ predominates. In the areas, where the impurities are present in microdoses and the change of the sign for $d\sigma / dT$ is observed, the oscillations and relaxation processes are possible, and generally the behavior of the thermodynamic system can be unstable. The change of the sign is not a simple substitution in the trend of any process, but as well a key opportunity to realization of absolutely new effects. The theory and practice of this phenomenon unite and describe a new class of effects widely spread in nature and is mostly interesting in local processes of interaction of light or laser radiation with matter. For example, CTCI gives new possibilities to control the liquid metal convection in the processes of welding and alloying.

Pre-history introduction. Still in the XIX century the phenomenon of a liquid surface layer overflow stimulated by a gradient of surface tension (Marangoni effect) was revealed. The so called Benard cells formed in a flat liquid layer uniformly heated from below have been known for a long time. Though instability of the system and origination of convective cells was initially ascribed to the forces of buoyancy (Archimedean forces), the defining role of capillary forces related to the dependence of liquid surface tension on temperature $\sigma = \sigma(T)$ was hereinafter shown. It was specified that the overflow of thin liquid films is also possible at the expense of differences in concentration of surface-active substances (SAS) by virtue of concentration dependence of surface tension $\sigma = \sigma(\xi)$. Some works pointed up the role of SAS in argon-arc welding. Thermocapillary convection was also studied in application to electron beam welding. Some certain interest to thermocapillary convection was recently aroused in the contributors engaged in studying the effect of laser radiation on materials. It can be stated that a good deal of experimental and theoretical works has been done in this line. Nevertheless no consideration was made of thermo- and concentration-capillary convection in connection with simultaneously flowing processes of components redistribution, their interaction, competitiveness and transition from one to another. This paper confirm that only for absolute pure substances the traditionally used regularity $d\sigma / dT < 0$ (where σ is the surface tension, and T is the temperature) is valid. As well as all natural substances are more or less «dirty», i.e. they necessarily contain impurities or microimpurities, the case $d\sigma / dT > 0$ occurs in experiments more often than the case $d\sigma / dT < 0$.

Thermodynamic principles of CTCI. Thermodynamics of surface effects makes a part of the Gibbs general theory of heterogeneous equilibrium. In line with the approach suggested by Van der Waals let us consider a surface layer of a finite thickness.

We make use of the general fundamental relationship for total internal energy E of the surface layer:

$$E = TS - PV + \sigma\Omega + \sum_{i=1}^{n} \mu_i m_i, \qquad (1)$$

where T is the temperature; S is the entropy; P is the pressure; V is the volume; σ is the surface tension; Ω is the discontinuity surface area; μ_i is the chemical potential of the i-th component; m_i is the mass of i-th component; n is the number of components.

From (1) we come to the equation

$$\Omega d\sigma = -SdT + VdP - \sum_{i=1}^{n} m_i d\mu_i, \qquad (2)$$

which, after being divided by the mass of surface layer $\sum_{i=1}^{n} m_i$, can be written as

$$\omega d\sigma = -sdT + vdP - \sum_{i=1}^{n} \xi_i d\mu_i, \qquad (3)$$

where ω is the molar surface; s is the molar entropy; v is the molar volume of the surface layer; ξ_i is the mole fraction of the i-th component in the surface layer.

At thermodynamic equilibrium, the chemical potentials for each of the components in the coexisting phases are equal, though the dependences of the chemical potentials on temperature, pressure and composition differ for different phases. So, for two phases separated by a surface layer it is possible to derive from (3) two independent equations and, having restricted ourselves to the case of a binary system, we can obtain the following expression that yields the differential dependence of σ on T at P = const:

$$\omega\left(\frac{d\sigma}{dT}\right)_P = s^{(1)} - s^{(\zeta)} + \frac{\xi_1^{(\zeta)} - \xi_1^{(1)}}{\xi_1^{(2)} - \xi_1^{(1)}}(s^{(2)} - s^{(1)}), \qquad (4)$$

where the superscript (1) corresponds to the first phase, (2) ---- to the second phase, (ζ) ---- to the surface layer.

The phase exhibiting a higher entropy $s^{(2)} - s^{(1)} > 0$ is chosen to be the second one. It follows from (4) that the temperature dependence of surface tension is substantially governed by the distribution of components between the coexisting phases and the surface layer.

Consider the case where the content of the first component in the surface layer far exceeds its content in both the coexisting phases: $\xi_1^{(\zeta)} >> \xi_1^{(1)}$ and $\xi_1^{(\zeta)} >> \xi_1^{(2)}$. The absolute value of the difference $\xi_1^{(2)} - \xi_1^{(1)}$ is much less than $\xi_1^{(\zeta)}$, and the fraction in the right-hand side of (4) will express a considerable value. An example of such a component is a SAS. Then, equation (4) produces the conditions

$$\left(\frac{d\sigma}{dT}\right)_P < 0 \text{ if } \xi_1^{(2)} < \xi_1^{(1)}; \qquad (5a)$$

$$\left(\frac{d\sigma}{dT}\right)_P > 0 \text{ if } \xi_1^{(2)} > \xi_1^{(1)}. \qquad (5b)$$

For the case of a liquid-vapor system inequalities (5a), (5b) show that the surface tension is reduced as the temperature rises, if the vapor is depleted of the SAS as against the liquid solution (SAS is a nonvolatile component). If the vapor is enriched with SAS as compared with the liquid solution (SAS has a higher volatility), the surface tension is increased.

In another case the first component is a surface-inactive substance (SIS). Its content is small both in the second phase and in the transition zone: $\xi_1^{(2)} << \xi_1^{(1)}$ and $\xi_1^{(\zeta)} << \xi_1^{(1)}$, and the multiplier for $(s^{(2)} - s^{(1)})$ in equation (4) will be a positive value approximating unity. The second phase shows higher entropy than the first one, so it can be assumed that, with rare exception (and always for solution-vapor systems), $s^{(2)} > s^{(\zeta)}$. This implies that the surface tension will increase with the temperature in this system under study too.

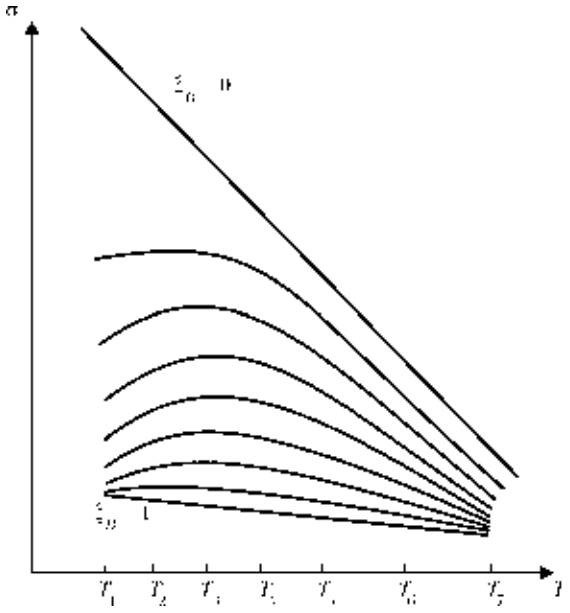

Figure 1. Schematic behavior of surface tension versus temperature for liquid system with A and B components ($\xi_A + \xi_B = 1$)

Only at considerable overheating of the liquid (far from the solidus temperature and near the critical point, where the surface tension aspires to zero) the temperature surface tension coefficient of solutions again becomes negative: $(\partial\sigma / \partial T)_{(\zeta)} < 0$. Therefore, in such systems the extremes of surface tension (Figure 1, intermediate curves) should be observed, and the value of $\partial\sigma / \partial T$ should be positive in some range of parameters T and ξ (Figure 2).

The free energy of the surface phase σ (surface tension) is one of the parameters of the thermodynamic system conditions and is connected to other parameters (as which can be selected temperature T, pressure P, adsorptions Γ_i of the components i, or structures ξ_i of the coexisting phases):

$$\sigma = \sigma[T, \Gamma_i, P] = \sigma[T, \Gamma_i(T, \xi_i), P]. \qquad (6)$$

The thermodynamic approach conducted for the case of stable equilibrium of phases of a multicompo-

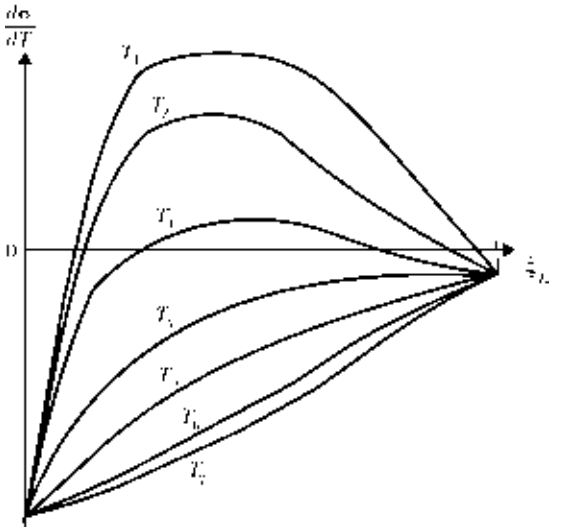

Figure 2. Concentration dependence of surface tension temperature coefficient for different temperatures

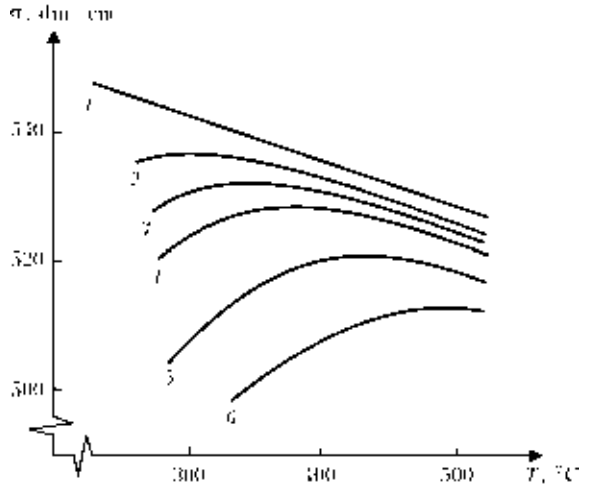

Figure 3. Sn–Te alloy polytherms for the tellurium concentration of 0 (*1*), 0.0046 (*2*), 0.0121 (*3*), 0.0177 (*4*), 0.0289 (*5*) and 0.0354 (*6*) %

nent system does not give concrete expressions for $\sigma = \sigma(T, \xi_i, P)$ but allows differential criterions to be formulated which describe the behavior of surface properties of the phase boundary. It would suffice to perform our analysis, because for convective force in a fluid not the σ absolute value, but the degree of its nonuniformity on the surface, i.e. its gradient (7), is important:

$$\begin{aligned} \text{grad}\ \sigma = (\delta\sigma / \delta T + \delta\sigma / \delta\Gamma\delta\Gamma / \delta / T)_\xi\ \text{grad}\ T + \\ + (\delta\sigma / \delta\Gamma\delta\Gamma / \delta\xi)_T\ \text{grad}\ \xi = \\ = (\partial\sigma / \partial T)_\xi\ \text{grad}\ T + (\partial\sigma / \partial\xi)_T\ \text{grad}\ \xi. \end{aligned} \tag{7}$$

Thus, by the example of a binary mixture with components *A* and *B* we shall consider how the surface tension σ can behave at simultaneous change of both temperature *T* and concentration ξ.

Some known examples from the literature. Figure 3 presents a set of polytherms of surface tension

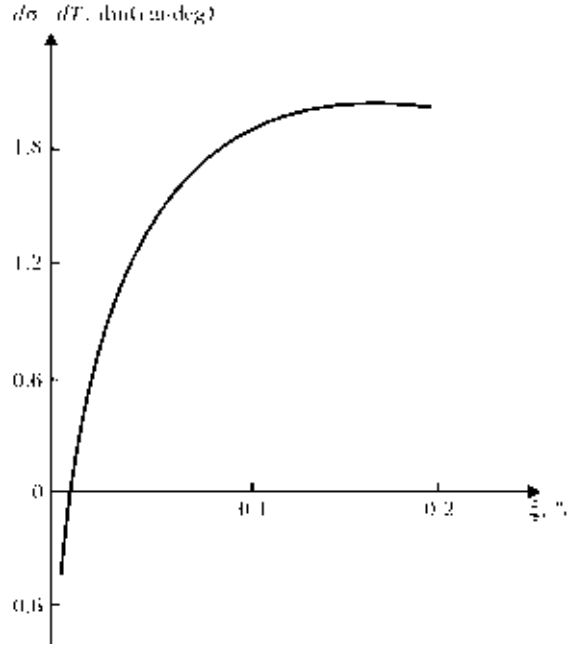

Figure 4. Dependence of surface tension temperature coefficient for Fe–O alloy versus concentration of oxygen

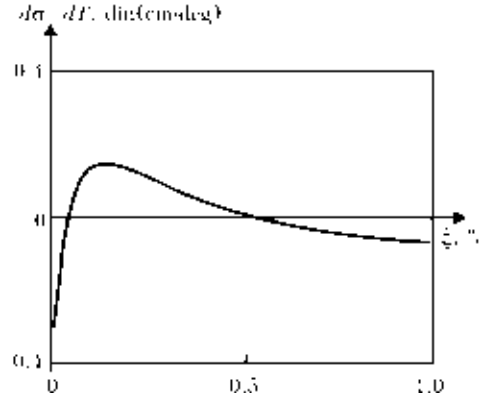

Figure 5. Dependence of surface tension temperature coefficient for Fe–Sn alloy versus concentration of tin

of the Sn–Te system (Figures 3 and 1 are similar, and it is necessary to pay attention to very strong influence of microdoses of the surface-active impurity); and Figures 4 and 5 illustrate concentration dependences of the temperature coefficient $\partial\sigma / \partial T$ for the systems Fe–O and Fe–Sn (the similarity of Figures 4, 5 and 2 is again obvious). In particular, from Figure 4 it is apparent that in laser heat treatment (melting) of iron-carbon alloys it is difficult to expect a pattern of streams in the liquid metal, typical for thermocapillary convection, because $\partial\sigma / \partial T < 0$ only for practically full absence of oxygen or other surface-active impurities ($\xi < 0.01$ %) in the processing zone.

So, it can be concluded that for solutions of any substances, both SAS and SIS, surface tension grows with temperature in the broad range of variation of the thermodynamic system parameters. In the areas, where the impurities are present in microdoses and the change of the $\partial\sigma / \partial T$ sign is observed, the oscillations and relaxation processes are possible, and generally the behavior of the thermodynamic system can be unstable and CTCI is realized. Besides the change of the $\partial\sigma / \partial T$ sign is not a simple variation in directionality of any processes, but also a key opportunity of absolutely new effects realization.

Convective movement in liquid melt at laser heating. All the experimental data show rather homogeneous distribution of an addition component over the liquid pool cross-section. It uniquely specifies the main role of convection in comparison with diffusion. The convective flows in the liquid pool are most simply described by 1D model of thermoinduced convec-

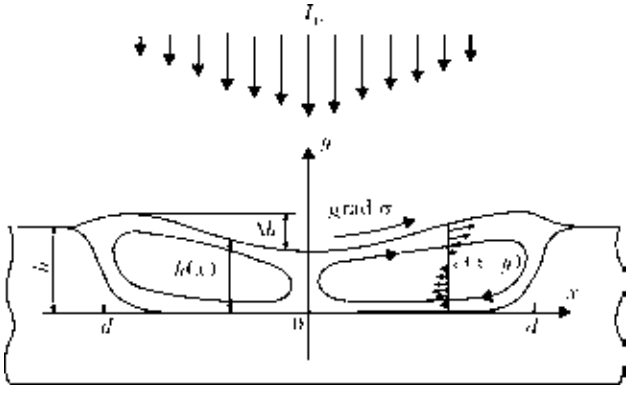

Figure 6. Schematic of fluid flow in molten pool

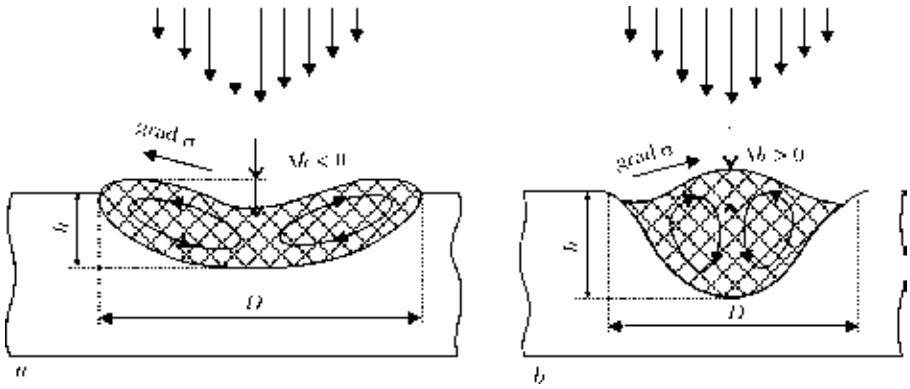

Figure 7. Thermo- (*a*) and concentration-capillary (*b*) effects in laser-melted zones

tion. It allows two most important parameters of alloying to be reasonably evaluated. Firstly, it is the characteristic velocity of melt movement and the degree of its intermixing (the number of convective cycles ---- revolutions of a melt movement during the liquid pool existence). Secondly, it is the degree of distortion of the alloyed zone profile. Within the framework of the indicated convection model we made the appropriate analytical calculations.

Consider the convection in the liquid melt pool in laser alloying (Figure 6). The calculations show that the stationary pattern of velocities over the cross-section in this case will be parabolic (8), and the depth of relief pattern is determined from expression (9), where $\Delta\sigma$ is the difference of surface tensions between the cross-sections $x = d$ and $x = 0$:

$$v_x = v_x^{\max}\left[3\left(\frac{y}{h}\right)^2 - 2\left(\frac{y}{h}\right)\right] = \frac{h}{4\mu}\frac{\partial\sigma}{\partial x}\times$$
$$\times\left[3\left(\frac{y}{h}\right)^2 - 2\left(\frac{y}{h}\right)\right] \approx \frac{h}{4\mu}\frac{\Delta\sigma}{d}\left[3\left(\frac{y}{h}\right)^2 - 2\left(\frac{y}{h}\right)\right]; \quad (8)$$

$$\Delta h = \frac{3}{2}\frac{\Delta\sigma}{\rho g h + \frac{\pi^2\sigma h}{d^2}} = \frac{3}{2}\frac{1}{\rho g h + \frac{\pi^2\sigma h}{d^2}}\frac{\partial\sigma}{\partial T}\times$$
$$\times\left[\frac{4a\mu d^2 I_0^2}{\lambda^2 h\left|\frac{\partial\sigma}{\partial T}\right|}\right]^{1/3}. \quad (9)$$

In our research it was shown that the nature of convective movement in a lamina of a liquid at local heating of its surface by laser radiation depends not only on temperature gradients, but also on the presence in the liquid the microimpurities, especially of SAS, which can entirely change the picture of convection.

In the absence of surface-active impurities the known common scheme of a thermocapillary convection (Figure 7, *à*) was realized, when the gradients and the liquid flow on the surface are directed from the center of the heated and melted zone to the edges. The addition a surface-active impurity to the sample resulted in the change of the sign of the gradients and, as a result of thermo-concentration capillary con-

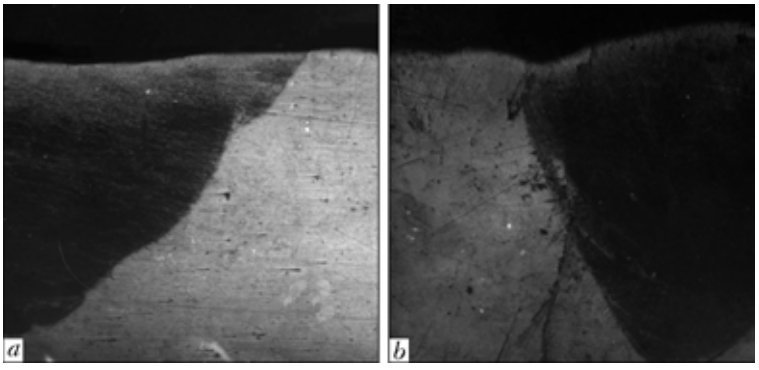

Figure 8. Laser-melted zone cross-section of the selenium-free 12Kh18N10T (*a*) and selenium-containing 12Kh18N10E (*b*) stainless steels

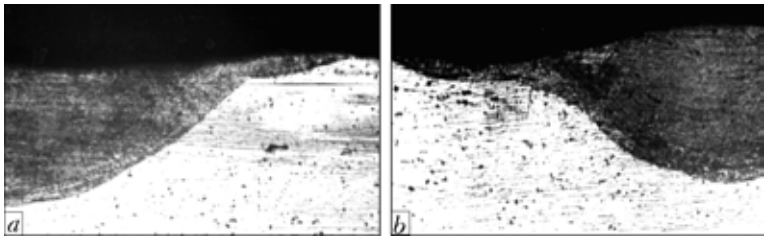

Figure 9. Samples of pure iron without (*a*) and with (*b*) sulfur in surface coating after laser melting

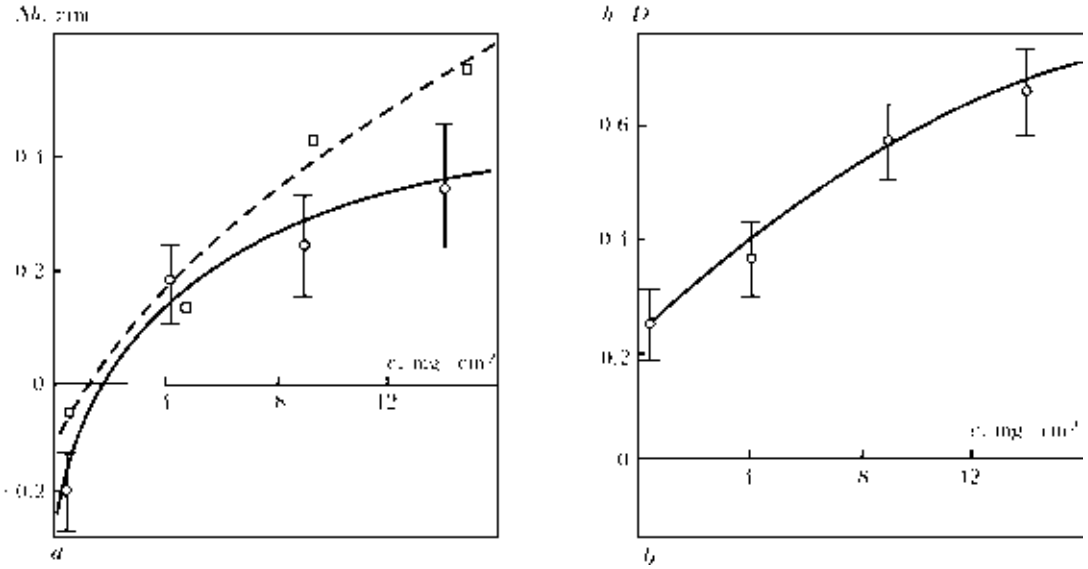

Figure 10. Surface ripple (*a*) and depth / width ratio (*b*) versus sulfur surface concentration at 1.5 kW CO_2-laser application: ❒ — pure iron; ❍ — steel

vection, the liquid in the melt pool moved to the center (Figure 7, *b*). Thus the use of selenium as a surface-active impurity in stainless steel forced the modification of the nature of convection (Figure 8). The addition of sulfur as a surface-active impurity to iron also resulted to thermo-concentration capillary convection (Figure 9). The change in difference of heights Δh of the alloyed path surface depending on the surface concentration of sulfur is shown in Figure 10.

The surface shapes and ripples of melted zones, obtained by many researchers after laser processing (generally, following any concentrated heating), are indicative of predominance of concentration effects, though the researchers themselves did not pay attention to it.

The purposeful use of SAS in production of doping compositions for laser alloying opens the path to active guidance of mass transfer processes and stabilization of parameters of modified layers in laser technologies.

CONCLUSION

The thermo-concentration instability phenomenon described makes itself most evident in those local enough conditions when surface tension forces start to prevail over other forces. The author makes the conclusion that in materials treatment with concentrated heat sources actually all technological processes are often governed by the above-stated phenomenon.

LASER STEREOLITHOGRAPHY — A NEW METHOD OF MAKING RELIEF MAPS FROM PHOTOGRAMMETRIC DATA

V.S. MAYOROV[1], A.V. EVSEEV[1], S.V. KAMAEV[1], A.P. MIKHAYLOV[2], M.V. KHOROSHEV[2], V.M. KURKOV[2] and A.B. VELYZHEV[2]

[1]Institute on Laser and Information Technologies of RAS, Shatura, Russia
[2]Moscow State University of Geodesy and Cartography, Russia

Relief maps (3D models of terrain) are used in many applications, especially when it is necessary to estimate fast some real picture from a mockup. Modern aerophotogeodetic activities are characterized by wide use of digital technologies in creating and updating maps of various purposes from materials of aerospace photography. Computer photogrammetric processing of these series of pictures allows a 3D model of an object to be made. From the 3D files generated, a real 3D mockup of any chosen territory (to the scale required) is created by the method of laser stereolithography. The present paper discusses the technique and technology developed and tested for expeditious making of such relief maps.

Peculiarities of photogrammetric processing of aerospace pictures. At present, photogrammetric processing of aerospace pictures is based on methods of digital photogrammetry and carried out on digital photogrammetric systems (DPS). A DPS makes the whole complex of work on building digital models of land relief and ortophotoplans necessary for creating relief maps as original materials.

The photogrammetric work processing includes definition of elements of external orientation of pictures by making spatial phototriangulation, digital relief models from stereo pairs of pictures and ortophotoplans. Some reference information is needed for photogrammetric processing; the elements of external orientation selected during the flight by means of inertial systems and the global positioning systems, as well as the reference points of the territory with fixed coordinates, can be used.

In most cases, digital terrain models (DTM) of two kinds — regular (a matrix of heights) or irregular (a Delaunay triangulation) — are generated from materials of aerospace photography. The DTM allows 3D visualizations and perspective views to be built, it also serving as a basis for resolving a number of applied problems.

The matrix of heights or digital elevation model (DEM) is a digital cartographical representation of the Earth's surface in the form of a regular grid whose corners set the value of the terrain elevations. The intervals between the neighboring nodes of the matrix are set to be equal along the X and Y axes of the local coordinate system and referred to as the grid step.

In the latter case, the model of the Earth's surface is built in the form of a Delaunay triangulation or triangulated irregular network (TIN) — a network of spatial triangles describing a second order surface. The vertices of the triangles are elevation pickets on the ground, providing an adequate description of the terrain by triangle planes. It is obvious that the density of the elevation pickets depends on the relief and its roughness. Besides elevation pickets, the structural lines of relief (thalwegs, watersheds, gully edge, slope soles and other fold lines) are used in generating a Delaunay triangulation.

The Delaunay triangulation provides a more adequate description of the Earth's surface as it takes into account all peculiarities of the relief as distinct from the height matrix where the level of the description detail of the surface is limited by the grid step. It is more convenient, however, to use a height matrix as a DTM for making ortophotoplans and resolving some applied problems (for example, creating relief maps). Therefore the Delaunay triangulation generated will be transformed into a regular matrix of heights, its grid step picked up with a minimum loss of accuracy describing the Earth's surface model.

Experimental work on generating a DTM from aerospace pictures has been executed on a Fotomod domestic DPS developed by Rakurs company, that makes it possible to carry out the whole complex of photogrammetric work processing of pictures.

As an example we will illustrate the results of constructing a DTM and ortophotoplan from pictures to a scale of 1:5000 taken by Wild RC-20 camera from a flying altitude of 900 m. Seven ground points with fixed geodetic coordinates and distinctly visible in pictures are used as reference points. Before processing on a Fotomod DPS the picture negatives were transformed into a digital form with the help of a photogrammetric scanner with a pixel size of 20 μm.

Figures 1–3 show a fragment of the picture with a Delaunay triangulation constructed as a DTM, a representation of the relief model by contours and a fragment of the ortophotoplan.

The digital relief model was transformed into a height matrix in DXF format to be used as original

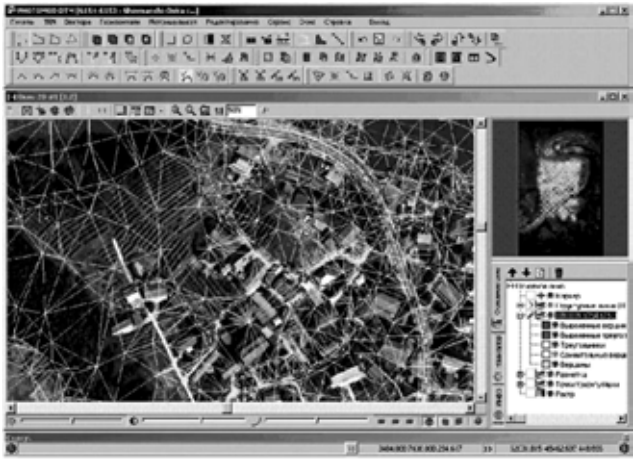

Figure 1. Generation of a Delaunay triangulation

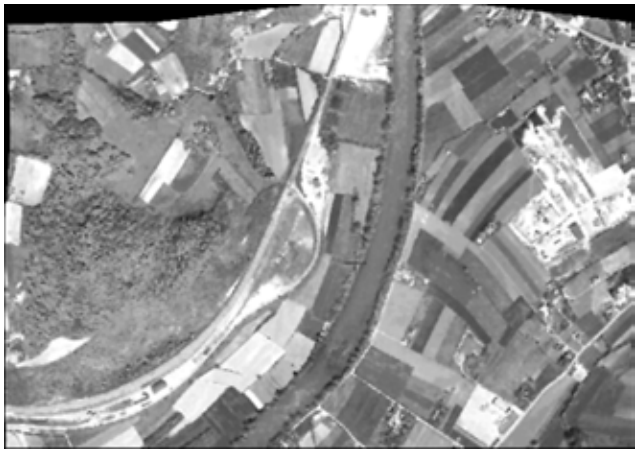

Figure 3. Terrain otophotoplan

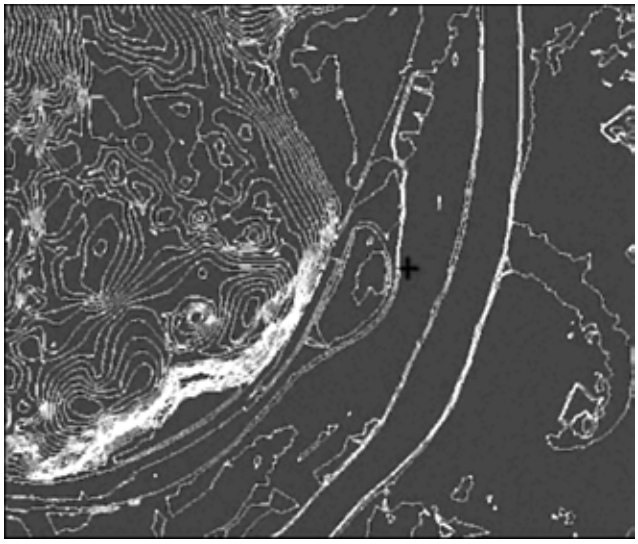

Figure 2. Relief model is represented by contours

materials for making a relief map of the terrain by means of laser stereolithography.

Manufacturing of terrain relief maps by means of laser stereolithography. Laser stereolithography, being one of the fast developing directions of expeditious manufacturing of prototypes, mockups and even functional objects from their 3D computer models, realizes the principle of direct image formation of 3D objects by consecutive (in particular, level-by-level) build-up of material. A local change of the phase condition of a homogeneous medium (transition from liquid to solid body state) as a result of the polymerization photoinitiated in a set volume provides the basis for stereolithography. Active centers are formed upon interaction of a photopolymerizing composition (PPC) with radiation of a certain spectral range. This spectral selectivity allows polymerization process to be made, in particular, under daylight conditions.

Laser stereolithography (Figure 4) includes creation of a 3D computer model of an object in STL format, its splitting into thin layers, calculation of

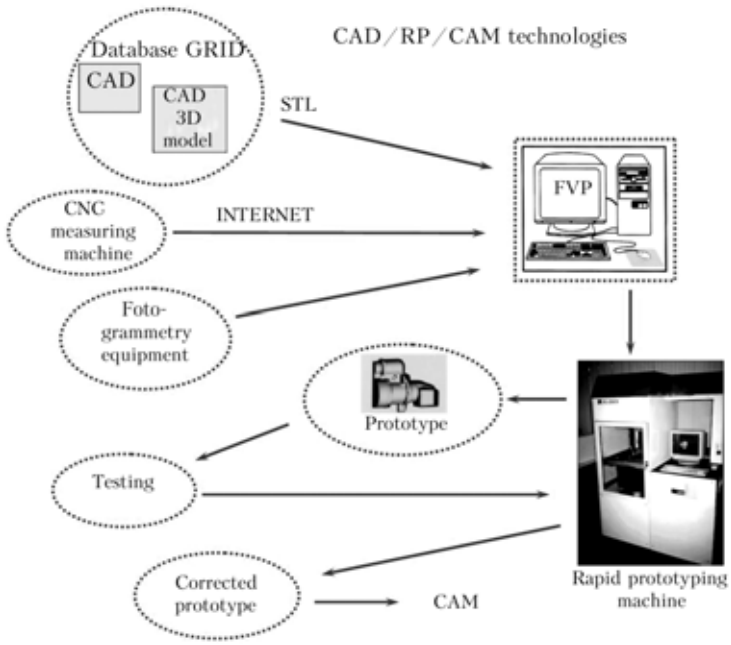

Figure 4. Step scheme of laser stereolithography

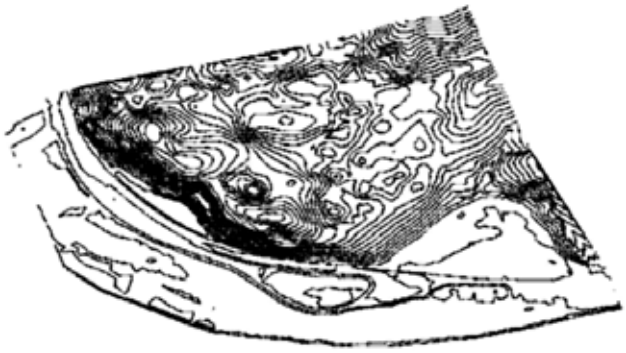

Figure 5. Set of contours

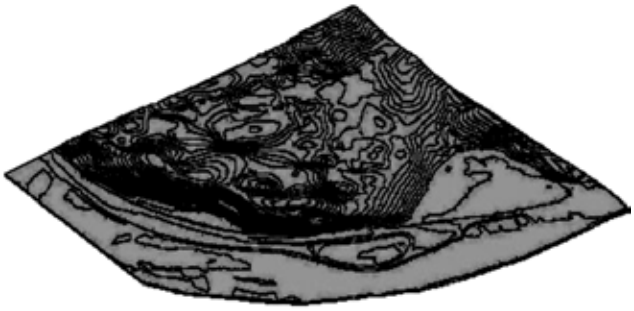

Figure 6. Level-by-level 3D computer model

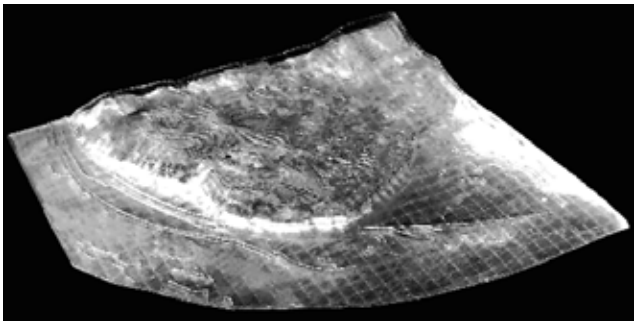

Figure 7. Plastic relief map

the motion trajectory of the laser beam filling in each section and consecutive reproduction of corresponding cross-sections on the liquid PPC surface by a focused laser ray initiating polymerization. In the area irradiated there is formed a film of solid polymer.

The original data for generating a 3D computer model of a portion of a terrain were a set of contours obtained as a result of transformation of photogrammetric data. The contours, with an interval of 2 m (in this case), have been presented in the form of DXF-files. Each contour was a closed or opened polyline (Figure 5). At the initial stage, each contour has been processed in order to eliminate defects (breaks and loops) resulted from an inadequate transformation. The files were exported in 3D CAD SolidWorks used for creating the 3D computer model.

The contours have been placed on a set of auxiliary planes, a certain thickness is imparted to each of the contours. The 3D model produced is a set of flat layers with the thickness equal to the distance between contours (Figure 6).

The 3D model has been exported in STL format and a plastic relief map (Figure 7) has been made of ILIT-3 PPC on an LS-400E machine. The vertical scale has been increased twice in comparison with the horizontal one to show better the peculiarities of the landscape relief.

In the photo presented, one peculiarity of the given map is noted, namely there is a sharp edge in transition from one layer to another one. The map has got a step structure that can be perceived as a set of lines of identical levels. It often happens, however, that it misrepresents the actual form of the landscape relief and makes it difficult for visual perception. Therefore a decision is made to apply special software developed in the Institute on Laser and Information Technologies of the Russian Academy of Sciences for transforming tomographic data in STL format in order to make a smoothed computer model.

DECISION SUPPORT SYSTEMS FOR OPTIMIZATION OF LASER MATERIALS PROCESSING

V.S. MAYOROV and **S.V. MAYOROV**
Institute on Laser and Information Technologies of RAS, Shatura, Russia

Computer databases are useful tools for laser machines. But it is only the first step in the utilization of intelligent computer programs. This paper presents the results of the development of decision support systems (DSS) to help technicians in the choice of best conditions for laser processing of materials. DSS include some important blocks and components: physical models and equations, databases, practical knowledge of experts, experimental results bank, some important criteria, algorithms for analysis and decision. Set of parameters was developed for the description of laser technological processes. Each process was characterized by the values of such parameters changing in some reasonable diapasons. The input group of parameters consisted of the main technical characteristics of laser, type of a material and demands on the quality of laser processing results. The output group of parameters consisted of the set of laser processing conditions recommended by DSS. Our DSS for laser cutting and laser heat treatment can be used as options to industry laser software. Such programs enables to define the necessary best operational modes for laser system without expensive and time-consuming experiments, technological samples and metallographical tests, thus enabling to avoid the waste of time as well as material and technical resources.

Many firms do not even think of their production facilities without technological lasers (TL), using them for such various treatment processes as cutting, hardening, surfacing, etc. The paper states the main principles of construction of expert systems (ES) and decision support systems (DSS) that grants consultations on the choice of modes of laser processing. The ES is based on the knowledge of the process experts and on the information from the databank of technological processes. The part played by DSS in solving the tasks of laser processing of materials will be shown, the structuring of data domain, decomposition of the task to subtasks and construction of the diagram of laser parameters influence will be described. Then the system offers the recommendations on the choice of the most important parameters of the process, for example, such output parameters as cutting rate, mode of laser generation, grade of gas, focal length, etc.

Main principles for DSS. The DSS includes some important blocks and components: physical models and equations, databases, practical knowledge of experts, experimental results bank, some important criteria, algorithms for analysis and decision (Figure 1). The database is only one part in DSS. The knowledge base has been developed that permits the information about laser processing to be stored in the appropriate database for the purpose of information support of reproduction of the above-said technologies. A process is characterized by a set of parameters describing the material under processing, the geometrical features of the produced parts outlines, the technical characteristics and capabilities of the specific TL. The system for representation and structuring of the information in the knowledge base allows it to be accumulated and upgraded, entering new sections of knowledge base and forming new links between the objects. Each record of the information entered in a database should be split to separate units having identical formats, dimensions, etc.

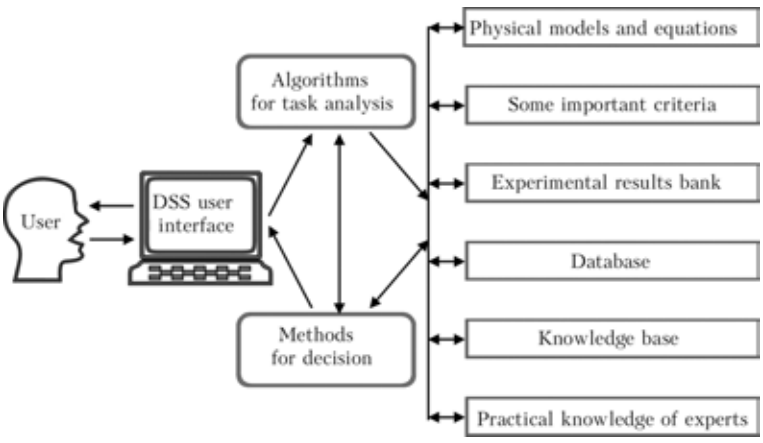

Figure 1. DSS structure

Structuring of data domain. In cooperation with the laser technology experts the structuring of the considered data domain was conducted and the main qualitative and quantitative criteria describing the input and output parameters of the laser processing were worked out. Thus, for laser cutting some parameters were selected as the input ones (type of laser; material; width of material; valid surface roughness; valid accuracy; presence of dross from the bottom of the cut; presence of small-sized holes and sharp corners; etc.) and another parameters were selected to be output (average power; continuous / pulse-periodic mode of cutting; pulse frequency; pulse duration; velocity; grade of gas; pressure; gas nozzle diameter; focal length; position of focal point and split between the nozzle and material surface; etc.).

The listed parameters can be considered as the names of fields of the database table, in which each of the records is considered to be a set of main parameters of the process. Thus, the recommendations offered by the process expert, as well as by the consulting model, should cover selected output parameters.

Diagram of influence and sequential decision. The decision for each of the listed parameters proceeds sequentially with allowance for dependencies of the parameters. The acyclic graph (diagram of influence), reflecting the relationship between the main parameters of the process under consideration, was constructed.

Let X is the set of data-ins $\{x_1, x_2, \ldots, x_m\}$; Y is the set of output parameters $\{y_1, y_2, \ldots, y_n\}$ and $Z = XUY$ is the set of all parameters. Then on a base of the constructed diagram of influence it is possible to formulate a sequential decision diagram on each of output parameters, each steps S_i can be written as follows: S_i:$\{x_1, x_2, \ldots, x_m\} \rightarrow y_i$, S_{i+1}:$\{x_1, x_2, \ldots, x_m, y_i\} \rightarrow y_{i+1}$.

For example, {laser, material, width of a material} → focal length; {laser, material, width of material, sharp corners, small holes, dross} → mode of cutoff; {laser, material, width of material, sharp corners, small holes, dross, roughness and heat-affected zone} → grade of gas and pressure; {laser, material, width of material, mode of cutoff} → average power; etc.

As many contributors in the field of an artificial intelligence mark, construction of a knowledge base mirroring procedural knowledge of the expert. In conditions of the given task the database on a master schedule of a laser cutoff was under construction on a base of interrogation of the experienced technologist. As a main method of construction of the system of the inference the approach of an opinion on precedents ---- case-based reasoning (CBR) ---- was selected. Such choice is not random, as from the designed consulting model level with the guideline on a master schedule the adapting to concrete TL is required also.

CBR technology. The CBR is a technology of solution of problems by the analysis of precedents (the tasks met before and successfully solved). The CBR system can fulfill various functions: adapt and use the existing solutions for the new tasks, give explanations on the ground of existing descriptions of similar situations, criticize the new solutions obtained from the analysis of the previous tasks, classify a new situation on available precedents.

The cycle of CBR operation can be in the general view circumscribed by the following steps: finding the precedent, closest in relation to the new task, or precedents; adapting retrieved before solution for close precedent in relation to the new task; and check in practice and saving of the obtained experience for operation with the new tasks.

That CBR system could realize these three steps, it is necessary to represent the available information by the way of precedents, to define a measure of their similarity among themselves and if necessary «to overlook» or «forget». During operation CBR technology uses algorithms having various assignment: search of the nearest precedents, estimation of similarity of the tasks among themselves etc. One of simple, effective and well recommending itself of algorithms is the algorithm of decision making on precedents ---- method k of the nearest neighbours (k–NN). Just this algorithm underlies the developed consulting model.

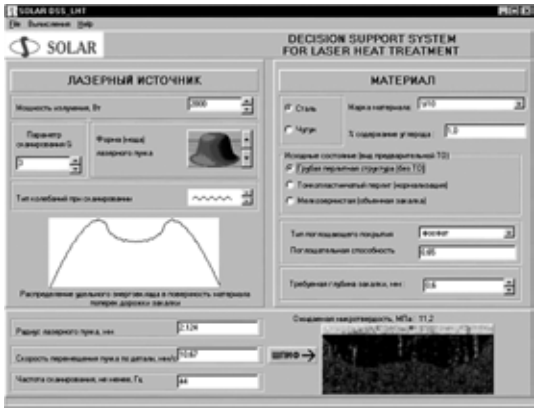

Figure 2. User interface of DSS for laser heat treatment

k–NN **method.** In each of the steps according to the sequential decision diagram for each of the output parameters, the search of the precedents, close in relation to the new task is carried out. During the search the function of complete similarity SIM (A, B) of two precedents A and B, described by p parameters is defined so that its value belongs to a segment [0.1):

$$SIM\ (A, B) = \frac{\sum_i sim_i\ (a_i, b_i)}{p},$$

where sim_i (a_i, b_i) are the local functions of similarity on separate parameters; a_i, b_i is the set of possible values of the parameter i precedents A and B, respectively. In some simple cases instead of a k–NN method it is possible to use the tree, beforehand worked with the expert.

DSS for laser heat treatment. DSS for Laser Heat Treatment© is presented if the form of computer program for defining the optimum laser hardening modes. This software is intended for production engineers involved in laser application in the plant. After initial data input (query formulation) the system gives out the recommended mode of laser heat treatment displaying everything on the screen (Figure 2). All this can be printed out as a report or a flow-process diagram.

The program can be used as an independent or additional option to industry laser software. The program enables to define the necessary best operational modes for laser system without expensive and time-consuming experiments, technological samples and metallographic tests, thus enabling to avoid the waste of time and material and technical resources.

CONCLUSION

The provision of the produced TL with modern facilities for data collection and analysis based on expert knowledge, allows consultations to be offered to beginner process engineers on choice of main parameters of laser processing. This will permit the available equipment to be used more effectively, and the conditions to be created for reproduction of laser treatment processes.

WEAR AND CORROSION PROPERTIES OF THE SiC REINFORCED SURFACE LAYERS IN MAGNESIUM AND ALUMINIUM ALLOYS OBTAINED BY LASER MELT INJECTION

H. POKHMURSKA[1], B. WIELAGE[1], H. PODLESIAK[1], Th. GRUND[1], T. HOENIG[2], K.-J. MATTHES[2], M. STUDENT[3], N. CHERVINSKA[3] and H. ZADOROZHNA[3]

[1]Institute of Composite Materials, Chemnitz University of Technology, Germany
[2]Institute of Welding Technology, Chemnitz University of Technology, Germany
[3]H.V. Karpenko Physico-Mechanical Institute of NASU, Lvov, Ukraine

The use of aluminium and magnesium alloys offers a great potential for weight reduction in aerospace, automotive and some engineering applications. The disadvantage of low wear and corrosion resistance can be overcome by different methods of surface modification. The use of high power lasers is a flexible tool in formation of protective layers on aluminium and magnesium alloys. Laser melt injection of alloying and reinforcing powders allows formation of near-surface layers with strongly increased wear resistance and improved corrosion properties. Reinforcement of aluminium (AA6082, AA7075) and magnesium (AM20, AE42, AZ31, AZ91) alloys is carried out by Nd:YAG CW laser with 2 kW maximum power using SiC powder or AlSi / SiC powder mixture. Additionally some of magnesium substrates are arc sprayed with Al or AlSi5 coatings in order to improve corrosion resistance. Microstructure of the produced layers is analyzed by optical and scanning electron microscopy. Corrosion behaviour is studied by immersion in NaCl solution, and electrochemical characteristics are investigated by current density-polarisation curves. Wear resistance of the coatings is determined by means of both corundum grinding disk and ASTM G65 wear test. It is shown that by method of laser melt injection uniform, pores- and cracks-free modified layers with homogeneous distribution of hard particles are formed in all investigated materials. Wear resistance on such layers strongly increases, especially under the conditions of abrasive wear (up to 70–100 times). Due to the refinement of microstructure of aluminium and magnesium, as well as because of partial alloying of matrix material after laser treatment, the improvement of corrosion properties is also observed.

During the last decades an increased amount of publications dedicated to the improvement of exploitation properties of aluminium and magnesium alloys concerning applications aimed on weight reduction of working parts appeared. Both alloys are known to have excellent physical and mechanical properties, in particular high strength-to-weight ratio of magnesium makes it very promising for a vehicle application [1–3]. Furthermore, magnesium substrates are completely recyclable [4]. The main reasons that limit aluminium and magnesium alloys applications are poor wear resistance and, especially for magnesium alloys, high susceptibility to corrosion, particularly in salt spray conditions.

Possibilities of enhancing the corrosion performance of aluminium and magnesium by means of laser surface treatment techniques are intensively investigated. Special attention is paid to local corrosion improvement. Already, when laser treatment is applied for surface melting of pure materials, increase of microhardness and a slight improvement of corrosion resistance to general corrosion of alloys is observed due to structural changes in irradiated areas [5, 6]. Nevertheless for the most part of applications much higher wear resistance and hardness of working part surfaces are required. Laser alloying with different elements or laser cladding allow forming on the surface of materials the modified layers with combined corrosion and wear protecting properties [7–10]. Another of the intensively investigated methods is the laser melt injection process, which is aimed on a formation of metal-matrix composite (MMC) layers directly in the near-surface region of a metal workpiece [11–13].

The aim of this work was to study an abrasion wear resistance under different load conditions and corrosion properties of surface layers of some aluminium and magnesium alloys reinforced by laser melt injection of SiC particles.

Materials and methods. Investigations are carried out on the plate substrates prepared from AA7075 and AA6082 aluminium alloys (80 × 100 × 8 mm) and magnesium alloys AZ31, AZ91, AM20 (50 × 100 × × 10 mm) with different content of aluminium. Chemical composition of investigated materials is given in Tables 1 and 2 respectively.

For a processing a pulsed CO_2-laser (wavelength of 10.6 μm) with middle beam energy 1350–1850 kW is applied. Process parameters are as follows: specimen traverse velocity of 60–150 cm / min, protective gas — argon, powder carrier gas — argon (gas flow of 2.3–2.5 l / min). Beam energy density is controlled with defocusing distance. The specimens are processed with different laser tracks overlapping that allow a concentration of hard particles in modified layers to be changed.

Powder feeding is realized with a cassette-type powder feeder. SiC particles of F100, F150 and F240 fractions (45, 82 and 129 μm mean size) or 50 / 50 powder mixture of SiC and AlSi40 powder (45–90 μm) are used.

Table 1. Chemical composition of investigated aluminium alloys, wt.%

Alloy	Al	Cr	Cu	Fe	Mg	Mn	Pb	Si	Ti	Zn	Other each	Other total
AA7075	87.1--91.4	0.18–0.28	1.2–2.0	max 0.5	2.1–2.9	max 0.3	–	max 0.4	max 0.2	5.1–6.1	max 0.05	max 0.15
AA6082	95.1--98.3	max 0.25	max 0.1	max 0.5	0.6–1.2	0.4–1.0	max 0.003	0.7–1.3	max 0.1	max 0.2	max 0.05	max 0.15

Table 2. Chemical composition of investigated magnesium alloys, wt.%

Alloy	Al	Zn	Mn	Si	Fe	Cu	Ni	Ca
AZ31	2.4–3.6	0.5--1.5	0.15–0.40	0.1	0.030	0.1	0.005	0.04
AM20	1.8–2.0	0.01--0.05	0.35–0.40	0.005–0.010	0.001	0.001	< 0.0005	< 0.001
AZ91	8.5–9.5	0.45--0.90	0.17–0.40	0.05	0.004	0.025	0.001	< 0.001

Additionally some of magnesium substrates are arc sprayed with Al or AlSi5 coatings in order to improve corrosion resistance. An injection of SiC particles was carried out in melt pool on the surface of samples being coated, and as a result alloyed / reinforced layers are obtained.

The microstructure of aluminium and magnesium alloys, before and after laser treatment, is examined on polished cross-sections. In addition to optical macroscopic observations, modified surface layers were investigated by scanning electron microscopy (SEM) equipped with an energy dispersive X-ray analyzer (EDX). Phase identification was conducted using an X-ray diffractometer and CuK_α radiation.

The abrasive resistance of the specimen surfaces was determined by using two test procedures, namely, in the process of friction against a rigidly fixed abrasive (abrasive wheel) and against an abrasive with not rigidly fixed particles (Rubber wheel test). Electrochemical measurements are carried out in tap water as well as in 0.1 M NaCl solution for polarisation curves (potential sweep 1 mV / s). Immersion test in 0.1 M NaCl solution is also carried out.

Experimental results and discussion. *Microstructure observations*. During the applied procedure the reinforcing particles are injected directly into the melt pool, which is formed by laser irradiation on the surface of the material being processed. Variation of treatment parameters, such as beam energy, scanning velocity and focus distance of beam, as well as amount and velocity of injected particles, provide a formation of layers with different depths and distribution of particles from incorporation of particles at the surface of samples exclusively to homogeneous distribution in the remelted layer.

For optimised process parameters a uniform distribution of reinforcing particles and good surface morphologies can be reached in the near-surface layers of the aluminium and magnesium alloys. Laser treatment results in the formation of a fine-grain structure of matrix material within the remelted layer due to extremely rapid solidification velocities. The substrate materials contain the intermetallic second phases in the form of relatively large precipitates. In the remelted layer a very fine distribution of intermatallic phase is observed. It is fine-dispersed or forms the kind of cell borders in the dendrite structured matrix. Injected SiC particles practically do not influence on the microstructure of laser remelted matrix material.

In Figure 1 the typical example of a modified layer formed in the AA7075 aluminium alloy obtained by consecutive overlapping of single tracks is shown.

The main process parameters that influence the properties of obtained layer are laser beam energy density, parameters concerning the reinforcement particles feeding and preheating temperature of specimen, which is in the range from 100 to 270 °C for aluminium and 100 °C for magnesium alloys.

During processing some chemical reactions between the substrate material and injected particles depending on the chemical composition of injected powder mixture and time-temperature parameters in melted pool occur [11, 14]. Reinforcement / alloying of aluminium alloys with AlSi / SiC powder mixture at the accelerated temperatures of 270 °C is accompanied with formation of needle-like aluminium carbide phase and precipitation of pure silicon phase, which appears in a shape of plates (Figure 2).

Decreasing of processing temperature, as well as application of pure SiC powder, leads to restriction of

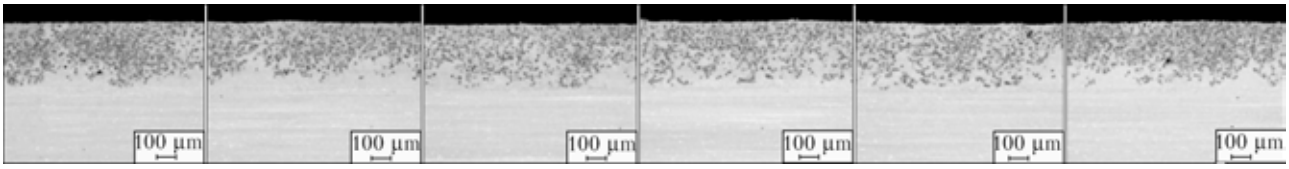

Figure 1. Panoramic view of cross-section of reinforced surface layer formed in AA7075 alloy by laser melt injection of SiC powder at the 1850 W beam power, 100 °C preheating temperature, 150 cm / min specimen traverse velocity and 50 % overlapping of tracks

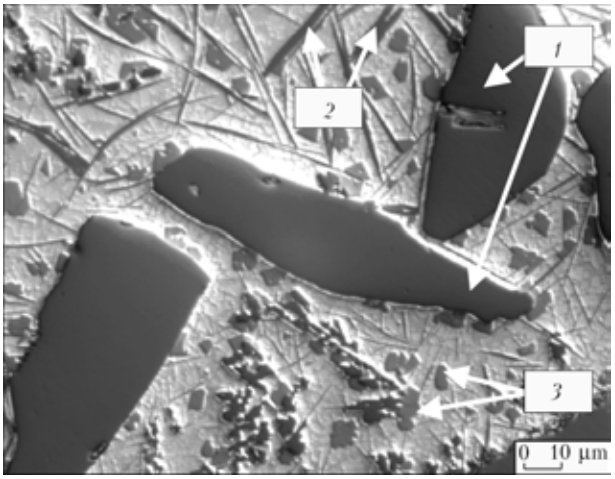

Figure 2. Typical cross-section optical micrograph showing the SiC particles in the AA7075 alloy substrate with 50:50 SiC:AlSi40 powder injected at the 1650 J / cm^2 beam energy density, 266 °C preheating temperature: *1* — SiC; *2* — Al_4C_3; *3* — Si

formation of Al_4C_3 and pure silicon phases. Only a small amount of needle-like Al_4C_3 crystals are detected mainly on the interface between the SiC particle and the matrix aluminium material (Figure 3, *c*, *f*).

Surface reinforcement of magnesium alloys is carried out with the average lower energy densities and pre-treatment temperatures. A distribution of hard particles in modified layers in magnesium alloys have some peculiarities to compare with those in aluminium substrate. Relatively larger difference in densities of matrix material and SiC in the case of magnesium reinforcement leads to a slight unevenness in particles distribution. In the thin near-surface region the particle poor layer is formed, while in the interface region a higher particle density is observed (Figure 4).

Wear resistance. Due to the reinforcement of surface layers of aluminium and magnesium alloys with hard particles an abrasive wear resistance is significantly improved for all investigated specimens. Wear resistance estimated in wear test with fixed abrasive (grinding wheel test) is 30–75 times and more than 2 orders of magnitude higher for SiC reinforced layers in aluminium and magnesium alloys respectively. Within the applied processing parameters the best results demonstrate the surface layers with the highest density of hard particles (Figure 5).

An improvement of abrasive wear resistance obtained in rubber wheel test is much lower and can

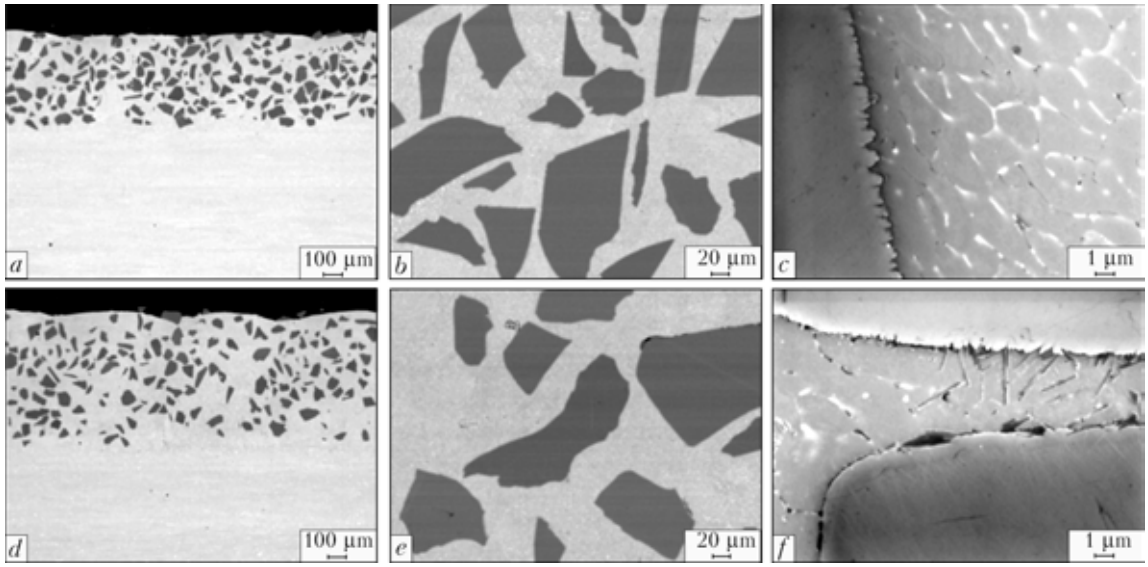

Figure 3. SEM images of cross-sections of SiC specimens reinforced AA7075 alloy at the 1850 kW laser beam power, 100 (*a–c*) and 250 (*d–f*) °C preheating temperature, 150 cm / min specimen traverse velocity and 30 % overlapping of tracks: *a*, *d* — general view; *b*, *e* — particles distribution; *c*, *f* — SiC particle / aluminium matrix interface

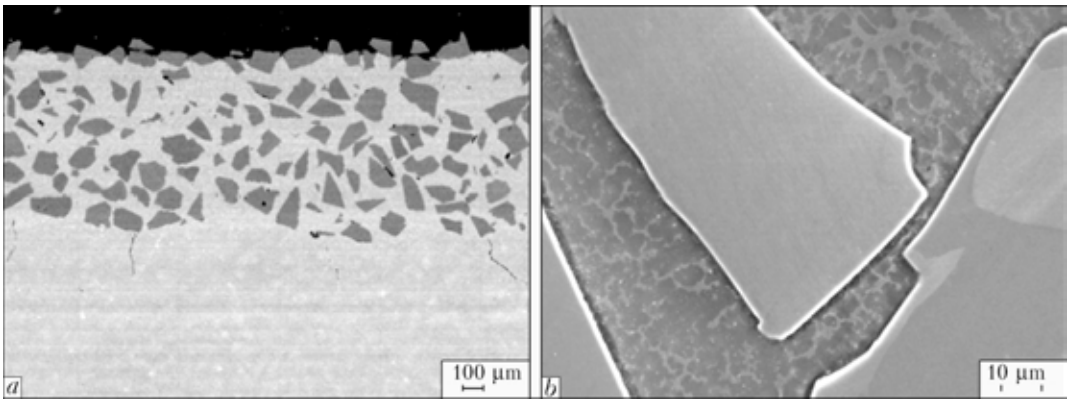

Figure 4. SEM images of cross-sections of SiC reinforced magnesium alloy AZ31 at the 1350 kW laser beam power, 100 °C preheating temperature, 150 cm / min specimen traverse velocity and 30 % overlapping of tracks: *a* — general view; *b* — SiC particle / magnesium matrix interface

reach the values 20–30 % higher to compare with base material. This difference in wear behaviour is explained due to different wear mechanisms that are responsible for material loss in these two tests [14]. In the case of grinding wheel the main role play the hard particles which are imbedded in matrix, while testing the specimens under conditions of not fixed abrasive course, first of all, the removal of soft matrix material. In this way the hard particles are permanently exposed from matrix and then pulled off from the base material, thus they do not fulfil their protection role. Moreover, removed by the rubber disc they can act as additional abrasive.

Corrosion properties. Laser remelting of aluminium and magnesium alloys provides a formation of surface layers with fine-dispersed microstructure due to rapid solidification. Uniform distribution of intermetallic phases along the cell boundaries in the matrix solid solution is observed. Laser melt injection of reinforcing SiC particles generally does not have significant influence on the base material microstructure, which is determined by cooling rate. As it was shown earlier, the resistance to general corrosion is moderately improved due to the surface treatment for tested alloys [15]. The effect on corrosion performance can be explained by microstructure modification together with the incorporation of non-equilibrium concentrations of alloying elements resulting from rapid cooling rates compared with conventional surface treatment techniques, which provides the basis for property enhancement.

SiC reinforcing particles do not demonstrate active electrochemical action on the corrosion process of investigated materials. An initiation of corrosion defects during immersion test in corrosion (0.1 M NaCl) solution occurs mainly on the interfaces with intermetallic phases rather than on the interface between embedded particles and matrix.

The susceptibility to pitting corrosion, namely the pitting potential of remelted layers, is not strongly improved by laser melting without addition of alloying elements. However, a number and size of pits were less developed in comparison with as-received samples.

An injection of SiC particles is also carried out in some of magnesium substrates which are arc sprayed with Al or AlSi5 coatings in melt pool on the surface in order to obtain alloyed / reinforced layers with improved corrosion resistance. However, rather poor morphology of such remelted layers to compare with specimens obtained by direct melt injection of powders, and some porosity in reinforced layer are the reasons of relatively moderate improvement of wear resistance of these layers.

CONCLUSION

It is shown that the method of laser melt injection for all investigated materials provides a formation of uniform modified layers with homogeneous distribution of hard particles, without pores and cracks. Wear resistance of SiC reinforced layers strongly increases, especially under conditions of abrasive wear with fixed abrasive (up to 70–100 times). The lower

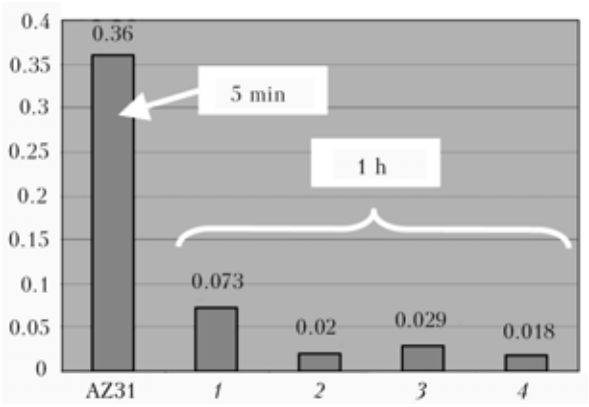

Figure 5. Abrasion wear resistance of AZ31 magnesium alloy and surface layers obtained by laser reinforcement with SiC particles at the 1350 W laser beam power, 150 cm / min specimen traverse velocity, 100 °C preheating temperature (*3*, *4*), 30 (*1*–*3*) and 50 (*4*) % overlapping of tracks

improvement of abrasive wear resistance obtained in rubber wheel test to compare with grinding wheel test is explained by the different wear mechanisms in these two tests. Improvement of corrosion properties is also observed due to the refinement of microstructure of aluminium and magnesium matrix as well as because of partial alloying of matrix material after laser treatment. Although the pitting potential of magnesium and aluminium alloys which are susceptible to pitting corrosion is not improved by laser melting, a number and size of pits are less developed in comparison with as-received samples.

1. Gray, J. E., Luan, B. (2002) Protective coatings on magnesium and its alloys — a critical review. *J. Alloys and Compounds*, **336**, 88–113.
2. Skar, I. (2002) *Magnesium technology*. Seattle, Washington: USA MT, 255–262.
3. *ASM Handbook*. Vol. 13A: Corrosion: fundamentals, testing, and protection. Product Code 06494G. www.ameritech.co.uk
4. (2005) *Magnesium surface treatment of magnesium substrates*. Ed. by K.U. Kainer.
5. Pokhmurska, H., Kwiatkowski, L., Kalita, W. et al. (2003) Corrosion behaviour of laser remelted aluminium alloy. In: *Proc. of SPIE* (Bellingham, USA, 2003), Vol. 5229, 260–265.
6. Abbas, G., Liu, Z., Skeldon, P. (2005) Corrosion behaviour of laser-melted magnesium alloys. *Appl. Surface Sci.*, 247(**1–4**), 347–353.
7. Majumdar, J.D., Galun, R., Mordike, B.L. et al. (2003) Effect of laser surface melting on corrosion and wear resistance of a commercial magnesium alloy. *Materials Sci. and Eng. A*, 361(**1 / 2**), 119–129.
8. Gaoa, Ya., Wanga, C., Panga, H. et al. (2007) Broad-beam laser cladding of Al–Cu alloy coating on AZ91HP magnesium alloy. *Appl. Surface Sci.*, 253(**11**), 4917–4922.
9. Ignat, S., Sallamand, P., Grevey, D. et al. (2004) Magnesium alloys laser (Nd:YAG) cladding and alloying with side injection of aluminium powder. *Ibid.*, 225(**1–4**), 124–134.
10. Dubourg, L., Hlawkab, F., Cornet, A. (2002) Study of aluminium–copper–iron alloys: application for laser cladding. *Surface and Coatings Technology*, **151 / 152**, 329–332.
11. Vreeling, J.A., Ocelik, V., Pei, Y.T. et al. (2000) Laser melt injection in aluminum alloys: on the role of the oxide skin. *Acta Materialia*, 48(**17**), 4225–4233.
12. Majumdar, J.D., Chandra, B.R., Mordike, B.L. et al. (2004) Laser surface engineering of a magnesium alloy with Al + Al_2O_3. *Surface and Coatings Technology*, 179(**2 / 3**), 297–305.
13. Dutta Majumdar, J., Ramesh Chandra, B., Manna, I. (2007) Friction and wear behavior of laser composite surfaced aluminium with silicon carbide. *Wear*, 262(**5 / 6**), 641–648.
14. Pokhmurska, H.V., Student, M.M., Chervinska, N.R. et al. (2005) Structure and properties of aluminium alloys modified with silicon carbide by laser surface treatment. *Fizyko-Khimichna Mekhanika Materialiv*, 41(**3**), 34–40.
15. Wielage, B., Wank, A., Pokhmurska, H. et al. (2005) Corrosion properties of surface layers of aluminium alloys reinforced with SiC particles by laser beam melt injection. *Surface Eng. A*, **2**, 147–153 (in Polish).

PECULIARITIES OF GAS-ASSISTED LASER CUTTING OF THICK METAL SHEETS

V. ROMANENKO, M. ANYAKIN and **R. ZHUK**
Laser Technology Research Institute of NTUU «KPI», Kiev, Ukraine

The paper presents the results of investigation of the process of gas-assisted laser cutting of thick metal sheets. It was shown that the increase of productivity and processing quality could be achieved by layer-by-layer cutting or by means of additional scanning with focused laser beam.

Gas-assisted laser cutting of thick metals is followed by the range of complications. First of all, it is the necessity of realizing the process of cutting at low velocities leaded to the appearance of so-called autogenous cutting mode that is followed by sizeable width of the cutting line and its high asperity. That is why gas-assisted laser cutting at low velocity is realized with high laser power density that is possible when using single-mode laser beam and more short-focus optical system. Such optical systems, in their turn, have limited depth of the focal zone that also has negative effect on the cutting parameters of thick materials.

Good results can be gained by the usage of pulse-periodic laser radiation in cutting metals of large thickness. But such laser complexes are rather expensive. At the same time, the velocity range of gas-assisted laser cutting of thick metals that guaranties optimal quality of the cutting lines has been defined theoretically and experimentally (the cutting velocity is v = = 1.0–2.5 m / min) [1]. However, as the thickness of cut metals considerably depends on the cutting velocity, it allows cutting metals not thicker than 5–7 mm. Consequently, traditional scheme of gas-assisted laser cutting allows one either to cut thick materials with low quality or to cut thin sheet metals with good one.

At the Laser Technology Research Institute of NTUU «KPI» the new schemes of gas-assisted laser cutting of thick metal materials have been developed; in their heart lies the method of laser radiation scanning all along the cutting line with the rating amplitude and within the limits of axially driven fluid jet.

During the development of new methods of cutting we considered the following points. The processed material must provide technological transference concerning laser radiation with the velocity low enough to guarantee complete cutting of thick metal. For the metal sheets with the thickness h = 10–15 mm the velocities lie in the range of 0.25–0.50 m / min.

At the same time, it is necessary to maintain the velocity of relative transference of the laser beam and the material being cut in the optimal range (v = 1.0–= 2.5 m / min) that will provide the required quality of cutting (cutting width b = 0.5–1.0 mm; surface asperity R_z = 20–40 μm; zone of thermal influence on the cutting lines of 0.25–0.50 mm). The required value of the relative transference of the beam and the material can be provided on the account of additional scanning movement of the laser beam along the destruction line. But for all that the amplitude of the scanning movement must exceed the diameter of laser radiation focused in the cutting zone and must be counted from the ratios of velocities of technological transference of the scanning movement of the laser beam and the material being cut.

Depending on the way of laser beam scanning it is possible to realize different mechanisms of destruction in the cutting zone.

There is a possibility of realizing schemes of layer-following and layer-counter destruction in the cutting zone. In the first scheme, the scanning movement of the beam is realized in the direction that follows the technological movement of the material. Meanwhile, the laser radiation gradually moves from the surface to the bottom. At the end of scanning the beam returns on the surface in spurts. In the second case, the laser beam moves counter the direction of the material, and the destruction comes from the inside to the surface. Then the beam returns inside the material in spurts.

At back-and-forth scanning of the beam the method of saw-shaped destruction of the material along the cutting line will be implemented. In such case during slow technological motion of the material the laser beam moves back-and-forth with a higher velocity, goes deeper inside the material and returns to the surface.

Let us assess the capacities of implementing each of the suggested schemes of cutting, their advantages and disadvantages.

The scheme of layer-following cutting totally corresponds to the conditions of cutting with the formation of furrows on the surface of destruction [1]. Remember that when the cutting velocities are in the measures of v = 1.0–2.5 m / min, the mechanism of formation of the cutting line greatly depends on the regularities which take place on the surface of the metal till the beginning of the process of destruction. During this transitional period the following processes take place: the rising of the heating of the surface of the material from the initial temperature T_{in} to the

destruction temperature T_0 and the acceleration of the interfacial failure to the speed v_0. At the same time, in the beginning the interfacial failure is constant and the heat is consumed for the formation of the next furrow, the width of which is defined by the mechanism of heat conductivity. When the temperature reaches T_0, the mechanism of destruction inside the material turns on in spurts, and the furrow that was formed near the surface deepens with the speed v_0.

As it follows from [1], the time t_0 of the beginning of destruction on the top of material at layer-following cutting of metals can be defined from the expression

$$t_0 = (2a / V_{sc}^2)[1 - (1 - k V_{sc}(T_0 - T_{in})/(a W_p))^{1/2}], \quad (1)$$

where k is the heat conductivity factor; a is the thermal diffusivity; W_p is the laser power density; V_{sc} is the scanning velocity of the laser beam.

During the time t_0 (this time is lost for destruction) the laser source moves on the surface of the material at a distance of $X_0 = V_{sc}t_0$. At the same time, the material itself makes a technological transference of $X_t = V_t t_0$) (here V_t — velocity of technological movement of the material), which partially compensates the time lost for heating. Then, within the limits of the rest of the scanning amplitude ($A - X_0 + X_t$), the cutting of the material to the required depth takes place.

The values of V_0 and $\dot{O}_0$, which characterize the process of assigned destruction, can be defined from solution of the following equations set of energy balance in the processing zone and kinetics of the oxidation reaction [1]:

$$V_0 = W_p[\rho c(T_0 - T_{in})(1.9 + a/(V_{sc}r_0)) + \Sigma L - G]^{-1}; \quad (2)$$

$$\dot{O}_0 = \dot{O}G \ln^{-1}(S_0 / V_0), \quad (3)$$

where G is the specific heat of burning reaction; ΣL is the total heat of phase change of the metal and its oxides; S_0 is the some constant close to sonic speed in the metal; $\dot{O}G$ is the reaction heat shown in degrees; ρ is the metal density; c is the its specific heat.

The depth of cutting, in such case, can be defined from the equation

$$h = (A - X_0 + X_t) V_0 / V_{sc}. \quad (4)$$

The velocity of technological movement can be defined from the condition of total cutting of the material during the time of focused laser beam passing through the diameter of its focal spot:

$$V_t = 2r_0 V_0 / h. \quad (5)$$

The choice of scanning amplitude will depend, first of all, on the ratio of velocities of technological transference of the material and laser radiation scanning. So,

$$A = 2r_0 V_{sc} / V_t. \quad (6)$$

From the given argumentation it is clear that the realization of this scheme of cutting doesn't cause special difficulty. The destruction surface cant is obvious to be more than during usual way of cutting as a result of laser scanning along the line of destruction. Consequently, the cant of furrows on the surface of the line which was cut will increase. It is also necessary to mention that one shouldn't overstate the velocity of relative movement of the laser beam and the material and establish it within the limits of V_{rel} = = 1.5–2.0 m / min in order to lessen the cant of the destruction surface, which will, in its turn, facilitate the passing of the process (in particular, the removal of destruction products from the processing zone with fluid jet). For this method of cutting the technological movement partially compensates the scanning movement of the laser beam. Consequently, $V_{sc} = V_{rel} + V_t$.

Among the disadvantages of this scheme of processing we should mention rough finish of the surface of the cutting line and it's a little high asperity (R_z = = 15–30 μm).

With the layer-following scheme of cutting laser radiation first falls on the lower deep-laid layers of the metal. When the time t_0, which is necessary for heating the cutting zone to the temperature $\dot{O}_0$ and the beginning of destruction, is up, the latter follows the cutting line within the measures of the left part of the beam scanning amplitude. This amplitude decreases to the value of $A - X_0 - X_t$ as a result of counter movement of the beam and the material.

When this scheme is implemented, a more long-focus optical system should be used to keep power density in the deep layers of the cut material high enough. Concerning the velocity of relative movement of the laser beam and the material V_{rel}, it must have minimum acceptable value in order to stabilize the process of destruction in the lower layers of the material (within the measures of V_{rel} = 1.0–1.5 m / min). As the technological movement of the material increases the scanning movement of the laser beam then $V_{sc} = V_{rel} - V_t$.

Another peculiarity of this scheme is the passing of the destruction process bottom-up. The upper layers are cut and the destruction products are removed down with the fluid jet. The surface of destruction cannot have rough finish because it is formed not as the result of heat conduction but on the account of passing of the destruction products in the cutting channel. As a result, the surface of the cutting line is cast-like with slight asperity (R_z = 5–15 μm).

It is obvious that the summing-up effect of the two methods above takes place in the realization of the scheme of «saw-shaped» destruction (Figure).

Among the advantages of this scheme of cutting we should mention stable mode of destruction in the processing zone because there are no interruptions of the cutting process connected with rapid shifts (spurts) of the laser beam to the new zones of processing. With all that near the upper and lower surfaces

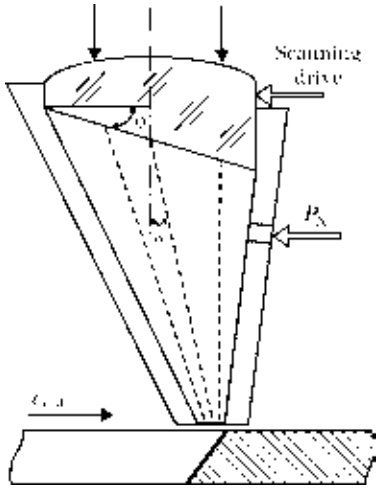

Scanning system

of the material there is additional heating of the material as a result of double movement of the laser beam (back-and-forth). It may cause the appearance of autogenous (uncontrolled) mode of cutting there. That is why when implementing this scheme the velocity of relative movement of the laser beam and the material must have the maximum acceptable value, which means V_{rel} = 2.0–2.5 m / min. When choosing the velocity of laser beam scanning the following aspects must be considered: in the phase of the following movement of the beam and the material the technological movement of the material partially compensates the scanning movement of the laser beam, which means $V_{rel} = V_{sc} - V_t$, unlike that in the phase of counter movement of the beam and the material ---- $V_{rel} = V_{sc} + V_t$. That is why the velocity of scanning is usually chosen from the measures of V_{sc} = 2.5–3.0 m / min.

The asperity of the cutting line surface in this case is slight (R_z = 10–25 μm) as a result of increased velocity of scanning and washing out of the lugs formed on the surface of the cutting line in the phase of counter movement of the beam and the material.

So, we should mention that all the suggested methods of processing could be successfully implemented in cutting rectilinear sections and materials with circle-arc forms and smooth curves of the contour. When processing acute angles gas-assisted cutting with the usage of pulse-periodic radiation is more acceptable.

1. Kovalenko, V.S., Romanenko, V.V., Oleshchuk, L.M. (1987) *Low-waist processes of laser cutting*. Kiev: Tekhnika.

MODELING OF PLASMA SHIELDING PHENOMENA

R. ROZMAN, E. GOVEKAR and **I. GRABEC**
University of Ljubljana, Slovenia

The plasma shielding phenomenon plays an important role in laser materials processing since it affects processing efficiency. Plasma shielding is caused by the laser beam absorption in plasma. Therefore, a model of plasma formation and laser beam absorption in plasma was developed. In this model, absorption is described by three different mechanisms: inverse bremsstrahlung, photoionization, and absorption process of light induced by small condensed clusters. Based on this model, numerical solutions are given for KrF laser beam irradiation (wavelength of 248 nm) impinging on a nickel substrate at various fluences. Results from the proposed model give the portion of absorbed laser beam energy in the plasma plume, which increases with the increase of laser beam fluence. The calculated results of our model are in good agreement with experimental measurements reported in the literature.

High-intensity laser beam material processing is accompanied by vaporization of the irradiated substrate [1]. Under certain conditions the vaporized material starts to ionize, and plasma is formed. Due to energy input into the plasma, the absorption coefficient of the plasma increases. The increase of the absorption coefficient in plasma causes an increase of laser beam energy absorbed in the plasma plume. Consequently, a portion of the laser beam energy does not reach the substrate surface, and heating of the substrate is decreased. This phenomenon is known as plasma shielding and plays an important role in laser material processing since it affects processing efficiency [1]. Therefore, plasma shielding is usually an unwanted phenomenon. To increase the efficiency of laser material processing, it would be of great benefit if optimal parameters that minimize the effect of plasma shielding could be estimated. For that purpose, a model of plasma formation is required. Therefore, the objective of this article is to define a physical model that relates laser material processing parameters to the formation of plasma and the plasma shielding phenomenon.

A brief overview and state-of-the-art of different modeling approaches available for laser material removal and plasma formation is given in the article [2]. In comparison with the state-of-the-art given in [2], the main step forward in our approach is determining the absorption coefficient of the plasma. In our model, three main absorption mechanisms are considered, namely inverse bremsstrahlung, photoionization, and absorption process of light induced by small condensed clusters.

In this article, a short presentation of the plasma formation model is given. By means of the numerical solutions of the model, the plasma shielding phenomenon is characterized by the calculated transmissivity of the plasma plume for the laser beam. Based on this model, numerical solutions for the case of KrF laser beam irradiation (wavelength of 248 nm) of a nickel substrate at various fluences are given.

Model. A plasma plume is formed from vaporizing material caused by laser beam irradiation on a substrate surface, therefore, the proposed model of plasma formation includes thermal phenomena caused by high-intensity laser beam irradiation of material, such as heating, melting, vaporization, ionization of vaporized material, and plasma plume formation.

The formation of vapor is described by the flux of particles j_s leaving the substrate surface. For this purpose we need to know the surface temperature T_s of the substrate. The heating of the substrate and the surface temperature T_s are defined by the heat equation

$$\rho_m c_p \frac{\partial T_m}{\partial t} = \nabla(\kappa \nabla T_m) + Q, \qquad (1)$$

where T_m is the temperature of the substrate; t is the time; Q is the energy source; and ρ_m, c_p and κ are the mass density, heat capacity and thermal conductivity of the substrate, respectively. Due to the thin liquid layer, the convection of material being melted in (1) is neglected. Furthermore, for the metal substrate, the optical penetration depth for the laser beam is typically very small [1]. Therefore, surface absorption is assumed and the laser energy source Q is described by boundary conditions [1].

Assuming thermally activated surface vaporization [1], the flux of particles j_s crossing the liquid–vapor interface is then determined by the actual surface temperature T_s, and it is used for the boundary conditons in the compressible Navier–Stokes system of equations that describes the flow of vapor from the substrate, vapor expansion and plasma formation. We treat the vapor as an ideal gas and assume that inlet flow velocity $\mathbf{v}_v$ from the substrate to the ambient is equal to the local sound velocity [1]. The Navier–Stokes equations are represented by the conservation equations for mass, momentum and energy:

$$\frac{\partial \rho}{\partial t} + \nabla(\rho \mathbf{v}) = 0; \qquad (2)$$

$$\rho\left(\frac{\partial \mathbf{v}}{\partial t} + (\mathbf{v}\nabla)(\mathbf{v})\right) = -\nabla p; \qquad (3)$$

$$\rho\left(\frac{\partial E}{\partial t} + (\mathbf{v}\nabla)E\right) = -p\nabla\mathbf{v} + \nabla(\kappa_{pl}\nabla T) + \frac{dP}{dV} - \varepsilon_{rad}. \quad (4)$$

In the above system of equations, the parameters ρ, $\mathbf{v}$, E, p, T, κ_{pl} and ε_{rad} represent mass density, velocity vector, total energy per unit mass, pressure, temperature, thermal conductivity and radiation power loss per unit volume, respectively. The aforementioned parameters refer to the mixture of vaporized material and ambient gas. dP / dV is the absorbed laser beam power per unit mass and is calculated by Beer–Lambert's law [1] using the absorption coefficient of the plasma α_{pl}. The thermal conductivity of the plasma κ_{pl} is defined by the kinetic theory of plasma [3], whereas the radiation power loss per unit volume ε_{rad} is calculated using the bremsstrahlung radiation mechanism [3, 4].

To solve the system of Navier–Stokes equations, three additional equations are needed: for the total energy per unit mass E, pressure p and internal energy per unit mass e of the gas mixture, which is treated as an ideal ionized gas. The relative concentration of electrons and ions can be calculated by the Saha-Eggart equations [3, 4], considering a thermal equilibrium between electrons, atoms and ions.

The plasma shielding phenomenon is caused by the absorption of laser beam energy in the plasma plume. Therefore, a description of the absorption of laser beam energy in the plasma plays an important role in characterizing plasma shielding. In (4) the absorption of the laser beam in the plasma is described by the absorbed power of the laser beam in the plasma per unit volume dP / dV, which is related to the absorption coefficient of the plasma α_{pl}. In most cases of plasma plume modeling, the absorption coefficient α_{pl} characterizes the absorption due to the inverse bremsstrahlung mechanism only [2]. However, it is known from the literature [5] that the photoionization and the absorption process of light induced by small condensed clusters known as the Mie absorption mechanism are important. Because of this and aside from the inverse bremsstrahlung absorption coefficient α_{ib}, the photoionization absorption coefficient α_{pi} and Mie absorption coefficient α_{Mie} are also taken into account in our model. Consequently, the absorption coefficient of the plasma α_{pl} is defined by $\alpha_{pl} = \alpha_{ib} + \alpha_{pi} + +\alpha_{Mie}$. The three aforementioned mechanisms of absorption are briefly presented below.

The inverse bremsstrahlung process involves the absorption of photons by free electrons traveling through the electric field of an ion [3, 4]. The inverse bremsstrahlung absorption process is dominant in the case of IR light. At lower wavelengths of IR light, the inverse bremsstrahlung is only important at high temperatures of the plasma, T, when the relative concentration of electrons is high.

The photoionization mechanism is described by absorption of a photon into the neutral atom, which becomes ionized [4]. If the energy of the atom in the ground electron level is lower than that of the photon, the atom cannot be ionized by photon absorption. In this case, ionization is only possible in thermally populated excited electron levels of the atom, where the energy difference between the ionized atom and the excited electronic level of the atom is lower than the photon energy. The excess of photon over electron binding energy is transformed into kinetic energy of the free electrons.

The Mie absorption mechanism involves the absorption of light induced by the clusters generated by the condensation of the supersaturated vapor. The size of the clusters is typically of about 10 nm [6] and is usually much smaller than wavelength λ of the incident laser beam radiation. Due to this, the absorption coefficient on small condensed clusters is described by the Mie absorption mechanism [7].

The different parts of the model of plasma formation are nonlinear and strongly coupled. On the one hand, laser–substrate interaction causes substrate heating and vaporization, and influences plasma plume formation. On the other hand, the absorption of the laser beam in the plasma represents important back-coupling, which leads to less efficient substrate heating. Due to the nonlinearity and strong coupling of the system of equations of the model, the system is solved numerically in 2D space with cylindrical symmetry. In the following, the numerical solution of the model of plasma plume formation is presented.

Numerical solution of the model. The proposed model of plasma formation was solved numerically in a 2D system with cylindrical symmetry. We considered in the model a motionless laser beam source with wavelength λ = 248 nm and pulse duration t_p = 50 ns with a uniform intensity profile in a radial direction r. The fluences F of pulses were between 2.5 and 10.5 J / cm^2.

The main outputs from our model are the temperature and velocity fields of the plasma above the substrate surface. An example of the time development of temperature and velocity fields of the plasma plume above the substrate calculated for three different fluences F is shown in Figure 1. Due to cylindrical symmetry, temperature and velocity fields along radial r and vertical z axes are presented. The temperature of the plasma T is shown by the scale, while the size and direction of plasma velocity $\mathbf{v}$ is indicated by arrows. From Figure 1 we can see that at time t = = 10 ns after the start of the laser beam pulse, the maximal temperature of the gas mixture is low ($\approx$ 5000 K). From time t = 20–40 ns, the absorption of laser beam power in the plasma increases. Consequently, the absorbed laser beam power heats the plasma plume and the temperature of the plume rapidly increases. Due to the end of the laser beam pulse at time t = 50 ns and due to the plasma expansion, the plasma is cooled down at the end of laser beam pulse. At higher laser beam fluences, higher plasma temperatures are observed. With increasing temperature T, the pressure p of the plasma plume also increases and the plume expands. Therefore, higher ve-

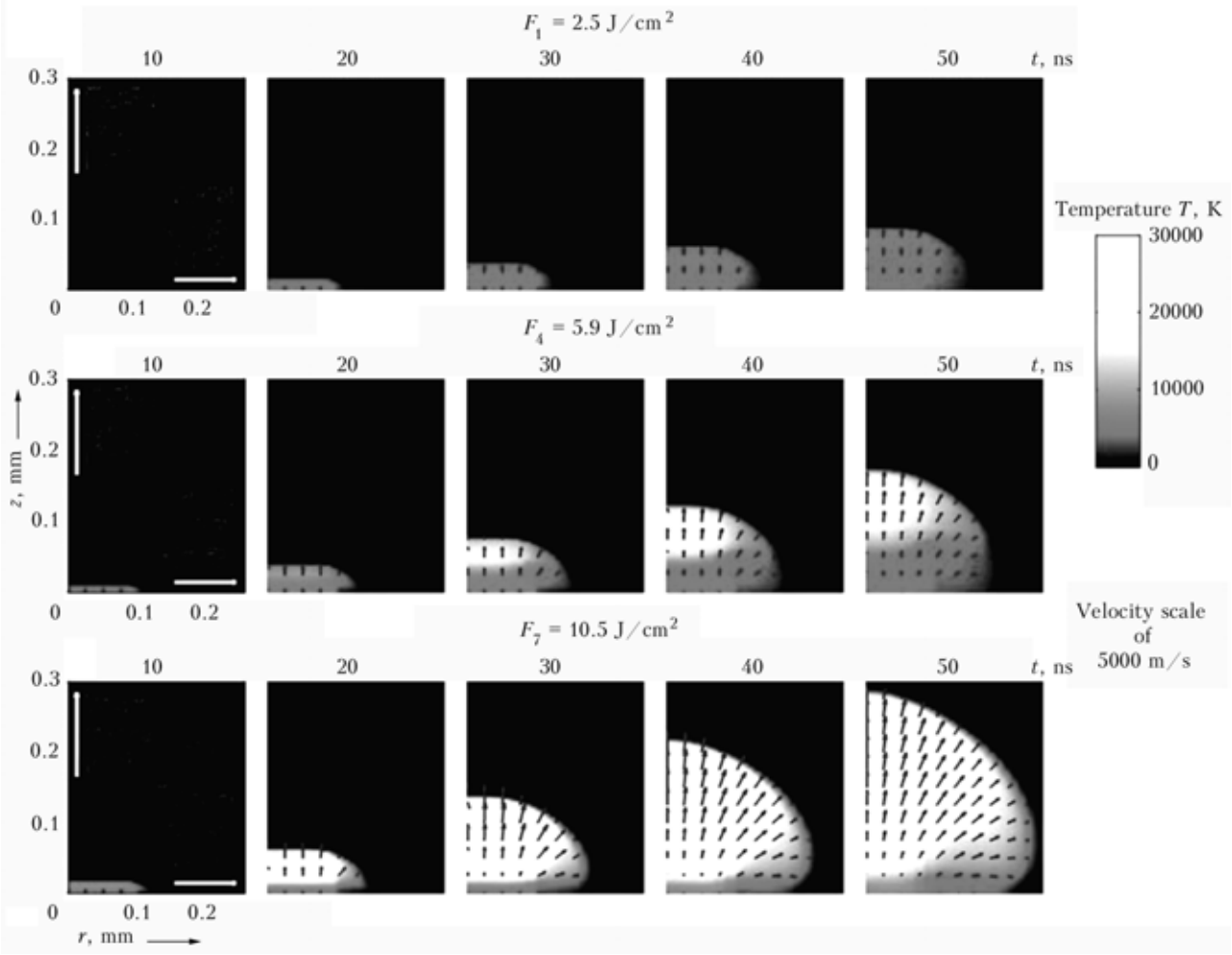

Figure 1. Temperature and velocity fields of the plasma above the substrate surface at various time t and fluence F

locities **v** of the plasma and larger sizes of the plasma plume are observed at higher laser fluences F.

Based on the model results, we see that the velocity and temperature fields of the plasma depend on laser beam fluence and time. Several parameters and relations between them can be calculated from the model. As expected, the results of the model show that the temperature of the plasma influences the absorption coefficient [1]. Consequently, a portion of laser beam energy is absorbed in the plasma and only a portion reaches the substrate surface. This phenomenon is known as plasma shielding and it is characterized in more detail below.

Plasma shielding plays an important role in laser material processing since it influences substrate surface temperature T_s. The substrate surface temperature T_s depends on plasma plume transmissivity for the laser beam τ and the absorption coefficient of plasma α_{pl}. The transmissivity τ of the plasma plume is defined as $\tau = P_s / P$ (here, P_s denotes the laser beam power that reaches the substrate surface, and P denotes laser beam power at the laser beam source). The absorption coefficient of the plasma α_{pl} is characterized by the average absorption coefficient α_a. It is defined by means of the Beer–Lambert's law $\tau = \exp(-\alpha_a h)$, which relates transmissivity τ with an average absorption coefficient α_a and the height of the plasma plume h. Both the transmissivity τ and the average absorption coefficient α_a depend on plasma temperature T, which is characterized by the maximal temperature of the plasma T_{max}. The vapor flow from the substrate influences the plasma plume and depends on the surface temperature T_s. Consequently, the plasma shielding phenomenon can be characterized by means of the parameters described above. Dependencies of the parameters T_{max}, α_a, τ and T_s versus time t for various fluences F are shown in Figure 2, *a*–*d*. In Figure 2, *a* the normalized laser beam power P_n versus time t is also shown.

From Figure 2, *a*–*c* we can observe that in general maximal temperature of plasma T_{max} and average absorption coefficient of plasma α_a increase with the increasing fluence F whereas the transmissivity τ decreases with an increase of the fluence F. In Figure 2, *d* an interesting property of the substrate surface temperature T_s can be seen. From the course of the temperature T_s it is evident that with lower laser beam fluences F, higher surface temperatures are achieved at the second part of the laser beam pulse. This can be explained by very low transmissivity τ of the plasma at higher fluences F.

Based on the results of the plasma plume model presented, we can say that plasma plume formation has a significant impact on the plasma transmissivity

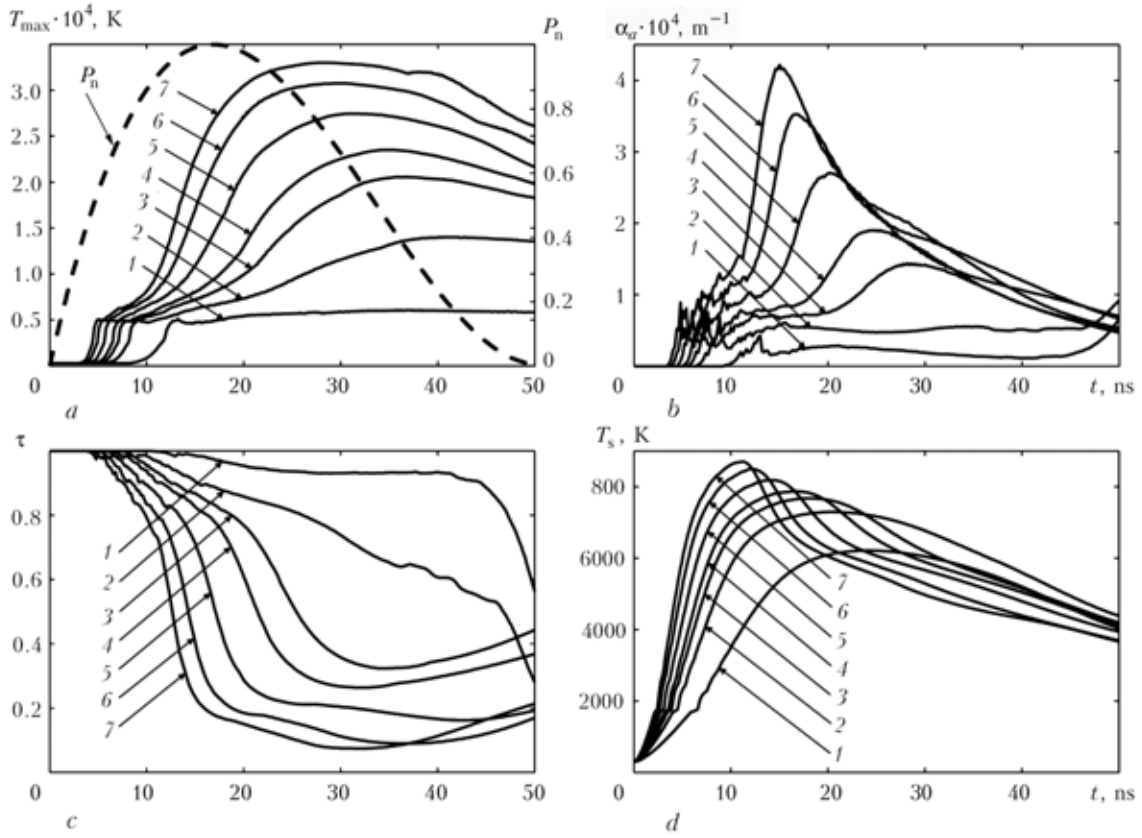

Figure 2. Maximal temperature of plasma T_{max} and normalized laser beam power P_n (*a*), average absorption coefficient of plasma α_a (*b*), plasma transmissivity τ (*c*), and substrate surface temperature T_s (*d*) versus time t for various fluence F of 2.5 (*1*), 4.2 (*2*), 5.2 (*3*), 5.9 (*4*), 7.3 (*5*), 9.0 (*6*) and 10.5 (*7*) J / cm^2

τ and on the corresponding plasma shielding phenomenon. Due to the onset of plasma shielding, the laser beam power that reaches the substrate surface P_s is significantly lower than the source power of the laser beam P. The model presented and results of the modeling of plasma plume formation and related phenomena of plasma shielding appear very promising for characterization and further optimization of the efficiency of laser material processing. However, for practical application of the model, experimental verification of the modeling results is necessary, that is given in [8] where the numerical results are compared by experimental ones given in [9].

CONCLUSION

In this article, a physical model of plasma plume formation and characterization of the related plasma shielding, are presented. The reason for the onset of the plasma shielding phenomenon is the absorption of laser beam power in the plasma plume. To characterize the absorption of the laser beam in the plasma, three different absorption mechanisms were taken into account in the model: inverse bremsstrahlung, photoionization, and the absorption process of light induced by small condensed clusters. The plasma shielding phenomenon was characterized based on the model results. Results show that plasma shielding varies with pulse duration and depends on laser beam fluence. Due to the onset of plasma shielding, the efficiency of laser material processing is significantly decreased. It has been shown that higher laser beam fluences cause more intensive plasma shielding and therefore lower processing efficiency. The numerically calculated results of the model were compared with experimental measurements from the literature and showed good agreement of calculated results with experimental results [8, 9]. This agreement indicates that the model of plasma plume formation presented in this article is sufficiently realistic and could be further used for optimization of laser material processing.

1. Baurle, D. (2000) *Laser processing and chemistry*. Springer.
2. Bogaerts, A., Chen, Z., Gijbels, R. et al. (2003) Laser ablation for analytical sampling: what can we learn from modeling? *Spectrochimica Acta B*, **58**, 1867–1893.
3. Mitchner, M., Kruger, C.H. (1992) *Partially ionized gases*. John Wiley & Sons.
4. Zeldovich, Ya.B., Raizer, Yu.P. (2002) *Physics of shock waves and high-temperature hydrodynamic phenomenon*. Dover Publ.
5. Mendes, M., Vilar, R. (2003) Influence of working atmosphere on the excimer laser ablation of Al_2O_3–TiC ceramics. *Appl. Surface Sci.*, 196–208.
6. Callies, G., Schittenhelm, H., Berger, P. et al. (1998) Modeling of the expansion of laser-evaporated matter in argon, helium and nitrogen and the condensation of clusters. *Idid.*, 134–141.
7. Bohren, C.F., Huffman, D.R. (1998) *Absorption and scattering of light by small particles*. John Wiley & Sons.
8. Rozman, R., Govekar, E., Grabec, I. (2006) Modeling of plasma shielding in laser material processing. In: *Proc. of 9th CIRP Int. Workshop on Modeling of Machining Operations* (Bled, Slovenia, May 11–12, 2006), 557–564.
9. Song, K.H., Xu, X. (1997) Mechanisms of absorption in pulsed excimer laser-induced plasma. *Appl. Physics A*, **65**, 477–485.

INVESTIGATION OF PECULIARITIES OF PROCESSES FOR LASER-ASSISTED DEPOSITION OF AMORPHOUS AND FINE-CRYSTALLINE LAYERS ON STEELS

V.D. SHELYAGIN[1], **V.Yu. KHASKIN**[1], **A.V. BERNATSKY**[1], **Yu.N. PEREVERZEV**[1] and **T.G. CHIZHSKAYA**[2]
[1]E.O. Paton Electric Welding Institute of NASU, Kiev, Ukraine
[2]National Technical University of Ukraine «KPI», Kiev, Ukraine

Formation of quasi-amorphous and microcrystalline coatings using laser beams with different wavelengths is investigated. It is shown that the efficiency of the process grows with decrease in the wavelength. Optimal parameters were established for the cases of laser and combined laser-microplasma spiral deposition of coatings on cylindrical surfaces.

Along with known laser cladding technologies [1], also the new laser-plasma technologies [2] are finding now commercial application for deposition of coatings. They are applied primarily for production of functional wear- and corrosion-resistant coatings. Production of amorphous and quasi-amorphous coatings is regarded as one of the most promising areas for development of such technologies [3]. Therefore, the purpose of our study was to explore the possibilities of producing such coatings by the laser and laser-microplasma methods using laser beams of different wavelengths to improve wear resistance of surfaces under conditions of dry friction at high temperatures, as well as to investigate their physical-chemical and mechanical properties.

Experiments were conducted using flow diagrams of the laser cladding and laser-microplasma deposition processes described in [4] and [5], respectively. The domestic 10 kW CO_2-laser LT-104 [6] and 200 W Nd:YAG laser LTN-103, as well as the Rofin-Sinar 2 kW diode laser DF 029 HQ (Germany) were employed in the experiments. The plasmatron, developed by the E.O. Paton Electric Welding Institute, equipped with the MPU-4 power supply was used to generate a microplasma jet. The treatment was performed on the in-house laboratory rigs, which provide linear velocities of the processes in a range of 10–600 m / h.

Critical thicknesses of the layers to be deposited, which allow amorphisation of these layers, were determined prior to the experiments by the calculation method suggested in [7]. For this, the temperature fields within the treatment zone, as well as the heating and cooling rates were calculated using the mathematical model of thermal processes occurring in laser cladding of materials of the Ni–Cr–B–Si and Fe–Ni–B–Si systems. Then, on the basis of these calculations, formation of microcrystalline or amorphous structures was predicted depending upon the portioned energy input into the treatment zone, and parameters of laser radiation were preliminarily identified for deposition of coatings with an optimal structure and, hence, with the assigned physical-mechanical properties for the given conditions. Permissible thickness of the coatings was found to be about 0.3 mm.

The next stage of investigations consisted in technological experiments conducted on cylindrical samples. Dependencies shown in Figure 1 were derived in the course of these experiments. As follows from the experimental results, for CO_2-laser the optimal diameter of the radiation spot on a surface treated is directly proportional to the power and equals 1 mm per 0.7–0.8 kW for process rates of 10–30 mm / s and cladding powder mass consumption of 0.1–0.3 g / s.

So, it can be concluded that the efficiency of the coating deposition processes grows with decrease in wavelength of the laser beam due to improvement of its absorption conditions. This conclusion is also confirmed by comparison of microstructures of the deposited layers (Figures 2 and 3). As seen from Figure 3, in the case of deposition of one bead, it is possible to provide amorphous structures in it.

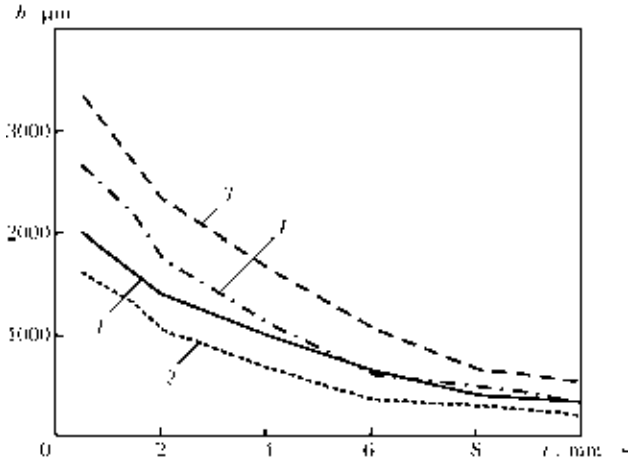

Figure 1. Effect of treatment parameters on coating thickness h for the Fe–Ni–B–Si material PG-N1: for CO_2-laser $q_0 = 2 \cdot 10^5$ (*1*) and $2 \cdot 10^4$ (*2*) W / cm^2; for laser DF020HQ $q_0 = 2 \cdot 10^5$ (*3*) and $2 \cdot 10^4$ (*4*) W / cm^2; v — treatment velocity

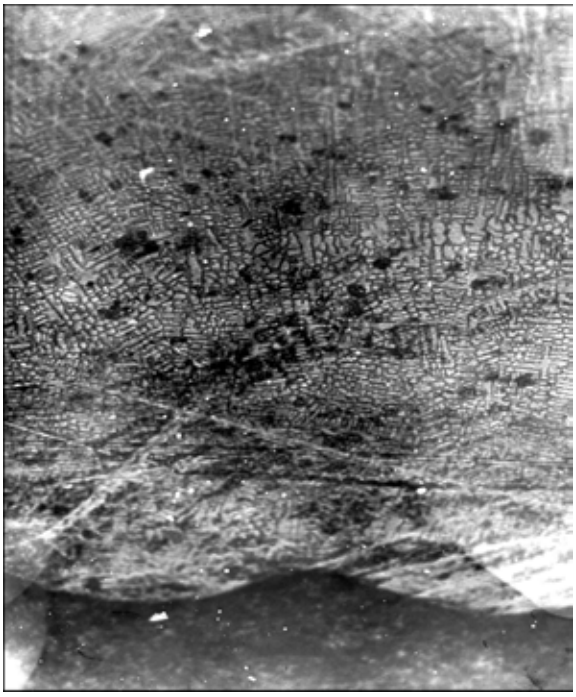

Figure 2. Microstructure of fine-crystalline coating of the Ni–Cr–B–Si system deposited on steel St3 using CO_2-laser at P = 1800 W and v = 1200 mm / min (×320)

Radiation of the CO_2-laser was used in the experiments on laser-microplasma deposition of coatings. Nevertheless, the rate of the process was substantially increased (3–5 times compared with laser cladding) in this case due to using a combination of the two heat sources. Claddings of alloys of the above systems featured an approximately 3 times decrease in grain size, compared with claddings produced by using the CO_2-laser.

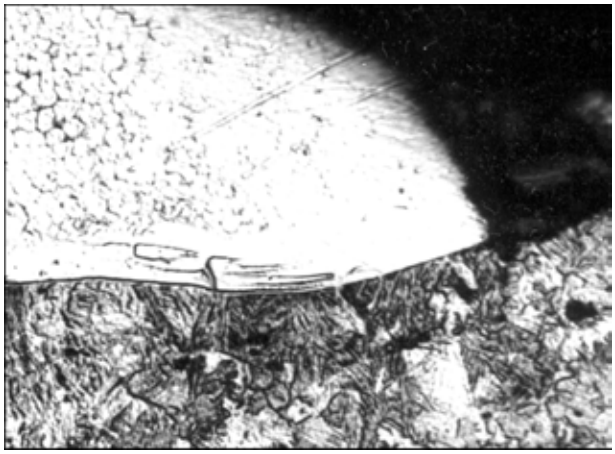

Figure 3. Microstructure of quasi-amorphous coating of the Ni–Cr–B–Si system deposited on steel 08kp (rimmed) using laser LTN-103 at P = 140 W and v = 100 mm / min (×400)

Samples with the deposited coatings were tested to friction and corrosion resistance. It was established that wear resistance of samples simulating internal combustion engine components grows by 50–100 % under the dry friction conditions, compared with the base metal (alloyed steels and cast irons). The rate of corrosion of the samples increased with decrease in grain size. Although differences in the rate were insignificant, for coatings with the amorphous-microcrystalline structure this indicator was higher than for coatings with the microcrystalline structure. This may serve as an indirect confirmation to the fact that the produced layers were not purely amorphous. Coatings deposited by the laser-microplasma method were tested to heat resistance. It was found that deposition of Al_2O_3 on carbon steel is accompanied by dissolution of a filler metal, which is the main cause of formation

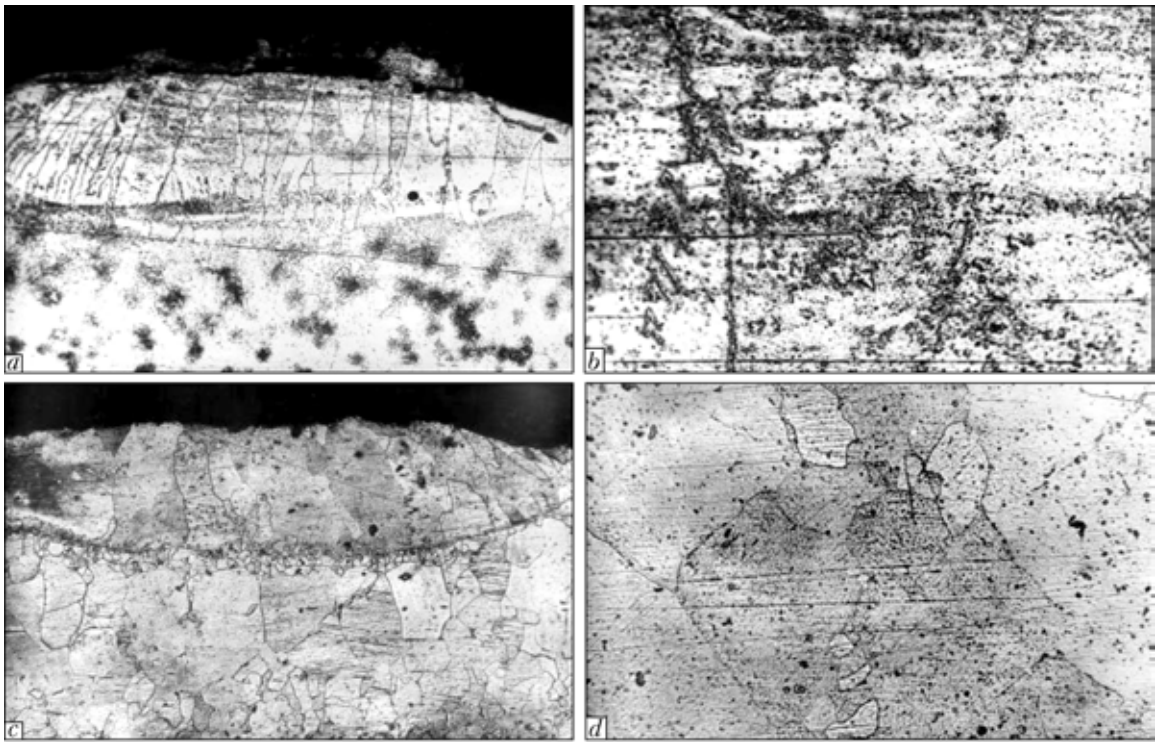

Figure 4. Structure of the Al_2O_3 coatings, deposited on steel St3ps (semi-killed) by the laser-microplasma method, before (*a* — ×100; *b* — ×1000) and after (*c* — ×100; *d* — ×1000) heat resistance tests

of an intermetallic compound of the Fe_2Al_5 type in a coating (Figure 4). And it is this compound that provides heat resistance.

CONCLUSIONS

1. Formation of amorphous, quasi-amorphous and microcrystalline coatings using laser beams with different wavelengths was investigated. It was found that the efficiency of the process increases with decrease in the wavelength. The most suitable parameters were identified for the cases of laser and combined laser-microplasma deposition of coatings on a cylindrical surface following the spiral path.

2. It was experimentally established that laser cladding provides only the surface, rather than complete, amorphisation of the deposited layer, which is attributable to directed solidification. Thickness of the amorphous layer depends upon the thermal-physical parameters of a deposited material and cooling rates within the treatment zone. Critical cooling rates were determined, which are required for amorphisation of the surface layer in laser cladding of materials of the Ni–Cr–B–Si and Fe–Ni–B–Si systems.

3. It was established as a result of a series of the tests to mechanical, corrosion and heat resistance that the amorphous-microcrystalline structure of coatings is optimal for parts operating in aggressive environments and / or under friction conditions. The coefficient of overlapping of deposited strips to ensure maximal corrosion resistance of the coatings should be 0.7–0.8.

4. The combined laser-microplasma process of deposition of thin (0.05–0.50 mm) wear- and corrosion-resistant coatings of the Ni–Cr–B–Si, Ni–Fe–B–Si and Al_2O_3 systems on low-carbon steels allows advantages of laser cladding to be combined with those of microplasma spraying. In addition, the process leads to increase in a coating to workpiece adhesion strength and elimination of microcracking, and makes it possible to avoid preliminary abrasive-jet blasting of the surface to be treated, owing to its guaranteed incipient melting to 5–20 μm.

5. Main process parameters of laser-microplasma deposition of coatings were determined. Mass consumption of a powder and coefficient of overlapping of coating strips have the highest effect on thickness of the coating deposited in one pass. The speed of displacement of a workpiece and laser beam power density affect to a lesser degree. Changes in an angle between the radiation axes and microplasma jet have almost no effect on the coating thickness.

1. Hoffman, J. (2001) Reconditioning of exchangeable parts using laser technologies. *The Paton Welding J.*, **12**, 33–34.
2. Zreris, R., Nowotny, S., Berger, L.-M. et al. (2003) Characterisation of coatings deposited by laser-assisted atmospheric plasma spraying. In: *Proc. of Thermal Spray Conf.* (Orlando, USA, 2003), 567–572.
3. Najdek, V.L., Likhoshva, V.P., Skripka, N.N. (2001) Properties of amorphous-microcrystalline laser coatings. *Protsessy Litia*, **4**, 45–51.
4. Velichko, O.A., Avramchenko, P.F., Molchan, I.V. et al. (1990) Laser cladding of cylindrical parts using powdered materials. *Avtomatich. Svarka*, **1**, 59–65.
5. Shelyagin, V.D., Khaskin, V.Yu., Pereverzev, Yu.V. (2006) Laser-microplasma alloying and coating of steels. *The Paton Welding J.*, **2**, 2–5.
6. Garashchuk, V.P., Shelyagin, V.D., Nazarenko, O.K. et al. (1997) Technological 10 kW CO_2-laser LT 104. *Avtomatich. Svarka*, **1**, 36–39.
7. Skripka, N.M. (2002) *Laser-assisted production of boron-containing amorphous-microcrystalline coatings with improved service characteristics*: Thesis for Dr. Techn. Sci. Degree. Kyiv: NTUU «KPI».

PECULIARITY OF PHASE TRANSFORMATION KINETICS AND CONTROL OF MATERIAL MICROSTRUCTURE FORMATION DURING LASER HYBRID WELDING

G. TURICHIN[1], **V. LOPOTA**[1], **E. VALDAITSEVA**[1], **E. ZEMLIAKOV**[1] and **Yu. BULKIN**[2]
[1]St.-Petersburg State Polytechnic University, Russia
[2]Federal Nuclear Research Center, Sarov, Russia

New hybrid processes, such as laser-arc and laser-light welding and surface treatment, allow controlling formation of metal microstructure parameters in weld and heat-affected zone. Thin structure of thermal cycle in hybrid technology, which contains several stages of high speed heating and cooling, gives possibility to control microstructure formation kinetics by changes of temporal shift between laser and addition heating source. The mathematical model of phase transformations in steels, which was developed on the base of reaction-diffusion kinetic problem, has been improved to take into account thermocycling and crystal lattice transformations. The model has been verified by experiments on laser-light welding of car body steels. Combination of this model with CAE system LaserCAD, which allow calculating thermal cycles for hybrid technology, was put on the base of choice of the welding mode parameters to provide prescribed properties of the welded joint.

To decrease the weight of new structural high-strength two- and three-phase steels are applied. Properties of such kind of steels are defined by parameters of ensembles of nano-dimension inclusions. In particular, in modern technologies of car bodies, based on tailored blanks, decrease in weight without strength decreasing is achieved by using high-strength biphasic steels in the blanks production instead of low-carbon ones; however there is a problem to provide of necessary plasticity of welds.

To solve this problem it is necessary to have a welding technology, which provides sufficient metal plasticity of the welds and welding quality, not yielding to quality of the laser welding used now. The use of high-speed heat cycling is most perspective to obtain set microstructure and mechanical properties [1]. It can be achieved in using for welding two heat sources following one after another, for example, tandem laser welding [2]. But from the economic point of view it is expedient to use cheap local sources of heating as the second source, such as a powerful lamp.

To choose the processing mode which provides necessary microstructure and material property it is necessary to have a quantitative description of temperature cycle influence on phase and structure transformations processes in the material, which would be based on their detail understanding. Modern concepts of phase transformation mechanisms at laser action on steels [3], which formed on the basis of phase transition thermodynamics, do not allow taking into account the non-equilibrium nature of fast transformation processes, which lead to appearance of non-equilibrium microstructures in laser-processed zone. For example, thermodynamics of transformation can't predict such effects as shifts of transformation temperature depending on heating and cooling rate, mutual influence of processes of a new phase growth and non-stationary diffusion, an initial state of the material. The quantitative description of microstructures is impossible without considering these factors and can be formulated only on the basis of the kinetic theory of phase transformations in steels [4]. For this purpose the exact calculation of a thermal cycle is necessary for the hybrid welding that is initial parameter for processes of phase transformations. Thus, it is necessary to pass consecutive steps of development of physical and mathematical models of welding processes, development of a material microstructure formation model in a zone being processed, creation of the experimental set-up and experimental researches of welding process. The present article is devoted to the description of this complex problem solution.

Simulation of metal microstructure formation in hybrid welding. Phase transformations in steels at the beam treatment defining the metal structure consist of two components. The first one is connected to decay (or formation) a solid solution of carbon in iron and formation (decay) of ferric carbide, and the second one is connected with crystal FCC–BCC lattice transformation at cooling and back at heating. To calculate parameters of carbide inclusions the kinetic model of formation and growth of the second phase inclusions for the solid solution decay has been developed.

The relation between the carbide inclusion volume and surface area depends on the inclusion shape. For initiation of the growth the inclusion can be treated as a «point» source of solute. The concentration field near the inclusion has a spherical symmetry, and one can consider the inclusion as a sphere with an effective radius a. The non-equilibrium growth of such new phase carbide inclusions is described by the kinetic equation of the chemical reaction:

$$\frac{da}{dt} = K_1(T)C - K_2(T), \qquad (1)$$

where $K_1(T)$ and $K_2(T)$ are the constants of velocities of the direct and inverse reaction; C is the free carbon

concentration on the inclusion surface; T and t are the local temperature and time.

The reaction speed constants are given by the Arrhenius formula:

$$K_{1,\,2}(T) = K_{1,\,2}^{(0)} \exp\,(U_{f,\,s}/kT),$$

where U_f, U_s are the activation energy of the direct and reverse reaction; $K_1^{(0)}$, $K_2^{(0)}$ are the frequency factors.

The superficial concentration in (1) is determined by a solution of the diffusion equation

$$\frac{dC}{dt} = D\Delta C = D\,\frac{1}{r^2}\,\frac{\partial}{\partial r}\left(r^2\,\frac{\partial C}{\partial r}\right). \qquad (2)$$

The boundary condition on the surface of the growing inclusion (at $r = a$) is the condition of the solute flux continuity:

$$-D\,\frac{\partial C}{\partial r}\Big|_{r=a} = K_1(T)C\,|_{r=a} - K_2(T). \qquad (3)$$

The admixture concentration far from the growing inclusion is determined by its average value $\tilde{N}_0$:

$$C\,|_{r\to\infty} \to C_0. \qquad (4)$$

The solution of this problem has been obtained by standard methods of mathematical physics. Having used a number of appropriate simplifications, one can obtain

$$C = C_0 - \frac{1.56}{d\sqrt{\pi}}\,\frac{(K_1C_0 - K_2)}{\left(\dfrac{K_1}{D} - \dfrac{1}{a}\right)}.$$

Taken into account mutual influence in the carbide inclusions ensemble and having denoted the carbon concentration in the cementite as C' (for Fe_3C $C' \cong$ $\cong 0.25$) and inclusion number density as n, one can get for the ensemble of spherical inclusions:

$$C_0 = C_0 - nC'\,\frac{4}{3}\,\pi a^3.$$

To determine a value of the parameter n, it is possible to connect the n value with a solubility limit, which can be determined from the thermodynamic phase diagram. Having denoted the solubility limit as $C_{\lim}(T)$, one can get from a substance conservation condition:

$$n = \frac{C_0 - C_{\lim}(293)}{\dfrac{4}{3}\,\pi a_{\lim}^3 C'},$$

where $a_{\lim}$ is the limit size of the growing inclusion.

Then the equation (1) can be rewritten as:

$$\frac{da}{dt} = K_1\left(C_0 - nC'\,\frac{4}{3}\,\pi a^2 - \frac{1.56}{\sqrt{\pi}D}\,\frac{K_1C_0 - K_2}{\dfrac{K_1}{D} - \dfrac{1}{a}}\right) - K_2. \qquad (5)$$

The Euler's method was used for solution of the equation for carbide grows (5). As the result of $a_{\lim}$ calculation has to be included in the equation, the «shooting» method of solution was used, i.e. such preliminary value of $a_{\lim}$ should be introduced, which provides the same final value of the inclusion radius a. The values of parameters, used for calculation in this article for low carbon steel, are given by the next list: $K_1^{(0)}$ = = 45 m / s, $K_2^{(0)}$ = 2.2 m / s, $U_f = 1.26\cdot10^{-19}$ J / atom, $U_s = 1.6\cdot10^{-19}$ J / atom, $D_0 = 2\cdot10^{-6}$ m^2 / s, U_d = $= 1.38\cdot10^{-19}$ J / atom.

The kinetic model of the crystal lattice transformation (α–γ transformation) has been formulated on the same principles, as the model of origin and growth of inclusions. Since the interphase border movement rate in this case is so that the diffusion Peclet number is not small, the diffusion equation, as against a problem about carbides growth, has been solved with considering a convective term. On the other hand, as the grain size in growing considerably exceeds a diffusion layer thickness the diffusion problem has been considered as one-dimensional. The joint solution of the connected problems about kinetics of growth of new phase grains and about carbon diffusion before its front allows calculating quantity of a new phase at any moment of a thermal cycle. Thus there has been obtained the self-consistent equations system describing completely material microstructure formation at high-speed heating and cooling. As parameters of initial metal structure there are taken into account both the initial carbides sizes, and the initial grains sizes influencing on the diffusion factor. The input parameter of model is the thermal cycle which parameters are defined by a technological mode of processing. The obtained solution allows calculating evolution of the steel phase composition in the processing zone.

Structure and properties of the weld metal in laser-light welding. The experiments for hybrid temperature cycle influence on microstructure formation have been carried out in the wide range of such parameters as welding speed and distance between laser and lamp spot on the target surface. The temperature cycle for hybrid laser-light welding has been calculated with the mathematical model described. For calculation of carbide inclusions a kinetic model, which also was described above, used. Changing the form of a temperature cycle, it is possible to achieve both size reduction, and enlargement of the carbide inclusions in comparison with a temperature cycle, which is typical for laser action without an additional heat source.

Influence of processing speed determining a time delay between the first and the second peaks of the thermocycle is illustrated by typical examples in Figures 1–3. It is obvious that decrease of the time delay between peaks results in significant size reduction of the carbide inclusions as it is predicted by the developed theory.

The analysis of distribution of microhardness average values on researched welds has shown that the hybrid-welded samples are characterized by considerably smaller difference of the microhardness values in comparison to the laser-welded samples. Decrease of martensite part in weld metal allows raising its plasticity. To research influence of pass from laser welding to the hybrid laser-light one on the technological plasticity, the welded samples have been tested by the Ericsen method. The carried out experiments have shown that, for example, for alloyed steel 08U pass from laser to hybrid welding increases technological plasticity by more than 40 %.

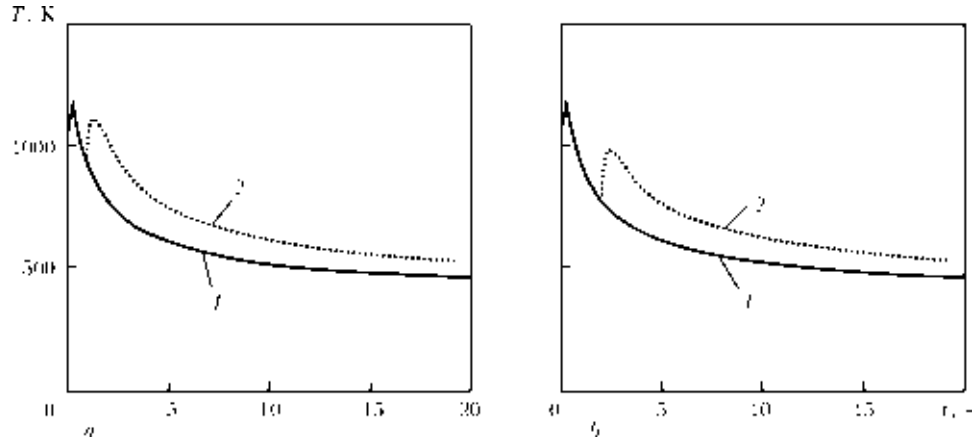

Figure 1. Temperature cycle for laser- (*1*) and hybrid-processed (*2*) steel 08U at delay between temperature peaks of 1 (*a*) and 2 (*b*) s

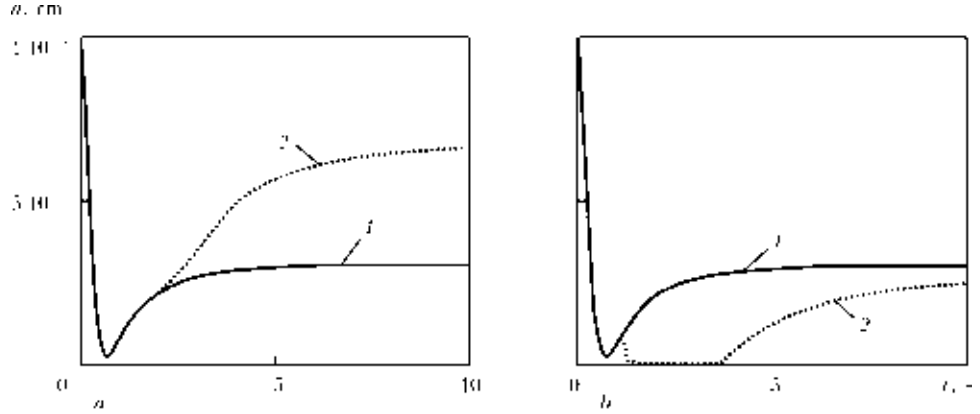

Figure 2. Calculation results for carbide nano-inclusion sizes for laser- (*1*) and hybrid-processed (*2*) steel 08U at delay between temperature peaks of 1 (*a*) and 2 (*b*) s

Model of weld pool and processing zone at hybrid influence. The mathematical model of the weld pool in hybrid welding, allowing calculation the thermal cycles of the weld and HAZ metal for various distances between action zones of laser and additional heat sources, both for welding with deep penetration, and for the surface melting case [5], has been formulated on the basis of solution of the connected problems about radiation absorption, convective heat transfer, melt hydrodynamics, gas-dynamics of evaporation products and laser-induced plasma kinetics. The numerical scheme with explicit allocation of the weld pool border has been used in solving. The laser heating source in case of deep penetration has been described according to [6]. Essential difference in this case is presence of the second heat source distributed on the weld pool surface, therefore use of assumption about 2D heat transfer as it was made for laser welding becomes impossible. And so for hybrid welding there have been obtained a 3D solution of thermal and hydrodynamic problems for the weld pool, taking into account influence of thermocapillary flow in the weld pool on the temperature distribution [7].

The target heating by the focused radiation of arc lamp leads to formation of the distributed moving heat source on the workpiece surface. The source energy distribution is determined by local values of radiation intensity and radiation absorption factor depending on the surface temperature. Thus, the problem about heating a material by the lamp (or arc)

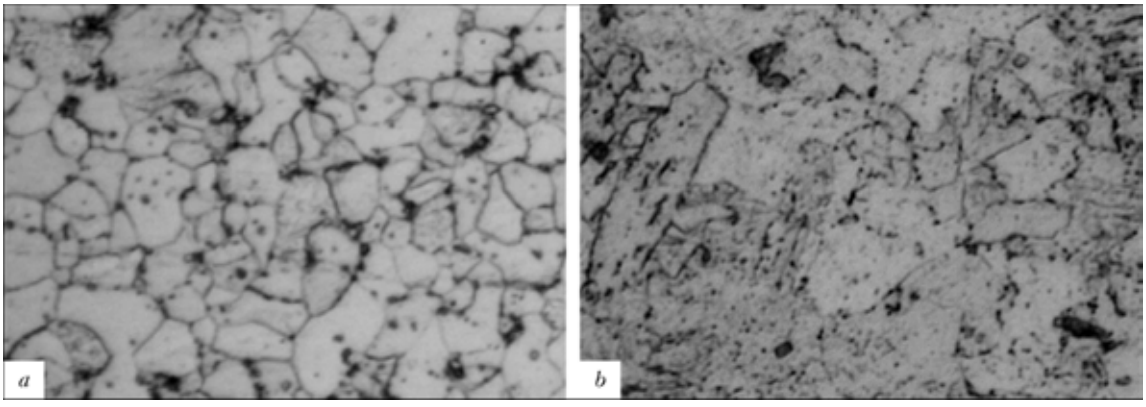

Figure 3. Microstructure after hybrid action at maximal heating temperature of 1200 K, field width of 50 μm and delay between temperature peaks of 1 (*a*) and 2 (*b*) s

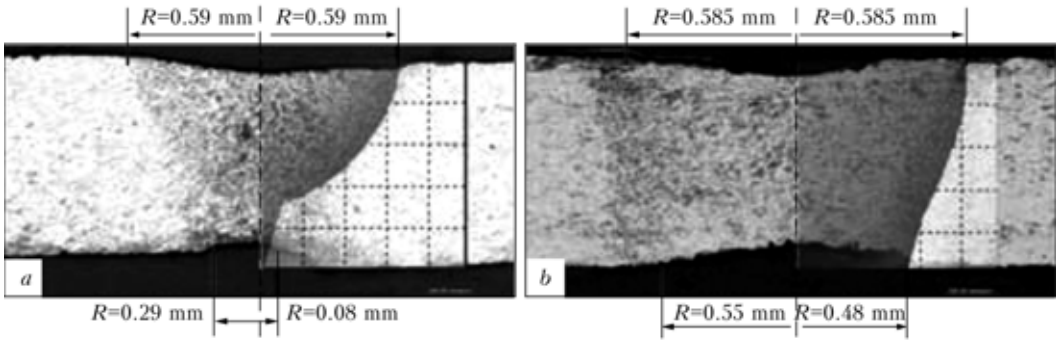

Figure 4. Comparison of calculation results on the developed model (*a*) with experiment (*b*) for low carbon steel 08U at 10 Hz laser frequency, 3.5 ms pulse duration, 4.5 kW radiation power, 5.726 kW lamp electric power and welding speed of 4 mm / s (*a*) and 5 Hz laser frequency, 7 ms pulse duration, 2.25 kW radiation power, 5.16 kW lamp electric power and welding speed of 2 m / s (*b*)

heat source is nonlinear since the heat source power depends on the surface temperature.

First we consider the problem as linear one. In this case, having used the known expression for the Green function of the 3D problem about heat conductivity in moving coordinate system, for the additional source heat field one can write

$$T(x, y, z) = \int\int \frac{A(T(x', y'))I(x', y')}{2\pi\lambda|\vec{R} - \vec{R'}|} \times$$

$$\times \exp\left(-\frac{v}{2\chi}(|\vec{R} - \vec{R'}| + (x - x'))\right) dx'dy'.$$

Here, integration is fulfilled with respect of the target surface illuminated by lamp light; $A(T)$ is the absorption factor; I is the radiation intensity; and v is the welding speed.

Considering the temperature dependence of absorption factor, this expression is an integral equation for which solution the following algorithm has been developed: at the first stage only the surface temperature is determined. Calculating the integral by summation over 2D grid we have got an algebraic nonlinear equation in each cell, and then it has been solved by the simple iteration method. At that the local temperature in each cell of the surface grid has been determined and the local value of absorbed energy of the lamp radiation has been found with its help. Then the heat field of the additional heat source is calculated with the known value of the absorbed energy distribution. This field without deep penetration has been summarized with a temperature field of the laser source. In case of deep penetration the temperature distribution of the additional source has been considered in calculating of the cavity sizes and shape as a distributed preheating temperature. The model realized as a computer program allows calculating size and shape of the weld pool, the temperature field and thermal cycles in the weld and HAZ metal. Comparison of the calculated results with

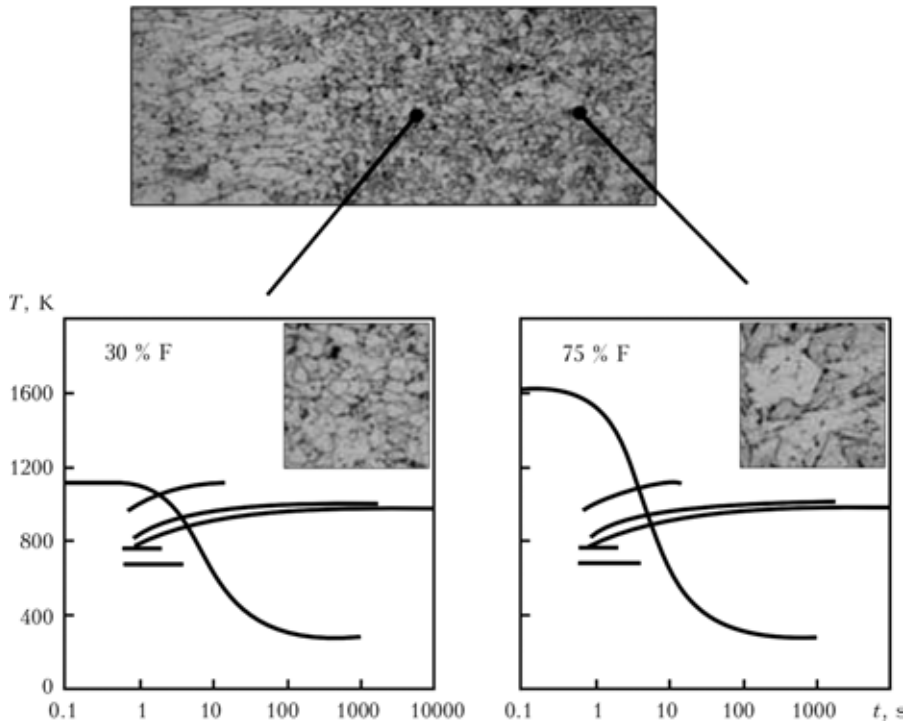

Figure 5. Comparison of calculation results of phase combination with experiment for low carbon steel 08U at laser frequency of 5 Hz, pulse duration of 7 ms, radiation power of 2.25 kW, lamp electric power of 5.16 kW and welding speed of 2 m / s

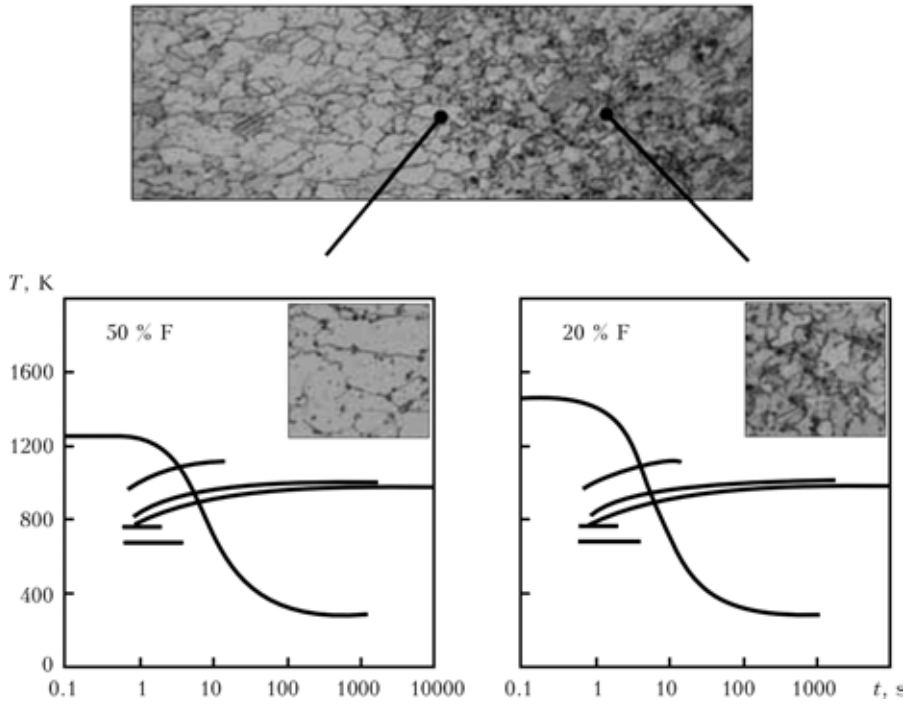

Figure 6. Comparison of calculation results for phase combination with experiment for low carbon steel 08U at laser frequency of 10 Hz, pulse duration of 3.5 ms, radiation power of 4.5 kW, lamp electric power of 5.726 kW and welding speed of 4 mm / s

experimental ones (Figure 4) confirms high accuracy of the developed model.

As stated above, the carbide precipitation and nature of thermal cycles influence on process of phase composition formation. For estimation the steels phase composition is usually used time-temperature transformation diagrams of austenite decay together with curves corresponding to thermal cycles. The method of phase composition quantitative assessment based on Quench factor analysis was described in [8] and successfully testing on aluminum alloys. Later the Quench factor analysis was applied for investigation possibility of prediction of steel mechanical properties during heat treatment [9], but in these works didn't consider processes of carbide formation and their influence on actual position of austenite decay *C*-curves. As was shown in [4], the non-equilibrium kinetics of new phase nucleus formation and non-stationary diffusion influence on phase condition formation in practical welding conditions. Such point of view was used for logical design of quantity precipitate calculation for low-carbon steel welding and realized as computer program in which for estimation thermal field was used the model described above. The calculation was carried out for steel 08U, the comparison of results and experimental data revealed their acceptable coincidence (Figure 5 and 6).

CONCLUSION

Use of the hybrid laser-light welding instead of laser one allows us to increase the melting efficiency and to provide stability of weld formation in welding metals of small thickness. The displacement of lamp spot from laser spot on workpiece surface can be used as control parameter for influence on welded metal microstructure. The laser-light welding with accompanying heat treatment in the investigated range of modes allows deep drawing depth to be increased and, accordingly, punch ability of the welds to be improved. The maximum value of the deep drawing depth has been observed when the axis of the focal spot of the laser beam has displaced from the light spot axis on 1.0–1.5 mm.

The analysis of a microstructure allows concluding that improvement of punch ability after the laser-light welding results from decrease of the martensite part in the microstructure of the weld and HAZ metal. It can be explained by influence of accompanying stress relieving due to action of the polychromatic heat source. Character of microhardness change in welds after the laser-light welding in comparison with laser one allows us to note significant decrease of microhardness variation on the HAZ and decrease of the maximum values of the metal microhardness in the weld and HAZ.

1. Gyulikhandanov, E.L., Khaidorov, A.D. (2002) Effect of thermocycling on the structure and properties of high-speed steel obtained by electroslag remelting. *J. Metal Sci. and Heat Treatment*, 44(**9 / 10**), 426.
2. Glumann, C., Rapp, J., Dausinger, F. et al. (1993) Welding with combination of two CO_2 lasers — advantages in processing and quality. In: *Proc. of ICALEO* (Orlando, USA), 672–678.
3. Gureev, D.M. et al. (1999) *Mechanisms of phase transformations in iron and steels at laser heating*. Samara: SSU.
4. Dilthey, U., Gumenyuk, A.V., Turichin, G.A. (2006) Calculation of the kinetics of diffusion phase transformations in low-alloyed steels in beam welding. *The Paton Welding J.*, **2**, 11–15.
5. Fuerst, B., Dahmen, M., Kaierle, S. et al. (1997) CALAS — a process model for laser beam welding. In: *Proc. on Laser Assisted Net Shape Eng.*, 193–201.
6. Lopota, V., Suhov, Yu., Turichin, G. (1997) Model of laser welding for application in technology. *Izvestiya RAN*, Series Physics, 61(**8**), 1613--1618.
7. Lopota, V., Turichin, G., Valdaitseva, E. et al. (2004) Marangoni convection in the rear part of molten pool in keyhole laser welding. *Priborostroenie*, **10**, 76–82.
8. Staley, J.T. (1987) Quench factor analysis of aluminium alloys. *Mater. Sci. Technol.*, 3(**11**), 923–935.
9. Totten, G.E., Sun, Y.H., Bates, C.E. (1999) Simplified property predictions AISI 4140 based on Quench factor analysis. In: *Proc. of 3rd Int. Conf. on Quenching and Control of Distortion* (Prague, March 24–26, 1999), 219-225.

THEORETICAL INVESTIGATION OF STABILITY OF MOLTEN POOL FOR HIGH SPEED WELDING WITH DEEP PENETRATION AND SUPERFICIAL WELDING USING HIGH POWER DENSITY HEAT SOURCE

G. TURICHIN[1], **E. VALDAITSEVA**[1], **E. POZDEEVA**[1], **U. DILTHEY**[2] and **A. GUMENIUK**[2]
[1]St.-Petersburg State Polytechnic University, Russia
[2]ISF Welding and Joining Institute, Aachen University, Germany

The article devoted to the simulation of dynamic phenomena of the laser welding process with deep penetration. The presented model is a future development of steady-state model of laser welding. It based on the approach of Lagrange mechanic and takes into account melt flow, wave motion on the cavity surface, melting viscosity, bubble pressure, recoil pressure and radiation parameters. The results of calculations describe self-oscillation nature of the cavity shape during welding. With the base of presented model a simulation of keyhole collapse, leading to defect formation, and a description of acoustic emission spectra from the cavity has been developed.

The processes of laser welding with deep penetration, as well as related processes of hybrid welding, are frequently accompanied by porosity appearance and spiking phenomena. The reason of these effects connected with self-oscillation nature of vapour cavity and melt pool in deep penetration welding. Results of experimental investigation of the laser welding prove that the process is not stationary even at stabilisation of all external effects on a weld pool. The experiments on high-speed filming of the laser welding of compound workpieces, consisting from metal and quartz glass [1], have shown a continuous change of the cavity shape, quay-periodic moving of zones of the maximum brightness on its depth and also availability of such zones on a back wall. The plasma plume filming above the keyhole has shown its quasi-periodic fluctuations [2]. The comparative researches of the liquid metal movement on the weld pool surface and process of spike formation have shown conformity between spiking and a melt tipping out from the melt pool. The same results were obtained later after X-ray filming [3].

The analysis of self-oscillations at action of high intensity energy fluxes on materials is conducted in [4] on the basis of the linear theory of stability. The further development of this approach is submitted in [5]. The stability is investigated on the basis of the joint analysis of the development of temperature, hydro- and gas-dynamic perturbations with the account of relaxation processes and target surface shielding by products of evaporation. The attempts to take into account a real geometry of a cavity surface in laser welding were undertaken by the authors of [6], and in [7] the linear stability of the cavity shape has been investigated. The description of temporary dynamics of cavity radius on the basis of a problem reduction to one ordinary differential equation is indicated in [8]. The authors used the axial symmetry of model problem for reduction of hydrodynamic equations to one ordinary differential equation, but this model predicts only attenuation of fluctuations.

For detail understanding of the nature of dynamic processes in the melt pool during deep penetration welding, it is necessary to have a dynamic model of welding process, based on the clear physical picture of the laser welding process with deep penetration.

Because such model could be applied for the aim of prediction of welding defect appearance and for creation of reliable monitoring and control systems, it should answer the following obvious demands to be used simultaneously for welded joint quality prediction and in the on-line control systems:

- physical equivalence;
- work in real time mode;
- work on available computer technology in the industry.

These requirements don't allow construction the dynamic model of the laser welding process on the base of the direct solution of all total combination of connected physical problems describing the laser welding processes, as it was done for steady-state process model [9–11]. The possible way to develop such dynamic model is using of minimum variation principles and Lagrange (or Hamilton) mechanics formalism, which allow reducing the model to several ordinary differential equations.

Description of the model. To use formalism of the Lagrange mechanics to derive the active zone dynamics equations, it is necessary to take into account such phenomena as wave motion of the cavity surface, change of the shape and sizes of the weld pool in time and influence of the cavity motion as the whole on

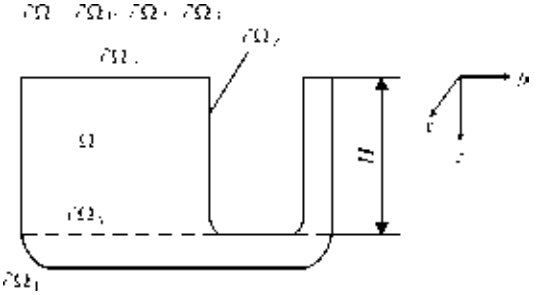

Figure 1. Suitable model form of the active zone

oscillations of its depth and radius. Besides the friction forces effect would be taken into account into the movement equations. We'll consider geometry of the model and its possible simplifications before deriving equations of motion by Lagrange formalism. For simplification let us apply that penetration depth $H >> a$, where a is the keyhole radius, and ignore inclination of the cavity and melt pool walls. Suitable model form of the active zone is show in Figure 1.

The melt flow is described by flow potential φ that answer Laplace equation $\Delta\varphi = 0$ and boundary conditions

$$\left.\frac{\partial\varphi}{\partial n}\right|_{\partial\Omega_1} = 0; \quad \left.\frac{\partial\varphi}{\partial n}\right|_{\partial\Omega_2} = f(\theta, t).$$

Here function f is determine by the cavity motion. It is impossible to get the analytic solution of task about the potential flow of the melt in the region shown in Figure 1, but it is possible to use a conform mapping to simplify the problem by transformation this task into determination of the melt velocity field in the region bounded by two co-axial cylinders with radii A and a. It is especially convenient to do it, if in the mapping space the energy is presented as function of the cavity section areas.

Taking into account the wave movement on the cavity surface and using Fourier expansion for cavity cross-section area $s(z) = s_0 + \sum_{n=1}^{\infty} s_n \cos\frac{\pi n z}{H}$ in the motionless (in respect to the target) coordinates system to describe the shape of surface, after using of the continuity equation one can obtain the following expression for the velocity v_z:

$$v_z = \frac{1}{S - s}\left(\dot{s}_0 z + s_0\dot{H} + \sum_{n=1}^{\infty}\frac{\dot{s}_n H}{\pi n}\sin\frac{\pi n z}{H}\right),$$

where S is the keyhole cross-section area.

For the melt between the target surface and parallel plane, passing through cavity bottom, after transformation it is possible to get

$$E = E_\perp + E_z,$$

where

$$E_\perp = \pi H a^2 \times$$
$$\times\left(\frac{\rho v_0^2}{2}\frac{A^2 + a^2}{A^2 - a^2} + \frac{\rho\dot{a}^2}{2}\frac{A^4}{(A^2 - a^2)^2}\left\{\ln\frac{A^2}{a^2} - 2\left(1 - \frac{1}{2}\frac{a^2}{A_2}\right)^2 + \frac{1}{2}\right\}\right);$$

$$E_z = \frac{\rho}{2(s - s_0)} \times$$
$$\times\left\{\dot{s}_0^2 H^2\left(\frac{1}{3} + \sum_{n=1}^{\infty}(-1)^n\frac{2s_n}{(\pi n)^2(S - s_0)}\right) + s_0^2\dot{H}^2 H + \sum_{n=1}^{\infty}\frac{H^3\dot{s}_n^2}{2(\pi n)^2} + \right.$$
$$+ s_0 H^2\dot{s}_0\dot{H}\left(1 + \sum_{n=1}^{\infty}\frac{2((-1)^n - 1)s_n}{(\pi n)^2(S - s_0)}\right) +$$
$$+\sum_{n=1}^{\infty}\sum_{k=1}^{\infty}\frac{1}{2}\dot{s}_0\dot{s}_n(s_{n-k} - s_{n+k})\frac{H^3}{p^2 nk(S - s_0)} - \sum_{n=1}^{\infty}(-1)^n\dot{s}_0\dot{s}_n\frac{H^3}{\pi^2 n} \times$$
$$\times\left[\frac{2}{n} + \sum_{k=1}^{\infty}(-1)^k\frac{1}{\pi}\frac{s_k}{S - s_0}\left(\frac{1}{(n + k)^2} + \frac{1 - \delta_{nk}}{(n - k)^2}\right)\right] +$$
$$+\sum_{n=1}^{\infty}s_0 H^2\dot{s}_n\dot{H}\frac{1}{\pi^2 n} \times$$
$$\left.\times\left[\frac{2(1 - (-1)^n)}{n} - \sum_{k=1}^{\infty}\frac{s_k}{S - s_0}\left(\frac{(-1)^{n+k} - 1}{n + k} + \frac{1 - \delta_{nk}}{n - k}\right)\right] - \right\};$$

A and a is the radii of the image circles of keyhole and the cavity on the plane of conform mapping, respectively.

The bottom part kinetic energy E_b can be calculated by the same way:

$$E_b = \frac{\rho}{2}\dot{H}^2\frac{4\pi a^2 A^5}{(A^2 - a^2)^2}\frac{A}{L - H}\sum_{i=1}^{\infty} \times$$
$$\times\left(\frac{J_1\left(l_i\frac{a}{A}\right)}{1_i^4 J_0(l_i)} + \frac{J_1\left(l_i\frac{a}{A}\right)}{3l_i^2 J_0(l_i)}\left(\frac{L - H}{A}\right)^2\right),$$

where l_i is the root of the equation $J_1(l_i) = 0$; L is the penetration depth.

Since potential energy of the active zone is superficial energy, it is enough to calculate a free surface area and multiply it by the value of the specific surface energy equal to surface tension coefficient σ. Having left parts containing the small parameter s_n / s_0 out, one can get

$$\Pi = \sigma\left\{\pi A^2 + 2\pi a H + \frac{\sqrt{\pi}}{4}\sum_{n=1}^{\infty}\frac{n^2 s_n^2}{H\sqrt{s_0}} + 2H_1(A + a)\right\}.$$

It is easy to get the expressions for generalised forces Q_i that corresponds to chosen generalised coordinates (s_0, s_n, H) by using definition $Q_i = \delta A_i / \delta q_i$, where δA_i is the virtual work on the virtual displacement δq_i. For Q_H it is easy to get $Q_H = (p - p_0)s_0$, where p is the vapour pressure inside the cavity; p_0 is the external pressure.

Taking into account the vapour jet reactive force, we have finally

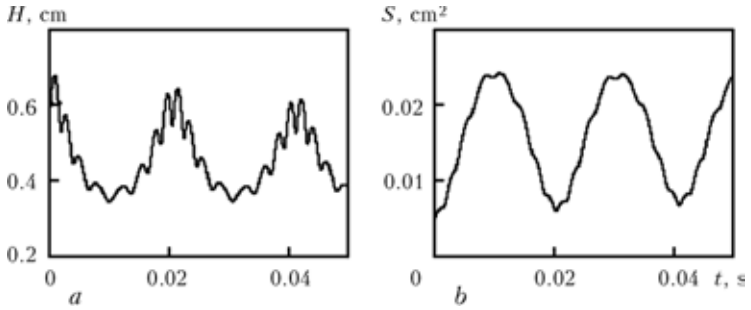

Figure 2. Temporal behavior of the cavity depth H (a) and its cross-section area S (b)

$$Q_H = (p - p_0 + \rho_0 v_0^2) s_0,$$

where ρ_0 and v_0 is the density and the velocity of vapour jet in the workpiece surface plane, respectively.

Let us evaluate Q_s. After several transformations, neglecting the small parts we have

$$Q_{s_0} = (p(s_0) - p_0)H - \frac{1}{3}\frac{\sigma}{a} H + (-1)^n \frac{2}{\pi^2}\frac{\sigma}{a}\frac{s_n}{s_0} H_n^2;$$

$$Q_{s_n} = H\left[\left.\frac{\partial p}{\partial s}\right|_{s = s_0} \frac{s_n}{s_0} + \frac{\sigma}{a}\frac{s_n}{s_0}(-1)^n \frac{1}{\pi^2 n^2} + \frac{2}{\pi^2}\frac{\sigma}{a}\sum_{\substack{k=1 \\ k \neq n}}^{\infty} \frac{s_k}{s_0}(-1)^{n+k} \frac{n^2 + k^2}{(n^2 - k^2)^2}\right].$$

To determine $p(s_0)$ and $\left.\frac{\partial p}{\partial s}\right|_{s = s_0}$ the non-stationary heat transfer problem has been solved analytically. Let us consider generalised viscous forces according to Lagrange mechanics formalism, having determined the dissipative function $D = \frac{dE}{dt}$, and the generalised friction force $R_i = \frac{1}{2}\frac{\partial D}{\partial Q_i}$. Solving task about the melt flow in the boundary layer at the melting front gives following expression for the dissipative function:

$$D_1 = -\rho L \sqrt{\frac{\nu}{\pi}} \int_{-\infty}^{t} \frac{d\tau}{\sqrt{t - \tau}} \int_0^H \frac{dv_0}{d\tau} v_0(t) dz,$$

where $L = 2\pi A$ is the melting front perimeter.

Now we can get Lagrange equation (dynamic model one) imagined as

$$\frac{d}{dT}\frac{\partial L}{\partial \dot{q}_i} - \frac{\partial L}{\partial q_i} = Q_i + R_i,$$

where q_i assumes H, s_0, s_1, ... s_n, ..., consecutively.

Modeling results and discussion. To fulfil calculates the system was «cut» in s_2, and the system obtained from four ordinary differential equations of second order was solved numerically by standard 6th order Runge–Kutt algorithm. The test calculations was made for welding of mild steel in the power range of 1–10 kW and welding speed from 0.3 till 5.0 cm / s. Examples of calculation results are shown in Figures 2 and 3 for radiation power Q = 3 kW, welding speed v = 1 cm / s, intensity distribution of the radiation corresponding to TEM_{00} mode with beam radius 0.015 in the focus (86 % of the full power inside), focus distance 20 cm and surface focusing. The initial conditions are taken from the calculation results of the stationary model of laser welding [10].

Analysis of the calculation results shows that when excess pressure inside the cavity and the capillary pressure being equal, force parts of the equations are zero. This condition is unstable balance point. Dense occupation of the limited regions on the phase portraits by the phase trajectories says about turbulent character of the cavity oscillations. It explains the calculation results independence upon initial conditions (when the initial point gets into the attractor). Sizes and shape of the attractor are determined by welding mode parameters.

Modelling show that different generalised coordinates have the different oscillations spectra. The lowest frequencies (less than 500 Hz) are typical for cavity radius oscillations. The amount of high frequency components in the spectra of the cavity depth oscillation is more than the same components in the spectra of the radius oscillation. The first s_1 and second s_2

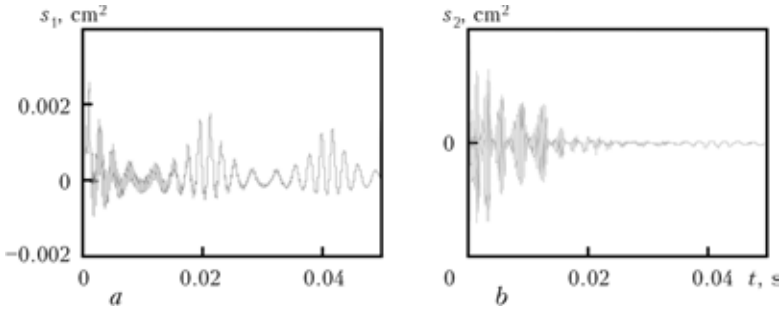

Figure 3. Temporal behavior of the first (a) and second (b) order waves on the cavity surface

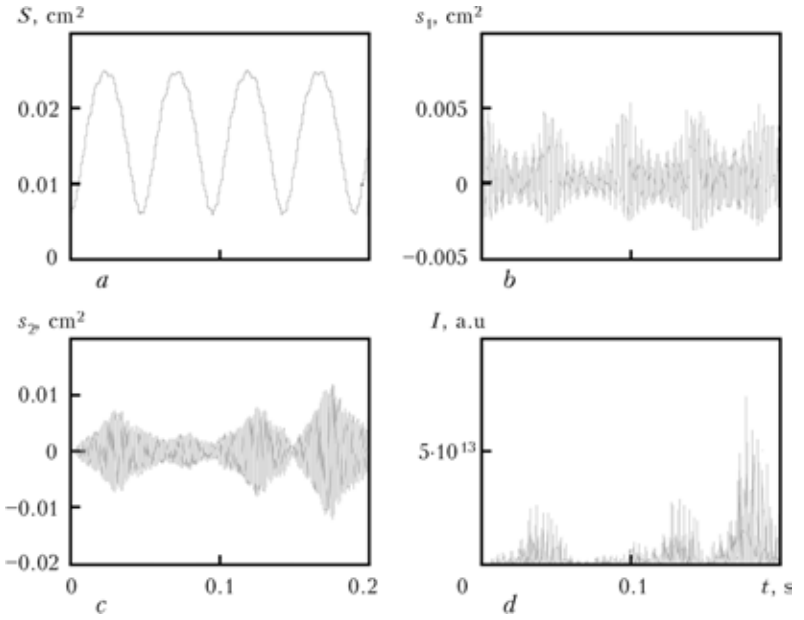

Figure 4. Temporal behavior of cavity area of cavity cross-section (*a*), amplitudes of waves on the cavity surface (*b*, *c*) and acoustic emission intensity (*d*)

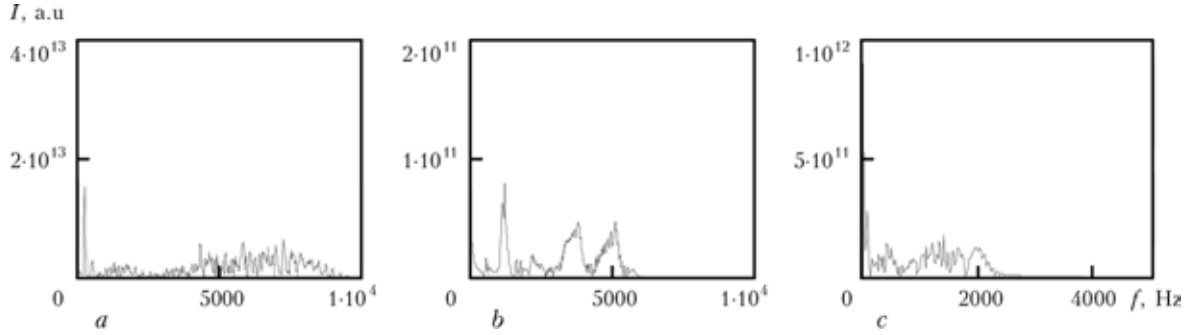

Figure 5. Frequency spectra of acoustic emission at welding speed 5 cm / s and penetration depth ≈ 0.25 cm (*a*), 3 cm / s and ≈ 0.42 cm (*b*), 1 cm / s and ≈ 1.1 cm (*c*)

order waves have the highest frequency spectra (up to 10 kHz). These spectra are also depending on the cavity depth. The feeding velocity increasing also decreases the low-frequency oscillations. Because of this model describes the non-linear cavity oscillation, amplitudes of which are not very small, it allows looking more precisely on the hydrodynamic stability of the cavity shape, as it was investigated in [8]. Accordingly

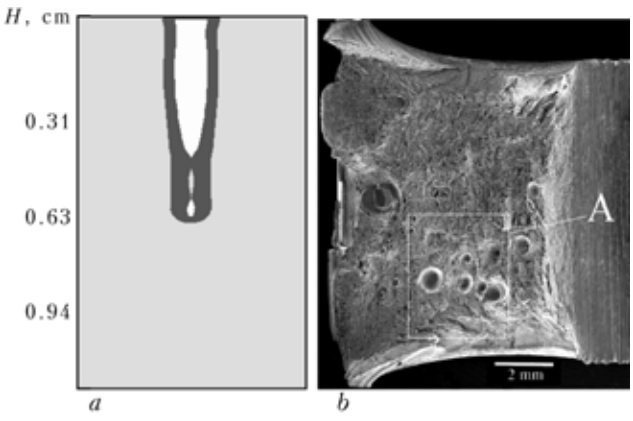

Figure 6. Simulation of porosity formation due to cavity collapse (*a*), and results of experimental observation of pores formed by this effect (*b*) during laser welding of pipe steel

[8], increase of the beam radius leads to increase of the wave amplitudes on the cavity surface.

To illustrate a dependence between the dynamics of cavity depth H, the area of cavity cross-section S and the amplitudes of waves on the cavity surface s_1 and s_2 from one side and acoustic emission parameters, the example of temporal behavior of this values and their frequently spectra are shown in Figure 4. The temporal dynamics of acoustic emission is more close to dynamics of banding around of the cavity generalised coordinate with highest frequency s_2, but frequency spectra lie in the region of lesser frequency.

The increases of power and, thus, increases of penetration depth lead to shift of spectra to direction of smaller frequencies that correlated with behavior of spectra of all generalised coordinates of cavity dynamic model. The changes of welding speed (Figure 5) lead to the same changes of spectra of acoustic emission, so the cavity depth is a value that in general determined a situation here.

The developed mathematical formalism has been implemented in CAE system LaserCAD. With this feature it is possible to use LaserCAD for dynamical analysis of porosity formation and spiking phenomena (Figure 6).

CONCLUSION

In this article, the dynamic model of the laser welding process with deep penetration based on the variation principles, is presented. The model takes into account melting flow, wave motion on the cavity surface, melting viscosity, bubble pressure, recoil pressure and radiation parameters. The model allows the welding process to be analysed both for continuous and for temporally modulated radiation. The model predicts self-oscillation character of the cavity behavior in welding, moreover the cavity oscillations are look like stochastic in general case.

1. Bashenko, V.V., Mitkevich, E.A., Lopota, V.A. (1983) Peculiarities of heat and mass transfer in welding using high energy density power sources. In: *Proc. of 3rd Int. Coll. on EBW* (Lion, 1983), 61–70.
2. Lopota, V.S. et al. (1989) State of material and its parameters in the beam interaction zone in laser welding with deep penetration. *Fizika i Khimiya Obrab. Materialov*, **2**, 104–115.
3. Matsunawa, A., Kim, J.-D., Seto, N. et al. (1998) Dynamics of keyhole and molten pool in laser welding. *J. Laser Appl.*, 10(**6**), 247–254.
4. Zuev, S.V., Selischev, V.I. et al. (1980) Self-oscillations under action of high density energy source on materials. *Fizika i Khimiya Obrab. Materialov*, **6**, 3–7.
5. Arutunyan, V.Yu., Baranov, E.P. et al. (1985) *Laws of pulse-periodic modes of deep penetration of metals*: Preprint IAE 4137 / 16. Moscow.
6. Uglov, S.V., Selischev, V.I. (1988). *Self-oscillations in action of high density energy fluxes on materials*. Moscow: Nauka.
7. Mirzoev, F.Kh. (1994) Vaporisation-capillary instability in deep gas-vapour keyholes. *Kvant. Elektronika*, 21(**2**), 147–150.
8. Turichin, A. (1996) Hydrodynamic aspects of cavity stability in beam welding. *Fizika i Khimiya Obrab. Materialov*, **4**, 74–82.
9. Kaplan, W. (1994) A model of deep penetration laser welding based on calculation of the keyhole profile. *J. Phys. D: Appl. Phys.*, **27**, 1805–1814.
10. Beyer, E., Dahmen, M., Fuerst, B. et al. (1995) A tool for efficient laser processing. In: *Proc. of ICALEO* (San Diego, USA).
11. Schulz, B., Fuerst, S., Kaierly, G. et al. (1996) Powerful features for LBW including theoretical aspects. In: *Proc. of ICALEO* (Detroit, USA).

STUDY OF ASSIST GAS FLOW IN TUBE WORKPIECE IN LASER CUTTING

R. ZHUK, M. ANYAKIN, P. KONDRASHEV, O. STEPURA, O. MUCKHOID and **V. KOVALENKO**
Laser Technology Research Institute of NTUU «KPI», Kiev, Ukraine

Laser technology has become a universal tool for different material processing applications but, unfortunately, the majority of physical mechanisms and their influence on processing quality are still far beyond understanding. Laser cutting of thin-walled tubes of small diameter for medical applications is an emerging technology and requires a detailed investigation. This paper presents an attempt to numerically simulate the cutting process of tubes from which medical stents are made, the propagation of an assist gas inside the tube, the temperature distribution on the outer and inner tube surfaces. Different assist gases, as well as various modulation frequencies and stand-off distances, were used.

Focused laser beam is widely used for precise cutting of almost any type of metal or alloy regardless of its mechanical and physical properties. There are two main cutting schemes which could be used for stent manufacturing, namely conventional laser cutting technique which results in the material evaporation with help of long-pulse diode and flash-lamp based Nd:YAG lasers and novel laser types with ultra-short pulses utilising the ablation processes for the material removal.

As was shown in [1], good cut quality could be achieved with help of gas-assisted laser cutting. Molten material is carried away downstream with help of assist gas which exits nozzle end under given pressure. But in most cases part of the molten material adheres to the bottom of the cutting kerf thus lowering its quality. Since the requirements to the quality of stent surface are very high, some means of surface quality increase have to be found.

Increasing of an assist gas pressure can in theory reduce the dross formation but it is very hard to achieve stable sonic or supersonic flow at the nozzle exit due to the pressure losses caused by the formation of Mach shock disks [1] occurred when the pressure at the nozzle exit exceeds 2 bar (for monatomic gas).

Versatile nozzle configurations and set-ups were designed in order to make the gas jet more uniform to obtain good cut quality. Among them are conical, ring and tailor-made Laval nozzles. The main purpose of these nozzles is to avoid shock formation and make gas flow more uniform.

At the very same time the results presented in [2] relate mainly to thin sheet metal. The interaction of laser beam and compressed gas jet with thin tube of small diameter is more complicated matters for several additional factors have to be taken into account. We have to consider the influence of laser beam on the lower surface of the tube and the influence of the assist gas pressure on the shape of the tube after laser cutting.

Experimental procedures. The cutting system used for the experiments consisted of motion unit, Nd:YAG laser, cutting head and tool for the control of laser cutting quality.

The focusing system comprises of a lens with focal distance of 50 mm and three types of diaphragms with the diameters of 2.0, 1.8 and 1.5 mm that are by turns positioned inside the resonator. The cutting head includes a focusing optics and an assist gas nozzle 72 mm long. At the initial stage, there was used an ordinary converging nozzle with the exit diameter of 1 mm. The length of the converging part of the nozzle is 10 mm, and the ratio of the inlet to exit diameter is 10:1.

There was also developed a measuring tool for cutting quality monitoring, principal scheme and general view of which is presented in Figure 1.

Nitinol-based tubes with the outer diameters of 1.5, 2.0 and 4.0 mm and thickness of 300 μm were cut in longitudinal direction at assist gas pressures of 4, 6 and 8 bar, respectfully.

Results. The following material removal techniques were chosen as a starting point for the investigation of laser cutting of stents:

- direct laser cutting –-- pure laser cutting (no assist gas), and gas-assisted laser cutting (air, oxygen, argon);
- layer-by-layer laser cutting (with help of additional laser beam scanning);
- layer-by-layer laser cutting (multiple pass cutting).

The first step was to model the propagation of assist gas out of a conical nozzle. Fluent 6.2 software with *k–e* turbulence model was used for computation. The goal of computations was to investigate the dynamic and stagnation pressure distribution along the nozzle axis and to see how it incorporates with the tube positioned in downstream the nozzle at a stand-off distance of 1.5 mm. The inlet pressure values of 5, 7 and 9 bar were set.

The results of computation clearly show that strong shockwaves are formed right after the nozzle exit. The higher the pressure, the greater the amplitudes of dynamic pressure and Mach number (Figures 2–5).

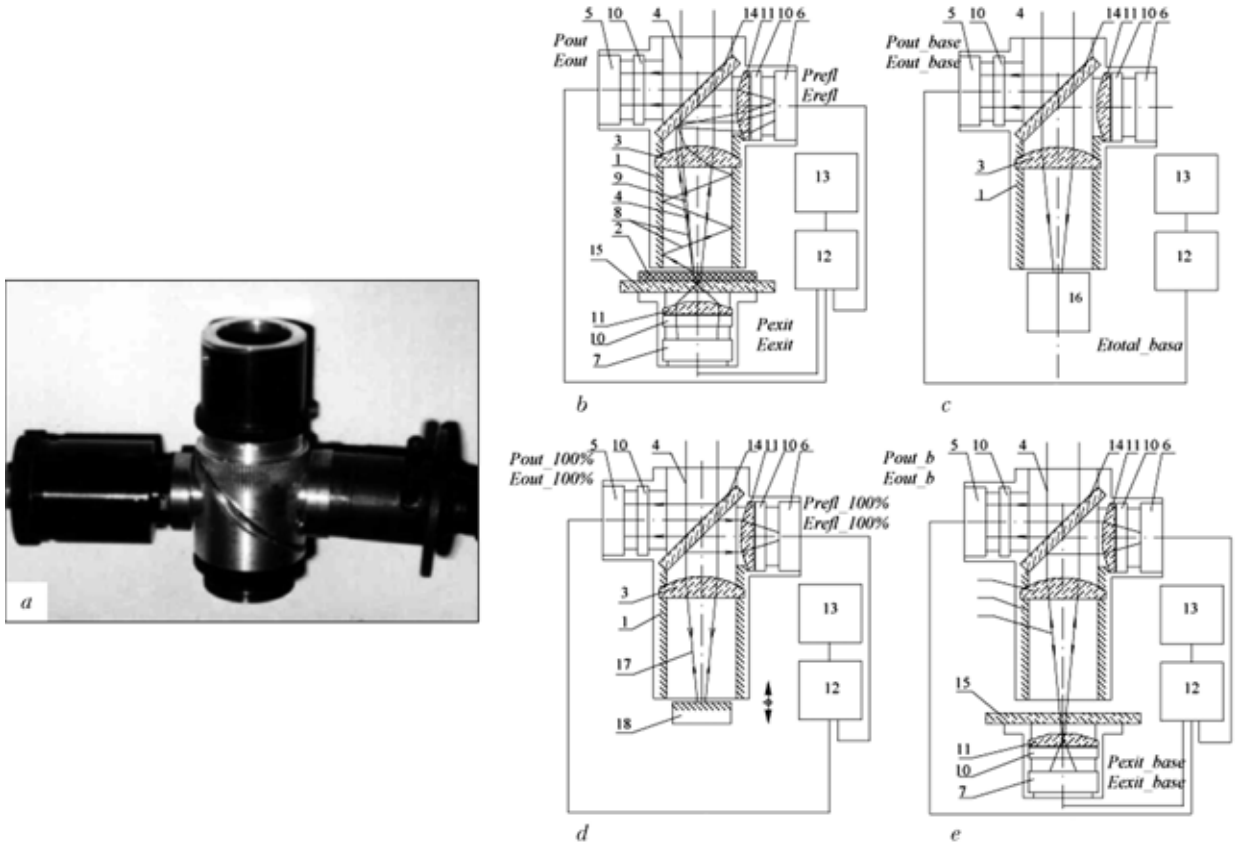

Figure 1. General view of tool for cutting process monitoring (*à*) and main stages of gauging (*b–e*): *1* — light-guide; *2* — specimen; *3* — focusing lens; *4* — laser beam; *5–7* — beam sensors; *8, 9* — beam traces; *10* — filters; *11* — objectives; *12* — control unit, *13* — computer; *14* — beam splitter; *15* — glass; *16* — energy meter; *17* — beam reflected from mirror; *18* — mirror

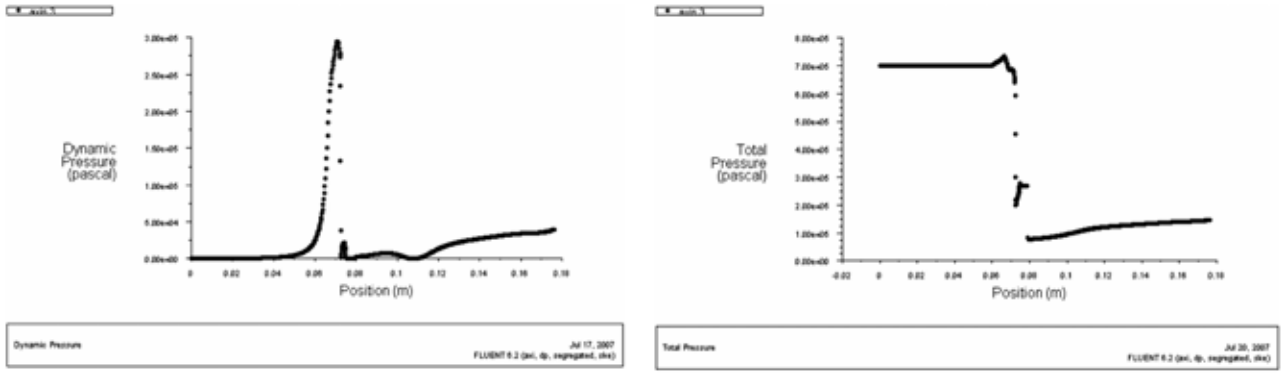

Figure 2. Dynamic (*a*) and total (*b*) pressure fluctuations along inside and outside of the nozzle at inlet pressure of 7 bar and nozzle total length of 0.072 m

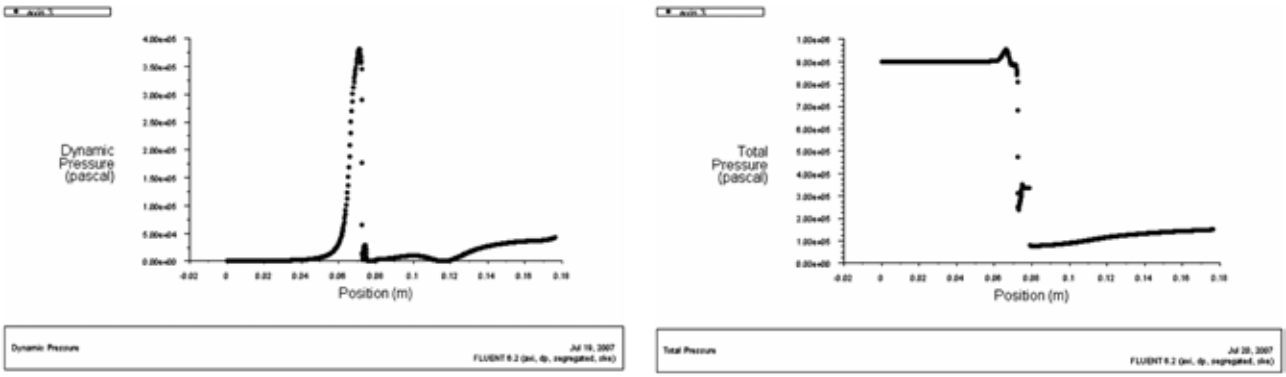

Figure 3. Dynamic (*a*) and total (*b*) pressure fluctuations inside and outside of the nozzle at inlet pressure of 9 bar and nozzle total length of 0.072 m

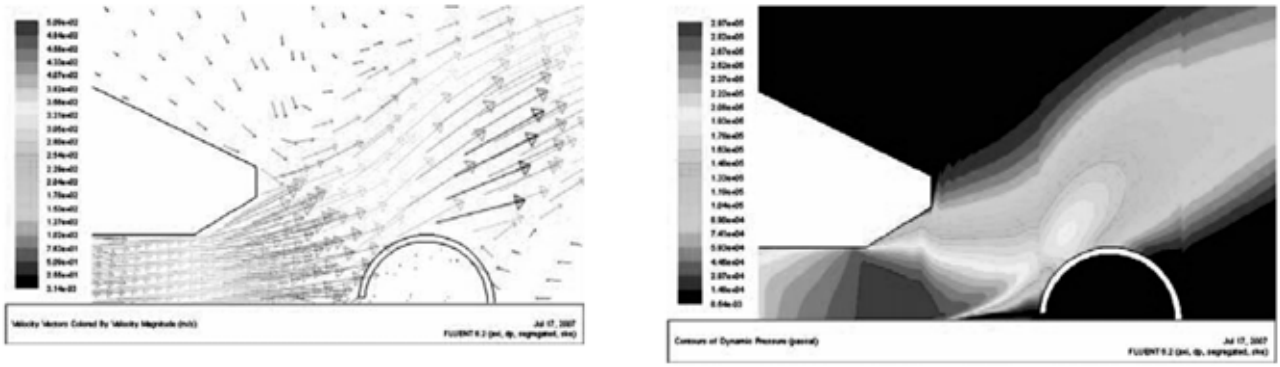

Figure 4. Contours of the velocity magnitude and dynamic pressure at inlet pressure of 7 bar

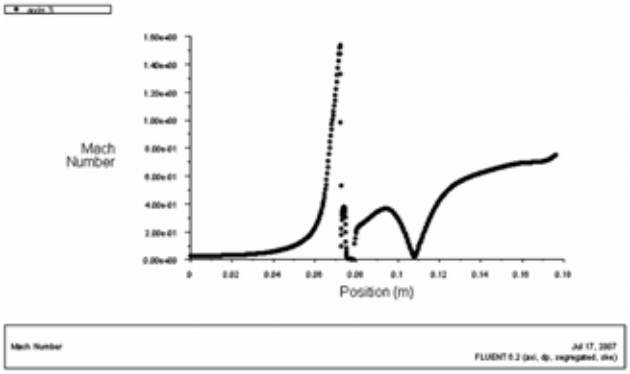

Figure 5. Mach number fluctuations inside and outside of the nozzle at inlet pressure of 7 bar

The emerged shock discs could have negative effect on the final quality of the stent. In combination with thermal effect of laser irradiation the gas jet could deflect from its propagation axis and cause deformations of the tube specimen.

Moreover, with help of the quality measuring tool (see Figure 1) we investigated the reflected signal from the processing zone. With its help we could observe the periodic formation of plasma plume represented on screen as a series of chaotic oscillations. At the very same time these oscillations were also periodically replaced by more uniform signals. It is possible to conclude that gas jet blew away the plasma plume during the cutting process.

A sudden total pressure drop is clearly seen on the plots in all cases. Since the stagnation pressure has a great influence on machining performance [3, 4], a special-purpose nozzle has to be designed in order to reduce shock formation and pressure drops. The best solution for this problem is to design tailor-made converging-diverging nozzles (also called Laval nozzles) but the use of these nozzles is limited for they could be designed only for specific pressure value. If the inlet pressure is decreased or increased then the good performance of these nozzles could not be guaranteed.

During the observation of gas-assisted laser cutting of thin-walled tubes it was found that assist gas has little influence on melt removal at given thicknesses. Shockwaves generated at the cutting nozzle exit stop the vapor expansion upstream in a periodic manner and the hot vapor under the shockwave partially assist the melting process. Assist gas also partially cools the melt on the upper surface of the tube. Whereas the bottom surface of the kerf still suffers from dross formation. The close-up photos of the cuts are presented in Figure 6.

For the purpose of clarity, the tube was later cut lengthwise and fattened (Figure 7).

The obtained results clearly show that the increase of pulse repetition rate can drastically decrease the cut width. A pressure was set to the value of 4 bar in order to avoid formation of strong oblique shocks.

CONCLUSIONS

1. Laser cutting of thin-walled tubes significantly differs from the other types of laser cutting. It is not advisable to use high pressure sonic and supersonic nozzles due to the shockwaves formation and narrow

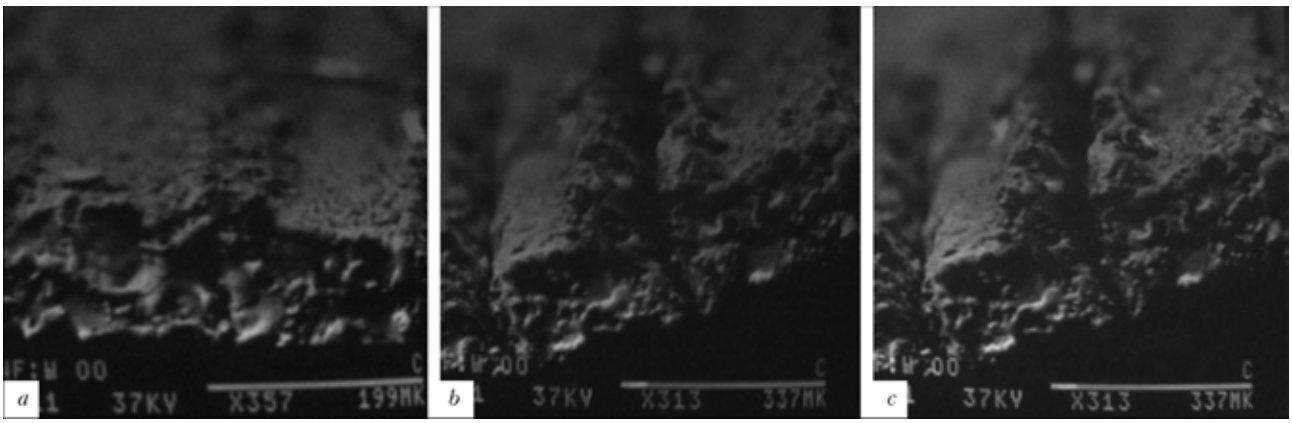

Figure 6. Close-up photos of laser cuts at pressure of 4 (*a*), 6 (*b*), 8 (*c*) bar and pulse frequency of 10 kHz

cutting kerfs and damage that could be done to the integrity and final shape of the product.

2. It is not recommended to use direct laser cutting method due to the poor laser quality. Assist gas has little influence on melt removal mechanisms in case of thin-walled tubes with small diameter but plays important role in melt formation process.

3. Strong shockwaves and Mach numbers higher than 1 occur in case of using ordinary conical nozzles. A tailor-made Laval nozzles have to be designed to minimize the shock formation and its influence on the tubes being cut.

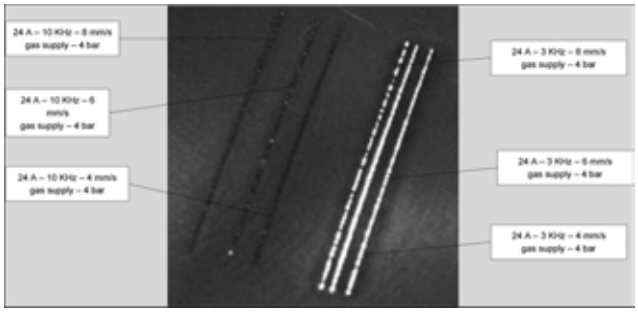

Figure 7. Influence of pulse frequency on the width of laser kerf at pressure of 4 bar (bottom view)

1. Schneider, M., Fabbro, R., Berthe, L. et al. (2005) Gas investigation on laser drilling. In: *Proc. of 24th Int. Congress on Applications of Lasers and Electro-Optics* (Miami, USA, Oct. 31–Nov. 3, 2005), Vol. 98.
2. Okamoto, Y., Uno, Y., Hosogaya, M. et al. (2005) Precision micro cutting of thin steel plate with newly designed Laval nozzle by pulsed YAG laser. *Ibid.*, Vol. 97.
3. Caristan, Ch.L. (2000) *Laser cutting guide for manufacturing.*
4. Chryssolouris, G. (1991) *Laser machining theory and practice.* Springer.

Name Index